Loop-induced form factors in light-meson physics

Dissertation
zur
Erlangung des Doktorgrades (Dr. rer. nat.)
der
Mathematisch-Naturwissenschaftlichen Fakultät
der
Rheinischen Friedrich-Wilhelms-Universität Bonn

vorgelegt von
Hannah Schäfer
aus
Freiburg im Breisgau

Bonn, 2025

Angefertigt mit Genehmigung der Mathematisch-Naturwissenschaftlichen Fakultät
der Rheinischen Friedrich-Wilhelms-Universität Bonn

Gutachter/Betreuer: PD Dr. Bastian Kubis
Gutachter: Prof. Dr. Christoph Hanhart
Tag der Promotion: 27.11.2025
Erscheinungsjahr: 2026

Abstract

The hadronic sector is a part of the Standard Model (SM) of particle physics that is not yet fully understood. Specifically, the energy dependence of the coupling of hadrons to photons, described by form factors, is an active field of research. We investigate two processes where form factors play a crucial role. In the first project, we calculate decay widths and branching ratios of rare semileptonic decays of the η and η' mesons into π^0/η and two leptons. These decays proceed via a two-photon intermediate state, which couples to the hadrons via transition form factors (TFFs). Different parameterisations of these TFFs are implemented and their effect on the results is discussed. Thus, we obtain a prediction for the SM contribution with some control over these systematic effects, which can be tested against future experimental results in order to investigate the possibility of beyond-the-SM (BSM) effects. In the second project, we construct a framework to dynamically generate doubly-virtual TFFs of the a_1 and a_2 mesons, for which not much experimental data exists, from a $\rho\pi$ intermediate state. For this, we describe the $\rho\pi \to \gamma^*\gamma^*$ system in a gauge-invariant way and, making use of unitarity, reconstruct it from left-hand cuts, taking care to remove kinematic singularities. We connect this system to the TFFs via the imaginary part of a loop diagram, reconstructing the real part dispersively; the convergence of said loop diagram limits our framework. These TFFs are relevant for a precise determination of the hadronic light-by-light contribution to the anomalous magnetic moment of the muon.

List of Publications

Chapter 2 of this thesis is published in the following article,

- H. Schäfer, M. Zanke, Y. Korte, and B. Kubis, *Semileptonic decays $\eta^{(\prime)} \to \pi^0\ell^+\ell^-$ and $\eta' \to \eta\ell^+\ell^-$ in the standard model*, Phys. Rev. D **108**, 074025 (2023) [arXiv:2307.10357 [hep-ph]].

Contents

Chapter 1

Introduction

I know it's hard to find
But somewhere along the line
It gets easier

Kalandra, *It Gets Easier* [1]

The hadronic sector is one of the most interesting, but also most challenging regimes of modern particle physics. In such an abstract field as particle physics, it is one of the more natural regimes to think about since nucleons in atomic nuclei and pions as the force-carriers between them seem relatively close to life. But if researchers have known about atomic nuclei since 1911 [2] and about nucleons since the 1930s [3–6], with pions as carriers of the nuclear force predicted in 1934 [7] and experimentally found in 1947 [8, 9], how is this still a field with open questions?

As simple as a problem with only a handful of involved particles may sound, the hadronic sector is still not fully understood. The reason is that although we know an underlying fundamental quantum field theory, Quantum Chromodynamics (QCD), it is not applicable for perturbative calculations due to the fact that its Landau pole, where the coupling constant diverges, lies right in the hadronic regime; the rich structure of states in this regime cannot be described on the level of quarks, which are confined into mesons and baryons. For hadronic calculations, QCD can only be used in lattice computations in a finite volume. In the last years, with increased computational power and improved algorithms, the field has produced competitive results. Alternatively, one can construct another perturbative theory with different degrees of freedom and a different parameter that converges and additionally utilise the most fundamental concepts of particle interactions, unitarity, analyticity, and symmetries.

Before going into details about the theoretical background for this work in the remainder of the introductory chapter, let us have a look at some open questions in the field. In particle physics in general, one wants to learn more about the most fundamental building blocks of nature, their dynamics, and how they play together such that we observe the Universe as we do. As we have already obtained more than a century worth of experimental results and have a theory, the Standard Model (SM) of particle physics, that describes most observations rather accurately, the quest is to learn what is beyond the SM and how to describe and integrate such phenomena as matter–antimatter asymmetry, neutrino oscillations, gravity, and Dark Matter.

Eventually, we want to find a suitable extension of the theory we are using so far, but in order to do so, we first need to identify more situations where it does not agree with observations. For this, experimentalists and theoreticians need to work closely together. There are different approaches: predicting and measuring at higher energies than before, either by building stronger accelerators for collider experiments or by detecting cosmic radiation; examples are the experiments at the LHC [10] and plans for possible future colliders at even higher energies [11].

Or one can focus on collecting more statistics and improving detectors and all other instrumentation,

including Monte-Carlo (MC) generators, in order to minimise systematic errors for a higher precision of results. On the theory side, this strategy includes taking into account higher-order effects. With this strategy, observables are predicted and measured in regimes that have already been researched in order to confirm or disprove conformity between experiment and theory at a higher precision. Examples include the anomalous magnetic moment of the muon, where it is still to be determined whether experiments [12–14] and SM prediction [15, 16] agree, and tests of discrete symmetries [17].

In order to understand and interpret results from experiments both at the high-energy and at the precision frontier and to compare them to existing theories, one needs a theoretical description of these processes as inclusive, accurate, and precise as possible. Since any quarks will be confined to hadrons at lower energies, for almost any given experiment, this requires a sufficient understanding of hadron dynamics, both for signal and for background processes.

From a theoretical point of view, the description of hadron dynamics is interesting as it is in general not clear what it the best way to approach a problem since there is not yet one theory that predicts all phenomena observed so far. Effective field theories are valid only in a specific energy regime; going beyond it, one needs to extend the theory or use a different one. A good example is Chiral Perturbation Theory (ChPT), which, for SU(2) symmetry, is only valid at the scale of pion masses or in situations where coupling to states with strangeness can be neglected, whereas it can describe the η meson and kaons when extended to SU(3). The η' meson, however, cannot be described in any of these, as its mass does not vanish in the chiral limit; one needs to extend the theory to large-N_c ChPT in order to obtain meaningful results. And while higher-spin resonances such as the vector mesons ρ, ω, and ϕ, axial-vector and tensor mesons can be introduced into ChPT as resonances [18–21], Resonance ChPT (RChPT) does not yield an appropriate dynamical description of said higher resonance states. S-matrix theory, on the other hand, is built from general principles, namely analyticity and unitarity of the scattering (S) matrix, which are associated with causality and probability conservation in physical amplitudes, complemented by crossing symmetry. These conditions should hold in all energy regimes; but as S-matrix theory needs input, *e.g.*, on scattering phases, its use is also limited to processes with enough experimental data or other constraints. Since all of these methods have their specific advantages and limitations, in practice, it is often useful to combine them. This allows also for a better understanding of nature, since each ansatz highlights different properties of a phenomenon.

One very important notion in hadron physics are *form factors* (FFs), which parameterise the coupling of hadrons to gauge bosons. The term comes from the notion of a FOURIER-transformed charge distribution of a particle that is not point-like, such that its elastic coupling to an electromagnetic current depends on this distribution. Generalising this term, one refers to many energy-dependent couplings of hadrons to gauge bosons as FFs, independent of the reference frame; if the process is inelastic, this is called a transition form factor (TFF). A FF parameterises any underlying dynamics of the coupling, which can be challenging to describe theoretically and to access experimentally. Having as accurate and precise a description as possible of FFs is imperative for any practical prediction at the precision frontier.

If a decay process is rare, there is typically a reason for it; often, a symmetry forbids it at tree level such that is is suppressed in terms of the perturbative expansion. In this case, it is necessary to calculate loop corrections. This is well-defined for photons running in the loop; one integrates over their virtualities, where it is important to take into account FFs depending on these virtualities. This is the case in the first project presented here, see Ch. 2, where we calculate the SM contribution to the decays $\eta \to \pi^0 \ell^+ \ell^-$ and $\eta' \to [\pi^0/\eta] \ell^+ \ell^-$, where $\ell^+ \ell^-$ are either electrons or muons. These decays are forbidden as tree-level processes with a one-photon exchange due to C and CP symmetry, but allowed via a two-photon exchange. Any BSM physics violating C and CP could potentially contribute at tree level, therefore, such contributions might be observable with future high-precision experiments.

Another example for the significance of form factors is the anomalous magnetic moment of the muon, which receives hadronic contributions via vacuum polarisation (HVP) and light-by-light scattering (HLbL), both being loop processes. Also in this case, we have to describe virtual photons coupling to mesons, and since both theory and experiment have proceeded to great precision, higher resonance states, including the axial-vector state a_1 and the tensor state a_2, have garnered interest. At the same

time, these states are experimentally hard to access and theoretically difficult to describe since they are slightly beyond the scale of the lightest mesons, the Goldstone bosons, and can at the same time not solely be understood as resonances in a system of two Goldstone bosons, as is the case for the ρ or the f_2 meson. Describing TFFs of the a_1 and a_2 is the goal of the second project in this thesis; see Ch. 3.

Before that, we give a brief introduction to the most important theoretical tools of the trade in the following sections, starting with quantum field theory and the SM in Sec. 1.1, followed by ChPT and its generalisations in Sec. 1.2, and dispersion theory in Sec. 1.3.

1.1 Quantum field theory and the Standard Model

One way to approach the calculation of an observable in particle physics is the perturbative method, and the framework for this is *quantum field theory* (QFT). The first QFT was developed in order to describe the interaction of electrons and photons and would eventually become Quantum Electrodynamics (QED), the beginnings lying in the 1920s [22].

A QFT consists of operators $\mathcal{O}$ acting on states $|\psi\rangle \in \mathcal{H}$ of a Hilbert space, a vector space over $\mathbb{R}$ or $\mathbb{C}$ with a scalar product, fulfilling conjugate symmetry $\langle\psi_2|\psi_1\rangle = \big(\langle\psi_1|\psi_2\rangle\big)^*$ and sesquilinearity, which is complete with regard to the metric induced by the scalar product. For a variable number of particles, one generalises $\mathcal{H}$ to a Fock space, the completion of the tensor product or exterior algebra of $\mathcal{H}$ for bosons or fermions, respectively. Symmetries are at the very basis of the construction of any QFT. First of all, the symmetries of relativistic space-time are encompassed in the Poincaré group $\mathbb{R}^{(1,3)} \rtimes O(1,3)$. The group action of the latter on the set of states $\{|\psi\rangle\}$ gives rise to orbits, subsets consisting of images of an element $|\psi\rangle$ under the group action. Physical observables are related to *matrix elements* $\langle\psi_2|\mathcal{O}|\psi_1\rangle$. Unitarity or antiunitarity of operators U ensures Poincaré invariance of matrix elements $\langle\psi_2|U^\dagger U|\psi_1\rangle = \langle\psi_2|\psi_1\rangle$ [23, 24].

Particles can be embedded into quantised fields that are irreducible unitary representations of the Poincaré group, *i.e.*, orbits under a Poincaré transformation, where irreducibility means that there is no subset transforming only amongst itself [25]. A field is here a mapping from a manifold, in this case the space-time, to the respective representation, and quantisation of a field means that it cannot take any value, but only discrete ones, which can be constructed with the help of creation and annihilation operators similar to the quantum mechanical harmonic oscillator. A given representation can be described by *quantum numbers* such as spin, intrinsic parity, charge, or behaviour under charge conjugation [26, 27]. The spin of a particle determines the number of degrees of freedom of the field as well as its statistics. Fermions, half-integer particles, obey the Fermi–Dirac statistics, where the Pauli exclusion principle holds, whereas bosons with integer spin behave according to the Bose–Einstein statistics.

Three discrete symmetries are of special interest, the combination of which has to be conserved by a large class of QFTs, namely parity P, charge parity C, and time reversal T. Parity and time reversal transform a space-time point as

$$(t,\vec{x}) \xrightarrow{\mathrm{P}} (t,-\vec{x}), \quad (t,\vec{x}) \xrightarrow{\mathrm{T}} (-t,\vec{x}), \tag{1.1}$$

whereas charge parity transforms particles into antiparticles and vice versa. A particle can be a positive or a negative eigenstate of P, which defines its intrinsic parity. This, together with spin, discriminates bosonic fields into (pseudo)scalars, (axial)vectors, and higher tensor fields. The CPT theorem states that the combination of time reversal, parity, and charge parity has to be conserved [28–32] if the QFT has suitably defined fields and operators, invariant under Poincaré transformations and fulfilling weak local commutativity as defined in Ref. [32]. However, P, C, and T do not need to be conserved separately, and indeed, the conservation of C and CP would be in contradiction with the observed asymmetry of matter and antimatter in the Universe [33].

In the Standard Model (SM) of particle physics, interactions between matter particles are mediated via gauge bosons. Matter particles, namely quarks and leptons, are fermions with spin 1/2. Three

generations of quarks and fermions exist: (u, d), (c, s), and (t, b) for the quarks and (e, ν_e), (μ, ν_μ), and (τ, ν_τ) for the leptons. For each matter particle, there exists an antimatter particle with equal mass and opposite charge. Each interaction can be associated with a gauge group, where the gauge boson emerges from the local gauge freedom.

The gauge group of the electromagnetic interaction is $\mathrm{U}(1)_{\mathrm{em}}$, and as it has one generator, there is one gauge boson, the photon, which has no rest mass and therefore two physical polarisations. Since it is embedded into a vector field, one needs to fix a gauge for any calculation [25], which is often done implicitly. If a photon is virtual, *i.e.*, not confined to its mass shell $p^2 = M^2 = 0$, the unphysical longitudinal polarisation is present and only the time-like polarisation is not propagated, but whenever the photon is measured, only the two transversal polarisations can contribute.[#1] All electrically charged particles take part in QED. $\mathrm{U}(1)_{\mathrm{em}}$ is an abelian group and therefore, the photon does not interact with itself at tree level; photons scatter on photons only via non-photon intermediate states. QED preserves all discrete symmetries and is the best-understood and -tested QFT.

All left-handed matter and right-handed antimatter particles take part in the weak interaction, whose force-carriers are the $W^\pm$ and Z bosons, which have masses of $M_{W^\pm} = 80.3692(133)\,\mathrm{GeV}$ and $M_Z = 91.1880(20)\,\mathrm{GeV}$, respectively [34]. The weak interaction and the electromagnetic interaction emerge via spontaneous symmetry breaking (SSB) from the electroweak interaction, whose gauge group is $\mathrm{SU}(2)_L \times \mathrm{U}(1)_Y$, as is stated in the GLASHOW–SALAM–WEINBERG theory [35–37]. This product of groups comes with $3 + 1$ massless generators $(W^0, W^1, W^2)_\mu$ and B_μ. After SSB, only the photon, a linear combination $A_\mu = \sin\theta_{\mathrm{W}} W^3_\mu + \cos\theta_{\mathrm{W}} B_\mu$ with the WEINBERG angle θ_{W}, stays massless, whereas $Z_\mu = \cos\theta_{\mathrm{W}} W^3_\mu - \sin\theta_{\mathrm{W}} B_\mu$ and $W^\pm_\mu = 1/\sqrt{2}\big(W^1_\mu \mp \mathrm{i} W^2_\mu\big)$ obtain a mass via the HIGGS mechanism [38, 39]. At energies significantly below these masses, the respective particles can be integrated out, which gives rise to the effective 4-FERMI theory [40] and its extension, the $V - A$ theory [41, 42], which was already known before electroweak theory, its UV completion.

As it couples only to left-handed particles and right-handed antiparticles, the weak interaction violates P and C symmetry; this was first experimentally shown by Wu [43]. If neutrinos are massless, as they are taken to be in the SM, this means that only left-handed neutrinos and right-handed antineutrinos can be observed; this is also what was found experimentally [44]. We know, however, from neutrino oscillations [45] that two out of the three neutrino generations must have a rest mass, as the oscillations come from a discrepancy between mass and flavour eigenstates, which can only occur if mass eigenstates are distinct. The transition between these different eigenstate bases is described by the PONTECORVO–MAKI–NAKAGAWA–SAKATA (PMNS) matrix [46, 47]. In the quark sector, the weak interaction is the only part of the SM that allows for flavour violation. The respective transition probabilities are collected in the CABIBBO–KOBAYASHI–MASKAWA (CKM) matrix [48, 49], which can be interpreted as the transition matrix between flavour eigenstates and weak eigenstates of the quarks, similar to the neutrino case.

The strong interaction is associated with the $\mathrm{SU}(3)_{\mathrm{colour}}$ gauge group, which gives rise to 8 massless gauge bosons, the gluons. A theory involving quarks was first proposed by NE'EMAN and GELL-MANN [50–52], and later, the additional gauge symmetry was discovered. Quarks are colour charged and therefore take part in the strong interaction; also the gluons themselves are colour charged, since the gauge group is non-abelian. Such a theory is referred to as a YANG–MILLS theory [53]. This difference to, *e.g.*, QED results in a different behaviour of the running coupling α_s compared to $\alpha_{\mathrm{QED}} \equiv \alpha$. The latter grows with increasing energy, such that QED becomes strongly coupled at high energies, culminating in the LANDAU pole of QED. For QCD, the LANDAU pole is located at low energies and the theory is strongly coupled there and weakly coupled at high energies. At low energies, quarks and gluons are confined to colour-neutral hadrons; with a large coupling constant, perturbative calculations are not possible. In the high-energy regime, where quarks are asymptotically free, calculations in the strong sector can be done with perturbative Quantum Chromodynamics (pQCD). However, measurements of particles in detectors happen at relatively low energies. Quarks and gluons hadronise

[#1] With some inconsistency, the three physical polarisations of a massive vector boson are often referred to as "transversal"; this includes then also the longitudinal polarisation, but excludes the time-like one. We will follow this inconsistency in this work.

into mesons and baryons and maybe states involving higher numbers of quarks or gluons, and any of these but the ones with the lowest masses decay before detection into the lightest hadrons and then via the electroweak interaction into leptons and photons. Any information about higher states in the hadronic spectrum is obtained via spectral analysis of detector data.

The weak interaction is the only part of the SM that violates the presented discrete symmetries, as the strong interaction conserves them, up to a possible extension via the θ term [54], which is constrained by neutron electric dipole moments [55–57].

At energies relevant for processes involving light hadrons, one can either do a direct numerical simulation on the basis of QCD in a discretised space-time and finite volume, which is done in Lattice QCD, or one can construct a new, effective QFT from the degrees of freedom that are relevant in this energy regime, making use of additional symmetries. This is done in ChPT and variants thereof, which we will discuss in the following section, Sec. 1.2. Alternatively or additionally, one can resort to the very basics of the theory, analyticity and unitarity, as is done in dispersion theory (DT); see Sec. 1.3.

1.2 Chiral Perturbation Theory and relatives

An effective field theory (EFT) is not the most fundamental theory possible; the idea is rather to work with the degrees of freedom relevant in the regime of interest and parameterise physics from other scales. We are specifically interested in physics of the strong interactions at energies up to and around 1 GeV, *i.e.*, in the hadronic regime, where pQCD is not applicable and hadrons are the relevant degrees of freedom.

The lightest hadrons are the pions, forming a triplet $\{\pi^+, \pi^0, \pi^-\}$, where $\pi^\pm$ have identical masses $M_{\pi^\pm} = 139.57039(17)\,\text{MeV}$ and π^0 is slightly lighter, $M_{\pi^0} = 134.9768(5)\,\text{MeV}$ [34]. This triplet together with the proton and the neutron in the baryonic sector gives a hint that there is a symmetry at play, which has different representations just as spin and is therefore called isospin [6]. In the quark model, it is interpreted as a symmetry between u and d quarks, and is associated with an SU(2) symmetry group. Its natural extension is flavour symmetry, which takes into account more quark flavours; in the regime of light hadrons, these are the three lightest quarks u, d, and s, and the associated symmetry group is SU(3).

Apart from isospin symmetry, one can observe a few other peculiarities about pions: why are they much lighter than all the other hadrons, the next ones being the kaons $K^{\pm,0}$ and the η around 500 MeV and after that the ρ and ω around 780 MeV, followed by a plethora of hadronic states?

Historically, current algebra was used to describe interactions of light hadrons. Various concepts, *e.g.*, vector-meson dominance (VMD), the notion that photons couple to hadrons dominantly via vector mesons, which can be understood through the matching quantum numbers [58, 59], and relations were found, such as consistency conditions, low-energy theorems, and sum rules [60–62]. Some processes are suppressed or forbidden due to a conspiracy of different quantum numbers; for this work, the Landau–Yang theorem is of special significance, which forbids the decay of spin-1 particles into two real photons [63, 64]. The systematic treatment of chiral symmetry enabled major progress in the field [65, 66].

The above observations about the lightest hadrons are used to construct the framework of Chiral Perturbation Theory (ChPT), an effective field theory with systematic power counting, which was done by Gasser and Leutwyler on the basis of the chiral symmetry that holds in QCD for vanishing light quark masses [67–73]. Initially, this was developed for SU(2) symmetry, *i.e.*, for two light quarks, and later extended to SU(3).

We will briefly review the main steps of the derivation for the SU(3) case, confining ourselves to mesons since baryons are not in the focus of this work and mostly following Refs. [74, 75], which are recommended for looking up any details left out here.[#2]

[#2] A pedagogical version of the first part of this summary was presented in a seminar at the International Conference of Physics Students in Tbilisi 2024 [76].

Starting from the QCD Lagrangian for light quarks,

$$\mathcal{L}_{\mathrm{QCD}} = \sum_{f\in\{u,d,s\}} \bar{q}_f \big(\mathrm{i}\not{D} - \mathtt{M}\big) q_f - \frac{1}{4} G_{\mu\nu,a} G^{\mu\nu,a}, \tag{1.2}$$

where $\not{D}$ is the covariant derivative, $\mathtt{M} = \mathrm{diag}\,(m_u, m_d, m_s)$ the quark mass matrix, and $G_{\mu\nu,a}$ the gluon field with colour index a, one can decompose the quark fields q into left- and right-handed components $q_{L/R}$ via projectors $P_{L/R} := (\mathbb{1} \mp \gamma^5)/2$. Since

$$\bar{q}\Gamma q = (\bar{q}_R + \bar{q}_L)\Gamma(q_L + q_R) = \begin{cases} \bar{q}_R\Gamma q_R + \bar{q}_L\Gamma q_L, & \Gamma \in \{\gamma^\mu, \gamma^\mu\gamma^5\}, \\ \bar{q}_R\Gamma q_L + \bar{q}_L\Gamma q_R, & \Gamma \in \{\mathbb{1}, \gamma^5, \mathrm{i}[\gamma^\mu, \gamma^\nu]/2\}, \end{cases} \tag{1.3}$$

the term with the covariant derivative decouples into $\bar{q}_L \not{D} q_L + \bar{q}_R \not{D} q_R$, while the mass term mixes the two components,

$$\bar{q}\mathtt{M}q = \bar{q}_R \mathtt{M} q_L + \bar{q}_L \mathtt{M}^\dagger q_R. \tag{1.4}$$

One can infer that $\mathcal{L}_{\mathrm{QCD}}$ would be invariant under separate unitary chiral transformations $U_{L/R} \in \mathrm{U}(3)_{L/R}$ if the mass term vanished. We refer to this hypothetical situation as the chiral limit; there, $\mathrm{U}(3)_L \times \mathrm{U}(3)_R$ is a global continuous symmetry of the Lagrangian. In reality, this symmetry is only approximate, and since the mass of the strange quark is significantly larger than the masses of u and d, ChPT with three flavours receives larger corrections than ChPT with only u and d. We can write an element of $\mathrm{U}(3)_{L/R}$ as

$$U_{L/R} = \exp\Big(-\mathrm{i}\sum_{a=1}^{8} \theta_a^{L/R} \frac{\lambda_a}{2}\Big) \exp\big(-\mathrm{i}\theta_0^{L/R}\big), \tag{1.5}$$

where λ_a are the GELL-MANN matrices and $\{\theta_0^{L/R}, \theta_a^{L/R}\}$ are 9 parameters. Accordingly, U(3) has 9 generators and the unitary decomposition Eq. (1.5) shows that the whole symmetry group can be decomposed into

$$\mathrm{U}(3)_L \times \mathrm{U}(3)_R \cong \mathrm{SU}(3)_L \times \mathrm{SU}(3)_R \times \mathrm{U}(1)_L \times \mathrm{U}(1)_R. \tag{1.6}$$

The NOETHER currents associated with the respective transformations of the fields $q \mapsto q + \theta_{0/a}^{R/L} \delta q$ can be calculated via $j^\mu = \partial\mathcal{L}/\big(\partial(\partial_\mu q)\big)\delta q$ to be

$$\begin{aligned} L_0^\mu &= \bar{q}_L \gamma^\mu q_L, & L_a^\mu &= \bar{q}_L \gamma^\mu \frac{\lambda_a}{2} q_L, \\ R_0^\mu &= \bar{q}_R \gamma^\mu q_R, & R_a^\mu &= \bar{q}_R \gamma^\mu \frac{\lambda_a}{2} q_R. \end{aligned} \tag{1.7}$$

Vector and axial-vector current are related to these left- and right-handed currents via

$$\begin{aligned} V &= L + R, & V_0^\mu &= \bar{q}\gamma^\mu q, & V_a^\mu &= \bar{q}\gamma^\mu \frac{\lambda_a}{2} q, \\ A &= L - R, & A_0^\mu &= \bar{q}\gamma^\mu\gamma^5 q, & A_a^\mu &= \bar{q}\gamma^\mu\gamma^5 \frac{\lambda_a}{2} q. \end{aligned} \tag{1.8}$$

According to NOETHER'S theorem [77], these currents are conserved if they correspond to continuous symmetries. An explicit calculation using the free DIRAC equation $\not{\partial} q = -\mathrm{i}\mathtt{M}q$ and $\bar{q}\overleftarrow{\not{\partial}} = \mathrm{i}\bar{q}\mathtt{M}$ yields

$$\begin{aligned} \partial_\mu V_0^\mu &= 0, & \partial_\mu V_a^\mu &= \mathrm{i}\bar{q}\big[\mathtt{M}, \frac{\lambda_a}{2}\big] q, \\ \partial_\mu A_0^\mu &= 2\mathrm{i}\bar{q}\gamma^5 \mathtt{M} q + \text{quantum corrections}, & \partial_\mu A_a^\mu &= \mathrm{i}\bar{q}\big\{\mathtt{M}, \frac{\lambda_a}{2}\big\} q. \end{aligned} \tag{1.9}$$

While V_0^μ is always conserved and V_a^μ and A_a^μ are conserved in the chiral limit, A_μ is conserved only on a classical level, but not in a quantum theory, where corrections enter from triangle diagrams. This fact is referred to as the axial or Adler–Bell–Jackiw anomaly [78, 79]. The conclusion is that the associated symmetry must also be broken, such that the symmetry group of $\mathcal{L}_{\text{QCD}}$ reduces to $\text{SU}(3)_L \times \text{SU}(3)_R \times \text{U}(1)_V$. An element $U_V \in \text{U}(1)_V$ transforms both left- and right-handed fields in the same way; this symmetry is associated with baryon number conservation. As a global symmetry, the baryon number B is not conserved due to anomalies in the electroweak sector, such that only $B - L$, the combination of baryon and lepton number, is conserved [80–82].

The axial symmetry breaking occurs on the level of the Lagrangian; for the vacuum, there is an additional subtlety at play. We can calculate the conserved charges associated with V_a^μ and A_a^μ as

$$Q_{V,a} = \int \mathrm{d}^3x\, V_a^0(\vec{x}, t), \qquad Q_{A,a} = \int \mathrm{d}^3x\, A_a^0(\vec{x}, t). \tag{1.10}$$

These conserved charges associated with the group generators can either annihilate the vacuum, then we say that the respective symmetries are realised in Wigner–Weyl mode; this mode would imply in the present case that every hadron has a parity partner since there are two copies of SU(3). Or a charge does not annihilate the vacuum, $Q|0\rangle \neq |0\rangle$, which is referred to as the Nambu–Goldstone mode [83–85]. Since parity doubling is not observed in the hadronic spectrum, the conclusion is that the Nambu–Goldstone mode must be realised for one set of symmetry generators. The Vafa–Witten theorem states that the global vector symmetry is unbroken [86], which implies that the axial-vector symmetry must be broken for the vacuum; this is referred to as SSB. According to the Goldstone theorem [87], for every broken generator a massless boson emerges as a consequence of SSB. The symmetry group of the vacuum is now reduced to $\text{SU}(3)_V \times \text{U}(1)_V$, whereas $\mathcal{L}_{\text{QCD}}$ is invariant under the larger group $\text{SU}(3)_L \times \text{SU}(3)_R \times \text{U}(1)_V$, and a set of 8 massless pseudoscalar Goldstone bosons has emerged.

Let $G = \text{SU}(3)_L \times \text{SU}(3)_R = \{(L, R) | L \in \text{SU}(3)_L, R \in \text{SU}(3)_R\}$ denote the symmetry group of $\mathcal{L}_{\text{QCD}}$. For building an effective Lagrangian, we need to establish building blocks with well-defined transformation properties under G and write down all possible invariant terms we can form with those, following Weinberg's principle that "if one writes down the most general possible Lagrangian, including *all* terms consistent with assumed symmetry principles, and then calculates matrix elements with this Lagrangian to any given order of perturbation theory, the result will simply be the most general possible S-matrix consistent with analyticity, perturbative unitarity, cluster decomposition and the assumed symmetry principle" [88].

Let $H = \{(V, V) | V \in \text{SU}(3)_V\} \leq G$ denote the subgroup that leaves the vacuum invariant and W the vector space of Goldstone boson fields $\Phi = (\phi_a)_{a=1}^8$. One can construct a mapping $\varphi : G \times W \to W$ that respects the group structure, which gives rise to an isomorphic mapping for the quotient group $G/H \times W \to W$. Implicitly, we introduced a space-time dependence for the fields and for the group elements, which is possible since the symmetry is actually local. This determines a group action and therewith the transformation properties of Φ under G, such that the Goldstone boson fields are logical degrees of freedom for the theory. One can write down a unitary matrix

$$U = \exp\left(\frac{\mathrm{i}}{F} \sum_{a=1}^{8} \phi_a \lambda_a\right) \tag{1.11}$$

collecting the Goldstone fields and transforming as $U \mapsto LUR^\dagger$, $U^\dagger \mapsto RU^\dagger L^\dagger$.

These symmetries hold for massless quarks, but for small quark masses, not everything is lost. One can reintroduce the quark mass matrix $\mathtt{M}$ as a spurious field transforming under G as $\mathtt{M} \mapsto L\mathtt{M}R^\dagger$. With this transformation property, the QCD mass term Eq. (1.4) is invariant. If we now use the same quark mass matrix in the effective Lagrangian, we ensure that the symmetry breaking due to finite quark masses happens in the same way as in QCD; in the effective theory, however, it has to be taken into account perturbatively. This yields a mass term for the previously massless Goldstone bosons; since we do not observe massless pseudoscalars, this fits experimental observations, and we can identify the

lightest pseudoscalar mesons, the pions $\pi^{\pm,0}$, the kaons $K^{\pm,0}, \bar{K}^0$, and the η, with the GOLDSTONE bosons. With the GELL-MANN matrices λ_a, the identification is

$$U = \exp\left(\frac{\mathrm{i}\lambda_a}{F}\phi_a\right) = \exp\left\{\frac{\sqrt{2}\mathrm{i}}{F}\begin{pmatrix} \frac{\pi^0}{\sqrt{2}} + \frac{\eta}{\sqrt{6}} & \pi^+ & K^+ \\ \pi^- & -\frac{\pi^0}{\sqrt{2}} + \frac{\eta}{\sqrt{6}} & K^0 \\ K^- & \bar{K}^0 & \frac{-2\eta}{\sqrt{6}} \end{pmatrix}\right\}, \tag{1.12}$$

where the charged physical pions relate to the ϕ_i via $\pi^\pm = (\phi_1 \pm \mathrm{i}\phi_2)/\sqrt{2}$.

The physical GOLDSTONE bosons form a flavour octet under G, and the pions, for which one can write down ChPT with SU(2), form an isospin triplet, being isovectors, whereas the kaons have $I = 1/2$ and the η is an isoscalar. Isospin is conserved under the strong interaction up to quark-mass corrections and for isovectors, one can define an additional quantum number, the so-called G-parity, as [89]

$$G = \mathrm{C}\exp(\mathrm{i}\pi I_2), \tag{1.13}$$

where I_2 is the second component of the isospin I. The charge-neutral ϕ_3 mixes in principle with the charge-neutral ϕ_8 from the flavour octet according to

$$\begin{pmatrix}\pi^0 \\ \eta\end{pmatrix} = \begin{pmatrix}\cos\theta_8 & -\sin\theta_8 \\ \sin\theta_8 & \cos\theta_8\end{pmatrix}\begin{pmatrix}\phi_3 \\ \phi_8\end{pmatrix}, \tag{1.14}$$

but since this is an isospin-breaking effect, $\theta_8 = 0$ as in Eq. (1.12) is an approximation sufficient for some applications.

We can take derivatives of U transforming as $\partial_\mu U \mapsto L\partial_\mu U R^\dagger$, $\partial_\mu U^\dagger \mapsto R\partial_\mu U^\dagger L^\dagger$ and build the ChPT Lagrangian order by order according to the number of derivatives corresponding to momenta p_μ as $\mathcal{L} = \mathcal{L}^{(0)} + \mathcal{L}^{(2)} + \mathcal{L}^{(4)} + \ldots$; a term of odd order in p_μ would not be LORENTZ invariant. This ordering scheme is particularly useful since ChPT is applied in the regime of low energies and momenta, such that terms $\sim p^{2n}$ are suppressed compared to terms $\sim p^{2n-2}$. $\mathcal{L}^{(0)}$ can only be proportional to $UU^\dagger = \mathbb{1}$, such that $\mathcal{L}^{(2)}$ is the leading term, given by

$$\mathcal{L}^{(2)} = \frac{F^2}{4}\langle\partial_\mu U\partial^\mu U^\dagger + 2B(\mathtt{M}U^\dagger + \mathtt{M}^\dagger U)\rangle, \tag{1.15}$$

where $\langle\ldots\rangle$ denotes the trace in flavour space. Note that U itself can be expanded, yielding coefficients in $1/F$. Relations between the masses of quarks and squared masses of GOLDSTONE bosons arise from expanding U to second order in the GOLDSTONE boson fields [67, 68, 90].

The constant F is not fixed from within ChPT, but can be determined by noting that the axial current is given by $A_a^\mu = -F\partial^\mu\phi_a + \mathcal{O}(\phi^3)$ and the matrix element accordingly yields

$$\langle 0|A_a^\mu|\phi_b(p)\rangle = \mathrm{i}p^\mu\delta_{ab}F. \tag{1.16}$$

Therefore, we can identify F with the pion decay constant F_π, which is measured in weak decays, mostly $\pi^+ \to \mu^+\nu_\mu$. Similarly, all low-energy constants (LECs) in ChPT have to be determined either from experiment or from other theoretical input.

Local symmetry parameters are related to gauge symmetries, and hence, there are chiral WARD identities, which can be seen via invariance under variation of external fields S, P, V^μ, and A^μ. In the QCD Lagrangian, these external fields can be included via [18, 75]

$$\mathcal{L}_{\mathrm{QCD}}^{\mathrm{ext}} = \bar{q}\gamma_\mu\left(V^\mu + \gamma^5 A^\mu\right)q - \bar{q}(S - \mathrm{i}\gamma^5 P)q. \tag{1.17}$$

In order to keep these chiral WARD identities intact for the effective Lagrangian, one has to include the external fields into $\mathcal{L}_{\mathrm{ChPT}}$ in such a way that the chiral transformation properties are the same [69]. For V^μ and A^μ, this is done via promoting the derivative ∂_μ to a covariant derivative D_μ

$$D_\mu U = \partial_\mu U - \mathrm{i}[V_\mu, U] - \mathrm{i}\{A_\mu, U\}. \tag{1.18}$$

S and P are included via terms

$$2B\left[(S+\mathrm{i}P)U^\dagger + (S+\mathrm{i}P)^\dagger U\right]. \tag{1.19}$$

The external currents can be identified with physical currents of matching quantum number. The mass matrix, *e.g.*, can be included as part of S, and the electromagnetic current as part of V_μ, which generates the coupling of Goldstone bosons to real photons via

$$D_\mu = \partial_\mu + \mathrm{i}eA^\gamma_\mu[Q,U], \tag{1.20}$$

where $Q = \mathrm{diag}\,(2/3,-1/3,-1/3)$ is the matrix of quark charges and against all convention, we denote the photon field by A^γ_μ in order to avoid confusion with the axial-vector current A_μ. Coupling to virtual photons receives corrections dependent the virtualities, which can be calculated including loop diagrams and higher-order LECs, which also capture the effects from higher resonances.

The terms discussed so far do not produce any term like $\pi^0 \to \gamma\gamma$ with an odd number of Goldstone bosons. Such a term must be of odd intrinsic parity and therefore contain the Levi-Civita tensor; since QCD admits odd intrinsic parity, ChPT should do so, as well. One can derive suitable Lagrangian terms from an action first written down by Wess and Zumino [91, 92], which yields terms at almost all orders in the chiral expansion, the lowest-order one being

$$\mathcal{L}_{\mathrm{WZW}} \ni -\frac{e^2}{32\pi^2 F}\pi^0 \epsilon^{\mu\nu\alpha\beta} F_{\mu\nu}F_{\alpha\beta}, \tag{1.21}$$

where $F_{\mu\nu}$ denotes the electromagnetic field strength tensor, which enters via integration by parts in the action with external fields. From the Lagrangian term in Eq. (1.21), the decay width of $\pi^0 \to \gamma\gamma$ can be calculated, which is associated with the axial anomaly. Witten found that the number of colours N_c shows up in the WZW action; it was argued in Refs. [82, 93, 94], however, that N_c cannot be obtained from $\Gamma_{\pi^0\gamma\gamma}$ due to subtle cancellation effects related to the violation of baryon number and the quark charges depending on N_c, which gives rise to the Goldstone–Wilczek term [95].

The term in Eq. (1.21) is already part of the next order of the Lagrangian $\mathcal{L}^{(4)}$, which consists of terms built from the same building blocks as $\mathcal{L}^{(2)}$. With increasing order, the number of possible terms rises, and each term comes with an LEC, which needs to be determined from external input. When calculating a process in ChPT to $\mathcal{O}(p^4)$, one has to take into account both the new terms from $\mathcal{L}^{(4)}$ and loops from $\mathcal{L}^{(2)}$. Since this pattern continues at every order, ChPT is a non-renormalisable theory, meaning that there are infinitely many loops that need to be renormalised. At the same time, there are infinitely many coupling constants, the LECs, which can be used to renormalise the theory order by order, *i.e.*, at a given order $2n$, one can renormalise all loops coming from Lagrangian terms up to and including $\mathcal{O}(p^{2n-2})$ using the LECs at $\mathcal{O}(p^{2n})$, which act as counter-terms. It is important to note that the LECs can upset the ordering scheme of ChPT if they are not all of the same order of magnitude, levering out the suppression due to powers of momenta. Therefore, if one actually wants to know how important higher-order corrections are, one has to do the calculation at the next order, for which one needs information about the corresponding LECs.

ChPT includes so far 8 Goldstone bosons identified with the lightest mesons; but experimentally, there is also the η' with the same quantum numbers as the η and a higher mass $M_{\eta'} = 957.78(6)\,\mathrm{MeV}$ [34], which looks suspiciously similar. One can include it into ChPT via an additional symmetry, under which the axial current A^μ_0 is conserved. The idea is to order terms according to their power of $1/N_c$, which is then combined with the ChPT counting scheme; it is therefore called large-N_c ChPT [96–98]. Since $1/N_c = 1/3$, the resulting perturbation theory has rather large corrections, but it allows to understand the presence and the properties of the η' as an additional Goldstone boson arising from the now spontaneously broken $U(1)_A$ symmetry. This symmetry has one generator and the emerging Goldstone boson is a singlet state. It can be included into the ChPT Lagrangian by adding a term $\phi_0\lambda_0$ to the sum $\sum_a \phi_a\lambda_a$ in U with $\lambda_0 = \mathbb{1}_3/\sqrt{3}$. This singlet state η_1 mixes with the

octet state η_8 to yield the physical states η and η' via

$$\begin{pmatrix}\eta'\\ \eta\end{pmatrix} = \begin{pmatrix}\cos\theta_1 & \sin\theta_1\\ -\sin\theta_1 & \cos\theta_1\end{pmatrix}\begin{pmatrix}\eta_1\\ \eta_8\end{pmatrix}. \tag{1.22}$$

Assuming ideal mixing, *i.e.*, $\theta_1 = \arcsin(-1/3)$, the unitary matrix can be extended to

$$\exp\left\{\frac{\mathrm{i}}{F}\left(\sum_{a=1}^{8}\phi_a\lambda_a + \frac{1}{\sqrt{3}}\eta_0\mathbb{1}_3\right)\right\} = \exp\left\{\frac{\sqrt{2}\mathrm{i}}{F}\begin{pmatrix}\frac{\pi^0}{\sqrt{2}} + \frac{\sqrt{2}\eta+\eta'}{\sqrt{6}} & \pi^+ & K^+\\ \pi^- & -\frac{\pi^0}{\sqrt{2}} + \frac{\sqrt{2}\eta+\eta'}{\sqrt{6}} & K^0\\ K^- & \bar{K}^0 & \frac{-\sqrt{2}\eta+2\eta'}{\sqrt{6}}\end{pmatrix}\right\}. \tag{1.23}$$

Large-N_c ChPT also provides a framework to include resonances of higher mass and spin, in principle similar to the source terms in Eq. (1.18). One can define suitable building blocks transforming under G similarly to their equivalents in a QCD Lagrangian with external currents. Writing down again all possible terms at a given order and systematically expanding yields all relevant terms at that order compatible with the respective symmetries [18–21, 99]. Such a Lagrangian describes how the dynamical degrees of freedom of ChPT, the pseudo-GOLDSTONE bosons, couple to higher resonances, but the latter are not dynamical fields in this theory in the sense that their dynamical behaviour cannot be described appropriately in this way. One can include mass and kinetic terms by choosing a representation that allows for propagation of the relevant degrees of freedom of the field. For a vector or axial-vector field, three degrees of freedom need to be propagated, which can be realised either in a vector representation V^μ/A^μ where the field strength tensor is written as $V^{\mu\nu} = \partial^\mu V^\nu - \partial^\nu V^\mu$ and similar for $A^{\mu\nu}$, or in an antisymmetric tensor representation $\tilde{V}^{\mu\nu}/\tilde{A}^{\mu\nu}$, where the additional degrees of freedom are removed by suitable conditions [18, 19, 100]. It was demonstrated that the two representations are equivalent, and also that the power counting for these (axial-) vector field terms is ambiguous. Such a representation allows to propagate a resonance field assuming it is stable. One intrinsic difficulty with these resonance states is that they are only well-defined as autonomous fields in a narrow-width or -resonance approximation (NWA), where they have to be on their mass shell; but at the same time, they are typically so short-lived that they have a non-negligible width compared to their mass, which should be taken into account in a hadronic calculation. One can include a finite width in the propagator of a resonance field; the easiest way to do so is via a BREIT–WIGNER function, which, however, breaks unitarity; see Sec. 1.3.

One would like to match LECs and masses of the resonances to QCD in the same limit of $N_c \to \infty$ at the level of correlators [21]. In practice, one does not know QCD in this limit and can only work on the basis of assumptions, especially a truncation of the hadronic spectrum after the lowest states. It is, however, possible to match large-N_c ChPT to ChPT in order to learn how resonances relate to LECs in ChPT, *e.g.*, whether a LEC in ChPT, which is related to loops at lower orders in the expansion, is saturated by resonances [101, 102]. Since vector (and axial-vector) mesons play a dominant role in this whenever quantum numbers allow it, this makes a connection to the empirical concept of VMD [18]. Large-N_c ChPT is built to produce all (strong) physics at tree level; instead of hadronic loops, higher resonances are introduced. This in combination with the truncations necessarily constrains the applicability of the theory. One can to some extent match hadronic processes at higher energies to pQCD by including effective poles as replacements for the states neglected by the truncation, via sum rules, and making use of an operator-product expansion (OPE) [103–111] and constrain the asymptotic behaviour from a light-cone expansion [112–115].

It is also possible to write down chiral theories for heavy mesons and baryons by introducing an additional expansion parameter $1/M_H^2$ into the series, the heavy mass scale [116–121]. One can utilise additional symmetries such as heavy-spin symmetry, relating heavy spin-0 and spin-1 states, and heavy-flavour symmetry, relating hadrons with b and c quark content.

1.3 Analytic S-matrix and dispersion theory

Another approach to understand the hadronic sector is dispersion theory, which has its roots in S-matrix theory. Originating in the 1960s before the development of QCD [122–124], S-matrix theory provides a non-perturbative approach to hadronic processes. It builds entirely on the idea that a physical scattering process should respect causality and conserve probability. The first constraint translates mathematically to analyticity, the second one to unitarity of the respective amplitude. The additional idea of crossing symmetry relates processes with the same particles involved, but different initial and final states, to one another, and together with analyticity fosters the idea of an S-matrix that is defined on the whole complex plane. Unitarity implies bounds on the asymptotic behaviour of $\mathcal{M}$ [125], originating from the *optical theorem* [126, 127]. It is easier to understand the connection between causality and analyticity on a classical or non-relativistic level [128], but we will focus here on the consequences for relativistic processes and refer the reader to more detailed literature on the subject [128–131].

Any scattering process with initial state $|i\rangle$ and final state $|f\rangle$ can be described as

$$\langle f|S|i\rangle. \tag{1.24}$$

The term *scattering process* refers typically to a $2 \to 2$ process, and we can discuss $1 \to 2$ and $1 \to 3$ processes as special cases. It does not make sense to discuss processes with more than two incoming particles due to the principle of *cluster decomposition* [132], the notion that interactions between particles are approximately local and particles before and after the interaction behave asymptotically as non-interacting. Processes with more outgoing particles, on the other hand, become increasingly complicated, and one has to hope that they factorise [133]. The canonical labelling for $2 \to 2$ scattering is $A(p_1) + B(p_2) \to C(q_1) + D(q_2)$, which gives rise to the definition of the Mandelstam variables

$$s = (p_1 + p_2)^2 = (q_1 + q_2)^2, \quad t = (p_1 - q_1)^2 = (p_2 - q_2)^2, \quad u = (p_1 - q_2)^2 = (p_2 - q_1)^2. \tag{1.25}$$

The relation

$$s + t + u = m_A^2 + m_B^2 + m_C^2 + m_D^2 \tag{1.26}$$

follows from energy-momentum conservation. *Crossing symmetry* relates the scattering process $A + B \to C + D$ to the decay process $A \to \bar{B} + C + D$ with $p_2 \mapsto -p_2$. The S-matrix maps the Hilbert space $\mathcal{H}$ onto itself, $S : \mathcal{H} \to \mathcal{H}$, and its symmetry properties are captured by the fact that it commutes with the respective symmetry operators. Per its Poincaré invariance, S is unitary, $SS^\dagger = \mathbb{1}$, and can only depend on Lorentz-invariant quantities, typically s, t, and u.

Observable quantities are related to (differential or integrated) cross sections $(\mathrm{d})\sigma$ that are proportional to the differential probability $\mathrm{d}P$ of scattering from this particular initial into this particular final state. The differential probability relates to the scattering matrix via

$$\mathrm{d}P = \frac{|\langle f|S|i\rangle|^2}{\langle f|f\rangle\langle i|i\rangle}\mathrm{d}\Pi, \tag{1.27}$$

where $\mathrm{d}\Pi$ is the differential phase space. The S-matrix can be separated into a non-interactive part, which is simply the identity matrix, and an interaction part denoted by the *transfer matrix* $\mathcal{T}$,

$$S = \mathbb{1} + \mathrm{i}\mathcal{T}. \tag{1.28}$$

Energy and momentum conservation are manifest when $\mathcal{T}$ is written as

$$\langle f|\mathcal{T}|i\rangle = (2\pi)^4\delta^{(4)}(\Sigma p_i - \Sigma p_f)\mathcal{M}, \tag{1.29}$$

where $\mathcal{M}$ is called the *matrix element*.

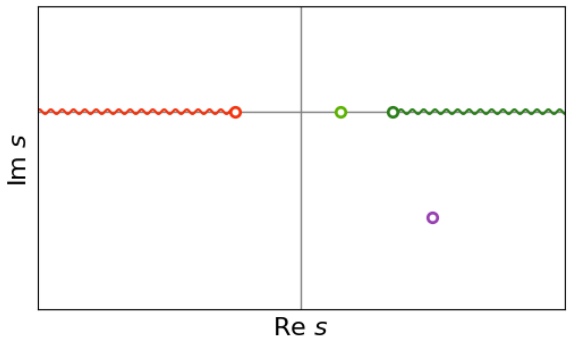

Figure 1.1: Poles and branch cuts with branch points in the complex plane. The light green circle on the real line denotes a bound state, the purple circle a resonance, the dark green wiggly line a right-hand cut, and the orange line a left-hand cut. The resonance lies on a non-physical sheet, separated from the physical sheet by a branch cut.

Due to causality, S can be analytically continued in the whole complex plane and is complex differentiable with the exception of poles and branch cuts, *i.e.*, it is a meromorphic function; see Fig. 1.1. Branch cuts emerge from complex square root and logarithm functions, which are multi-valued, *i.e.*, their domain extends to more than one RIEMANN sheet. Different RIEMANN sheets are connected smoothly with the exception of the branch point where the branch cut opens. As an example, consider the different branches of a square root and a logarithm in Fig. 1.2: the square root has two RIEMANN sheets, which are smoothly connected across the branch cut, which is situated at $(-\infty, 0]$, *i.e.*, it is a left-hand cut (LHC). A right-hand cut (RHC) emerges from $\sqrt{-z}$. If one starts at some point in $\mathbb{C}\backslash 0$ and circumnavigates the origin twice, one arrives at the same point. The logarithm, on the other hand, has infinitely many RIEMANN sheets; if one starts at some point in $\mathbb{C}\backslash 0$ and circumnavigates the origin in one direction, one will never return to the original point, but for every round, the imaginary part increases by 2π. Therefore, it is important to define on which RIEMANN sheet these functions are to be evaluated in a calculation. Measurements of any physical observable always happen for real values of the MANDELSTAM variables s, t, and u, the input variable of the S-matrix. The input variables are also restricted by energy and momentum conservation. The RIEMANN sheet that is smoothly connected to the upper part of the branch cut is called the *physical sheet*, all other sheets are called *unphysical*.

We recapitulate some central results from complex analysis and point out their significance for the context of this work, refraining from stating the most general versions of the theorems and from reproducing any proofs, which can be found in the abundant literature on the subject.

Analyticity, *i.e.*, the fact that one can expand f on a disc around z_0 in a convergent power series

$$f(z) = \sum_{n=0}^{\infty} c_n (z - z_0)^n \tag{1.30}$$

with a positive radius of convergence, is equivalent with the function being holomorphic in z_0. This is a powerful constraint since complex differentiability of a function $f : \mathbb{C} \to \mathbb{C}, z = x + \mathrm{i}y \mapsto f(z) = u(x, y) + \mathrm{i}v(x, y)$ is a significantly stronger property than real differentiability. It implies that the CAUCHY–RIEMANN differential equations hold,

$$\frac{\partial u}{\partial x} = \frac{\partial v}{\partial y}, \qquad \frac{\partial u}{\partial y} = -\frac{\partial v}{\partial x}. \tag{1.31}$$

With this and STOKE's theorem, one can prove CAUCHY's theorem, which states that if a function $f(z)$ is holomorphic on a simply connected open set U, then its contour integral along any closed curve $C \in U$ vanishes,

$$\int_C \mathrm{d}z f(z) = 0. \tag{1.32}$$

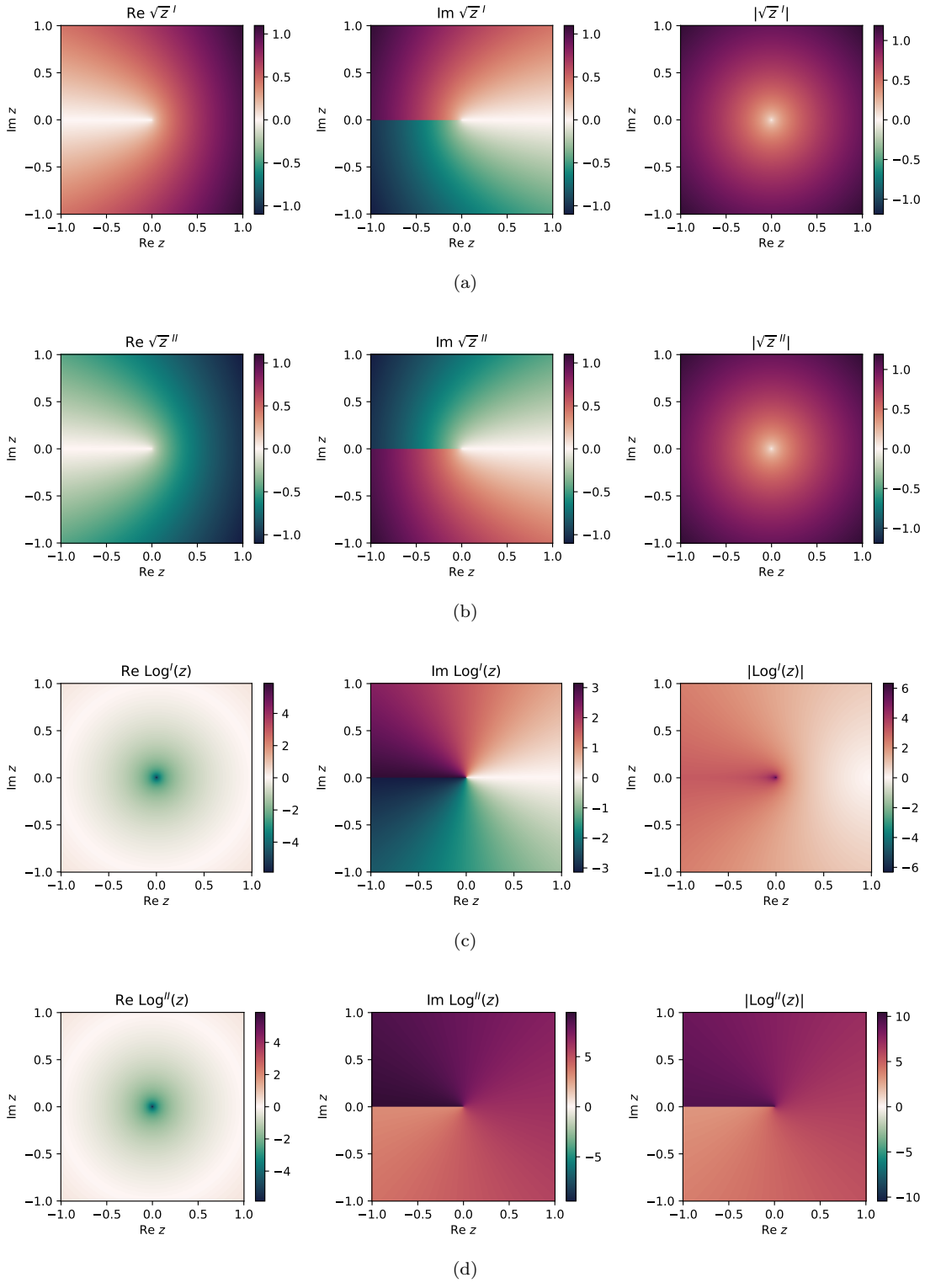

Figure 1.2: Examples for branch cuts: the functions $\sqrt{s}$ on the first (a) and second (b) sheet, and $\log(s)$ on the first (c) and second (d) sheet in the complex s-plane, where branch cuts open in the imaginary part at the branch point $s_{\mathrm{thr}} = 0$. For each function, the first diagram depicts the real part, the second one the imaginary part, and the third one the absolute.

From this, CAUCHY's integral formula follows,

$$f(z) = \frac{1}{2\pi \mathrm{i}} \int_C \mathrm{d}\zeta \, \frac{f(\zeta)}{\zeta - z}, \tag{1.33}$$

where $C \subset U$ is the counterclockwise oriented boundary of a disc $D = \{z \in \mathbb{C} : |z - z_0| \leq r\} \subset U$ for some radius $r > 0$ and centre $z_0 \in U$ with $z \in D$, and $f(z)$ is holomorphic on the open simply-connected set $U \subseteq \mathbb{C}$. This is the fundamental case of a simple pole; the residue theorem deals with the more general situation of finitely many singularities at positions $z_i \in U, i \in N$ with residues $\mathrm{Res}\,(f, z_i)$ and a closed rectifiable curve $C \subset U \backslash \{z_i, i \in N\}$. One needs to track how many times C winds around each singularity z_i counterclockwise and denotes the number by $\mathrm{I}(C, z_i)$. $f(z)$ is taken to be holomorphic on $U \backslash \{z_i, i \in N\}$ or meromorphic on U, which is still a simply-connected open subset of C. Then the contour integral along C is given by

$$\int_C \mathrm{d}z \, f(z) = 2\pi \mathrm{i} \sum_{i=1}^{N} \mathrm{I}(C, z_i) \mathrm{Res}\,(f, z_i). \tag{1.34}$$

The identity theorem states that any two functions analytic on an open and connected domain $D \subseteq \mathbb{C}$ which agree on a subset $A \subseteq D$ with an accumulation point in D agree on D. This implies that if a function is known on a suitable subset of $\mathbb{C}$, *e.g.*, an open subset of the real line, its analytic continuation to the whole complex plane is unique. Actually, it is not even necessary to know the full function, it is enough to know its *discontinuity* $\mathrm{disc} f$: as mentioned earlier, complex square roots and logarithms give rise to branch cuts, and a discontinuity is defined as the difference between values of the function on either side of the branch cut,

$$\mathrm{disc} f(z) := f(z + \mathrm{i}\epsilon) - f(z - \mathrm{i}\epsilon), \tag{1.35}$$

compare Fig. 1.2. If $f(z)$ is holomorphic outside of a right-hand branch cut, it can be reconstructed at any point z via CAUCHY's theorem by deforming the integration path C,

$$\begin{aligned} f(z) &= \frac{1}{2\pi \mathrm{i}} \int_C \mathrm{d}\zeta \, \frac{f(\zeta)}{\zeta - z} = \frac{1}{2\pi \mathrm{i}} \int_{C_1} \mathrm{d}\zeta \, \frac{f(\zeta)}{\zeta - z} + \frac{1}{2\pi \mathrm{i}} \int_{C_2} \mathrm{d}\zeta \, \frac{f(\zeta)}{\zeta - z} \\ &= \frac{1}{2\pi \mathrm{i}} \int_{z_{\mathrm{thr}}}^{\infty} \mathrm{d}\zeta \, \frac{f(\zeta + \mathrm{i}\epsilon) - f(\zeta - \mathrm{i}\epsilon)}{\zeta - z} = \frac{1}{2\pi \mathrm{i}} \int_{z_{\mathrm{thr}}}^{\infty} \mathrm{d}\zeta \, \frac{\mathrm{disc} f(\zeta)}{\zeta - z}, \end{aligned} \tag{1.36}$$

where C_1 is the arc from $R + \mathrm{i}\epsilon$ to $R - \mathrm{i}\epsilon$ as depicted in (a) in Fig. 1.3 and C_2 is the path from $R - \mathrm{i}\epsilon$ to the branch point $z_{\mathrm{thr}} - \mathrm{i}\epsilon$, around z_{thr} to $z_{\mathrm{thr}} + \mathrm{i}\epsilon$ without crossing the branch cut, and from $z_{\mathrm{thr}} + \mathrm{i}\epsilon$ to $R + \mathrm{i}\epsilon$. If $f(z)$ falls fast enough, *i.e.*, faster than $1/z$, the integral along C_1 vanishes in the limit $R \to \infty$; the small arc around z_{thr} in C_2 vanishes for $\epsilon \to 0$, such that we are left with an integral along either side the branch cut, which can be written as an integral from the branch point to ∞ over $\mathrm{disc} f(\zeta)/(\zeta - z)$. If $f(z)$ does not decrease fast enough, one needs to artificially force it to do so and introduce a subtraction, *i.e.*, for $z_0 < z_{\mathrm{thr}}$, where $f(z)$ is holomorphic, write

$$\begin{aligned} g(z) &= \frac{f(z) - f(z_0)}{z - z_0} = \frac{1}{2\pi \mathrm{i}} \int_{z_{\mathrm{thr}}}^{\infty} \mathrm{d}\zeta \, \frac{\mathrm{disc}\, g(\zeta)}{(\zeta - z)} = \frac{1}{2\pi \mathrm{i}} \int_{z_{\mathrm{thr}}}^{\infty} \mathrm{d}\zeta \, \frac{\mathrm{disc} f(\zeta)}{(\zeta - z_0)(\zeta - z)} \\ \Rightarrow f(z) &= f(z_0) + \frac{z - z_0}{2\pi \mathrm{i}} \int_{z_{\mathrm{thr}}}^{\infty} \mathrm{d}\zeta \, \frac{\mathrm{disc} f(\zeta)}{(\zeta - z_0)(\zeta - z)}. \end{aligned} \tag{1.37}$$

This procedure can be repeated until the integrand decreases sufficiently fast for large arguments. For each such subtraction, one obtains a subtraction constant $f(z_0)$ that needs to be fixed by additional input, *e.g.*, an experimental value for the amplitude at z_0 or a theory constraint.

If there is, additionally to a RHC, also a LHC involved, and maybe also poles corresponding to one-particle intermediate states, one has to integrate around those in a similar manner, see (b) in Fig. 1.3; for isolated poles, one just picks up the residue.

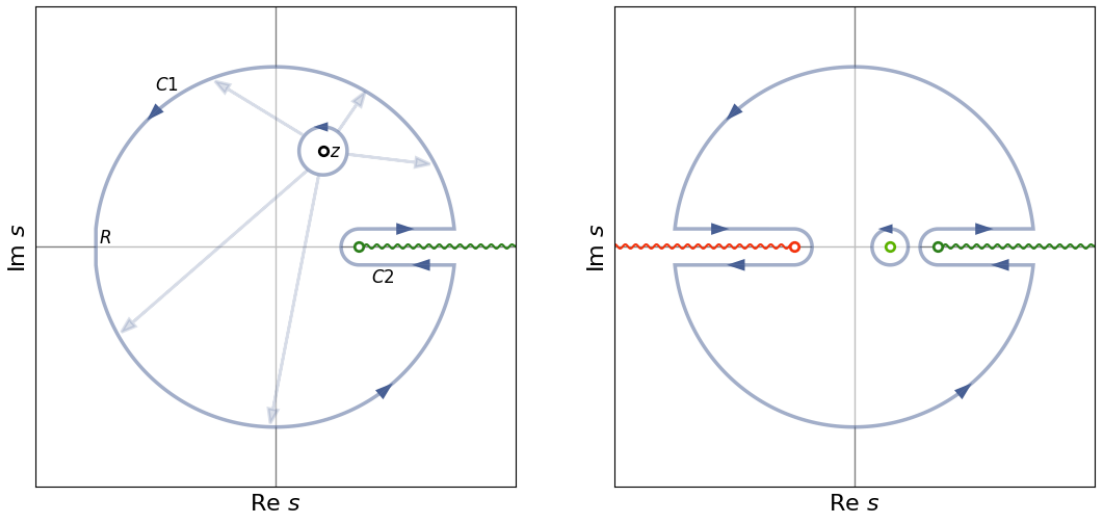

(a) (b)

Figure 1.3: Deformation of the integration path around z to a radius R, avoiding a RHC (a), or around a RHC, a LHC, and a pole on the real axis (b).

If $f(z)$ fulfils the Schwarz reflection principle, $f(z^*) = \big(f(z)\big)^*$, which holds if $f(z)$ is holomorphic on an open subset U of the upper (or lower) half plane and only takes real values on the real line, then the discontinuity can be written as

$$\mathrm{disc} f(z) = f(z + \mathrm{i}\epsilon) - \big(f(z + \mathrm{i}\epsilon)\big)^* = 2\mathrm{i}\,\mathrm{Im}\, f(z), \tag{1.38}$$

and the integral in Eq. (1.36) becomes

$$f(z) = \frac{1}{\pi} \int_{z_{\mathrm{thr}}}^{\infty} \mathrm{d}\zeta\, \frac{\mathrm{Im}\, f(\zeta)}{\zeta - z}. \tag{1.39}$$

Expressing $f(z) = \mathrm{Re}\, f(z) + \mathrm{i}\,\mathrm{Im}\, f(z)$, we can obtain the real and imaginary part of the integral via the Sokhotski–Plemelj theorem [134], which implies for integrations along the real line

$$\lim_{\epsilon \to 0} \int_a^b \frac{\mathrm{d}x}{x \pm \mathrm{i}\epsilon} = \fint \frac{\mathrm{d}x}{x} \mp \mathrm{i}\pi, \tag{1.40}$$

where $\fint$ denotes the Cauchy principal value integral. With this,

$$f(z) = \frac{1}{\pi} \fint_{z_{\mathrm{thr}}}^{\infty} \mathrm{d}\zeta\, \frac{\mathrm{Im}\, f(\zeta)}{\zeta - z} + \mathrm{i}\,\mathrm{Im}\, f(z), \qquad \mathrm{Re}\, f(z) = \frac{1}{\pi} \fint_{z_{\mathrm{thr}}}^{\infty} \mathrm{d}\zeta\, \frac{\mathrm{Im}\, f(\zeta)}{\zeta - z} \tag{1.41}$$

for the non-subtracted version; from the sign of $\mathrm{i}\epsilon$, we see that we need to approach the real line from below with the integrand. An integral as in Eq. (1.39) is called a *dispersion integral*; the name goes back to the Kramers–Kronig relations between absorption and refraction of light in a medium [126, 135]. When implementing a dispersion integral in practice, it is sometimes preferable to write

$$f(z) = f(z_0) + \frac{z - z_0}{\pi} \int_{z_{\mathrm{thr}}}^{\infty} \mathrm{d}\zeta\, \frac{\mathrm{Im}\,\big[f(\zeta) - f(z)\big]}{(\zeta - z_0)(\zeta - z)} + \frac{(z - z_0)\mathrm{Im}\, f(z)}{\pi} \int_{z_{\mathrm{thr}}}^{\infty} \mathrm{d}\zeta \frac{1}{(\zeta - z_0)(\zeta - z)}, \tag{1.42}$$

where the integrand in the first integral is non-singular at $\zeta = z$ and the latter integral can be solved analytically to be

$$\begin{aligned}
&\int_{z_{\rm thr}}^{\infty} \mathrm{d}\zeta \frac{1}{(\zeta - z_0)(\zeta - z)} = \frac{1}{z - z_0} \log\left(\frac{z_{\rm thr} - z_0}{z_{\rm thr} - z}\right) \\
=&\frac{1}{z - z_0}\left[\log\left(\left|\frac{z_{\rm thr} - z_0}{z_{\rm thr} - z}\right|\right) + \mathrm{i}\arg\left(\frac{z_{\rm thr} - z_0}{z_{\rm thr} - z}\right)\right] = \frac{1}{z - z_0}\left[\log\left(\left|\frac{z_{\rm thr} - z_0}{z_{\rm thr} - z}\right|\right) + \mathrm{i}\pi\theta(z - z_{\rm thr})\right]. \quad (1.43)
\end{aligned}$$

Here, we need either a subtracted dispersion integral as above or an integrand that falls faster than $1/z^2$ and therefore can be written as $z \cdot f(z)/z$, otherwise, the second integral will diverge.

The imaginary part of a process $\langle f|i\rangle$ is connected to the amplitudes $\langle f|n\rangle$ and $\langle i|n\rangle$ for any possible intermediate state $|n\rangle$ via a generalisation of the optical theorem [126, 127], which is a consequence of unitarity,

$$\begin{aligned}
&\mathbb{1} = S^\dagger S = (\mathbb{1} - \mathrm{i}\mathcal{T}^\dagger)(\mathbb{1} + \mathrm{i}\mathcal{T}) = \mathbb{1} - \mathrm{i}(\mathcal{T}^\dagger - \mathcal{T}) + \mathcal{T}^\dagger\mathcal{T} \\
&\Rightarrow \mathrm{i}(\mathcal{T}^\dagger - \mathcal{T}) = \mathcal{T}^\dagger\mathcal{T} \\
&\Rightarrow \mathrm{i}\langle f|(\mathcal{T}^\dagger - \mathcal{T})|i\rangle = \mathrm{i}\,(2\pi)^4\delta^{(4)}(\Sigma p_i - \Sigma p_f)\left[\mathcal{M}^*(f \to i) - \mathcal{M}(i \to f)\right] \\
&\quad = \langle f|\mathcal{T}^\dagger\mathcal{T}|i\rangle = \sum_n \frac{1}{S_n}\int\left(\prod_{j=1}^{N_n}\widetilde{\mathrm{d}k_j}\right)\langle f|T^\dagger|n\rangle\,\langle n|T|i\rangle \\
&\quad = \sum_n \frac{1}{S_n}\int\left(\prod_{i=1}^{N_n}\widetilde{\mathrm{d}k_j}\right)(2\pi)^4\delta^{(4)}(\Sigma p_f - \Sigma k_j)\mathcal{M}^*(f \to n)\,(2\pi)^4\delta^{(4)}(\Sigma p_i - \Sigma k_j)\mathcal{M}(i \to n). \quad (1.44)
\end{aligned}$$

Here, S_n is the symmetry factor of an intermediate state n, $\{k_j\}_{j=1}^{N_n}$ are its momenta, and the (N_n-particle) phase space is given by

$$\prod_{j=1}^{N_n}\widetilde{\mathrm{d}k_j} = \prod_{j=1}^{N_n}\frac{\mathrm{d}^3k_j}{(2\pi)^3 2k_j^0}. \quad (1.45)$$

Let us consider a concrete example, the two-point correlation function of a real scalar field $\phi(x)$ with mass M [25, 131, 136], and express it in terms of the *spectral function* or *spectral density* $\rho(s)$, which carries all information about the process,

$$\begin{aligned}
\langle 0|\phi(x)\phi(y)|0\rangle &= \sum_n \int\prod_{j=1}^{N_n}\widetilde{\mathrm{d}k_j}\langle 0|\phi(x)|n\rangle\,\langle n|\phi(y)|0\rangle = \sum_n\int\prod_{j=1}^{N_n}\widetilde{\mathrm{d}k_j}e^{-\mathrm{i}(\Sigma_j k_j)(x-y)}|\langle 0|\phi(x)|n\rangle|^2 \\
&= \int\frac{\mathrm{d}^4p}{(2\pi)^4}e^{-\mathrm{i}p(x-y)}\sum_n\int\prod_{j=1}^{N_n}\widetilde{\mathrm{d}k_j}(2\pi)^4\delta^{(4)}\big(p - (\Sigma_j k_j)\big)|\langle 0|\phi(x)|n\rangle|^2 \\
&=: \int\frac{\mathrm{d}^4p}{(2\pi)^4}e^{-\mathrm{i}p(x-y)}2\pi\theta(p^0)\rho(p^2), \quad (1.46)
\end{aligned}$$

where we introduced a complete set of states in the first line and a δ function in the second, and defined $\rho(p^2)$ in the last line. The time-ordered correlator is then given by

$$\begin{aligned}
\langle 0|T\{\phi(x)\phi(y)\}|0\rangle &= \langle 0|\phi(x)\phi(y)|0\rangle\theta(x^0 - y^0) + \langle 0|\phi(y)\phi(x)|0\rangle\theta(y^0 - x^0) \\
&= \mathrm{i}\int\frac{\mathrm{d}^4p}{(2\pi)^4}e^{\mathrm{i}p(x-y)}\int_0^\infty \mathrm{d}s\,\frac{\rho(s)}{p^2 - s + \mathrm{i}\epsilon}. \quad (1.47)
\end{aligned}$$

This is similar to the derivation of the FEYNMAN propagator via the advanced and retarded propagator [25]. Indeed, the lowest intermediate state is given by $|n\rangle = |\phi\rangle$, which yields the FEYNMAN

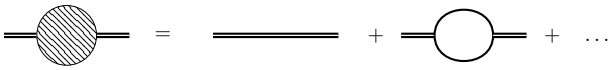

Figure 1.4: The lowest-order contributions to the two-point function of ϕ, which is denoted by a double line; single lines denote η.

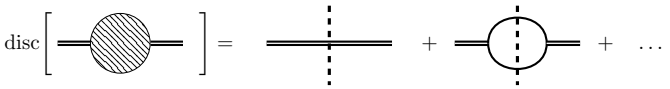

Figure 1.5: The discontinuity of the two-point function of ϕ can be obtained from the sum over its cuts.

propagator as the lowest-order result, *i.e.*, $\rho(p^2) = \delta(p^2 - M^2) + \dots$. The Källén–Lehmann representation [137, 138] of the two-point function in momentum space is given by

$$\int \mathrm{d}x\,\mathrm{d}y\, e^{\mathrm{i}(px+p'y)} \langle 0|T\{\phi(x)\phi(y)\}|0\rangle = \mathrm{i}(2\pi)^4 \delta^{(4)}(p+p') \int_0^\infty \mathrm{d}s \frac{\rho(s)}{p^2 - s + \mathrm{i}\epsilon} =: \mathrm{i}(2\pi)^4 \delta^{(4)}(p+p') D(p^2). \tag{1.48}$$

Using the Sokhotski–Plemelj theorem, one can relate the spectral function to the imaginary part of $D(p^2)$,

$$\rho(p^2) = -\frac{1}{\pi} \mathrm{Im}\, D(p^2). \tag{1.49}$$

We already know that $\delta(p^2 - M^2)$ contributes to the imaginary part, yielding an isolated pole.

For a second intermediate state in the sum in Eq. (1.46), assume there is another scalar particle η with mass m in the model, such that $M > 2m$, and an interaction term $\mathcal{L}_{\mathrm{int}} \ni \frac{\lambda}{2}\phi\eta^2$. Then the next contribution to the two-point function is given by an η loop; see Fig. 1.4. After evaluating the diagram, one finds for the imaginary part

$$\mathrm{Im}\, \mathcal{M}_{\mathrm{loop}}(p^2) = -\frac{\lambda^2}{32\pi} \sqrt{1 - \frac{4m^2}{p^2}}\, \theta(p^2 - 4m^2), \tag{1.50}$$

which yields a branch cut starting at $p^2 = 4m^2 =: s_{\mathrm{thr}}$ from the square root. We have identified contributions to the imaginary part from the one-particle intermediate state ϕ and the two-particle intermediate state 2η with support where the respective intermediate states can go on-shell.

In order to include contributions from all intermediate states, one considers the sum over all possible one-particle irreducible (1PI) contributions, which is given by the self-energy of ϕ denoted by $\Pi(p^2)$. Taking care of renormalisation implicitly and making use of the geometric series, one can express the two-point function as

$$D(p^2) = \frac{1}{p^2 - M^2 - \Pi(p^2) + \mathrm{i}\epsilon}, \qquad \mathrm{Im}\, D(p^2) = \frac{\mathrm{Im}\left[\Pi(p^2)\right]}{|p^2 - M^2 - \Pi(p^2)|^2}. \tag{1.51}$$

The real part of $D(p^2)$ can be calculated from the imaginary part dispersively,

$$\mathrm{Re}\, D(p^2) = \frac{1}{\pi} \fint_{s_{\mathrm{thr}}}^\infty \mathrm{d}s\, \frac{\mathrm{Im}\, D(s)}{s - p^2}. \tag{1.52}$$

For other theories and more complicated correlators, $\rho(s)$ will similarly exhibit poles at the squared masses of one-particle intermediate states and branch cuts from higher intermediate states; the procedure to determine the correlator is similar. Systematically, one can obtain the imaginary part or,

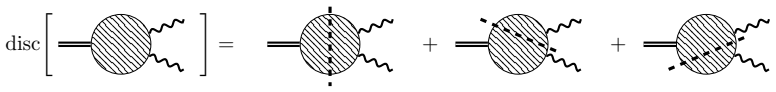

Figure 1.6: The discontinuity of a three-point function can be obtained from the sum over cuts in three different kinematic variables.

more generally, the discontinuity by cutting a diagram in all possible ways, each time replacing the propagators of particles whose lines were cut by delta functions $-2\pi\mathrm{i}\,\delta(p^2 - M^2)$ in order to retain the on-shell contribution. Summing over these expressions yields the discontinuity since it captures all ways in which an intermediate state can go on-shell. The procedure to obtain the discontinuity from the sum over all cuts is known as CUTKOSKY or cutting rules [139], where the latter term refers both to the cuts in the diagrams and to the resulting branch cuts.

The first two diagrams in the previously discussed example of the scalar two-point function admit only one cut each; see Fig. 1.5. Higher-order intermediate states with more loops will admit more cuts, but all in the same variable. For a three-point function, one can cut in three different kinematic variables, as depicted in Fig. 1.6. In that case, the imaginary part and the discontinuity are in general not equivalent since a function depending on several variables can approach the real axis in several ways; *e.g.*, let $\mathcal{M}(s,t)$ depend on two kinematic variables and consider its imaginary part, which is not equal to the discontinuity in s (or t),

$$\begin{aligned} 2\mathrm{i}\,\mathrm{Im}\,\mathcal{M}(s,t) &= [\mathcal{M}(s+\mathrm{i}\epsilon, t+\mathrm{i}\epsilon) - \mathcal{M}(s-\mathrm{i}\epsilon, t-\mathrm{i}\epsilon)] \\ &\neq [\mathcal{M}(s+\mathrm{i}\epsilon, t+\mathrm{i}\epsilon) - \mathcal{M}(s-\mathrm{i}\epsilon, t+\mathrm{i}\epsilon)] = \mathrm{disc}_s \mathcal{M}(s,t). \end{aligned} \tag{1.53}$$

Differences occur if there is not only a cut in s, but also one in t, such that the two limits $t+\mathrm{i}\epsilon$ and $t-\mathrm{i}\epsilon$ differ by $\mathrm{disc}_t\,\mathcal{M}$. The discontinuity arising from a cut in t also shows up if one projects to s via a partial-wave analysis (PWA). Due to the projection, a pole or a cut in t manifests itself as a branch cut in s; one refers to such a cut as a LHC since it occurs on the negative real axis in the s plane (but on the positive real axis in the t plane).

A correlation function can exhibit resonant behaviour, which is associated with a short-lived one-particle intermediate state. For example, a two-particle initial state can produce a one-particle resonance, which subsequently decays back to the two-particle state. This is associated with a pole in the corresponding correlation function, which, however, does not lie on the real axis as in the case before, where ϕ could also occur as an asymptotic state. In contrast, a resonance state cannot exist asymptotically and corresponds to a pole in the complex plane away from the real axis; due to analyticity, it can only lie on unphysical sheets [128]. The square root of the complex pole position s_R corresponds to the mass $m_R = \mathrm{Re}\,\sqrt{s_R}$ and the width $\Gamma_R = 2\mathrm{Im}\,\sqrt{s_R}$ of the resonance state, the residue of a correlation function at s_R is associated with the coupling strength of the initial state to the resonance. While the non-resonant part of a two-particle intermediate state is described by square roots and logarithms, the resonant part has a finite peak shape, depending on the position of the resonance pole with respect to the real axis, where physical measurements take place, and to other structures such as branch cuts. Examples of resonances occuring in the context of hadron physics include the $\rho(770)$ as a vector isovector resonance in the two-pion system, whereas the $f_0(500)$ is a scalar isoscalar two-pion resonance. While these resonances are rather broad, the vector isoscalar resonances $\omega(782)$ and $\phi(1020)$ are much narrower, coupling mainly, but not exclusively, to 3π and $K\bar{K}$, respectively. If a resonance couples to more than one system, one needs a coupled-channel formalism for an accurate description, such as for the $f_0(980)$, which has an $s\bar{s}$ component and therefore couples to $\pi\pi$ and $K\bar{K}$ [140, 141].

For a narrow resonance located not too too close to other singularities, one can parameterise its peak on the real axis with a BREIT–WIGNER (BW) function [142]

$$D_{\mathrm{BW}}(s) = \frac{1}{s - m_{\mathrm{BW}}^2 + \mathrm{i} m_{\mathrm{BW}} \Gamma_{\mathrm{BW}}}, \tag{1.54}$$

with parameters m_{BW} and Γ_{BW} that are similar to the pole parameters described above. This description of a resonance peak is, however, not unitary for more than one resonance, and for resonance poles far in the complex plane, the line shape can deviate significantly from a BW shape; examples for this are the scalar resonances $f_0(500)$ and $f_0(980)$ [34]. In the latter situation, BW parameters do not yield an accurate description of the resonance. When several resonances with the same quantum numbers couple to the same channel and the respective BW functions would overlap, a more refined treatment such as the K-matrix formalism should be used [143]. More details on resonances can be found in the review on the topic in Ref. [34].

One can improve a Breit–Wigner description by including an energy-dependent width $\Gamma(s)$ with support above the lowest production threshold of the resonance. With this, a dispersively improved BW propagator can be constructed similar to a full spectral function [144],

$$D_{\mathrm{BW}}^{\mathrm{impr}}(p^2) = -\frac{1}{\pi}\int_{s_{\mathrm{thr}}}^{\infty} \mathrm{d}s\, \frac{\mathrm{Im}\left[D_{\mathrm{BW}}(s)\right]}{p^2 - s + \mathrm{i}\epsilon}, \qquad \mathrm{Im}\left[D_{\mathrm{BW}}(s)\right] = \frac{-\sqrt{s}\Gamma(s)}{(s - m_{\mathrm{BW}}^2)^2 + s\Gamma(s)^2}. \tag{1.55}$$

Chapter 2

Semileptonic $\eta^{(\prime)}$ decays in the Standard Model

Like memories in cold decay
Transmissions echoing away
Far from the world of you and I
Where oceans bleed into the sky

Linkin Park, *The Catalyst* [145]

2.1 Prologue

The content of this chapter is based on the publication

- H. Schäfer, M. Zanke, Y. Korte, and B. Kubis, *Semileptonic decays $\eta^{(\prime)} \to \pi^0\ell^+\ell^-$ and $\eta' \to \eta\ell^+\ell^-$ in the standard model*, Phys. Rev. D **108**, 074025 (2023) [arXiv:2307.10357 [hep-ph]].

It was presented in the following talks:

- *The semileptonic decays $\eta^{(\prime)} \to \pi^0\ell^+\ell^-$ and $\eta' \to \eta\ell^+\ell^-$ in the standard model*, Precision tests of fundamental physics with light mesons, Trento 2023.
- *Semileptonic $\eta^{(\prime)}$ decays in the standard model*, The 11th International Workshop on Chiral Dynamics, Bochum 2024.

The second one entails the proceeding

- H. Schäfer, M. Zanke, Y. Korte, and B. Kubis, *Semileptonic $\eta^{(\prime)}$ decays in the Standard Model*, Proceedings of The 11th International Workshop on Chiral Dynamics — PoS(CD2024), 2025, 479, 035.

Tests of discrete symmetries are part of the endeavour to understand limitations of the SM in order to eventually extend it. The violation of C and CP is one of the conditions necessary for a matter–antimatter asymmetry in the Universe [33]. The SM does not provide enough CP violation to match the observations as electromagnetic interactions preserve CP, weak interactions violate it only via the CKM phase [49], and strong interactions conserve it; one can introduce the θ-term [54], which provides a mechanism for P and CP violation, but the corresponding parameter is heavily constrained by upper

limits on an electric dipole moment of the neutron [17, 56, 57, 146–148]. Decays of $\eta^{(\prime)}$ mesons provide a good opportunity to search for BSM sources of C and CP violation since these light pseudoscalars are C and P eigenstates. The semileptonic decays $\eta^{(\prime)} \to \pi^0\ell^+\ell^-$ and $\eta' \to \eta\ell^+\ell^-$, for $\ell \in \{e, \mu\}$, are forbidden in the SM as tree-level processes and therefore rare, such that a potential BSM contribution at tree-level might be observable against the SM background. Current experimental results yield only upper limits for these decays [149–151]; however, the upcoming REDTOP experiment [152] is expected to produce unprecedented numbers of $\eta^{(\prime)}$ mesons, yielding results of such high precision that a comparison to SM predictions might be feasible. This requires a prediction of the SM contributions with uncertainty estimates including both uncertainties from phenomenological input and an assessment of systematic effects from the model.

The leading SM contribution includes a C-preserving two-photon intermediate state. The photons couple to $\pi\eta$ primarily via a vector-meson exchange in the t- and u-channel, such that vector–pseudoscalar–photon ($VP\gamma$) couplings are to be determined. The coupling constants were calculated phenomenologically by Marvin ZANKE and the author of this thesis, and relative signs were fixed by symmetry considerations in discussions with Bastian KUBIS. Due to the virtual nature of the photons in the loop diagram, it is important to take into account their virtualities via the introduction of $VP\gamma$ form factors; this also ensures that the loop calculation converges. In the spirit of vector-meson dominance (VMD), these are modelled as either monopole or dipole form factors, where the latter effect the expected high-energy behaviour. Previous calculations based on VMD did not take these photon virtualities into account, thus missing a systematic effect. Another systematic effect that was not consired previously for these decays is scalar s-channel rescattering. Yannis KORTE had already worked out and implemented a framework for such contributions in $\eta\pi^0 \to \gamma\gamma$ processes in collaboration with Bastian KUBIS. This effect and its interplay with the VMD contribution in the context of semileptonic decays was discussed between Bastian KUBIS, Yannis KORTE, Marvin ZANKE, and the author of this thesis; the numerical implementation was done by Yannis KORTE and this thesis' author.

The groundwork of the project was presented in the master's thesis of the author of this thesis [153], where the general framework was investigated and first results for form factors with constant decay widths were obtained, which improved previous theoretical calculations [154]. Since then, the calculation has been significantly refined by the inclusion of energy-dependent widths both for the exchanged vector meson and in the form factors. The dispersive improvement of vector-meson propagators with spectral functions according to the procedure outlined in Ref. [144] was proposed by Marvin ZANKE and Bastian KUBIS. The details of several form factor parameterisations were worked out by Marvin ZANKE, Bastian KUBIS, and the author of this thesis in order to estimate systematic effects.

Since the combination of the loop integrals and the integration over the three-particle phase space is a numerical highly non-trivial task—especially when complemented by additional integrals from spectral functions—the numerical evaluation was set up and carried out independently by Marvin ZANKE and the author of this thesis in order to provide cross-checks. Hereby, the author of this thesis focused on the implementation of the monopole form factors with constant and with energy-dependent widths, which were cross-checked by Marvin ZANKE. The latter implemented dipole form factors with constant and energy-dependent widths and compared them to cross-checks provided by this thesis' author.

In the course of this, a comparison between two libraries for the evaluation of PASSARINO–VELTMAN master integrals, which are needed to calculate the loop integral, was carried out since *LoopTools* [155] proved to be numerically instable in specific settings with dispersive parameters. These numerical instabilities were investigated by Marvin ZANKE and the author of this thesis and discussed with Bastian KUBIS. Marvin ZANKE presents and discusses more details on this in Ref. [156]. For the `Fortran` library *Collier* [157–160], an interface to `C++` was developed by Marvin ZANKE and the author of this thesis, with helpful input concerning `Fortran` from Andreas NOGGA and insightful communication with Ansgar DENNER regarding *Collier*. In order to carry out the numerical evaluation at the required precision, it had to be performed partly on the computer cluster of the institute with kind help of Bernard METSCH and partly on the university's HPC cluster *bonna* with support from the High Performance Computing and Analytics Lab at Bonn University.

With the framework implemented as described, (differential) decay widths, normalised decay widths, and branching ratios for the semileptonic decays and corresponding photonic decays were calculated. Uncertainties were estimated for these observables, and the calculation was done for the various form factor parameterisations described above, including a variant with constant couplings as a benchmark and for comparison with previous theoretical calculations. For this, a similar pattern of cross-checks was adopted; Marvin Zanke focused on calculating observables with different variants of monopole form factors and this thesis' author cross-checked them, while the latter calculated observables with different variants of dipole form factors, which were subsequently cross-checked by Marvin Zanke. The calculation of scalar rescattering contributions to the observables was carried out by the author of this thesis in collaboration with Yannis Korte. The text of this article was written collaboratively by all four authors, where the main part was done by Marvin Zanke and the author of this thesis; the plots of the differential decay widths were produced by Marvin Zanke.

2.2 Introduction

Within the Standard Model (SM) of particle physics, the strong and electromagnetic interactions conserve the symmetries parity (P), charge conjugation (C), and time reversal (T) separately. For this reason, the decays $\eta^{(\prime)} \to \pi^0\ell^+\ell^-$ and $\eta' \to \eta\ell^+\ell^-$ can—mediated via the strong and electromagnetic force—only proceed via a C-even two-photon mechanism due to $\mathrm{C}(\eta^{(\prime)}) = \mathrm{C}(\pi^0) = +1$; *i.e.*, they appear as one-loop processes at lowest order.[#1] As a result, the SM contribution to those decays is strongly suppressed, rendering them well-suited candidates for searches for physics beyond the SM (BSM). In fact, BSM contributions to the discussed decays, either mediated via a C-odd one-photon exchange [161–164] or due to other BSM mechanisms such as new light scalars [17] and unconventional sources of CP violation [165], are themselves subject to ongoing analyses.

Historically, calculations of $\eta \to \pi^0\ell^+\ell^-$ were based on different models for the $\eta \to \pi^0\gamma^*\gamma^*$ vertex function, as the conversion $\gamma^*\gamma^* \to \ell^+\ell^-$ depends solely on quantum electrodynamics (QED) and is, hence, in principle straightforward. This is not unlike the rare dilepton decays of the lightest flavour-neutral pseudoscalars, $P \to \ell^+\ell^-$, $P = \pi^0$, η, η', similarly loop-induced and completely calculable once the corresponding transition form factors $P \to \gamma^*\gamma^*$ are known; see Refs. [166–168] for recent work and references therein. For these decays, a reasonable behaviour of the transition form factors for large photon virtualities is not only a requirement for a precision calculation, but a necessity to regularise the otherwise ultraviolet-divergent loop integral. This was similarly realised in early theoretical work on $\eta \to \pi^0\ell^+\ell^-$ in the late 1960s, which was based on the simplest possible, point-like effective operator for $\eta \to \pi^0\gamma\gamma$ [169, 170]: the loop was rendered finite either with an *ad-hoc* form factor [169] or reconstructed dispersively from the unambiguously calculable imaginary part, using a finite energy cutoff [170]. As the effective operator only contained S-wave interactions in either case—leading to helicity suppression of the resulting dilepton mechanism—these calculations only determined a subdominant contribution, underestimating in particular the $\eta \to \pi^0 e^+e^-$ rate by orders of magnitude.

On the other hand, a first vector-meson-dominance (VMD) model calculation [171], which based the $\eta \to \pi^0\gamma\gamma$ amplitude on ρ and ω exchange, $\rho \equiv \rho^0(770)$, $\omega \equiv \omega(782)$, required no such further regularisation: the additional vector-meson propagators, singularities in the crossed channels providing so-called left-hand cuts, dampen the high-energy behaviour sufficiently such that the loop integral is convergent; see Fig. 2.1. The coupling constants for the $V \to P\gamma$ transitions, $V = \rho, \omega$, $P = \eta, \pi^0$, largely unknown at the time, had to be estimated in a quark model. In this way, realistic rates $\mathcal{B}(\eta \to \pi^0 e^+e^-)/\mathcal{B}(\eta \to \pi^0\gamma\gamma) \approx 10^{-5}$ were obtained. In the 1990s, the two decays $\eta \to \pi^0 e^+e^-$ and $\eta \to \pi^0\mu^+\mu^-$ were reconsidered by calculating unitarity bounds [172, 173]. These are based on the observation that the amplitude $\eta \to \pi^0\gamma\gamma$ (with real photons) model-independently determines the imaginary part of the dilepton amplitudes, thus providing a lower limit to the corresponding rates. The diphoton decays were calculated in VMD, supplemented with scalar $a_0(980)$ exchange [172], or

[#1] Contributions from the weak interactions are also required to vanish at tree level.

	Branching ratio	Ancillary information	Reference
$\eta \to \pi^0 e^+ e^-$	9.9×10^{-9}	VMD model	[171]
$\eta \to \pi^0 e^+ e^-$	$8.4^{+4.6}_{-3.8} \times 10^{-10}$	Unitarity bounds, VMD model	[172]
$\eta \to \pi^0 e^+ e^-$	$9.2(1.5) \times 10^{-10}$	Quark-box model, $m_q = 330\,\text{MeV}$	[173]
$\eta \to \pi^0 \mu^+ \mu^-$	$3.8^{+2.3}_{-1.5} \times 10^{-10}$ $6.9^{+4.6}_{-3.8} \times 10^{-10}$	Unitarity bounds, VMD model As above, supplemented by a_0	[172]
$\eta \to \pi^0 \mu^+ \mu^-$	$3.3(5) \times 10^{-9}$	Quark-box model, $m_q = 330\,\text{MeV}$	[173]
$\eta \to \pi^0 e^+ e^-$	$< 7.5 \times 10^{-6}$	3×10^7 η events	WASA-at-COSY [151]
$\eta \to \pi^0 \mu^+ \mu^-$	$< 5 \times 10^{-6}$	2×10^7 η events	Dzhelyadin *et al.* [149]
$\eta' \to \pi^0 e^+ e^-$	$< 1.4 \times 10^{-3}$	1.3×10^6 η' events	CLEO [150]
$\eta' \to \pi^0 \mu^+ \mu^-$	$< 6 \times 10^{-5}$	10^7 η' events	Dzhelyadin *et al.* [149]
$\eta' \to \eta e^+ e^-$	$< 2.4 \times 10^{-3}$	1.3×10^6 η' events	CLEO [150]
$\eta' \to \eta \mu^+ \mu^-$	$< 1.5 \times 10^{-5}$	10^7 η' events	Dzhelyadin *et al.* [149]

Table 2.1: Historical theoretical results on the branching ratios for $\eta \to \pi^0 \ell^+ \ell^-$ and experimental upper limits for the different decay channels $\eta^{(\prime)} \to [\pi^0/\eta] \ell^+ \ell^-$, the latter all at 90% confidence level. Note that, for reasons of consistency with the experimental upper limits, we converted the theoretical results from decay widths to branching ratios by using an up-to-date central value [174] for the η width; see also Table 2.13.

based on a constituent-quark-box model [173]. The numerical results of these older calculations are collected in Table 2.1.

Today, we understand the mechanism for $\eta \to \pi^0 \gamma\gamma$ (and the related η' decays) much better, while precision calculations are still a challenge. Chiral perturbation theory [70] allows us to understand this reaction in terms of a systematic expansion at low momenta: the dominant contribution originates from a set of next-to-next-to-leading-order counterterms [101, 102], whose size can phenomenologically be estimated in terms of vector-meson exchanges. The resulting predictions agree with the data [175–177] rather well [178], and rescattering corrections in the scalar channel [179, 180] are moderate in size [181]. Similarly, vector-meson exchanges dominate the decays $\eta' \to \pi^0 \gamma\gamma$ and $\eta' \to \eta\gamma\gamma$ [182], with only minor S-wave corrections to the $\gamma\gamma$ spectra.

The most recent theoretical work on the decays $\eta^{(\prime)} \to \pi^0 \ell^+ \ell^-$ and $\eta' \to \eta \ell^+ \ell^-$ [154] employs this modern knowledge to a large extent. It once more models the two-photon amplitudes with a VMD ansatz, superseding Ref. [171] by retaining all lepton mass effects and Ref. [172] by calculating the real parts of the amplitudes explicitly; the current phenomenological information on vector–pseudoscalar–photon couplings is used therein. Perhaps surprisingly, what has still not been implemented is the dependence on the photon virtualities, *i.e.*, the vector-to-pseudoscalar transition form factors [183, 184]. These have garnered significant interest in the last few years, both phenomenologically [185–188] and, in particular for the $\rho \to \pi$ transition form factor, on the lattice [189–192]. Furthermore, the behaviour of these form factors for asymptotically large momentum transfers is known [113, 114, 193–195]. This is the major novelty of this article and the main advance compared to Ref. [154]: by providing a realistic model for $\eta^{(\prime)} \to \pi^0 \gamma^* \gamma^*$ and $\eta' \to \eta \gamma^* \gamma^*$, including the dependence on the photon virtualities, we are able to give a more reliable prediction for the rates of the corresponding dilepton decays in the SM. Furthermore, by lifting the (somewhat artificial) dependence of the loop regularisation on the left-hand cuts, we can, for the first time, also test the effect of S-wave rescattering contributions. Varying the form-factor models allows us to assess the remaining theoretical uncertainties of our predictions.

Experimentally, the decay $\eta \to \pi^0 e^+ e^-$ has been searched for since the 1960s [196–198], motivated by the search for possible C violation in the strong and electromagnetic interactions. To date, only

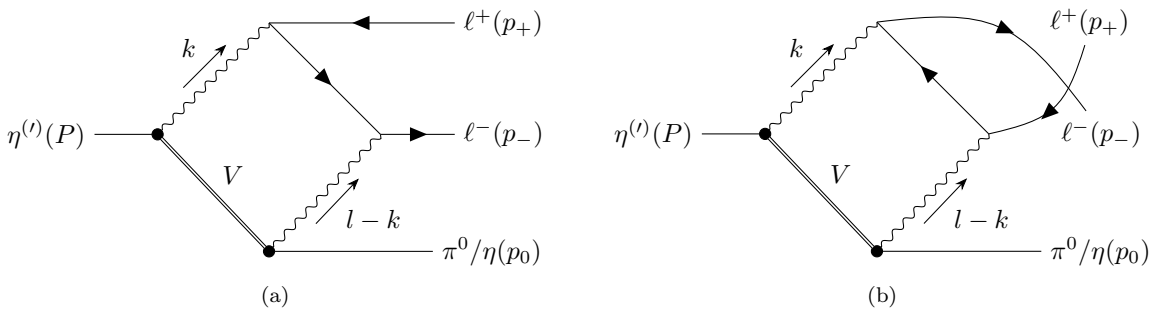

Figure 2.1: The t- (a) and u-channel (b) diagrams that contribute to $\eta^{(\prime)} \to [\pi^0/\eta]\ell^+\ell^-$ under the assumption that the underlying two-photon amplitudes are dominated by the exchange of the vector mesons $V = \rho, \omega, \phi$.

upper limits have been established for all decays studied in this article, the most rigorous ones being collected in Table 2.1.[#2] The most stringent upper limits, those for $\eta \to \pi^0 e^+ e^-$ from WASA-at-COSY [151] and for $\eta \to \pi^0 \mu^+ \mu^-$ from Lepton-G [149], are still more than three orders of magnitude above the theoretical SM branching ratios; for the η' decays, this margin is even larger. There is, even so, the prospect of improved experimental results by the REDTOP collaboration [152, 199], which plans to search for rare decays with an unprecedented number of η and η' events.

This article is structured as follows. In Sec. 2.3, we construct the amplitudes for the decays $\eta^{(\prime)} \to \pi^0\ell^+\ell^-$ and $\eta' \to \eta\ell^+\ell^-$ as well as the corresponding two-photon analogs, with the latter serving as normalisation channels. For the semileptonic decays, a set of form factors that incorporate the non-perturbative physics of the process is introduced and their normalisations are determined from phenomenological input. These form factors are then parameterised in Sec. 2.4 by means of two distinct VMD models, including the construction of dispersively improved variants. In Sec. 2.5, we discuss the calculation of observables—branching ratios as well as differential distributions—via a Passarino–Veltman (PV) decomposition. Scalar rescattering contributions are analysed in Sec. 2.6. Our numerical results are discussed in Sec. 2.7, and we summarise our findings in Sec. 2.8. Further details are provided in the appendices.

2.3 Amplitudes

The construction of the C-even decay amplitudes for

$$\begin{aligned} \eta^{(\prime)}(P) &\to \pi^0(p_0)\ell^+(p_+)\ell^-(p_-), \\ \eta'(P) &\to \eta(p_0)\ell^+(p_+)\ell^-(p_-), \end{aligned} \tag{2.1}$$

where $\ell = e, \mu$, is based on the assumption that the underlying $\eta^{(\prime)} \to \pi^0\gamma^*\gamma^*$ and $\eta' \to \eta\gamma^*\gamma^*$ amplitudes are dominated by the exchange of the vector mesons $V = \rho, \omega, \phi$, $\phi \equiv \phi(1020)$; see Fig. 2.1. For our analysis, we define the Mandelstam variables $s = (p_+ + p_-)^2$, $t = (p_- + p_0)^2$, and $u = (p_+ + p_0)^2$, which describe the invariant mass squares of the lepton pair and the lepton–pseudoscalar subsystems, respectively; they fulfill the relation $\Sigma = s + t + u = M^2_{\eta^{(\prime)}} + M^2_{\pi^0/\eta} + 2m^2_\ell$. The relevant vector-to-pseudoscalar transition form factors $\mathcal{F}_{VP}(q^2)$ are defined according to

$$\langle P(p)|j_\mu(0)|V(p_V)\rangle = e\,\epsilon_{\mu\nu\alpha\beta}\epsilon^\nu(p_V)p^\alpha q^\beta \mathcal{F}_{VP}(q^2), \tag{2.2}$$

[#2] Note that those upper limits were obtained assuming a flat Dalitz-plot distribution, which our results indicate to be an insufficient assumption; see the discussion in Sec. 2.7.1 below.

	$\Gamma/\,\mathrm{keV}$ [174]	$\lvert\mathcal{F}_{VP}(0)\rvert/\,\mathrm{GeV}^{-1}$
$\rho \to \pi^0\gamma$	69(12)	0.73(6)
$\omega \to \pi^0\gamma$	725(26)	2.33(4)
$\phi \to \pi^0\gamma$	5.61(21)	0.1355(26)
$\rho \to \eta\gamma$	44.2(3.1)	1.58(6)
$\omega \to \eta\gamma$	3.91(35)	0.449(20)
$\phi \to \eta\gamma$	55.3(1.1)	0.691(7)
$\eta' \to \rho\gamma$	55.5(1.9)	1.299(23)
$\eta' \to \omega\gamma$	4.74(20)	0.401(9)
$\phi \to \eta'\gamma$	0.264(9)	0.712(12)

Table 2.2: The normalisations $|\mathcal{F}_{VP}(0)|$ at the real-photon point obtained from Eq. (2.3) and phenomenological input determined from Ref. [174]; see also Table 2.13.

where $j_\mu = e(2\bar{u}\gamma_\mu u - \bar{d}\gamma_\mu d - \bar{s}\gamma_\mu s)/3$ denotes the electromagnetic current, and $q = p_V - p$. The normalisations $|\mathcal{F}_{VP}(0)|$ at the real-photon point can be derived from phenomenological input in a straightforward manner,

$$\begin{aligned}\Gamma(V \to P\gamma) &= \frac{\alpha(M_V^2 - M_P^2)^3}{24M_V^3}|\mathcal{F}_{VP}(0)|^2,\\ \Gamma(P \to V\gamma) &= \frac{\alpha(M_P^2 - M_V^2)^3}{8M_P^3}|\mathcal{F}_{VP}(0)|^2,\end{aligned} \tag{2.3}$$

where $\alpha = e^2/(4\pi)$ is the fine-structure constant, leading to Table 2.2 with input from Ref. [174].

Using Eq. (2.2) and summing over the t- and u-channel diagrams shown in Fig. 2.1 as well as $V = \rho, \omega, \phi$, we find the amplitude $\mathcal{M} \equiv \mathcal{M}(\eta^{(\prime)} \to [\pi^0/\eta]\ell^+\ell^-)$ to be

$$\begin{aligned}\mathcal{M} = \mathrm{i}\frac{\alpha^2}{\pi^2}\sum_V \int \mathrm{d}^4k\; g^{\beta\tilde{\beta}}\epsilon_{\mu\nu\alpha\beta}\epsilon_{\tilde{\mu}\tilde{\nu}\tilde{\alpha}\tilde{\beta}}P^\alpha k^\mu\big(P^{\tilde{\alpha}}k^{\tilde{\mu}} - P^{\tilde{\alpha}}l^{\tilde{\mu}} + k^{\tilde{\alpha}}l^{\tilde{\mu}}\big)P_V^{\mathrm{BW}}\big((P-k)^2\big)P_\gamma(k^2)P_\gamma\big((l-k)^2\big)\\ \times \mathcal{F}_{V\eta^{(\prime)}}(k^2)\mathcal{F}_{V[\pi^0/\eta]}\big((l-k)^2\big)\bar{u}_s\left[\gamma^{\tilde{\nu}}\frac{\not{k} - \not{p}_+ + m_\ell}{(k-p_+)^2 - m_\ell^2}\gamma^\nu + \gamma^\nu\frac{\not{p}_- - \not{k} + m_\ell}{(p_- - k)^2 - m_\ell^2}\gamma^{\tilde{\nu}}\right]v_r,\end{aligned} \tag{2.4}$$

with $\bar{u}_s \equiv \bar{u}_s(p_-)$ and $v_r \equiv v_r(p_+)$. Here, we defined $l = p_+ + p_-$ and the [BREIT–WIGNER (BW)] propagators

$$P_V^{\mathrm{BW}}(q^2) = \frac{1}{q^2 - M_V^2 + \mathrm{i}M_V\Gamma_V}, \quad P_\gamma(q^2) = \frac{1}{q^2 + \mathrm{i}\epsilon}, \tag{2.5}$$

where M_V is the mass of the respective vector meson and Γ_V its width. Due to their narrowness, a constant-width approximation is well justified for the ω and ϕ, whereas the broad ρ meson necessitates an energy-dependent width to avoid sizable unphysical imaginary parts below threshold. We will implement such a parameterisation for the ρ in Sec. 2.4.3, where we will use a dispersively improved BW propagator. Our final results will be quoted for both a variant with constant widths for all vector mesons (CW) and a variant that instead employs an energy-dependent width for the ρ (VW).

For the eventual computations, it will turn out useful to apply the DIRAC equation and make the replacements

$$\begin{aligned}\bar{u}_s\gamma^{\tilde{\nu}}(\not{k} - \not{p}_+ + m_\ell)\gamma^\nu v_r &= \bar{u}_s(\gamma^{\tilde{\nu}}\not{k}\gamma^\nu - 2p_+^\nu\gamma^{\tilde{\nu}})v_r,\\ \bar{u}_s\gamma^\nu(\not{p}_- - \not{k} + m_\ell)\gamma^{\tilde{\nu}}v_r &= \bar{u}_s(2p_-^\nu\gamma^{\tilde{\nu}} - \gamma^\nu\not{k}\gamma^{\tilde{\nu}})v_r\end{aligned} \tag{2.6}$$

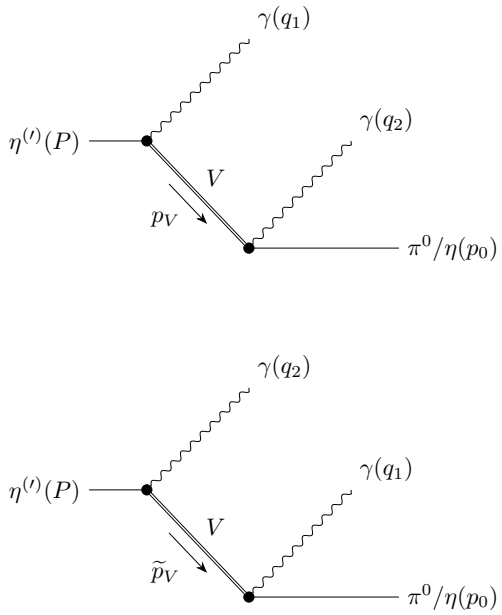

Figure 2.2: The two diagrams contributing to the two-photon decay $\eta^{(\prime)} \to [\pi^0/\eta]\gamma\gamma$, which are related via $q_1 \leftrightarrow q_2$.

in Eq. (2.4).

The branching ratios of the semileptonic decays are commonly normalised to the two-photon analogs

$$\begin{aligned} \eta^{(\prime)}(P) &\to \pi^0(p_0)\gamma(q_1)\gamma(q_2), \\ \eta'(P) &\to \eta(p_0)\gamma(q_1)\gamma(q_2); \end{aligned} \tag{2.7}$$

see also Fig. 2.2. For these decays, we define the Mandelstam variables[#3]

$$s = (q_1+q_2)^2, \quad t_\gamma = (q_2+p_0)^2, \quad u_\gamma = (q_1+p_0)^2, \tag{2.8}$$

which fulfill $\Sigma_\gamma = s + t_\gamma + u_\gamma = M^2_{\eta^{(\prime)}} + M^2_{\pi^0/\eta}$, and denote the corresponding helicity amplitudes by $H_{\lambda\lambda'}$,

$$\begin{aligned} &\langle\gamma(q_1,\lambda)\gamma(q_2,\lambda')|\, S\,|\eta^{(\prime)}(P)[\pi^0/\eta](p_0)\rangle \\ &= \mathrm{i}(4\pi\alpha)(2\pi)^4\delta^{(4)}(P+p_0-q_1-q_2)\, e^{\mathrm{i}(\lambda-\lambda')\varphi} H_{\lambda\lambda'}. \end{aligned} \tag{2.9}$$

Here, $\lambda^{(\prime)}$ are the helicities of the photons and we factored out the dependence on the electric charge $(4\pi\alpha)$ and the azimuthal angle φ for convenience. Using Eq. (2.2) and the normalisation of the form factors, $|C_{VP\gamma}| = |\mathcal{F}_{VP}(0)|$, as will be introduced in Sec. 2.4, we express the VMD helicity amplitudes as

$$H_{\lambda\lambda'} = \epsilon_\lambda^{\alpha_1\,*}(q_1)\epsilon_{\lambda'}^{\alpha_2\,*}(q_2)\sum_V C_{V\eta^{(\prime)}\gamma} C_{V[\pi^0/\eta]\gamma}\big[P_V^{\mathrm{BW}}(t_\gamma)H^t_{\alpha_1\alpha_2} + P_V^{\mathrm{BW}}(u_\gamma)H^u_{\alpha_1\alpha_2}\big], \tag{2.10}$$

where $\epsilon^*_\lambda(q_i)$ denote the polarisation vectors of the outgoing photons and

$$\begin{aligned} H^t_{\alpha_1\alpha_2} &= g^{\mu_1\mu_2}\epsilon_{\mu_1\nu_1\alpha_1\beta_1}\epsilon_{\mu_2\nu_2\alpha_2\beta_2} p_V^{\nu_1} q_1^{\beta_1} p_0^{\nu_2} q_2^{\beta_2}, \\ H^u_{\alpha_1\alpha_2} &= g^{\mu_1\mu_2}\epsilon_{\mu_1\nu_1\alpha_1\beta_1}\epsilon_{\mu_2\nu_2\alpha_2\beta_2} p_0^{\nu_1} q_1^{\beta_1} \widetilde{p}_V^{\nu_2} q_2^{\beta_2}, \end{aligned} \tag{2.11}$$

with $p_V = q_2 + p_0$ and $\widetilde{p}_V = q_1 + p_0$ the momenta of the intermediate vector mesons.

[#3] Note that the Mandelstam variable $s = (P-p_0)^2$ is identical in the semileptonic and the diphoton case.

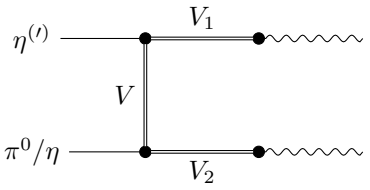

Figure 2.3: The modeling of the two-photon decay mechanism in the VMD framework via two vector mesons V_1 and V_2. Constraints on (V_1, V_2) in dependence of the initial and final state as well as V are given in Table 2.3.

2.4 Form factors

In order to parameterise the form factors $\mathcal{F}_{VP}(q^2)$, we use the VMD framework. As a consequence, the photon couplings at the $VP\gamma^*$ vertices of the diagrams in Fig. 2.1 are mediated via two intermediate vector mesons V_1 and V_2; see Fig. 2.3. We will construct two distinct such models: a monopole (MP) parameterisation with $V_i = \rho, \omega, \phi$ and a dipole (DP) ansatz with $V_i = \rho^{(\prime)}, \omega^{(\prime)}, \phi^{(\prime)}$, $\rho' \equiv \rho^0(1450)$, $\omega' \equiv \omega(1420)$, and $\phi' \equiv \phi(1680)$, that ensures the expected high-energy behaviour of the form factors [113, 114, 193–195]. For reference, we also include a model calculation with constant form factors, *i.e.*, a point-like (PL) interaction, which closely resembles the parameterisation of Ref. [154].

The conservation of isospin—and thus G parity combined with C—imposes constraints on V_1 and V_2 in dependence on the initial and final states as well as the t- or u-channel vector meson V. However, some of the couplings, namely $\eta^{(\prime)}\omega\phi^{(\prime)}$, $\eta^{(\prime)}\phi\omega^{(\prime)}$, $\pi^0\rho\phi^{(\prime)}$, and $\pi^0\phi\rho^{(\prime)}$, are, although isospin-allowed, vanishing under the assumption of U(3) flavour symmetry and ideally mixed vector-meson multiplets; see Appendix 2.9.1. Since the contribution of $V = \phi$ would otherwise vanish entirely for $\eta^{(\prime)} \to \pi^0\ell^+\ell^-$, we nonetheless include the OKUBO–ZWEIG–IIZUKA-suppressed (OZI-suppressed) [200–202] couplings $\pi^0\phi\rho^{(\prime)}$ in our calculations; the remaining vector mesons V_i are collected in Table 2.3.

2.4.1 Monopole model

The MP model only takes the lowest-lying vector mesons ρ, ω, and ϕ into account, so that the form factors are parameterised according to

$$\mathcal{F}_{VP}(q^2) = C_{VP\gamma} M_{V_i}^2 P_{V_i}^{\mathrm{BW}}(q^2), \tag{2.12}$$

with the assignments of $V_i \in \{\rho, \omega, \phi\}$ according to Table 2.3. Here, we assume $|C_{VP\gamma}| = |\mathcal{F}_{VP}(0)|$ at the real-photon point, see Table 2.2, which determines the coupling constants $C_{VP\gamma}$ up to an overall phase. This assumption omits corrections due to the constant, non-zero widths in the BW propagators, which are negligible for $V = \omega, \phi$ but potentially significant for $V = \rho$.[#4] Since the energy-dependent width of the ρ meson will be chosen to have the proper threshold behaviour, these complications only exist for the variant CW but not for VW. All coupling constants are assumed to be real in the following. In order to fix the relative signs between them, we resort to U(3) flavour symmetry and analyses of $e^+e^- \to 3\pi$ and $e^+e^- \to \pi\gamma$ [203–205]; see Appendix 2.9.1. Without loss of generality, we adopt a positive sign for the coupling $C_{\rho\eta\gamma}$ and establish the consistent sign convention collected in Table 2.4.

2.4.2 Dipole model

Given that the asymptotic behaviour of the vector-to-pseudoscalar transition form factors is expected to be $\mathcal{F}_{VP}(q^2) \propto q^{-4}$ [113, 114, 193–195], we can additionally include the next-higher multiplet of

[#4] Note that $P_V^{\mathrm{BW}}(0) \simeq -1/M_V^2$, so that $\mathcal{F}_{VP}(0) = -C_{VP\gamma}$, which, however, corresponds to an unobservable overall phase.

	$V\pi^0\gamma$			$V\eta^{(\prime)}\gamma$		
V	ρ	ω	ϕ	ρ	ω	ϕ
V_i	$\omega^{(\prime)}$	$\rho^{(\prime)}$	$\rho^{(\prime)}$	$\rho^{(\prime)}$	$\omega^{(\prime)}$	$\phi^{(\prime)}$

Table 2.3: The constraints on the vector mesons V_i of Fig. 2.3 in dependence of V derived from isospin conservation and U(3) flavour symmetry with ideally mixed vector-meson multiplets. We include the OZI-suppressed couplings $\phi\pi^0\rho^{(\prime)}$; see text and Appendix 2.9.1 for more information.

vector mesons, ρ', ω', and ϕ', to achieve this property by tuning a free parameter ϵ_V.[#5] For the DP model, we thus make the ansatz

$$\widetilde{\mathcal{F}}_{VP}(q^2) = C_{VP\gamma}\big[(1-\epsilon_{V_i})M_{V_i}^2 P_{V_i}^{\mathrm{BW}}(q^2) + \epsilon_{V_i} M_{V_i'}^2 P_{V_i'}^{\mathrm{BW}}(q^2)\big], \tag{2.13}$$

where we assume the excited vector states to couple according to the exact same symmetry restrictions as the ground-state multiplet; *cf.* Table 2.3. Here, $P_{V'}^{\mathrm{BW}}(q^2)$ is defined as in Eq. (2.5), with $M_{V'}$ and $\Gamma_{V'}$ the mass and width of the respective excited vector meson. Due to the large widths of the excited vector mesons, a constant-width approximation leads to a rather poor description of these mesons, however. We will therefore, analogously to the ρ, construct dispersively improved BW propagators for ρ', ω', and ϕ' based on energy-dependent widths in Sec. 2.4.3, leading to replacements of the kind $P_{V'}^{\mathrm{BW}}(q^2) \to P_{V'}^{\mathrm{disp}}(q^2)$. Similarly to the MP, our final results for the DP will be quoted for both the variant CW with constant widths for all vector mesons and the variant VW, *i.e.*, using constant widths for the ω and ϕ but energy-dependent ones for $\rho^{(\prime)}$, ω', and ϕ'. The form factors in Eq. (2.13) are assumed to be normalised such that $\widetilde{F}_{VP}(0) = -C_{VP\gamma}$, which, as for the MP, holds up to potential corrections due to the constant widths in the propagators. In order to achieve the desired high-energy behaviour, the free parameter needs to be chosen as $\epsilon_V = M_V^2/(M_V^2 - M_{V'}^2)$.

2.4.3 Spectral representation

While the variant CW has its own *raison d'être* as a simple approximate description, the large widths of the mesons $\rho^{(\prime)}$, ω', and ϕ' actually require an energy-dependent parameterisation to avoid significant unphysical imaginary parts below threshold.[#6] In this section, we construct these energy-dependent widths; to ensure the correct analytic properties when inserting the form factors into the amplitude, Eq. (2.4), we will furthermore introduce dispersively improved variants [217] of the form factors that contain a $\rho^{(\prime)}$-, ω'-, or ϕ'-meson propagator, which lay the foundation for the variant VW in both the MP and DP model.

For the ρ meson, we will use the energy-dependent width [144]

$$\begin{aligned}\Gamma_\rho(q^2) &= \theta(q^2 - 4M_{\pi^\pm}^2)\frac{\gamma_{\rho\to\pi^+\pi^-}(q^2)}{\gamma_{\rho\to\pi^+\pi^-}(M_\rho^2)} f(q^2)\Gamma_\rho,\\ \gamma_{\rho\to\pi^+\pi^-}(q^2) &= \frac{(q^2 - 4M_{\pi^\pm}^2)^{3/2}}{q^2},\end{aligned} \tag{2.14}$$

where the so-called barrier factor [218, 219]

$$f(q^2) = \frac{\sqrt{q^2}}{M_\rho}\frac{M_\rho^2 - 4M_{\pi^\pm}^2 + 4p_R^2}{q^2 - 4M_{\pi^\pm}^2 + 4p_R^2}, \tag{2.15}$$

[#5] Data both on $e^+e^- \to \omega\pi^0$ [206] and $e^+e^- \to \rho^0\eta$ [207–209] suggest that the required cancellation indeed largely occurs between the contributions of the two lowest vector states, ρ and ρ' in those cases.

[#6] In principle, such unphysical imaginary parts could be avoided for the ρ exchange by reconstructing the latter in terms of dispersion relations for $\gamma^{(*)}\pi \to \pi\pi$ [192, 210, 211] and $\eta^{(\prime)} \to \pi\pi\gamma^{(*)}$ [209, 212–214]; *cf.* also Refs. [215, 216]. We here refrain from further refining the amplitude in such a way.

$C_{\rho\pi^0\gamma}$	$C_{\omega\pi^0\gamma}$	$C_{\phi\pi^0\gamma}$
$+$	$+$	$-$
$C_{\rho\eta\gamma}$	$C_{\omega\eta\gamma}$	$C_{\phi\eta\gamma}$
$+$	$+$	$-$
$C_{\rho\eta'\gamma}$	$C_{\omega\eta'\gamma}$	$C_{\phi\eta'\gamma}$
$+$	$+$	$+$

Table 2.4: The signs $\mathrm{sgn}[C_{VP\gamma}]$ of the couplings constants defined in Eq. (2.12). Here, we fixed the global sign of $C_{\rho\eta\gamma}$ to be positive; see Appendix 2.9.1 for details.

$p_R = 202.4\,\mathrm{MeV}$, has been introduced to ensure convergence of the superconvergence relations evaluated in Eq. (2.24) below. We calculate the dispersive ρ propagator via

$$P_V^{\mathrm{disp}}(q^2) = -\frac{1}{\pi}\int_{s_{\mathrm{thr}}}^{\infty} \mathrm{d}x\, \frac{\mathrm{Im}\,[P_V^{\mathrm{BW}}(x)]}{q^2 - x + \mathrm{i}\epsilon},$$
$$\mathrm{Im}\,[P_V^{\mathrm{BW}}(x)] = \frac{-\sqrt{x}\,\Gamma_V(x)}{(x - M_V^2)^2 + x\Gamma_V(x)^2}, \tag{2.16}$$

where $s_{\mathrm{thr}} = 4M_{\pi^\pm}^2$ is the threshold for $\rho \to \pi^+\pi^-$. The spectral representations of the form factors $\mathcal{F}_{VP}(q^2)$ for $VP \in \{\rho\eta^{(\prime)}, \omega\pi^0, \phi\pi^0\}$ are thus given by

$$\widehat{\mathcal{F}}_{VP}(q^2) = \frac{C_{VP\gamma}}{N_\rho} M_\rho^2 P_\rho^{\mathrm{disp}}(q^2), \tag{2.17}$$

where the normalisation constant

$$N_\rho = -M_\rho^2 P_\rho^{\mathrm{disp}}(0) \approx 0.898 \tag{2.18}$$

is introduced in order to retain $\widehat{\mathcal{F}}_{VP}(0) = -C_{VP\gamma}$, *i.e.*, to ensure that the coupling constants have the same meaning in the original and the dispersively improved VMD parameterisation. For reasons of consistency, we also replace the ρ propagator in the left-hand cuts, $P_\rho^{\mathrm{BW}}(q^2)$ in Eq. (2.4), by a dispersively improved variant, *i.e.*,

$$P_\rho^{\mathrm{BW}}(q^2) \to \frac{1}{N_\rho^{\mathrm{LHC}}} P_\rho^{\mathrm{disp}}(q^2), \tag{2.19}$$

where the normalisation constant

$$N_\rho^{\mathrm{LHC}} = \mathrm{i}M_\rho\Gamma_\rho P_\rho^{\mathrm{disp}}(M_\rho^2) \approx 1 \tag{2.20}$$

is introduced in order to retain $P_\rho^{\mathrm{BW}}(M_\rho^2) = 1/(\mathrm{i}M_\rho\Gamma_\rho)$, in line with the VMD assumption.[#7] With these conventions, we will drop the distinction between $\mathcal{F}_{VP}(q^2)$ and $\widehat{\mathcal{F}}_{VP}(q^2)$ in the following, and it will always be clear from context which representation is used.

For the dipole variant, the widths of the excited vector mesons ρ', ω', ϕ' are modeled using the dominant quasi-two-particle thresholds. We condense the decays $\rho' \to \omega\pi$, $\omega' \to \rho\pi$, and $\phi' \to K^*\bar{K}$, $K^* \equiv K^*(892)$, in the notation $V' \to VP$, such that

$$\Gamma_{V'}(q^2) = \theta\big(q^2 - (M_V + M_P)^2\big)\frac{\gamma_{V'\to VP}(q^2)}{\gamma_{V'\to VP}(M_{V'}^2)}\Gamma_{V'},$$
$$\gamma_{V'\to VP}(q^2) = \frac{\lambda(q^2, M_V^2, M_P^2)^{3/2}}{(q^2)^{3/2}}, \tag{2.21}$$

[#7] We ignore the fact that the ρ pole in the complex plane does not exactly agree with the BREIT–WIGNER parameters.

ϵ_ρ	$(-0.47)^{-0.07}_{+0.06}$	$\widetilde{N}_\rho$	$0.99^{+0.04}_{-0.03}$
ϵ_ω	$(-0.43)^{-0.25}_{+0.16}$	$\widetilde{N}_\omega$	$1.10^{+0.17}_{-0.10}$
ϵ_ϕ	$(-0.42)^{-0.08}_{+0.06}$	$\widetilde{N}_\phi$	$1.03^{+0.05}_{-0.04}$

Table 2.5: The values of the parameter ϵ_V derived from the superconvergence relations, Eq. (2.25), and the normalisation constants of Eq. (2.23). Here, tiny imaginary parts in the normalisation constants have been neglected. The uncertainties refer to the variations of $\Gamma_{\rho'}$, $\Gamma_{\omega'}$, and $\Gamma_{\phi'}$, see Table 2.13, and are omitted in the subsequent analysis.

where $\lambda(x,y,z) = x^2+y^2+z^2-2xy-2xz-2yz$ is the KÄLLÉN function. Here, we disregard any distinction between the various charge channels and use the neutral masses for numerical evaluation. The dispersive ρ', ω', and ϕ' propagators and spectral functions are defined similarly to Eq. (2.16), with $s_{\text{thr}} = (M_V + M_P)^2$ for the thresholds. In analogy to Eq. (2.13), the dipole form factors read

$$\widetilde{\mathcal{F}}_{VP}(q^2) = \frac{C_{VP\gamma}}{\widetilde{N}_{V_i}}\big[(1-\epsilon_{V_i})M_{V_i}^2 P_{V_i}(q^2) + \epsilon_{V_i} M_{V_i'}^2 P_{V_i'}(q^2)\big], \tag{2.22}$$

where the simplifying assumption of constant widths for ω and ϕ propagators is always implicitly understood, with $P_{V_i'}(q^2) \in \{P_{V_i'}^{\text{BW}}(q^2), P_{V_i'}^{\text{disp}}(q^2)\}$. Here, we introduced the normalisation constants

$$\widetilde{N}_V = -\big[(1-\epsilon_V)M_V^2 P_V(0) + \epsilon_V M_{V'}^2 P_{V'}(0)\big], \tag{2.23}$$

which, once more, ensure $\widetilde{\mathcal{F}}_{VP}(0) = -C_{VP\gamma}$. The parameters ϵ_V have to be tuned differently in the dispersively improved variant, namely via the superconvergence relations

$$0 = (1-\epsilon_V)M_V^2 P_V^0 + \epsilon_V M_{V'}^2 P_{V'}^0, \tag{2.24}$$

$$P_V^0 = \begin{cases} 1\,, & V = \omega, \phi, \\ -\dfrac{1}{\pi}\displaystyle\int_{s_{\text{thr}}}^{\infty} \mathrm{d}x\, \mathrm{Im}\left[P_V^{\text{BW}}(x)\right], & V = \rho^{(\prime)}, \omega', \phi', \end{cases}$$

such that the terms of $\mathcal{O}(1/q^2)$ in the form factors cancel. We collect the numerical results for

$$\epsilon_V = \frac{M_V^2 P_V^0}{M_V^2 P_V^0 - M_{V'}^2 P_{V'}^0} \tag{2.25}$$

and $\widetilde{N}_V$ in Table 2.5, where we include the uncertainties due to the large errors on $\Gamma_{V'}$; in the following, their effect is, however, assumed to be insignificant and thus discarded.

2.5 Observables

The phenomenological analysis in this article will be performed in terms of doubly- and singly-differential decay widths as well as integrated branching ratios. We define $\nu = t - u$ for the MANDELSTAM variables t and u, in terms of which the twofold differential decay width $\mathrm{d}\Gamma \equiv \mathrm{d}\Gamma(\eta^{(\prime)} \to [\pi^0/\eta]\ell^+\ell^-)$ is given by [174]

$$\mathrm{d}\Gamma = \frac{1}{(2\pi)^3}\frac{1}{64 M_{\eta^{(\prime)}}^3}|\overline{\mathcal{M}}|^2 \mathrm{d}s\,\mathrm{d}\nu. \tag{2.26}$$

Here, $|\overline{\mathcal{M}}|^2$ is the spin-summed square of the amplitude, Eq. (2.4), and the integration region is bounded by the available phase space

$$\begin{aligned} &s \in [4m_\ell^2, (M_{\eta^{(\prime)}} - M_{\pi^0/\eta})^2], \\ &\nu \in [-\nu_{\max}, \nu_{\max}], \quad \nu_{\max} = \sigma(s)\sqrt{\lambda(s)}, \end{aligned} \tag{2.27}$$

	$C_\rho/\,\mathrm{GeV}^{-2}$	$C_\omega/\,\mathrm{GeV}^{-2}$	$C_\phi/\,\mathrm{GeV}^{-2}$
$\eta \to \pi^0\ell^+\ell^-$	1.16(11)	1.05(5)	0.0936(20)
$\eta' \to \pi^0\ell^+\ell^-$	0.95(8)	0.937(26)	−0.0965(25)
$\eta' \to \eta\ell^+\ell^-$	2.05(8)	0.180(9)	−0.492(10)

Table 2.6: Numerical values of the coupling constants defined in Eq. (2.30) for the different processes.

with

$$\sigma(s) = \sqrt{1 - \frac{4m_\ell^2}{s}}, \quad \lambda(s) \equiv \lambda(s, M_{\eta^{(\prime)}}^2, M_{\pi^0/\eta}^2). \tag{2.28}$$

The singly-differential decay width $\mathrm{d}\Gamma/\mathrm{d}s$ follows from an integration of Eq. (2.26) over ν and the branching ratio

$$\mathcal{B}(\eta^{(\prime)} \to [\pi^0/\eta]\ell^+\ell^-) = \frac{\Gamma}{\Gamma_{\eta^{(\prime)}}} \tag{2.29}$$

is obtained after performing the full three-body phase-space integration, *i.e.*, by also integrating over s.

In order to calculate $|\overline{\mathcal{M}}|^2$, we perform a PV decomposition of Eq. (2.4) with *FeynCalc* [220–222] after inserting explicit expressions for the form factors. For both the MP and DP model and in both variants CW and VW, this results in an expression of the generic form

$$\begin{aligned} \mathcal{M} &= 16\pi^2\alpha^2\big[\mathcal{M}_{\mathrm{QED}}^{uv}\mathcal{M}_{\mathrm{H}}^{uv} + \mathcal{M}_{\mathrm{QED}}^{u0v}\mathcal{M}_{\mathrm{H}}^{u0v}\big], \\ \mathcal{M}_{\mathrm{QED}}^{uv} &= m_\ell\,\bar{u}_s v_r, \quad \mathcal{M}_{\mathrm{QED}}^{u0v} = \bar{u}_s \not{p}_0 v_r, \\ \mathcal{M}_{\mathrm{H}}^{u(0)v} &= \sum_V C_V \mathcal{M}_V^{u(0)v}, \quad C_V = C_{V\eta^{(\prime)}\gamma} C_{V[\pi^0/\eta]\gamma}, \end{aligned} \tag{2.30}$$

where the quantities $\mathcal{M}_V^{u(0)v}$ account for the different vector-meson contributions in the result of the PV decomposition, *cf.* the sum in Eq. (2.4); they amount to cumbersome expressions containing PV functions.[#8] The numerical values of the process-specific coupling constants C_V are provided in Table 2.6. Upon squaring and spin-summing, the above amplitude leads to

$$\begin{aligned} |\overline{\mathcal{M}}|^2 = 256\pi^4\alpha^4\big[&C_\rho^2\,|\overline{\mathcal{M}}_{\rho,\rho}|^2 + C_\omega^2\,|\overline{\mathcal{M}}_{\omega,\omega}|^2 + C_\phi^2\,|\overline{\mathcal{M}}_{\phi,\phi}|^2 \\ &+ C_\rho C_\omega\,|\overline{\mathcal{M}}_{\rho,\omega}|^2 + C_\rho C_\phi\,|\overline{\mathcal{M}}_{\rho,\phi}|^2 + C_\omega C_\phi\,|\overline{\mathcal{M}}_{\omega,\phi}|^2\big], \end{aligned} \tag{2.31}$$

where we defined

$$\begin{aligned} |\overline{\mathcal{M}}_{V,V}|^2 &= |\overline{\mathcal{M}}_{\mathrm{QED}}^{uv}|^2|\mathcal{M}_V^{uv}|^2 + |\overline{\mathcal{M}}_{\mathrm{QED}}^{u0v}|^2|\mathcal{M}_V^{u0v}|^2 \quad + 2\,\overline{\mathcal{M}}_{\mathrm{QED}}^{uv,u0v}\mathrm{Re}\left[\mathcal{M}_V^{uv}\mathcal{M}_V^{u0v*}\right], \\ |\overline{\mathcal{M}}_{V_1,V_2}|^2 &= 2\,|\overline{\mathcal{M}}_{\mathrm{QED}}^{uv}|^2\mathrm{Re}\left[\mathcal{M}_{V_1}^{uv}\mathcal{M}_{V_2}^{uv*}\right] + 2\,|\overline{\mathcal{M}}_{\mathrm{QED}}^{u0v}|^2\mathrm{Re}\left[\mathcal{M}_{V_1}^{u0v}\mathcal{M}_{V_2}^{u0v*}\right] \\ &\quad + 2\,\overline{\mathcal{M}}_{\mathrm{QED}}^{uv,u0v}\mathrm{Re}\left[\mathcal{M}_{V_1}^{uv}\mathcal{M}_{V_2}^{u0v*} + \mathcal{M}_{V_1}^{u0v}\mathcal{M}_{V_2}^{uv*}\right] \end{aligned} \tag{2.32}$$

for $V_1 \neq V_2$, with

$$|\overline{\mathcal{M}}_{\mathrm{QED}}^{uv}|^2 = 2m_\ell^2(s - 4m_\ell^2), \qquad |\overline{\mathcal{M}}_{\mathrm{QED}}^{u0v}|^2 = \frac{1}{2}\big[\lambda(s) - \nu^2\big], \qquad \overline{\mathcal{M}}_{\mathrm{QED}}^{uv,u0v} = -2m_\ell^2\nu. \tag{2.33}$$

Similarly to the semileptonic decays, the branching ratio of the two-photon analogs is defined by

$$\mathcal{B}(\eta^{(\prime)} \to [\pi^0/\eta]\gamma\gamma) = \frac{\Gamma_\gamma}{\Gamma_{\eta^{(\prime)}}}, \tag{2.34}$$

[#8] These expressions are attached as supplemental materials to the published article [223].

where $\Gamma_\gamma \equiv \Gamma(\eta^{(\prime)} \to [\pi^0/\eta]\gamma\gamma)$ and

$$\mathrm{d}\Gamma_\gamma = \frac{1}{(2\pi)^3}\frac{(4\pi\alpha)^2}{64 M_{\eta^{(\prime)}}^3}|\overline{H}|^2 \mathrm{d}s\,\mathrm{d}\nu_\gamma, \tag{2.35}$$

with the phase space bounded by

$$s \in [0, (M_{\eta^{(\prime)}} - M_{\pi^0/\eta})^2], \quad \nu_\gamma \in [-\nu_\gamma^{\max}, \nu_\gamma^{\max}], \quad \nu_\gamma^{\max} = \sqrt{\lambda(s)}. \tag{2.36}$$

Due to the indistinguishability of the two photons in the final state, an additional factor of $1/2$ has to be taken into account upon integration. From Eq. (2.10), one finds the polarisation-summed amplitude squared

$$\begin{aligned}|\overline{H}|^2 = \frac{1}{8}\Bigg[&\sum_V C_V^2 \Big(\big|P_V(t_\gamma)\big|^2 |H^{t,t}|^2 + \big|P_V(u_\gamma)\big|^2 |H^{u,u}|^2 + 2\mathrm{Re}\left[P_V(t_\gamma)P_V^*(u_\gamma)\right]|H^{t,u}|^2\Big) \\ &+ \sum_{\{V_1,V_2\}} 2C_{V_1}C_{V_2}\Big(\mathrm{Re}\left[P_{V_1}(t_\gamma)P_{V_2}^*(t_\gamma)\right]|H^{t,t}|^2 \\ &+ \mathrm{Re}\left[P_{V_1}(u_\gamma)P_{V_2}^*(u_\gamma)\right]|H^{u,u}|^2 + \mathrm{Re}\left[P_{V_1}(t_\gamma)P_{V_2}^*(u_\gamma) + P_{V_1}(u_\gamma)P_{V_2}^*(t_\gamma)\right]|H^{t,u}|^2\Big)\Bigg],\end{aligned} \tag{2.37}$$

where the second sum extends over $\{V_1, V_2\} = \{\rho,\omega\}, \{\rho,\phi\}, \{\omega,\phi\}$ and we introduced

$$\begin{aligned}|H^{t,t}|^2 &= g^{\alpha_1\tilde{\alpha}_1} g^{\alpha_2\tilde{\alpha}_2} H^t_{\alpha_1\alpha_2} H^t_{\tilde{\alpha}_1\tilde{\alpha}_2}, \\ |H^{u,u}|^2 &= g^{\alpha_1\tilde{\alpha}_1} g^{\alpha_2\tilde{\alpha}_2} H^u_{\alpha_1\alpha_2} H^u_{\tilde{\alpha}_1\tilde{\alpha}_2}, \\ |H^{t,u}|^2 &= g^{\alpha_1\tilde{\alpha}_2} g^{\alpha_2\tilde{\alpha}_1} H^t_{\alpha_1\alpha_2} H^u_{\tilde{\alpha}_1\tilde{\alpha}_2}.\end{aligned} \tag{2.38}$$

As in Eq. (2.22), the propagators $P_V(x)$ are to be understood as BW propagators for all V in the CW approximation and BW propagators for $V = \omega, \phi$ but dispersively improved variants for $V = \rho$ in the variant VW. Inserting the kinematics of the process, these expressions simplify to

$$\begin{aligned}|H^{t,t}|^2 &= |H^0|^2 + t_\gamma^2(s^2 + u_\gamma^2), \\ |H^{u,u}|^2 &= |H^0|^2 + u_\gamma^2(s^2 + t_\gamma^2), \\ |H^{t,u}|^2 &= |H^0|^2 + t_\gamma u_\gamma(s^2 + t_\gamma u_\gamma),\end{aligned} \tag{2.39}$$

where we defined

$$\begin{aligned}|H^0|^2 = M_{\pi^0/\eta}^4\big(&s^2 + t_\gamma^2 + u_\gamma^2 + 2st_\gamma + 2su_\gamma + 4t_\gamma u_\gamma\big) \\ &- 2M_{\pi^0/\eta}^2 \Sigma_\gamma t_\gamma u_\gamma - 2M_{\pi^0/\eta}^6 \Sigma_\gamma + M_{\pi^0/\eta}^8.\end{aligned} \tag{2.40}$$

Finally, we consider the normalised semileptonic branching ratios

$$\widehat{\mathcal{B}}(\eta^{(\prime)} \to [\pi^0/\eta]\ell^+\ell^-) = \frac{\mathcal{B}(\eta^{(\prime)} \to [\pi^0/\eta]\ell^+\ell^-)}{\mathcal{B}(\eta^{(\prime)} \to [\pi^0/\eta]\gamma\gamma)}, \tag{2.41}$$

which are particularly useful from the theoretical point of view, since they reduce the effect of the uncertainties from the coupling constants.

We perform the phase-space integrations of the differential decay widths, Eq. (2.26) and Eq. (2.35), numerically with the *Cuhre* and *Vegas* algorithm from the *Cuba* library [224]. For the numerical evaluation of the PV functions contained in the quantities $\mathcal{M}_V^{u(0)v}$, see Eq. (2.30), we use *Collier* [157–160].[#9] The integration is carried out following the decomposition of Eqs. (2.31) and (2.37),

$$\begin{aligned}\Gamma_{(\gamma)} = &C_\rho^2 \Gamma^{(\gamma)}_{\rho,\rho} + C_\omega^2 \Gamma^{(\gamma)}_{\omega,\omega} + C_\phi^2 \Gamma^{(\gamma)}_{\phi,\phi} \\ &+ C_\rho C_\omega \Gamma^{(\gamma)}_{\rho,\omega} + C_\rho C_\phi \Gamma^{(\gamma)}_{\rho,\phi} + C_\omega C_\phi \Gamma^{(\gamma)}_{\omega,\phi}.\end{aligned} \tag{2.42}$$

[#9] A C++ interface to the native Fortran library *Collier* written for this purpose, including an executable demo file, is attached as supplemental material to the published article [223].

Numerical results for the auxiliary quantities $\Gamma^{(\gamma)}_{V_1,V_2}$ are listed in Appendix 2.9.2.[#10]

2.6 Scalar rescattering contributions

While there are good reasons to assume that the VMD model captures the most significant contributions to the semileptonic $\eta^{(\prime)}$ decays, we will assess scalar rescattering contributions explicitly by calculating them for the $\eta \to \pi^0\ell^+\ell^-$ channels. For the η' channels, the vector mesons have sufficient energy to go quasi on-shell, so that an even stronger dominance of the VMD mechanism is expected.

2.6.1 Isolating the *S*-wave in the hadronic sub-amplitude

With the decay $\eta \to \pi^0\ell^+\ell^-$ being driven by the two-photon intermediate state, as discussed in Ch. 1, the hadronic sub-process we consider is again $\eta \to \pi^0\gamma\gamma$. The corresponding sub-amplitude $H_{\lambda\lambda'}$, defined in Eq. (2.9), can be expressed in terms of the tensor amplitude $H_{\mu\nu}$ according to

$$e^{\mathrm{i}(\lambda-\lambda')\varphi} H_{\lambda\lambda'} = \epsilon^{*\mu}_{\lambda}(q_1)\epsilon^{*\nu}_{\lambda'}(q_2)\, H_{\mu\nu}. \tag{2.43}$$

In the following, we choose

$$\begin{aligned}\epsilon^{\mu}_{\pm}(q_1) &= \frac{1}{\sqrt{2}}(0, \mp 1, -\mathrm{i}, 0),\\ \epsilon^{\mu}_{\pm}(q_2) &= \frac{1}{\sqrt{2}}(0, \mp 1, \mathrm{i}, 0)\end{aligned} \tag{2.44}$$

as the explicit form for the polarisation vectors. In the context of the hadronic process $\eta \to \pi^0\gamma\gamma$, we use the MANDELSTAM variables s, t_γ, and u_γ as defined in Eq. (2.8). For on-shell photons, the tensor amplitude $H^{\mu\nu}$ can be written in terms of two independent tensor structures $T^{\mu\nu}_{1/2}$ [181],

$$\begin{aligned}T^{\mu\nu}_1 &= \frac{1}{2} s\, g^{\mu\nu} - q_2^\mu q_1^\nu,\\ T^{\mu\nu}_2 &= 2s\Delta^\mu\Delta^\nu + 4(q_1\Delta)(q_2\Delta)g^{\mu\nu}\\ &\quad - 4(q_2\Delta)\Delta^\mu q_1^\nu - 4(q_1\Delta)q_2^\mu\Delta^\nu,\end{aligned} \tag{2.45}$$

with $\Delta^\mu = (P + p_0)^\mu$, which manifestly fulfill the necessary WARD identities. The expansion of the tensor amplitude in this basis involves two scalar amplitudes A and B and reads

$$H^{\mu\nu} = A(s, t_\gamma)T^{\mu\nu}_1 + B(s, t_\gamma)T^{\mu\nu}_2. \tag{2.46}$$

Contracting the tensor amplitude (2.46) with the polarisation vectors gives an expression for the helicity amplitudes in terms of the scalar amplitudes,

$$\begin{aligned}H_{++}(s, t_\gamma) &= -\frac{s}{2}A(s, t_\gamma) - s\big[2(M_\eta^2 + M_{\pi^0}^2) - s\big]B(s, t_\gamma),\\ H_{+-}(s, t_\gamma) &= \big[(t_\gamma - u_\gamma)^2 - \lambda_{\pi^0\eta}(s)\big]B(s, t_\gamma).\end{aligned} \tag{2.47}$$

Here and in the following, we use the abbreviation

$$\lambda_{P_1P_2}(s) \equiv \lambda(s, M_{P_1}^2, M_{P_2}^2). \tag{2.48}$$

[#10] Using *LoopTools* [155] for the evaluation of the PV functions, we observed severe numerical instabilities for some integrations in the variant VW. These issues were most extreme in Γ_{V_1,V_2} with at least one $V_i = \phi$ for the decays $\eta^{(\prime)} \to \pi^0 e^+e^-$ but also notably problematic in $\Gamma_{\omega,\omega}$ for $\eta' \to \pi^0 e^+e^-$. They can be traced back to problems with the evaluation in certain regions of the phase space and might be related to vanishing GRAM determinants in the PV reduction procedure, but their exact origin remains obscure to us, in particular because a decomposition into coefficient functions does not improve this behaviour and the evaluation with *Collier* using scalar functions does not suffer from such instabilities.

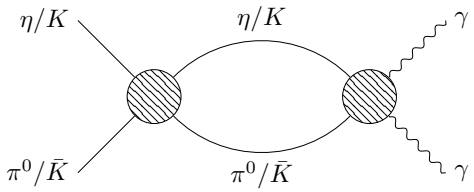

Figure 2.4: The two intermediate states $\pi^0\eta/K\bar{K}$ contributing to the two-photon amplitudes. The dispersive representation of those amplitudes is constructed in Ref. [181].

To isolate the S-wave, we will neglect D- and higher partial waves, including the whole H_{+-} contribution, since its partial-wave expansion starts with D-waves. Consequently, we are required to set the scalar amplitude B to zero, which leads to the S-wave contributing only through the tensor structure $T_1^{\mu\nu}$. Furthermore, setting B to zero allows us to use the S-wave amplitude $h_{++}^{L=0}$ to fix the scalar amplitude A via Eq. (2.47),

$$A^0(s) = -\frac{2}{s}\, h^0_{++}(s). \tag{2.49}$$

Note that the $(++)$ helicity amplitude has a soft-photon zero at $s = 0$, such that $A^0(s)$ has no singularity at that point despite the factor $1/s$.

2.6.2 Rescattering effects in the hadronic sub-process

In Ref. [181], the rescattering effects in $\eta \to \pi^0\gamma\gamma$ are described by means of a coupled-channel analysis, taking into account $\pi^0\eta$ and $K\bar{K}$ intermediate states; *cf.* Fig. 2.4. Using the Omnès matrix $\Omega(s)$ for the $\pi^0\eta/(K\bar{K})_{I=1}$ system constructed therein, one can write a dispersive representation for the S-wave amplitudes,

$$\begin{aligned}\begin{pmatrix} h^0_{++}(s) \\ k^0_{1,++}(s) \end{pmatrix} = \Omega(s)\Bigg\{ \begin{pmatrix} a \\ b \end{pmatrix} s + \frac{s^2}{\pi}\Bigg(\sum_V \int_{-\infty}^{s_V} \mathrm{d}z\, \frac{\Omega^{-1}(z)}{z^2(z-s)}\, \mathrm{Im} \begin{pmatrix} h^{0,V}_{++}(z) \\ k^{0,V}_{++}(z) \end{pmatrix} \\ - \int_{s_{\pi\eta}}^{\infty} \mathrm{d}z\, \frac{\mathrm{Im}\left(\Omega^{-1}(z)\right)}{z^2(z-s)} \begin{pmatrix} 0 \\ k^{0,\mathrm{Born}}_{1,++}(z) \end{pmatrix} \Bigg) \Bigg\},\end{aligned} \tag{2.50}$$

with $s_{\pi\eta} = (M_\eta + M_{\pi^0})^2$ the threshold for the $\pi^0\eta$ intermediate state and

$$s_V = -\frac{1}{M_V^2}\left(M_V^2 - M_\eta^2\right)\left(M_V^2 - M_{\pi^0}^2\right) \tag{2.51}$$

the onset of the left-hand cut. Here, we include the VMD contributions from the ρ, ω, and ϕ mesons for the $\pi^0\eta$ channel ($h^{0,V}_{++}$) and the K^* for the $K\bar{K}$ channel ($k^{0,V}_{++}$) in the zero-width approximation. Using the polarisation vectors (2.44) and the coupling constants C_V defined in Eq. (2.30), the VMD amplitude for the $\pi^0\eta$ channel for photons with polarisation $(++)$ as well as the corresponding S-wave amplitude are given by

$$\begin{aligned} H^V_{++}(s,t_\gamma) &= \frac{C_V}{4}\frac{s t_\gamma}{M_V^2 - t_\gamma - \mathrm{i}\epsilon} + (t_\gamma \leftrightarrow u_\gamma), \\ h^{0,V}_{++}(s) &= \frac{C_V}{2}\left(\frac{s M_V^2}{\lambda^{1/2}_{\pi^0\eta}(s)} \log\left[\frac{X_V(s)+1}{X_V(s)-1}\right] - s\right), \\ X_V(s) &= \frac{2M_V^2 - (M_\eta^2 + M_{\pi^0}^2) + s}{\lambda^{1/2}_{\pi^0\eta}(s)}\,. \end{aligned} \tag{2.52}$$

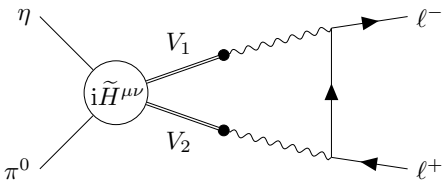

Figure 2.5: The triangle loop contributing to $\pi^0\eta \to \ell^+\ell^-$, which contains the tensor amplitude $\widetilde{H}^{\mu\nu}$ that captures the rescattering effects in $\pi^0\eta \to \gamma\gamma$, with the photon virtualities modeled via vector-meson propagators. This process is related to the corresponding η decay via crossing symmetry.

The logarithm in Eq. (2.52) induces the left-hand cut starting from s_V. The VMD contribution to the $K\bar{K}$ channel, K^V_{++}, can be treated in complete analogy. In the $K\bar{K}$ channel, the QED BORN term projected onto isospin $I = 1$ is included in addition,

$$K^{\mathrm{Born}}_{1,++}(s,t_\gamma) = \frac{\sqrt{2}\,s\,M_K^2}{(t_\gamma - M_K^2)(u_\gamma - M_K^2)},$$
$$k^{0,\mathrm{Born}}_{1,++}(s) = \frac{2\sqrt{2}M_K^2}{s\,\sigma_K(s)}\log\left[\frac{1+\sigma_K(s)}{1-\sigma_K(s)}\right], \tag{2.53}$$

with $\sigma_K(s) \equiv \sqrt{1-4M_K^2/s}$. In Eq. (2.50), the soft-photon zero is already taken care of; the remaining subtraction constants a and b are determined in accordance with Ref. [181], where an ADLER zero at $s_A = M_\eta^2$ is implemented to fix one of these and the other one is fit to experimental data.

Subtracting the VMD contributions (2.52) from the complete S-wave amplitude h^0_{++} (2.50) allows us to isolate the rescattering effects in Eq. (2.49),

$$A^0_{\mathrm{resc}}(s) = -\frac{2}{s}\left(h^0_{++}(s) - \sum_{V=\rho,\omega,\phi} h^{0,V}_{++}(s)\right). \tag{2.54}$$

With this, we can now construct the S-wave tensor amplitude containing only the rescattering contributions,

$$\widetilde{H}^{\mu\nu} = A^0_{\mathrm{resc}}(s)\,T_1^{\mu\nu}. \tag{2.55}$$

2.6.3 Loop calculation

In order to calculate the contribution of S-wave rescattering effects to the decay $\eta \to \pi^0\ell^+\ell^-$, we retain the tensor amplitude (2.55) for the $\eta \to \pi^0\gamma\gamma$ vertex. This reduces the loop from a box to a triangle topology; see Fig. 2.5. We denote the tensor QED sub-amplitude for $\gamma\gamma \to \ell^+\ell^-$ by $L^{\mu\nu}$. At tree level, the construction is straightforward, and after simplifying with Eq. (2.6), one finds

$$L^{\mu\nu} = -\bar{u}_s\frac{2p_-^\mu - \gamma^\mu \not{q}_1}{(p_- - q_1)^2 - m_\ell^2 + \mathrm{i}\epsilon}\gamma^\nu v_r. \tag{2.56}$$

Note that we do not have to concern ourselves with calculating the S-wave projection of the QED sub-amplitude $\gamma^*\gamma^* \to \ell^+\ell^-$, since the loop integration will take care of the projection automatically. Furthermore, to avoid double counting, we do not include the crossed channel, which is described by the same amplitude due to the symmetry of the triangle loop.

When taking into account the photon virtualities, the gauge-invariant tensor structure $T_1^{\mu\nu}$, in particular, acquires additional terms [225–227],

$$T_1^{\mu\nu}(q_1^2,q_2^2) = \frac{1}{2}\big(s - q_1^2 - q_2^2\big)g^{\mu\nu} - q_2^\mu q_1^\nu. \tag{2.57}$$

The impact of the photon virtualities is then further modeled by including factors $M_V^2 P_V^{\mathrm{BW}}(q^2)$ for both photons, resulting in a hadronic tensor amplitude for off-shell photons on the basis of the on-shell one,

$$\begin{aligned}\widetilde{H}^{\mu\nu}(q_1^2, q_2^2) = M_{V_1}^2 P_{V_1}^{\mathrm{BW}}(q_1^2) M_{V_2}^2 P_{V_2}^{\mathrm{BW}}(q_2^2) \\ \times A_{\mathrm{resc}}^0(s) T_1^{\mu\nu}(q_1^2, q_2^2).\end{aligned} \tag{2.58}$$

This is a naive generalisation to virtual photons that corresponds to a scalar-resonance approximation. It avoids the known complications, *e.g.*, from the modified partial-wave projections of the VMD amplitudes; see Refs. [228, 229] for a more rigorous treatment. We deem this approximation sufficient in the context of the semileptonic decays. The prescription in Eq. (2.58) is consistent with the monopole model for the form factors constructed in Sec. 2.4.

The rescattering contribution to the $\eta \to \pi^0 \ell^+ \ell^-$ amplitude is then given by

$$\mathrm{i}\,\widetilde{\mathcal{M}}(s) = \left(\frac{\alpha}{\pi}\right)^2 \int \mathrm{d}^4 q_1 \, \frac{\widetilde{H}^{\mu\nu}(q_1^2, q_2^2)}{q_1^2 + \mathrm{i}\epsilon} \frac{L_{\mu\nu}}{q_2^2 + \mathrm{i}\epsilon}, \tag{2.59}$$

with $q_2 = p_+ + p_- - q_1$.

Understanding the S-wave amplitude as an enhancement due to the $a_0(980)$ resonance with $I^G(J^{PC}) = 1^-(0^{++})$, only the combination of ρ and ω is allowed for the vector mesons V_1 and V_2. With that, the S-wave rescattering contribution is given by

$$\begin{aligned}\widetilde{\mathcal{M}}(s) = -\mathrm{i} \left(\frac{\alpha}{\pi}\right)^2 M_\rho^2 M_\omega^2 A_{\mathrm{resc}}^0(s) \\ \times \int \mathrm{d}^4 q_1 \, P_\rho^{\mathrm{BW}}(q_1^2) \, P_\omega^{\mathrm{BW}}(q_2^2) \, \frac{T_1^{\mu\nu}(q_1^2, q_2^2) \, L_{\mu\nu}}{(q_1^2 + \mathrm{i}\epsilon)(q_2^2 + \mathrm{i}\epsilon)}.\end{aligned} \tag{2.60}$$

Note that with $T_1^{\mu\nu} \propto \mathcal{O}(q_1^2)$, the integral is convergent only due to the dependence on the photon virtualities introduced in Eq. (2.58). This is a consequence of the reduction from a box to a triangle loop. Contracting the tensor structures and performing a PV decomposition allows us to separate a factor of $m_\ell s/(M_\rho^2 M_\omega^2)$ with only the $\bar{u}_s v_r$ spinor structure from Eq. (2.30) contributing,

$$\widetilde{\mathcal{M}}(s) = \mathrm{i}\,(4\pi\alpha)^2 s \, A_{\mathrm{resc}}^0(s) \widetilde{\mathcal{M}}_{\mathrm{H}}^{uv}(s) \mathcal{M}_{\mathrm{QED}}^{uv}. \tag{2.61}$$

Here, $\widetilde{\mathcal{M}}_{\mathrm{H}}^{uv}(s)$ contains the remaining PV master integrals.

2.7 Results and discussion

We present the results for the semileptonic decays in the form of branching ratios as well as singly- and doubly-differential decay widths. The branching ratios are particularly apt to demonstrate the effects of the different form-factor models. Furthermore, we examine the contribution of scalar rescattering effects to the branching ratios and normalise these to the corresponding two-photon analogs. For all of our results, the quoted uncertainties stem from the experimental uncertainties that enter via the coupling constants and amount to $\sim 10\%$. The uncertainties from the numerical integration, on the other hand, are at least one order of magnitude smaller and therefore omitted.

2.7.1 Differential decay widths

The doubly- and singly-differential distributions of the semileptonic decays exhibit distinct characteristics, with the most prominent differences being observable between the decays with electrons and muons in the final state; see Figs. 2.6–2.8. While the majority of the doubly-differential distribution for the electron channels is contained in a small fraction close to the threshold in the invariant

lepton mass, the decays with muons in the final state display a spread-out distribution that covers large parts of the available phase space. For the electron final state, in particular, it is important to take account of the region close to the threshold in the invariant lepton mass both when integrating over the phase space and when performing a measurement, as significant parts of the decay width are readily missed otherwise. Furthermore, the logarithmic scale shows that the distributions possess a minimum for $\nu = 0$, where $\nu \propto \cos\theta_s$, with θ_s the s-channel scattering angle. With only even partial waves contributing to the decays, this feature can be attributed to the dominance of D-waves over the helicity-suppressed S-waves—which do not show such an angular distribution—whereas for the muon channels, this suppression is less pronounced. Beyond the difference in the final-state leptons, the principal visible differentiations concern the size of the phase space, which is significantly larger for $\eta' \to \pi^0\ell^+\ell^-$ than for $\eta \to \pi^0\ell^+\ell^-$ and $\eta' \to \eta\ell^+\ell^-$.

For all decay channels, the obtained DALITZ plots do not follow a flat distribution, which was assumed for the experimental analysis of $\eta \to \pi^0 e^+e^-$ in Ref. [151]. This assumption is justified for a potential C-violating contribution [164] but inaccurate for the standard-model result; we therefore propose a reevaluation of the experimental data and a reassessment of the reported upper limit.

The singly-differential distributions for the electron channels explicitly resolve a strongly peaked structure for invariant lepton masses close to the threshold and a subsequent rapid decrease. For muons in the final state, the singly-differential distribution is much different, with a broad peak that is situated more centrally in the phase space. This behaviour is in correspondence with the observation that for $m_\ell \approx 0$, the threshold in s approximately collapses to the threshold of the two-photon intermediate state, $s = 0$, where the two-photon cut induces a behaviour $\propto \log(s)$ [171]. Hence, for the electron final state, this logarithmic divergence manifests itself as a peak close to the threshold in s, regularised by a phase-space factor and forced to zero at $s = 4m_\ell^2$, see Eq. (2.27), whereas the muon channels have a much higher threshold, far from the logarithmic divergence.

2.7.2 Branching ratios in the different models

The sensitivity of the semileptonic decays to the different form-factor parameterisations, *i.e.*, a point-like, monopole, or dipole interaction, each with constant or energy-dependent widths, can be probed by comparing the results for the branching ratios collected in Table 2.7.

Our results for the decays $\eta \to \pi^0\ell^+\ell^-$ obtained with constant form factors and widths are compatible with the results of Ref. [154], which similarly assumed a point-like interaction. Instead of determining the coupling constants purely from phenomenology, the authors modeled these using a symmetry-driven quark model, which results in only slightly different numerical values. For the η' decays, on the other hand, we find significant disagreement, which might be due to numerical difficulties when calculating the box diagrams in a non-automated way via FEYNMAN parameters.

Implementing non-trivial form factors leads to a significant decrease of the branching ratio for all decays, with the muon channels being subject to a larger reduction than the electron channels and the η' decays to less reduction than the η decays. More specifically, the decrease amounts to $\sim 35\%$ for $\eta \to \pi^0 e^+e^-$ and $\sim 50\%$ for $\eta \to \pi^0\mu^+\mu^-$. For $\eta' \to \pi^0\ell^+\ell^-$, the branching ratios are reduced by $\sim 20\%$ for electrons and $\sim 35\%$ for muons in the final state. Regarding $\eta' \to \eta\ell^+\ell^-$, the branching ratios decrease by $\sim 10\%$ for electrons and $\sim 25\%$ for muons in the final state. This gives strong indication that the photon virtualities cannot be neglected in the analysed processes, since constant form factors are likely to overestimate the decay widths.

The dipole form factors, which feature the expected high-energy behaviour $\sim 1/q^4$, further assess the sensitivity on the precise parameterisation of the form factors. Compared to the variation observed between constant form factors and the monopole parameterisation, their effect is, however, negligible, leading to a further decrease for $\eta \to \pi^0\ell^+\ell^-$, $\eta' \to \pi^0\mu^+\mu^-$, and $\eta' \to \eta\mu^+\mu^-$ and a slight increase for $\eta' \to \pi^0 e^+e^-$ and $\eta' \to \eta e^+e^-$, both at most at the level of 5%.

Using spectral representations to implement energy-dependent widths for the broad vector mesons, *i.e.*, $\rho^{(\prime)}$, ω', and ϕ', leads to a decrease in the branching ratio of less than 4% for all decays with constant form factors and an increase of not more than 8% both in the monopole and dipole models,

		Branching ratio/10^{-9}			
		PL	MP	DP	Ref. [154]
$\eta \to \pi^0 e^+ e^-$	CW	2.10(23)	1.35(15)	1.33(15)	2.0(2)
	VW	2.06(22)	1.40(15)	1.36(15)	
$\eta \to \pi^0 \mu^+ \mu^-$	CW	1.37(15)	0.70(8)	0.66(7)	1.1(2)
	VW	1.32(14)	0.71(8)	0.67(7)	
$\eta' \to \pi^0 e^+ e^-$	CW	3.82(33)	3.08(27)	3.14(27)	4.5(6)
	VW	3.81(33)	3.30(28)	3.30(28)	
$\eta' \to \pi^0 \mu^+ \mu^-$	CW	2.57(23)	1.69(15)	1.68(15)	1.7(3)
	VW	2.53(23)	1.81(16)	1.81(16)	
$\eta' \to \eta e^+ e^-$	CW	0.53(4)	0.48(4)	0.49(4)	0.4(2)
	VW	0.51(4)	0.50(4)	0.50(4)	
$\eta' \to \eta \mu^+ \mu^-$	CW	0.287(26)	0.213(18)	0.207(18)	0.15(5)
	VW	0.280(25)	0.225(20)	0.240(21)	

Table 2.7: The branching ratios of the semileptonic decays, Eq. (2.29), resulting for the models PL, MP, and DP in both variants CW and VW. The uncertainty is entirely due to the dominant experimental uncertainty of $|\mathcal{F}_{VP}(0)|$; see Table 2.2. For reference, we also give the corresponding results from Ref. [154], where we added the quoted uncertainties in quadrature.

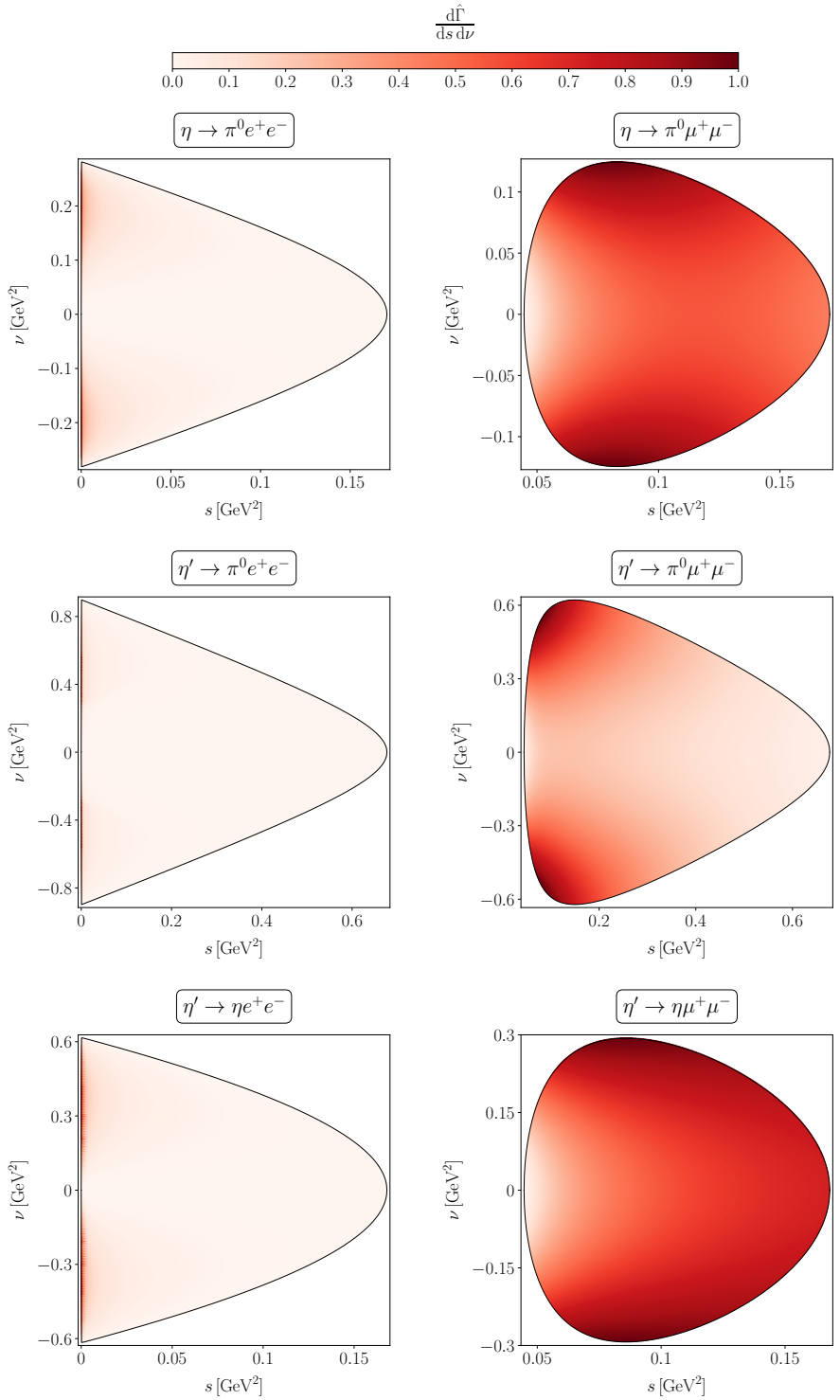

Figure 2.6: DALITZ plots for the MP model in the variant CW, normalised to the maximum value within the available phase space of the respective channel, $\mathrm{d}\hat{\Gamma}/\mathrm{d}s\,\mathrm{d}\nu = [\mathrm{d}\Gamma/\mathrm{d}s\,\mathrm{d}\nu]/[\max \mathrm{d}\Gamma/\mathrm{d}s\,\mathrm{d}\nu]$.

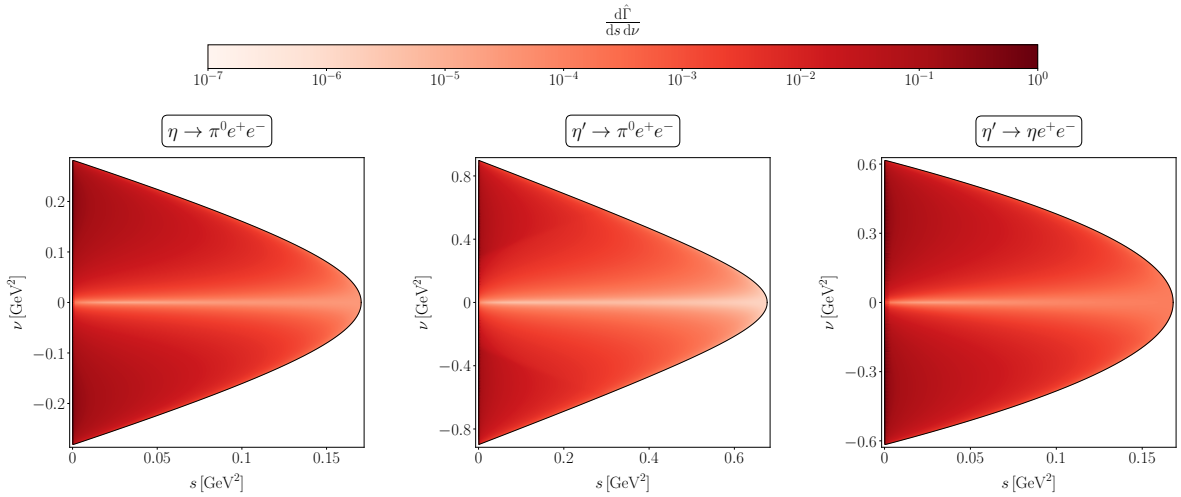

Figure 2.7: Logarithmic Dalitz plots for the electron channels with the MP model in the variant CW, normalised to the respective maximum value within the available phase space; see Fig. 2.6.

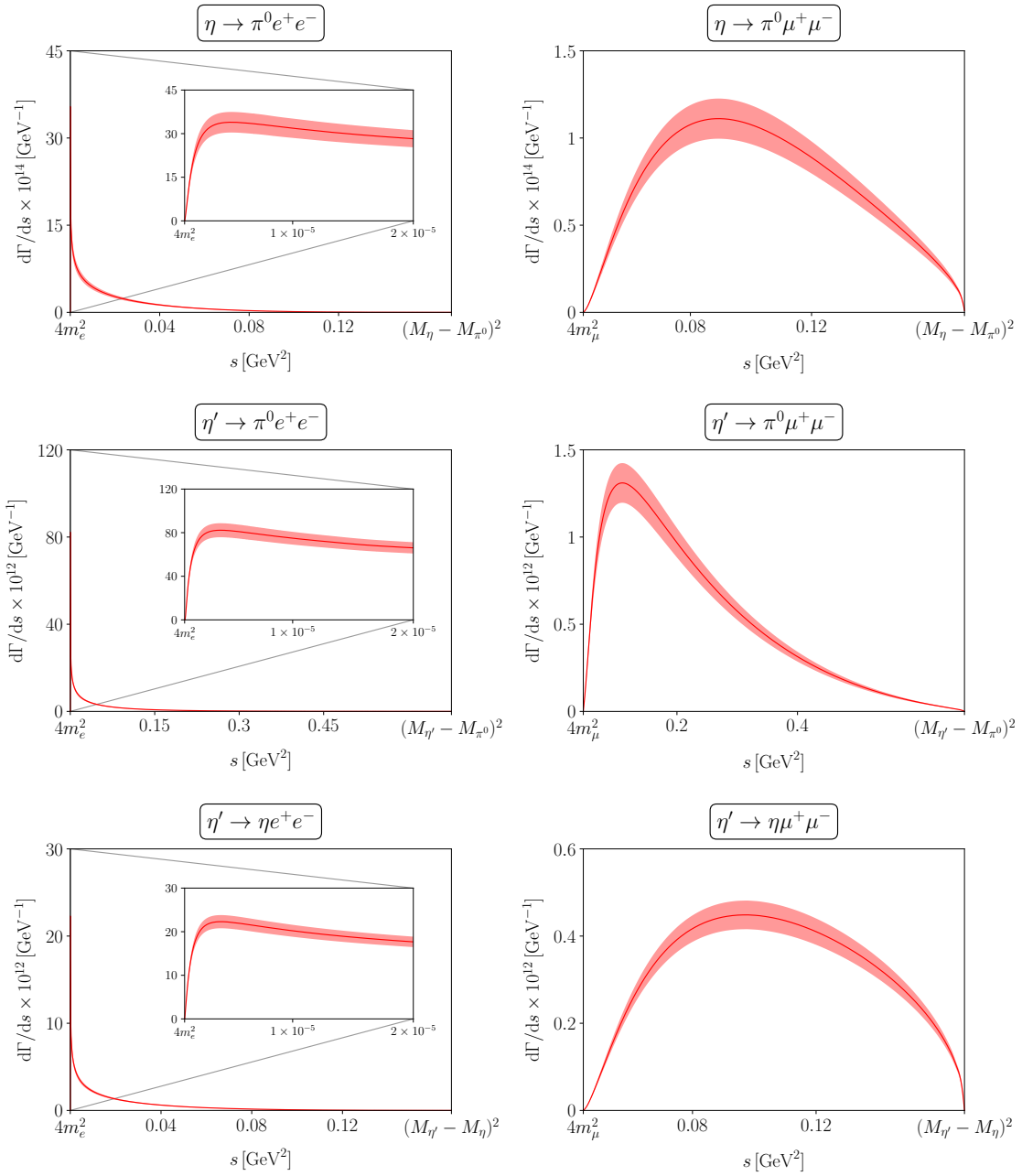

Figure 2.8: Singly-differential decay widths in the MANDELSTAM variable s, obtained with the MP model in the variant CW. Here, the inlays amplify the behaviour close to the lower threshold of the phase space, where the distribution shows a strong peak for the channels with electrons in the final state. The uncertainty is entirely due to the dominant phenomenological uncertainty of $|\mathcal{F}_{VP}(0)|$; see Table 2.2.

	Branching ratio		
	VMD	rescattering	mixed
$\eta \to \pi^0 e^+ e^-$	$1.36(15) \times 10^{-9}$	2.5×10^{-13}	4.6×10^{-13}
$\eta \to \pi^0 \mu^+ \mu^-$	$0.67(7) \times 10^{-9}$	2.8×10^{-11}	-2.6×10^{-11}

Table 2.8: The scalar rescattering contributions to the branching ratios of $\eta \to \pi^0 \ell^+ \ell^-$, Eq. (2.62), separated into the pure rescattering and mixed term, as well as the corresponding VMD contributions from Table 2.7 for comparison.

with the exception of $\eta' \to \eta \mu^+ \mu^-$, where the increase even reaches $\sim 15\%$.

All these variations are small compared to the difference between the results in the PL model and any other model and mostly even small compared to the phenomenological uncertainties. We thus infer the semileptonic decays to be rather insensitive to the precise parameterisation of the photon virtualities in the form factors. Therefore, we restricted our discussion of the Dalitz and singly-differential plots in Sec. 2.7.1 to the monopole model, as finer details would not be discernible.

2.7.3 Scalar rescattering contributions

We have calculated the S-wave rescattering contributions exemplarily for the $\eta \to \pi^0 \ell^+ \ell^-$ decay channels. Adding these to the VMD amplitude leads to two additional terms on the level of the squared amplitude in the branching ratio: one pure rescattering term and one term mixing rescattering and VMD effects,

$$|\mathcal{M} + \widetilde{\mathcal{M}}|^2 = |\mathcal{M}|^2 + |\widetilde{\mathcal{M}}|^2 + 2\mathrm{Re}\left(\mathcal{M}\widetilde{\mathcal{M}}^*\right). \tag{2.62}$$

The two contributions to the branching ratios can be found in Table 2.8. For $\eta \to \pi^0 e^+ e^-$, both the rescattering and the mixed contribution are of $\mathcal{O}(10^{-4})$ compared to the VMD result. This seems plausible, given that a spin flip is necessary to couple a scalar resonance to two leptons, resulting in an amplitude proportional to m_ℓ. For $\eta \to \pi^0 \mu^+ \mu^-$, the rescattering and mixed contributions are at the level of 5% in comparison to the VMD contributions, still notably below the uncertainties of the latter. In addition, the two contributions have opposite signs, such that they largely cancel, leading to a suppression of $\mathcal{O}(10^{-3})$. In light of the negligible contributions of the rescattering effects, we consider it unnecessary to calculate errors on them. Apart from the impact of the uncertainties on the coupling constants C_V within the dispersive integral in Eq. (2.50), such a calculation would also have to take into account the uncertainties from fixing the subtraction constants as estimated in Ref. [181].

A similar order of magnitude is expected for the respective corrections to the other decay channels $\eta' \to [\pi^0/\eta]\ell^+\ell^-$, an explicit demonstration of which is, however, beyond the scope of this article.

2.7.4 Photonic decays and normalised branching ratios

The primary motivation for calculating the branching ratios for the two-photon decays $\eta^{(\prime)} \to [\pi^0/\eta]\gamma\gamma$ within our VMD framework is the normalisation (2.41) of the corresponding semileptonic decays. Numerical results for these are collected in Table 2.9 and Table 2.10, respectively. Currently, however, there is also thriving interest in resolving a discrepancy arising from an updated experimental measurement of the $\eta \to \pi^0\gamma\gamma$ decay [230]. The effect of implementing dispersively improved ρ propagators amounts to less than 2% and is therefore insignificant, as the phenomenological uncertainties range between (6–11)%.

Our branching ratios with constant widths are in agreement with the VMD results of Ref. [182]; supplementing those with a linear-σ-model scalar contribution and chiral loops, the authors quote $\mathcal{B}(\eta \to \pi^0\gamma\gamma) = 1.35(8) \times 10^{-4}$, $\mathcal{B}(\eta' \to \pi^0\gamma\gamma) = 2.91(21) \times 10^{-3}$, and $\mathcal{B}(\eta' \to \eta\gamma\gamma) = 1.17(8) \times 10^{-4}$

	Branching ratio/10^{-4}	
	CW	VW
$\eta \to \pi^0\gamma\gamma$	1.21(13)	1.18(13)
$\eta' \to \pi^0\gamma\gamma$	27.8(1.7)	28.1(1.8)
$\eta' \to \eta\gamma\gamma$	1.10(8)	1.10(8)

Table 2.9: The branching ratios of the two-photon decays, Eq. (2.34), in both variants CW and VW. The uncertainty is entirely due to the dominant experimental uncertainty of $|\mathcal{F}_{VP}(0)|$; see Table 2.2.

		Normalised branching ratio/10^{-6}		
		PL	MP	DP
$\eta \to \pi^0 e^+e^-$	CW	17.422(28)	11.197(11)	11.032(9)
	VW	17.510(20)	11.855(7)	11.531(4)
$\eta \to \pi^0 \mu^+\mu^-$	CW	11.371(20)	5.781(7)	5.450(6)
	VW	11.197(25)	6.020(10)	5.647(5)
$\eta' \to \pi^0 e^+e^-$	CW	1.37(7)	1.11(6)	1.13(6)
	VW	1.36(7)	1.17(6)	1.18(6)
$\eta' \to \pi^0 \mu^+\mu^-$	CW	0.92(5)	0.610(35)	0.603(35)
	VW	0.90(5)	0.64(4)	0.65(4)
$\eta' \to \eta e^+e^-$	CW	4.77(7)	4.38(6)	4.41(6)
	VW	4.65(7)	4.56(7)	4.56(7)
$\eta' \to \eta \mu^+\mu^-$	CW	2.60(6)	1.93(4)	1.88(4)
	VW	2.54(5)	2.05(4)	2.18(4)

Table 2.10: The same as Table 2.7 but for the normalised branching ratios of the semileptonic decays, Eq. (2.41). Due to partial cancellations in this ratio, the quoted uncertainties are given with the caveat that they are likely to underestimate the genuine uncertainty; see main text.

based on empirical couplings. These results are slightly larger than the plain VMD numbers but still compatible within uncertainties, indicating that the effects of these model extensions are insignificant at the current level of precision [182].

The dispersive analysis of $\eta \to \pi^0\gamma\gamma$ [181] referenced in Sec. 2.6 also includes the $a_2 \equiv a_2(1320)$ tensor resonance as well as isospin-breaking $\pi^+\pi^-$ contributions, with the result $\mathcal{B}(\eta \to \pi^0\gamma\gamma) = 1.81^{+0.46}_{-0.33} \times 10^{-4}$ showing a $\sim 50\%$ discrepancy with the VMD model. This deviation can be traced back largely to the a_2 contribution, suggesting that the impact of this resonance might be relevant for $\eta \to \pi^0\gamma\gamma$, specifically at very low diphoton invariant masses.

In light of this finding, it is important to note that we have not included any tensor-meson effects for $\eta \to \pi^0\ell^+\ell^-$ in Sec. 2.6. For electrons in the final state, the lower threshold in s is close to the two-photon threshold, so that an effect of similar size as in the photonic case is within the bounds of possibility; the higher threshold for muons, on the other hand, is expected to exclude the region where the a_2 resonance is most relevant. For the η' decays, the exchanged vector mesons can go quasi on-shell, so that the VMD mechanism is even more likely to dominate the effect of the tensor resonance.

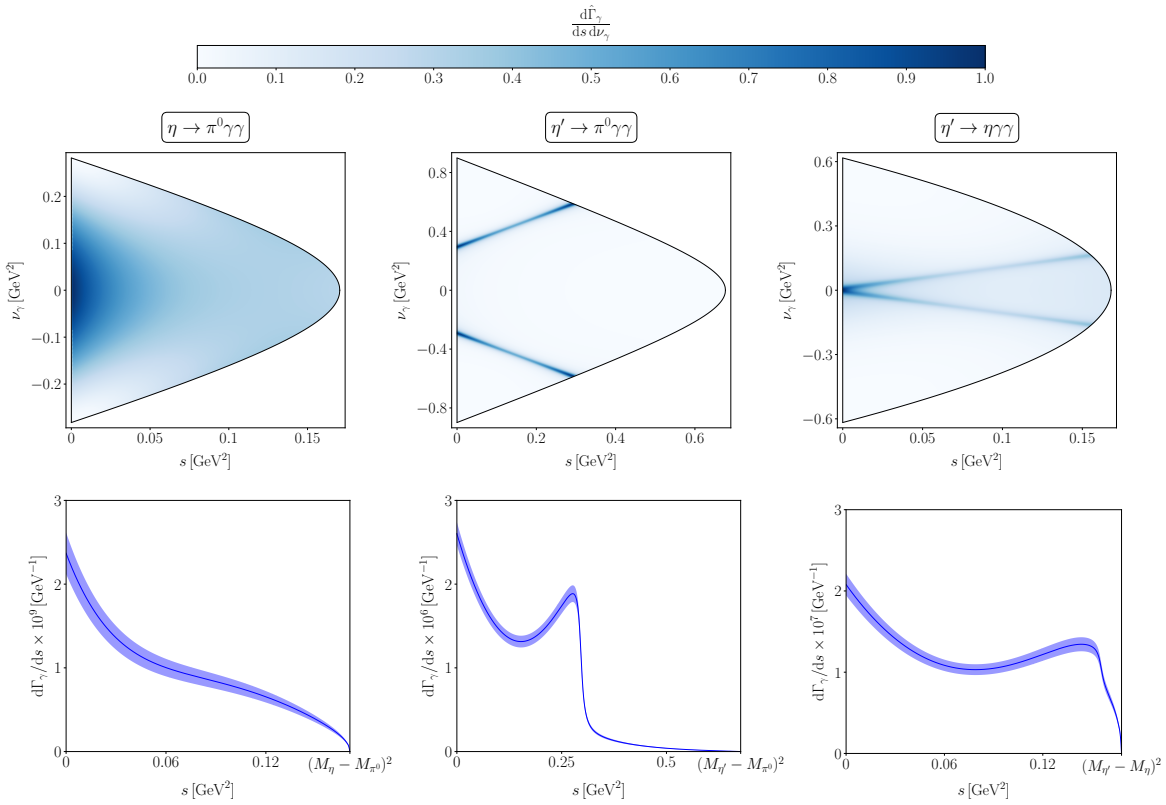

Figure 2.9: Dalitz plots for the two-photon decays in the variant CW (*top*), normalised to the maximum value within the available phase space of the respective channel, $\mathrm{d}\hat{\Gamma}_\gamma/\mathrm{d}s\,\mathrm{d}\nu_\gamma = [\mathrm{d}\Gamma_\gamma/\mathrm{d}s\,\mathrm{d}\nu_\gamma]/[\max \mathrm{d}\Gamma_\gamma/\mathrm{d}s\,\mathrm{d}\nu_\gamma]$, and singly-differential decay widths in the Mandelstam variable s, obtained in the variant CW (*bottom*).

While our results for the two-photon decays of the η' meson are compatible with the experimental results from BESIII, $\mathcal{B}(\eta' \to \pi^0\gamma\gamma) = 3.20(24)\times10^{-3}$ [231] and $\mathcal{B}(\eta' \to \eta\gamma\gamma) = 8.3(3.4)\times10^{-5}$ [232],[#11] the experimental situation for $\eta \to \pi^0\gamma\gamma$ is presently inconclusive. For this decay, the PDG average $\mathcal{B}(\eta \to \pi^0\gamma\gamma) = 2.55(22) \times 10^{-4}$ [174]—the main input being $\mathcal{B}(\eta \to \pi^0\gamma\gamma) = 2.52(23) \times 10^{-4}$ from the A2 experiment at MAMI [177]—is in agreement with the theoretical calculation performed in Ref. [181] but in severe tension with the preliminary result from the KLOE-2 collaboration, $\mathcal{B}(\eta \to \pi^0\gamma\gamma) = 0.99(26) \times 10^{-4}$ [230], which corroborates the older KLOE measurement $\mathcal{B}(\eta \to \pi^0\gamma\gamma) = 0.84(30) \times 10^{-4}$ [233] and is consistent with the VMD-only result.

The results for the normalised branching ratio can be found in Table 2.10, and the discussion of the differences between the distinct form-factor parameterisations is analogous to Sec. 2.7.2. Due to partial cancellations in this ratio, the quoted uncertainties are reduced drastically, however with the caveat that they are likely to underestimate the genuine uncertainty, lest some neglected systematic effect beyond the error estimates of the couplings potentially becomes dominant here. At the same time, potential corrections to the semileptonic branching ratios that are not included in the plain VMD model, *e.g.*, the a_2 resonance, are assumed to partially cancel as well because they emerge in the hadronic part of the amplitudes that is shared with the photonic decays.

The doubly- and singly-differential decay widths for the two-photon decays are displayed in Fig. 2.9.

[#11] Here and in the following, we combine statistical and systematic uncertainties of experimental branching ratios in quadrature for simplicity.

While the η decay does not show much structure in either plot—being dominated by a D-wave at low and an S-wave at high diphoton invariant masses—the η' decays are dominated by vector-meson resonances that can go quasi on-shell. The ω resonance is clearly visible as two narrow bands in the DALITZ plots and as a peak in the singly-differential distributions, whereas the ρ is disguised in comparison due to its much larger width. The angular dependence perceivable as a less saturated band in the DALITZ plots and as a dip in the singly-differential distributions can be attributed to the fact that the $\omega \to [\pi^0/\eta]\gamma$ decay must be in a P-wave due to parity.

2.8 Summary

We have reanalysed the standard-model contribution to the semileptonic decays $\eta^{(\prime)} \to \pi^0\ell^+\ell^-$ and $\eta' \to \eta\ell^+\ell^-$, where $\ell = e, \mu$. Since C parity is conserved in the strong and electromagnetic interactions, these processes are mediated via a two-photon mechanism and therefore loop-induced. This two-photon mechanism is known to be dominated by vector exchanges; as a major improvement compared to the existing literature, we have, for the first time, implemented a realistic dependence of the hadronic sub-process on the photon virtualities via vector-to-pseudoscalar transition form factors. To assess the sensitivity to the chosen parameterisations, we compared three different schemes: constant couplings (as a reference point), monopole form factors, and dipole form factors. The last of those three are motivated by having the correct asymptotic behaviour at high virtualities. In addition, dispersively improved variants of all form factors have been probed. Non-trivial form factors turn out to be important in order not to overestimate the branching ratios. We thereby improve previous theoretical results for the semileptonic $\eta^{(\prime)}$ decays. On the other hand, the observables are mostly insensitive to the details of the parameterisation at the level of uncertainty induced by the phenomenological coupling constants.

All predicted branching ratios are, as expected, well below the current experimental upper limits. For the latter, we however recommend a reanalysis, given the far-from-flat DALITZ-plot distributions of the standard-model contributions. With improved experimental sensitivities in the future, our theoretical branching ratios of these rare $\eta^{(\prime)}$ decays can hopefully be compared to experiment and thus help cast a light on possible symmetry violations and physics beyond the standard model in the light-meson sector.

2.9 Appendix

2.9.1 U(3) flavour symmetry

For the U(3) parameterisations of the pseudoscalar and vector-meson multiplets, we write

$$\Phi^P = \begin{pmatrix} \pi^0 + \frac{\sqrt{2}\,\eta+\eta'}{\sqrt{3}} & 0 & 0 \\ 0 & -\pi^0 + \frac{\sqrt{2}\,\eta+\eta'}{\sqrt{3}} & 0 \\ 0 & 0 & \frac{-\sqrt{2}\,\eta+2\eta'}{\sqrt{3}} \end{pmatrix},$$

$$\Phi_\mu^{V^{(\prime)}} = \begin{pmatrix} \rho_\mu^{0\,(\prime)} + \omega_\mu^{(\prime)} & 0 & 0 \\ 0 & -\rho_\mu^{0\,(\prime)} + \omega_\mu^{(\prime)} & 0 \\ 0 & 0 & -\sqrt{2}\phi_\mu^{(\prime)} \end{pmatrix}, \tag{2.63}$$

where we only retain flavour-neutral states. Here, mixing effects between the (physical) mesons are taken into account via the pattern

$$\begin{pmatrix} \eta' \\ \eta \end{pmatrix} = \begin{pmatrix} \cos\theta_P & \sin\theta_P \\ -\sin\theta_P & \cos\theta_P \end{pmatrix} \begin{pmatrix} \eta_1 \\ \eta_8 \end{pmatrix},$$

$$\begin{pmatrix} \omega^{(\prime)} \\ \phi^{(\prime)} \end{pmatrix} = \begin{pmatrix} \cos\theta_{V^{(\prime)}} & \sin\theta_{V^{(\prime)}} \\ -\sin\theta_{V^{(\prime)}} & \cos\theta_{V^{(\prime)}} \end{pmatrix} \begin{pmatrix} \omega_1^{(\prime)} \\ \omega_8^{(\prime)} \end{pmatrix}, \tag{2.64}$$

with η_1, η_8 and $\omega_1^{(\prime)}$, $\omega_8^{(\prime)}$ denoting the isoscalar singlet and octet states of the pseudoscalar and vector-meson multiplets, respectively. In the above, the mixing angles are assumed to be given by $\theta_P = \arcsin(-1/3)$ for the pseudoscalar nonet (canonical mixing) and $\theta_{V^{(\prime)}} = \arcsin(1/\sqrt{3})$ for the vector mesons (ideal mixing). We furthermore introduce the charge matrix according to

$$\mathcal{Q} = \frac{1}{3}\mathrm{diag}\,[2,-1,-1]. \tag{2.65}$$

Using Eq. (2.63), we calculate $\mathrm{Tr}\,[\Phi^P\Phi_\mu^V\Phi_\nu^{V^{(\prime)}}]$ to find the allowed couplings $\eta^{(\prime)}\rho\rho^{(\prime)}$, $\eta^{(\prime)}\omega\omega^{(\prime)}$, $\eta^{(\prime)}\phi\phi^{(\prime)}$, $\pi^0\rho\omega^{(\prime)}$, and $\pi^0\omega\rho^{(\prime)}$. To derive the relative signs between the corresponding coupling constants $C_{VP\gamma}$ introduced in Sec. 2.4.1, we calculate $\mathrm{Tr}\,[\Phi^P\Phi_\mu^V\mathcal{Q}]$ and take the appropriate ratios of coefficients that emerge in Eq. (2.4). For our analysis, we furthermore included the OZI-suppressed coupling $C_{\phi\pi^0\gamma}$, whose sign thus cannot be determined from U(3) symmetry. Instead, we resort to analyses of $e^+e^- \to 3\pi$ and $e^+e^- \to \pi\gamma$ [203–205], which suggest that the product of the $\phi\gamma$ and $\phi\pi\gamma$ couplings carries a relative sign as compared to the product of the $\omega\gamma$ and $\omega\pi\gamma$ couplings. Hence, calculating $\mathrm{Tr}\,[\Phi_\mu^V\mathcal{Q}]$ indicates a relative sign between $C_{\phi\pi^0\gamma}$ and $C_{\omega\pi^0\gamma}$. Fixing the sign of $C_{\rho\eta\gamma}$ to be positive, the sign convention of Table 2.4 follows.

2.9.2 Intermediate results

The numerical values of the auxiliary quantities $\Gamma^{(\gamma)}_{V_1,V_2}$ defined in Eq. (2.42), for a point-like interaction (PL), monopole form factors (MP), and dipole form factors (DP), are collected in Table 2.11 and Table 2.12.

2.9.3 Constants and parameters

We collect the masses and widths used throughout the calculations in Table 2.13.

			$\Gamma_{\rho,\rho}/\,\mathrm{MeV}^5$	$\Gamma_{\omega,\omega}/\,\mathrm{MeV}^5$	$\Gamma_{\phi,\phi}/\,\mathrm{MeV}^5$	$\Gamma_{\rho,\omega}/\,\mathrm{MeV}^5$	$\Gamma_{\rho,\phi}/\,\mathrm{MeV}^5$	$\Gamma_{\omega,\phi}/\,\mathrm{MeV}^5$
$\eta \to \pi^0 e^+ e^-$	PL	CW	0.5302	0.5684	0.1864	1.077	0.6041	0.6485
		VW	0.4992			1.065	0.6060	
	MP	CW	0.3463	0.3627	0.1093	0.6914	0.3707	0.3966
		VW	0.3422	0.3814	0.1151	0.7226	0.3945	0.4174
	DP	CW	0.3419	0.3573	0.1033	0.6814	0.3615	0.3835
		VW	0.3285	0.3630	0.09942	0.7160	0.3869	0.3903
$\eta \to \pi^0 \mu^+ \mu^-$	PL	CW	0.3440	0.3686	0.1383	0.7022	0.4222	0.4498
		VW	0.3123			0.6785	0.4136	
	MP	CW	0.1772	0.1870	0.06392	0.3569	0.2029	0.2173
		VW	0.1697	0.1972	0.06742	0.3657	0.2123	0.2293
	DP	CW	0.1674	0.1764	0.05756	0.3366	0.1888	0.2009
		VW	0.1603	0.1802	0.06073	0.3473	0.1916	0.2102
$\eta' \to \pi^0 e^+ e^-$	PL	CW	154.6	283.5	57.20	405.1	125.7	183.3
		VW	152.8			406.5	138.9	
	MP	CW	125.8	227.7	37.08	323.0	82.41	126.6
		VW	133.7	241.9	39.93	349.2	103.0	135.4
	DP	CW	128.1	232.0	35.95	328.3	84.42	128.8
		VW	131.5	253.1	38.66	340.9	101.0	134.6
$\eta' \to \pi^0 \mu^+ \mu^-$	PL	CW	121.2	169.8	55.13	284.5	131.0	168.1
		VW	116.9			281.7	139.1	
	MP	CW	80.02	111.0	30.42	185.6	70.21	94.91
		VW	83.84	119.3	32.79	199.8	84.77	101.9
	DP	CW	79.10	109.8	28.68	183.4	68.78	92.80
		VW	80.95	121.1	29.78	201.0	82.23	97.28
$\eta' \to \eta e^+ e^-$	PL	CW	19.68	50.07	6.701	60.79	8.303	14.86
		VW	19.47			60.64	10.11	
	MP	CW	16.44	48.33	5.100	48.56	−1.684	10.79
		VW	18.50			57.98	6.724	
	DP	CW	16.54	51.24	4.902	47.02	−2.518	12.45
		VW	18.37	46.79	4.827	57.81	6.109	10.82
$\eta' \to \eta \mu^+ \mu^-$	PL	CW	12.45	20.56	4.847	31.57	10.52	15.70
		VW	12.38			31.86	11.66	
	MP	CW	8.240	16.03	3.170	19.66	2.342	9.959
		VW	9.471			24.59	6.988	
	DP	CW	7.980	16.28	2.944	18.15	1.682	10.13
		VW	10.05	15.35	2.937	23.61	6.266	9.555

Table 2.11: Numerical results for the auxiliary quantities defined in Eq. (2.42) for the models PL, MP, and DP in both variants CW and VW, rounded to four significant digits.

		$\Gamma^{\gamma}_{\rho,\rho}/\,\mathrm{MeV}^5$	$\Gamma^{\gamma}_{\omega,\omega}/\,\mathrm{MeV}^5$	$\Gamma^{\gamma}_{\phi,\phi}/\,\mathrm{MeV}^5$	$\Gamma^{\gamma}_{\rho,\omega}/\,\mathrm{MeV}^5$	$\Gamma^{\gamma}_{\rho,\phi}/\,\mathrm{MeV}^5$	$\Gamma^{\gamma}_{\omega,\phi}/\,\mathrm{MeV}^5$
$\eta \to \pi^0\gamma\gamma$	CW	3.154×10^4	3.193×10^4	8.719×10^3	6.175×10^4	3.218×10^4	3.335×10^4
	VW	2.921×10^4			6.108×10^4	3.189×10^4	
$\eta' \to \pi^0\gamma\gamma$	CW	3.088×10^7	4.586×10^8	4.286×10^6	1.097×10^8	1.115×10^7	1.884×10^7
	VW	3.341×10^7			1.130×10^8	1.386×10^7	
$\eta' \to \eta\gamma\gamma$	CW	3.203×10^6	6.537×10^7	4.473×10^5	1.425×10^7	2.031×10^5	7.406×10^5
	VW	3.280×10^6			1.411×10^7	5.056×10^5	

Table 2.12: Numerical results for the auxiliary quantities defined in Eq. (2.42) in both variants CW and VW, rounded to four significant digits.

	Variable	Value [174]
π^0	M_{π^0}	134.9768(5) MeV
$\pi^\pm$	$M_{\pi^\pm}$	139.57039(18) MeV
K^0	M_K	497.611(13) MeV
η	M_η	547.862(17) MeV
	Γ_η	1.31(5) keV
$\eta'(958)$	$M_{\eta'}$	957.78(6) MeV
	$\Gamma_{\eta'}$	188(6) keV
$\rho^0(770)$	M_ρ	775.26(23) MeV
	Γ_ρ	147.4(8) MeV
$\omega(782)$	M_ω	782.66(13) MeV
	Γ_ω	8.68(13) MeV
$K^{*0}(892)$	M_{K^*}	895.55(20) MeV
$\phi(1020)$	M_ϕ	1019.461(16) MeV
	Γ_ϕ	4.249(13) MeV
$\rho^0(1450)$	$M_{\rho'}$	1465(25) MeV
	$\Gamma_{\rho'}$	400(60) MeV
$\omega(1420)$	$M_{\omega'}$	1410(60) MeV
	$\Gamma_{\omega'}$	290(190) MeV
$\phi(1680)$	$M_{\phi'}$	1680(20) MeV
	$\Gamma_{\phi'}$	150(50) MeV

Table 2.13: The masses and widths needed for the calculations in this article, with the values taken from Ref. [174].

Chapter 3

Axial-vector and tensor meson transition form factors

> Der Tümpel ist trüb und es tanzen die Teilchen im Licht.
>
> Dota Kehr, *Licht* [234]

3.1 Prologue

The results of this chapter are not yet published, but have been presented in a talk,

- H. Schäfer in collaboration with P. Sánchez-Puertas, E. Lymperiadou, and B. Kubis, *Axial-vector and tensor meson transition form factors*, 8th Plenary workshop of the Muon $g-2$ Theory Initiative, Orsay 2025.

Transition form factors (TFFs) of hadrons, depending on the photon virtualities, reflect the fact that hadrons are not fundamental, point-like particles. They are, *inter alia*, of special interest in processes where photon loops occur, such as in the anomalous magnetic moment of the muon, $(g-2)_\mu$. There, the dominant uncertainty comes from hadronic effects in photon loops. Resonance states, which are not stable under the strong interaction, have garnered interest in this context as they contribute to $(g-2)_\mu$ in the intermediate regime between the region where the pseudo-Goldstone bosons dominate and the high-energy region where perturbative quantum chromodynamics (pQCD) is applicable, interfering with both. At the same time, it is not straightforward to describe hadronic resonances since, on the one hand, pQCD is not applicable in this regime, and on the other hand, pure chiral perturbation theory (ChPT) breaks down at this scale. It was developed to describe the dynamics of light pseudo-Goldstone bosons [67–73] and extended to include the effect of resonance states such as vector, axial-vector, and tensor mesons on the pseudo-Goldstone boson dynamics [18–21], but the actual resonance properties of these states are not sufficiently represented in resonance ChPT (RChPT). Additionally, the power-counting scheme in RChPT is ambiguous due to the fact that the respective states can be embedded in different representations, such as the vector or the antisymmetric tensor representation [18, 19, 100].

Dispersion theory is a useful framework for many form factor calculations. One needs, however, input such as scattering phases or transition amplitudes in order to make predictions. The TFFs of the isovector C-even axial-vector and tensor states a_1 and a_2 have not been described precisely since there is not much experimental data to work with. In this project, we present the first steps towards a

parameterisation that takes into account the dynamical generation of these states in a $3\pi \equiv \rho\pi$ system on the basis of unitarity, crossing symmetry, and analyticity. This introduces inevitably a model dependence, which is hard to avoid given the scarcity of experimental data and the lack of theoretical insight. For axial-vector mesons, the decay into two real photons is forbidden by the LANDAU–YANG theorem [63, 64]. The total decay width of the a_1 has a rather large uncertainty, especially since a determination using a BREIT–WIGNER fit and another one using a complex pole description are incompatible [34]. Still, it is clear that it is not a narrow resonance and that its main decay channel is 3π. Tensor mesons are not restricted by the LANDAU–YANG theorem. The a_2 decays mainly into $\rho\pi$ with a branching ratio of 70.1(2.7)%, the next-important decay channels are $\pi\eta$, $\omega\pi\pi$, and $K\bar{K}$; for these (and even more) channels, experimental decay rates are available. Extracting information on the coupling to (virtual) photons from this involves the introduction of a dynamical model.

To this end, the $\rho\pi \to \gamma^*\gamma^*$ system is investigated and a decomposition into gauge-invariant tensor structures and scalar functions is performed following the BARDEEN–TUNG–TARRACH (BTT) procedure [225, 226]. This ansatz was suggested by Bastian KUBIS and Pablo SÁNCHEZ-PUERTAS and performed by the latter and the author of this thesis independently in order to cross-check the result. Since a description free of kinematic zeros and singularities is necessary for the subsequent dispersive treatment, poles introduced in the BTT procedure have to be removed. Additionally, redundancies associated with kinematic zeros are taken into account and a minimal generating set of tensor structures is constructed. This was done, again, by Pablo SÁNCHEZ-PUERTAS and the author of this thesis independently. Since it proved to be more involved than initially assumed, discussions between these two and Bastian KUBIS were essential to the progress, as well as additional discussions with Gio CHANTURIA, Simon MUTKE, and Maximilian ZILLINGER. Additional constraints necessary for removing kinematic singularities and zeros were identified by Pablo SÁNCHEZ-PUERTAS and this thesis' author.

For the scalar functions of the $\rho\pi \to \gamma^*\gamma^*$ system, the lowest-lying intermediate states in the crossed channels t and u are considered, namely one-particle ρ and π states, and the scalar functions reconstructed dispersively from these. This model was suggested by Bastian KUBIS and Pablo SÁNCHEZ-PUERTAS and calculated by the latter, Eirini LYMPERIADOU, and the author of this thesis. Pablo SÁNCHEZ-PUERTAS and the author of this thesis constructed a mapping in order to relate this input to the gauge-invariant description free of kinematic zeros and singularities. The author of this thesis formalised this procedure to some extent.

In order to connect the $\rho\pi \to \gamma^*\gamma^*$ system to the a_1 and a_2 TFFs, $\rho\pi$ are coupled to $a_{1/2}$. It is not possible to calculate the TFFs naively from the resulting loop as the preceding construction implies on-shell ρ and π states. Therefore, a dispersive reconstruction utilising only the unambiguous imaginary part of the loop is performed, which was suggested by Bastian KUBIS and discussed and developed by the latter, Pablo SÁNCHEZ-PUERTAS, and the author of this thesis. This was accomplished by computing the associated loop diagram via a PASSARINO–VELTMAN decomposition, which was implemented by Eirini LYMPERIADOU, Pablo SÁNCHEZ-PUERTAS, and this thesis' author, an evaluation of the corresponding master integrals, which was done by the latter and cross-checked by Pablo SÁNCHEZ-PUERTAS, and an implementation of the dispersion integral. The last step was done by the author of this thesis with the help of Gio CHANTURIA.

A projection to the a_1 and a_2 TFFs of the results obtained this way was constructed by Pablo SÁNCHEZ-PUERTAS, Eirini LYMPERIADOU, and the author of this thesis. The couplings of $a_{1/2}$ to $\rho\pi$ have been calculated phenomenologically by Pablo SÁNCHEZ-PUERTAS and the author of this thesis. Results for different configurations of this model have been calculated by the author of this thesis and discussed by the latter, Pablo SÁNCHEZ-PUERTAS, and Bastian KUBIS. Plots of the results have been prepared by the author of this thesis.

Since the divergence of the loop integrals limits the extraction of the a_1 TFFs to a simplified model and prohibits it entirely for the a_2, discussions between Pablo SÁNCHEZ-PUERTAS, Bastian KUBIS, Eirini LYMPERIADOU, and Martin HOFERICHTER have resulted in ideas to improve the framework, which are to be implemented in the future.

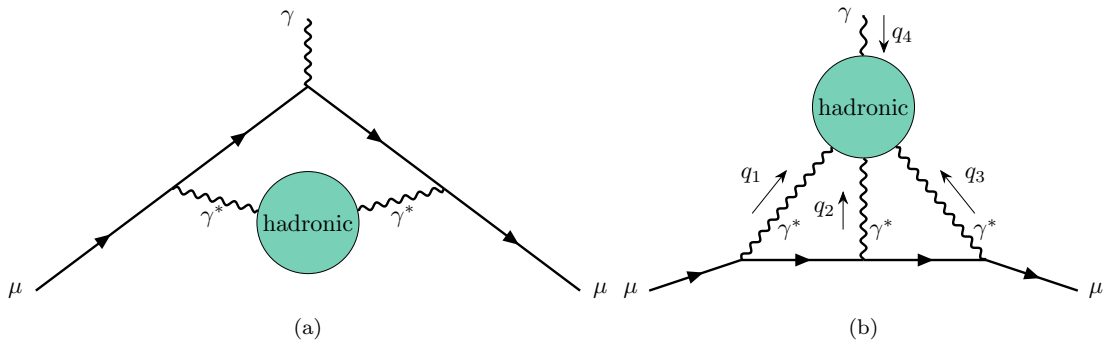

Figure 3.1: Hadronic contributions to a_μ: (a) HVP and (b) HLbL.

3.2 Introduction

From an outside view, it may seem that the question of the anomalous magnetic moment of the muon $(g-2)_\mu = 2a_\mu$ is settled. The long-standing discrepancy between the experimental value and the theory prediction has vanished with the current experimental world average $a_\mu^{\text{exp}} = 116592071.5(14.5) \times 10^{-11}$, including the latest results from BNL E821 [12] and Fermilab E989 [13, 14], and the latest White Paper (WP25) of the Theory Initiative [16], which quotes $a_\mu^{\text{WP25}} = 116592033(62) \times 10^{-11}$[108, 109, 111, 227, 235–290].[#1] The previous White Paper (WP20) [15, 107, 204, 235, 242, 243, 263, 265–268, 270, 285, 286, 291–297] had a value of $a_\mu^{\text{WP20}} = 116591810(43)$, which was in tension with the experimental result. In the following paragraphs, we follow the argumentation in WP25 [16].

The Standard Model (SM) prediction receives its main contribution from quantum electrodynamics (QED), $a_\mu^{\text{QED}} = 116584718.8(2) \times 10^{-11}$ [235–241], an electroweak correction $a_\mu^{\text{EW}} = 154.4(4) \times 10^{-11}$ [242–245], and then hadronic contributions, namely from hadronic vacuum polarisation (HVP) and hadronic light-by-light scattering (HLbL); see Fig. 3.1. While historically the HLbL contribution, which is of higher order in the perturbative expansion, was less understood and model-dependent, presently, the HVP contribution is the concerning part. a_μ^{HVP} was estimated from experimental data on $e^+e^- \to$ hadrons in WP20 and already then showed a discrepancy to the result from lattice QCD. While more independent lattice results for the leading-order HVP contribution are available now with higher precision than before [246–262], the community agreed that at the time of WP25, no data-driven leading-order HVP result can be quoted due to the large discrepancies between the different experimental results entering this calculation. The leading-order HVP result from the lattice, on the other hand, is systematically larger than the previous data-driven result and shifts a_μ^{WP25} such that it is compatible with the experimental result. While this seems like a step back and one might loose hope to find new physics in this regime, the current situation is a physics puzzle in itself that is worth solving: why do the different experimental results for $e^+e^- \to$ hadrons disagree? Why do most of them disagree with the lattice results? How can the community address such questions that require meticulous error estimation and comparisons between experiment, theory, and lattice?

On the other hand, in the sector of the once-problematic HLbL, significant progress has been made in the last years. There are also lattice results [286–290], and on the phenomenological side [108, 109, 111, 227, 244, 266–284], the picture is much clearer now. A dispersive framework has been set up in order to systematically include hadronic intermediate states in a manner consistent with analyticity and unitarity. For this, one needs a generating set of tensor structures and scalar functions for the

[#1] The theory predictions for the anomalous magnetic moment of the muon in WP25 and WP20 are based on input from the references cited here.

$\gamma^*\gamma^*\gamma^*\gamma$ system, which generates the full HLbL tensor

$$\Pi^{\mu\nu\lambda\sigma}(q_1,q_2,q_3) = -\mathrm{i}\int \mathrm{d}^4x\,\mathrm{d}^4y\,\mathrm{d}^4z\,e^{-\mathrm{i}(q_1\cdot x+q_2\cdot y+q_3\cdot z)}\langle 0|T\{j^\mu_{\mathrm{em}}(x)j^\nu_{\mathrm{em}}(y)j^\lambda_{\mathrm{em}}(z)j^\sigma_{\mathrm{em}}(0)\}|0\rangle, \tag{3.1}$$

with $j^\mu_{\mathrm{em}} := \bar{q}Q\gamma^\mu q$ the electromagnetic (EM) currents, defined in pure QCD for the lightest quarks $q = (u,d,s)^T$, and the charge matrix $Q = \mathrm{diag}\,(2/3,-1/3,-1/3)$. In Ref. [227], a decomposition into 54 tensor structures $T_i^{\mu\nu\lambda\sigma}$ and scalar functions Π_i ,

$$\Pi^{\mu\nu\lambda\sigma}(q_1,q_2,q_3) = \sum_{i=1}^{54} T_i^{\mu\nu\lambda\sigma}\Pi_i, \tag{3.2}$$

was constructed such that the tensor structures are gauge-invariant and the scalar functions free of kinematic singularities. However, this decomposition is redundant, as there are only 41 independent helicity amplitudes, which matches the number of independent tensor structures. The reason to work with this generating set instead of a basis is that there seems to be no way to construct such a basis valid in all kinematic limits. We encounter a similar problem in this work and will explain the details in the next section. For the evaluation of a_μ^{HLbL}, one takes the limit $q_4 \to 0$ (since the fourth photon is always soft) and applies DIRAC-space projection operator techniques [298] to find the so-called master formula

$$a_\mu^{\mathrm{HLbL}} = \frac{\alpha^3}{432\pi^2}\int_0^\infty \mathrm{d}\Sigma\,\Sigma^3\int_0^1 \mathrm{d}r\,r\sqrt{1-r^2}\int_0^{2\pi}\mathrm{d}\phi\sum_{i=1}^{12} T_i(\Sigma,r,\phi)\bar{\Pi}_i(Q_1^2,Q_2^2,Q_3^2) \tag{3.3}$$

with Euclidean photon virtualities $Q_i^2 = -q_i^2$, which can be expressed in terms of the integration variables Σ, r, and ϕ. The $\bar{\Pi}_i$ emerge as unambiguous linear combinations of the Π_i in the limit $q_4 \to 0$. One can reconstruct the real parts of these scalar functions from their imaginary parts, which via unitarity are related to all possible intermediate states. The choice of a suitable framework to describe these intermediate states depends on the scale of the Q_i^2 and how they relate to each other. Higher virtualities correspond to shorter distances, therefore one refers to contributions in this regime as short-distance constraints (SDCs). For three large virtualities $Q_1^2 \approx Q_2^2 \approx Q_3^2 \gg \Lambda_{\mathrm{QCD}}$, one can calculate quark loops in an operator product expansion (OPE) framework [108, 109, 270]. In the so-called mixed or MELNIKOV–VAINSHTEIN region where w.l.o.g. $Q_1^2 \approx Q_2^2 \gg Q_3^2$ [296], the axial current dominates, and higher-order corrections can be estimated again in OPE [110, 111]. Additional corrections come from gluonic contributions.

For low virtualities, a dispersive treatment takes into account discrete hadronic states up to some point and is then matched to the SDCs. This can be done in different frameworks. One version, which is in use in WP25, works in four-point kinematics, where the tensor structures $T_i^{\mu\nu\lambda\sigma}$ are written in terms of $q_1, q_2, q_3, q_4 := q_1 + q_2 + q_3$, and dispersion relations for Π_i are derived for fixed photon virtualities in the limit $q_4^2 = 0$; the limit $q_4 \to 0$ is taken afterwards [227, 267]. In this approach, the scalar functions Π_i exhibit kinematic singularities in q_i^2, which vanish in the end due to a set of sum rules; these connect different hadronic intermediate states, which themselves still contain spurious kinematic singularities. In Ref. [278], an optimised basis has been constructed, where these kinematic singularities only occur for intermediate states with spin ≥ 2, *i.e.*, tensor states.

On the other hand, one can take the limit $q_4 \to 0$ early on before setting up the dispersion relations, thus working in three-point kinematics. This ansatz is followed in Ref. [299], and it yields scalar functions manifestly free of kinematic singularities, but one has to take into account additional cuts and intermediate states for the dispersive reconstruction, which complicates the calculation and requires input for additional sub-processes [300]. In the end, these two frameworks, complemented by SDCs, have to yield equivalent results; on the level of intermediate states, however, they can differ, since contributions get shuffled between them, as was shown for the simpler case of the hadronic VVA correlator [244].

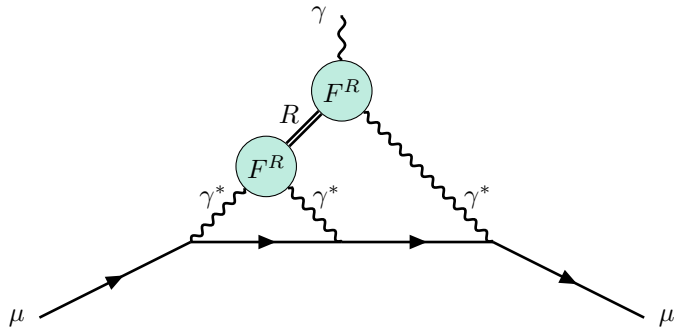

Figure 3.2: Contribution of a resonance R to HLbL, where TFFs of R occur.

The leading contributions in the hadronic regime are given by light pseudoscalar $\pi, \eta^{(\prime)}$ pole terms, followed by the pion box. Next in order are S-wave $\pi\pi/(K\bar{K})_{I=0}$ rescattering effects and pole contributions from scalar, axial-vector, and tensor mesons. In four-point kinematics, these higher pole contributions are estimated via a narrow-resonance (or narrow-width) approximation (NWA) [278, 282, 301]. For this, doubly-virtual transition form factors (TFFs) of the corresponding states are needed as input; see Fig. 3.2. The NWA takes into account only the residues and not the full generation of these intermediate states. One side effect of this is that imaginary parts of the TFFs are difficult to treat in the framework. For compatibility, the TFFs are ideally also described in the NWA, such that their imaginary parts vanish. Alternatively, one could adapt the HLbL dispersive framework such that it includes more intermediate states and imaginary parts can cancel between them. This, however, is a challenging task.

In this work, we focus on isovector axial-vector and tensor-meson intermediate states. The lightest axial-vector mesons are organised in a triplet of two isoscalar states $f_1(1285) \equiv f_1$ and $f_1(1420) \equiv f_1'$ and one isovector state $a_1(1260) \equiv a_1$. Similarly, the lowest-lying tensor states are $f_2(1270) \equiv f_2$, $f_2(1525) \equiv f_2'$, and $a_2(1320) \equiv a_2$. Masses and widths used in this work are collected in the appendix in Table 3.2.

In the current evaluation of a_μ^{HLbL}, tensor intermediate states are affected by the spurious kinematic singularities, which eventuates in the fact that one can include either F_1^T and F_2^T or F_1^T and F_3^T. Ideally, one finds a good reason for a hierarchy between one of these pairs of TFFs and the rest. Currently there exists a simple quark model [282, 301, 302]

$$F_1^T(q_1^2, q_2^2) = F_1^T(0,0) \times \left(\frac{\Lambda_T}{\Lambda_T - q_1^2 - q_2^2}\right)^2, \qquad F_{2-5}^T \equiv 0, \tag{3.4}$$

where the scale is set to $\Lambda_T = M_\rho$. The effect of tensor-meson contributions on a_μ has also been estimated in holographic QCD (hQCD) [284], where only F_1^T and F_3^T are non-zero. In hQCD, there is also a prediction for the axial-vector TFFs [276], and SDCs are implemented in the same framework. Experimentally, for the f_2, the f_2', and the a_2, mass and width as well as branching fractions for the main decay channels $\pi\pi$, $K\bar{K}$, and 3π, respectively, as well as a few subleading channels are known.

In the axial-vector sector, the f_1 is the state about which most is know as several decay and production channels have been measured. A fit to all available data on the basis of a vector-meson dominance (VMD) model was performed in Refs. [144, 277]. Since there is no such data available for the a_1 and the f_1', their contributions are estimated in analogy to the f_1 via U(3) symmetry. Making use of several constraints, the $F_2^{a_1}$ TFF was estimated in Ref. [244], finding a good agreement with the U(3) estimate. One major constraint for axial vectors is that their decay to real photons is forbidden by the Landau–Yang theorem [63, 64].

In this work, we want to relate the a_1 and a_2 TFFs to the well-known pion vector form factor F_π^V, the $\rho\pi$ TFF F_{VP}, and the ρ FFs $G_i, i \in \{1,2,3\}$, making use of the knowledge that the main decay channel is $3\pi \equiv \rho\pi$. For this, we study the $\rho\pi \to \gamma^*\gamma^*$ amplitude in Sec. 3.3 and Sec. 3.4 and then

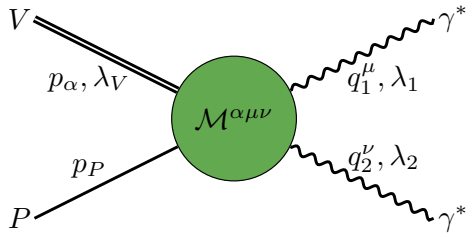

Figure 3.3: The process $VP \to \gamma^*\gamma^*$ with definitions of momenta and helicities.

relate it to $a_{1/2} \to \gamma^*\gamma^*$ and the TFFs $F_i^{a_{1/2}}$ in Sec. 3.5. The numerical evaluation is described in Sec. 3.6 and results are discussed in Sec. 3.7. We conclude in Sec. 3.8.

3.3 $VP \to \gamma^*\gamma^*$ basis

We want to construct a gauge-invariant tensor basis free of kinematic zeros and singularities for the subprocess $\rho\pi \to \gamma^*\gamma^*$; see Fig. 3.3. Since the following considerations are valid for any vector meson V and pseudoscalar P, we construct this in a more general notation and switch back to $\rho\pi$ when we use physical input. We start with the most general set of tensor structures and employ the BARDEEN–TUNG–TARRACH (BTT) procedure [225, 226]. In this section, we treat the vector and the pseudoscalar particle as asymptotic states, *i.e.*, in a NWA. The amplitude is defined as

$$\begin{aligned}
&\langle\gamma^*(q_1,\lambda_1)\gamma^*(q_2,\lambda_2)|V(p)P(p_P)\rangle \\
&= -e^2(2\pi)^4\delta(q_1+q_2-p-p_P)\epsilon_\mu^*(q_1,\lambda_1)\epsilon_\nu^*(q_2,\lambda_2)\int \mathrm{d}^4z\, e^{-\mathrm{i}q_1z}\langle 0|T\{j_{\mathrm{em}}^\mu(z)j_{\mathrm{em}}^\nu(0)\}|V(p)P(p_P)\rangle \\
&= \mathrm{i}e^2(2\pi)^4\delta(q_1+q_2-p-p_P)\epsilon_\mu^*(q_1,\lambda_1)\epsilon_\nu^*(q_2,\lambda_2)\epsilon_\alpha^{\lambda_V}(p,\lambda_V)\mathcal{M}^{\mu\nu\alpha}(q_1,q_2,p),
\end{aligned} \tag{3.5}$$

with the matrix element

$$\mathrm{i}\int \mathrm{d}^4z e^{-\mathrm{i}q_1z}\langle 0|T\{j_{\mathrm{em}}^\mu(z)j_{\mathrm{em}}^\nu(0)\}|V(p)P(p_P)\rangle = \epsilon_\alpha^{\lambda_V}(p,\lambda_V)\mathcal{M}^{\mu\nu\alpha}(q_1,q_2,p). \tag{3.6}$$

We made use of the LEHMANN–SYMANZIK–ZIMMERMANN (LSZ) reduction formula [303] and the equations of motion for photons,

$$\partial_\mu F^{\mu\nu}(x) = ej_{\mathrm{em}}^\nu(x), \tag{3.7}$$

in order to switch back and forth between writing photons as external particles and as currents,

$$\begin{aligned}
\langle \mathrm{out}|\gamma(q,\lambda),\mathrm{in}\rangle &= -\mathrm{i}e\epsilon_\mu(q,\lambda)\int \mathrm{d}^4e^{-\mathrm{i}q\cdot x}\langle \mathrm{out}|j_{\mathrm{em}}^\mu(x)|\mathrm{in}\rangle, \\
\langle \gamma(q,\lambda),\mathrm{out}|\mathrm{in}\rangle &= -\mathrm{i}e\epsilon_\mu^*(q,\lambda)\int \mathrm{d}^4e^{\mathrm{i}q\cdot x}\langle \mathrm{out}|j_{\mathrm{em}}^\mu(x)|\mathrm{in}\rangle.
\end{aligned} \tag{3.8}$$

3.3.1 Gauge invariance and cancellation of poles

The BARDEEN–TUNG–TARRACH (BTT) procedure [225, 226] addresses the problem that an amplitude with external photons is not gauge-invariant when written down naively, *i.e.*, unphysical degrees of freedom are not removed. If we do not have any further information about an amplitude but its external particles and the symmetries that it has to fulfil, we can decompose it into a sum over all possible LORENTZ tensor structures T_i with generic scalar coefficient functions,

$$\mathcal{M} = \sum_i \mathcal{F}_i T_i. \tag{3.9}$$

The scalar functions $\mathcal{F}_i$ depend on all available LORENTZ scalars, and *a priori*, we do not have any information about their behaviour. The goal is then to extract from a set of all possible tensor structures the gauge-invariant linear combinations, to find a generating set for those, and to remove any kinematic zeros and singularities from the tensor structures, such that the corresponding scalar functions are free of kinematic singularities and zeros and singularities.

For a minimal decomposition, it would be ideal to construct a basis, which manifestly avoids any double counting. This is not always compatible with the other conditions, as we will see. The procedure has been used and explained, *e.g.*, in Refs. [227, 304, 305], some investigations concerning symmetries between the kinematic variables are collected in Ref. [306]. We do not only explain the steps necessary to construct a basis of tensor structures and the reasons why we extend this basis to a generating set, but describe in addition the mathematical procedure of transforming simultaneously the scalar functions $\mathcal{F}_i$. In order to do so, we alternate between the concrete example of the process $VP \to \gamma^*\gamma^*$ and more general considerations which outline how this can be done for other processes.

The initial set of all possible tensor structures is constructed by writing down all possible combinations of independent momenta q_i and the metric tensor g with respect to all free LORENTZ indices of the process. The free indices correspond to the external polarisation vectors via $\mathcal{M} = \epsilon_{\alpha_1} \dots \epsilon_{\alpha_n} \mathcal{M}^{\alpha_1 \dots \alpha_n}$, where α_i is the (multi-)index of the polarisation vector ϵ_i. Depending on the parity of the process, one needs to include a LEVI-CIVITA tensor $\varepsilon^{\mu\nu\alpha\beta}$[#2] in order to accommodate the correct behaviour under parity transformations, such as for $VP \to \gamma^*\gamma^*$. Therefore, the construction for the latter process starts from

$$\mathcal{M}^{\mu\nu\alpha} \sim \mathcal{M}^{\mu\nu\alpha\beta\gamma\delta\epsilon} \varepsilon_{\beta\gamma\delta\epsilon}. \tag{3.10}$$

The tensor structures of $\mathcal{M}^{\mu\nu\alpha\beta\gamma\delta\epsilon}$ are now built from $\{q_1, q_2, p\}^{\{\mu,\nu,\alpha,\beta,\gamma,\delta,\epsilon\}}$ and $g^{\mu\nu}$ with all possible index variations, where we only take into account combinations that are not related via relative minus signs. We find a total number of 60 resulting´ structures $T_i^{\text{in},\mu\nu\alpha}$, which are listed in Sec. 3.9.1.

From a linear algebra perspective,[#3] the tensor structures T_i of a process with N external particles of given spin and intrinsic parity form a vector space over the field $\mathbb{C}$. Note that there is no canonical scalar product defined on this vector space, which complicates the procedure of constructing a basis significantly. The dimension of the vector space depends only on the number of external particles and their spin and parity, and it can be assessed by counting helicity amplitudes $H_{\lambda_1 \dots \lambda_N}$, where $\lambda_n, n \in \{1, \dots, N\}$ are the helicity eigenvalues. The number of helicity amplitudes is determined from all possible combinations $\lambda_1 \dots \lambda_N$, where those that violate helicity conservation are removed. For 3 external particles, this implies $\lambda_1 = \lambda_2 - \lambda_3$, but for more than three particles, there is more freedom and no such relation holds. Lastly, one identifies amplitudes that are identical up to a sign due to parity.

This leads to, *e.g.*, 3 helicity states for $A \to \gamma^*\gamma^*$ and 5 amplitudes for $T \to \gamma^*\gamma^*$. For real photons, this reduces to 2 amplitudes for $T \to \gamma\gamma$ and 1 for $A \to \gamma\gamma$; the latter one, however, has to vanish since the decay of a spin-1 particle into two photons is forbidden by the LANDAU–YANG theorem [63, 64]. It is demonstrated in Ref. [308] that this happens. For $VP \to \gamma^*\gamma^*$, the helicity amplitudes are defined as

$$\epsilon_\mu^*(q_1, \lambda_1) \epsilon_\nu^*(q_2, \lambda_2) \epsilon_\alpha(p, \lambda_V) \mathcal{M}^{\mu\nu\alpha}(q_1, q_2, p) = e^{i(\lambda_1 - \lambda_2)\varphi} H_{\lambda_1 \lambda_2; \lambda_V}. \tag{3.11}$$

In the centre-of-momentum system (CMS) of the two photons, momentum vectors are given by

$$\begin{aligned} q_1 &= (E_1, 0, 0, |\vec{q}|), \qquad q_2 = (E_2, 0, 0, -|\vec{q}|), \\ p &= (E_V, |\vec{p}| \sin\theta \cos\varphi, |\vec{p}| \sin\theta \sin\varphi, |\vec{p}| \cos\theta), \\ p_P &= (E_P, -|\vec{p}| \sin\theta \cos\varphi, -|\vec{p}| \sin\theta \sin\varphi, -|\vec{p}| \cos\theta), \end{aligned} \tag{3.12}$$

[#2] We adopt the convention $\epsilon^{0123} = 1$.

[#3] We will use some linear algebra terminology and concepts in the following without explicit definitions and refer the reader to any textbook on the topic, *e.g.*, Ref. [307].

where the energies and magnitudes of three-momenta in terms of the MANDELSTAM variable $s = (p+p_P)^2 = (q_1+q_2)^2$ are

$$\begin{aligned} E_1 &= \sqrt{q_1^2+|\vec{q}|^2} = \frac{s+q_1^2-q_2^2}{2\sqrt{s}}, & E_2 &= \sqrt{q_2^2+|\vec{q}|^2} = \frac{s-q_1^2+q_2^2}{2\sqrt{s}}, & |\vec{q}| &= \frac{\lambda^{1/2}(s,q_1^2,q_2^2)}{2\sqrt{s}}, \\ E_V &= \sqrt{p^2+|\vec{p}|^2} = \frac{s+p^2-p_P^2}{2\sqrt{s}}, & E_P &= \sqrt{p_P^2+|\vec{p}|^2} = \frac{s-p^2+p_P^2}{2\sqrt{s}}, & |\vec{p}| &= \frac{\lambda^{1/2}(s,p^2,p_P^2)}{2\sqrt{s}}. \end{aligned} \tag{3.13}$$

Here, $\lambda(a,b,c) := a^2+b^2+c^2-2ab-2ac-2bc$ denotes the KÄLLÉN function. A set of polarisation vectors that fulfil $\epsilon_r^*(q)\cdot\epsilon_s(q) = -\delta_{rs}$ and $\epsilon_r(q)\cdot q = 0$ for $r,s\in\{\pm,0\}$ and $q\in\{q_1,q_2,p\}$ is given by

$$\begin{aligned} \epsilon_\pm(q_1) &= \mp\frac{1}{\sqrt{2}}\big(0,1,\pm\mathrm{i},0\big), \quad \epsilon_0(q_1) = \frac{1}{\xi_1}\big(|\vec{q}|,0,0,E_1\big), \\ \epsilon_\pm(q_2) &= \mp\frac{1}{\sqrt{2}}\big(0,1,\mp\mathrm{i},0\big), \quad \epsilon_0(q_2) = \frac{1}{\xi_2}\big(-|\vec{q}|,0,0,E_2\big), \\ \epsilon_+(p) &= \frac{1}{\sqrt{2}}\big(0,-\cos\theta\cos\varphi+\mathrm{i}\sin\varphi,-\cos\theta\sin\varphi-\mathrm{i}\cos\varphi,\sin\theta\big), \\ \epsilon_-(p) &= \frac{1}{\sqrt{2}}\big(0,\cos\theta\cos\varphi+\mathrm{i}\sin\varphi,\cos\theta\sin\varphi-\mathrm{i}\cos\varphi,-\sin\theta\big), \\ \epsilon_0(p) &= \frac{1}{\xi_V}\big(|\vec{p}|,E_V\sin\theta\cos\varphi,E_V\sin\theta\sin\varphi,E_V\cos\theta\big), \end{aligned} \tag{3.14}$$

where the polarisation vectors of the vector meson $\epsilon_r(p), r\in\{\pm,0\}$, have been obtained by rotating the polarisation vectors of the photon $\epsilon_r(q_1)$ accordingly. The longitudinal polarisation vectors ϵ_0 are normalised to 1 for $\xi_{1/2/V} = \sqrt{q_1^2/q_2^2/p^2}$.

These polarisation vectors are mapped as $\epsilon_\pm \mapsto -\epsilon_\mp$ and $\epsilon_0 \mapsto \epsilon_0$ under a parity transformation followed by a rotation around the y-axis [309]. Combinatorically, there are 27 different amplitudes; from the parity considerations, we see that $H_{00;0}$ vanishes and 13 out of the remaining amplitudes are independent,

$$\begin{aligned} H_{++;+} &= H_{--;-}, & H_{++;-} &= H_{--;+}, & H_{++;0} &= -H_{--;0}, & H_{+-;+} &= H_{-+;-}, \\ H_{+-;-} &= H_{-+;+}, & H_{+-;0} &= -H_{-+;0}, & H_{+0;+} &= -H_{-0;-}, & H_{+0;-} &= -H_{-0;+}, \\ H_{+0;0} &= H_{-0;0}, & H_{0+;+} &= -H_{0-;-}, & H_{0+;-} &= -H_{0-;+}, & H_{0+;0} &= H_{0-;0}, \\ H_{00;+} &= H_{00;-}, & H_{00;0} &= -H_{00;0} \equiv 0. \end{aligned} \tag{3.15}$$

In the on-shell case, there are 12 helicity amplitudes, of which 6 are independent, matching the number of structures for the on-shell amplitude $VP\to\gamma\gamma$ in Ref. [310].

Constructing gauge-invariant tensor structures is done by contracting the initial structures $T_i^{\mathrm{in},\mu\nu\alpha}$ with a projector

$$I_i^{\mu\nu} = g^{\mu\nu} - \frac{q_j^\mu q_i^\nu}{q_i\cdot q_j} \tag{3.16}$$

for every external photon $\gamma(q_i,\lambda_i)$, where q_j is another LORENTZ vector in the process. Such a projector fulfils the following properties for an amplitude $\mathcal{M} = \epsilon_\mu(q_i,\lambda_i)\mathcal{M}^\mu$: any gauge-invariant tensor structure $T^\mu\in\mathcal{M}^\mu$ it gets contracted with stays intact as the second part vanishes due to $q_{i\mu}T^\mu = 0$, and any unphysical structure $\mathcal{M}^\mu \ni T^\mu \sim q_i^\mu$ projects to zero because the two parts of the sum cancel.

A gauge projection maps the set of LORENTZ structures onto a subspace of lower dimension, which contains only gauge-invariant structures T_i^{proj}.[#4] The mapping can be put in terms of a non-invertible matrix M^{proj}, which manifestly expresses the projected structures as linear combinations of the original ones. The corresponding coefficients can contain poles in $q_i \cdot q_j$, the maximal pole order is given by the number of projectors. In the case of $VP \to \gamma^*\gamma^*$, the gauge projection together with the condition that the vector meson has only 3 propagating degrees of freedom, removing the scalar time-like degree of freedom,[#5] reduces the set of 60 initial structures to a smaller set of 36 gauge-invariant structures with poles up to second order. Here, the explicit contraction is performed as

$$\left[g^{\rho\mu} - \frac{q_2^\rho q_1^\mu}{q_1 \cdot q_2}\right]\left[g^{\nu\sigma} - \frac{q_2^\nu q_1^\sigma}{q_1 \cdot q_2}\right] T_i^{\text{in},\mu\nu\alpha}, \tag{3.17}$$

and subsequently, the indices are renamed again via $\rho, \sigma \mapsto \mu, \nu$.

Cancelling the poles is done order by order. For each order, we form all possible linear combinations of the projected structures with non-singular coefficients that cancel a pole and collect the respective coefficients in an invertible matrix. All poles of a given order that cannot be cancelled this way need to be removed via multiplication of the respective structure by $q_i \cdot q_j$; the number of cases where this is necessary can be determined from M^{proj}. Multiplying all structures with poles by the respective pole positions would introduce zeros in the tensor structures. We note that the matrix collecting the multiplications by $q_i \cdot q_j$ is singular in the limit $q_i \cdot q_j \to 0$.

Furthermore, we can examine how the tensor structures behave under symmetries such as BOSE symmetry; sometimes it is useful to build (anti-)symmetric combinations. For the $VP \to \gamma^*\gamma^*$ system, we symmetrise with respect to $(q_1, \mu) \leftrightarrow (q_2, \nu)$, which corresponds to crossing of the two photons.

3.3.2 Linear relations and construction of a basis

The generating set of gauge-invariant pole-free symmetrised tensor structures we have obtained so far is still not necessarily minimal since there might be linear dependencies. In order to find a minimal set, we need to remove some structures by exploiting those linear relations. It is easiest to write down such a linear relation in terms of the initial tensor structures,

$$\sum_i a_i T_i^{\text{in}} = 0, \tag{3.18}$$

since the identification of the T_i^{in} is simple and does not require any projection techniques. As we want to use this relation in order to reduce the set of pole-free gauge-invariant structures to a basis, we are actually interested in

$$\sum_i \tilde{a}_i T_i^{\text{pl.-fr.}} = 0, \tag{3.19}$$

where the coefficients $\tilde{a}_i$ of the pole-free gauge-invariant structures $T_i^{\text{pl.-fr.}}$ differ in general from the coefficients a_i. Hence, we need to project and transform the a_i accordingly. In order to do so, we employ the framework of dual vector spaces and dual mappings. Linear relations can be seen as linear forms on the vector space of tensor structures. The space of linear forms on a vector space V is called the dual space V^*. For a basis $\mathcal{B} = \{b_i\}$ of V, we can define a dual basis $\mathcal{B}^* = \{b_i^*\}$ of V^* with

[#4] Massive vector particles do not have such a gauge symmetry, but in any physical amplitude, time-like degrees of freedom do not contribute. In terms of polarisation vectors, this means that $\epsilon_\mu(q_i) q_i^\mu$ has to vanish, and the condition for the amplitude is again that terms $T^\mu \sim q_i^\mu$ do not contribute. One can construct a similar projector as in the photon case and contract it with the corresponding free index; we found, however, that it is equivalent and easier to check this condition after the rest of the steps are done via contraction with the usual vector spin sum $g^{\mu\nu} - (q_i^\mu q_i^\nu)/q_i^2$, which is not possible for photons, where $1/q_i^2$ can become singular.

[#5] We demand that $\varepsilon(p, \lambda_\rho)_\alpha T_i^{\mu\nu\alpha} = 0$ if $T_i^{\mu\nu\alpha} \sim p^\alpha$, and as we will contract with the vector meson polarisation later on, we can ignore the respective structures. The tensor basis where this condition is not implemented can be obtained from our basis Eq. (3.23) by contracting with $g_{\tau\alpha} - p_\tau p_\alpha / p^2$.

$b_i^*(b_j) = \delta_{ij}$. The dual basis depends by construction on the choice of $\mathcal{B}$. With this, a linear relation can be written as

$$\varphi = \sum_i \varphi_i b_i^* \in V^*, \quad \varphi(b_j) = \sum_i \varphi_i b_i^*(b_j) = \sum_i \varphi_i \delta_{ij} =: a_j, \tag{3.20}$$

from which we see that the coefficients depend on the basis $\mathcal{B}$. Note that the linear form in Eq. (3.20) is not defined on the whole vector space, but only at very specific points, namely where it maps to $0 \in \mathbb{C}$.

Let $f : V \to W$ denote a mapping between two vector spaces V and W, and $\varphi : W \to \mathbb{C}$ a linear form, $\varphi \in W^*$. Then, the dual mapping of f is defined by $f^* : W^* \to V^*, \varphi \mapsto f^*(\varphi) := \varphi \circ f$. This implies in the case of an invertible mapping f that a mapping f^* of such a linear form is performed using the transposed matrix with respect to the dual basis of V^* and the inverse of the transposed matrix with respect to the basis of V [307], which is also what we have to do in order to find the coefficients $\tilde{a}_i$. In the case of non-invertible mappings such as the gauge projection, one has to construct the dual mapping in a more pedestrian way, making use of the fact that $\mathrm{Im}\, f^* = (\mathrm{Ker} f)^0$ and $\mathrm{Ker} f^* = (\mathrm{Im}\, f)^0$, where $U^0 := \{\varphi \in V^* : \varphi(u) = 0 \quad \forall u \in U\} \subset V^*$ denotes the annihilator of a subspace $U \subset V$. For the gauge projection, it is enough to take the transpose of the matrix that reduces the dimension of the vector space according to the BTT projection,

$$M_{ij}^{\mathrm{red}} = \delta_{ij} \times \begin{cases} 0 & , \text{ if structure } T_i \text{ is projected to } 0 \\ 1 & , \text{ else .} \end{cases} \tag{3.21}$$

Here, $\mathrm{Ker} f$ consists of the structures that get projected to $0 \in V$, and its annihilator $(\mathrm{Ker} f)^0$ are the linear forms that send such structures to $0 \in \mathbb{C}$, which are therefore in the image of f^*. A similar situation occurs when multiplying some structures by $q_i \cdot q_j$ in order to remove remaining poles. Since such a multiplication is a singular operation in the kinematic limit $q_i \cdot q_j \to 0$, one needs to find the appropriate dual operation to this, which is the identity mapping for $q_i \cdot q_j \neq 0$ and similar to Eq. (3.21) in the limit $q_i \cdot q_j \to 0$.

Such linear relations can come from constraints regarding the degrees of freedom of the physical fields involved; *e.g.*, in the case of a tensor-meson field parameterised by two polarisation indices, any physical amplitude has to be symmetric under the exchange of these indices, a condition which can be expressed in terms of linear equations of the T_i^{in}.[#6] In case of P-odd structures, as with $VP \to \gamma^*\gamma^*$, a set of linear equations arises due to the four dimensions of space-time via the so-called SCHOUTEN identity,

$$\varepsilon^{\mu\nu\rho\sigma} g^{\lambda\tau} = \varepsilon^{\tau\nu\rho\sigma} g^{\lambda\mu} + \varepsilon^{\mu\tau\rho\sigma} g^{\lambda\nu} + \varepsilon^{\mu\nu\tau\sigma} g^{\lambda\rho} + \varepsilon^{\mu\nu\rho\tau} g^{\lambda\sigma}. \tag{3.22}$$

For $VP \to \gamma^*\gamma^*$, all possible combinations of free indices, while the remaining indices are contracted with available momenta and the metric tensor, yield 39 equations relating the initial structures to each other. Of these, 32 are independent; they are collected in App. 3.9.2. In terms of the gauge-invariant pole-free (and symmetrised) tensor structures, we find 30 linear relations, 23 of which are independent. We obtain the coefficients for these new relations via dual mappings as explained above. The relations can be used to find a minimal set of (linear combinations of) structures that generates the full set of projected tensor structures. This procedure is, of course, ambiguous; we choose a basis $\{T_i^{\mathrm{b},\mu\nu\alpha}\}_{i=1}^{13}$ of structures with the lowest mass dimension possible, given by

$$\begin{aligned}
T_1^{\mathrm{b},\mu\nu\alpha} &= \varepsilon^{\alpha\nu q_1 q_2} q_2^\mu + \varepsilon^{\alpha\mu q_1 q_2} q_1^\nu + \varepsilon^{\alpha\mu\nu q_1}(q_1 \cdot q_2) + \varepsilon^{\alpha\mu\nu q_2}(q_1 \cdot q_2), \\
T_2^{\mathrm{b},\mu\nu\alpha} &= -\varepsilon^{\alpha\nu q_1 q_2} q_2^\mu + \varepsilon^{\alpha\mu q_1 q_2} q_1^\nu + \varepsilon^{\alpha\mu\nu q_1}(q_1 \cdot q_2) - \varepsilon^{\alpha\mu\nu q_2}(q_1 \cdot q_2), \\
T_3^{\mathrm{b},\mu\nu\alpha} &= \varepsilon^{\alpha p q_1 q_2} g^{\mu\nu} - \varepsilon^{\alpha\nu p q_1} q_2^\mu + \varepsilon^{\alpha\mu p q_2} q_1^\nu + \varepsilon^{\alpha\mu\nu p}(q_1 \cdot q_2),
\end{aligned}$$

[#6] In the tensor representation of a tensor meson, there are initially 16 degrees of freedom. The symmetry condition brings this down to 10, tracelessness is one further condition, and the 4 conditions from space-like polarisations leaves us then with 5 degrees of freedom, which matches the number of helicity states.

$$
\begin{aligned}
T_4^{\mathrm{b},\mu\nu\alpha} &= \varepsilon^{\mu\nu q_1 q_2}(q_1+q_2)^\alpha,\\
T_5^{\mathrm{b},\mu\nu\alpha} &= \varepsilon^{\mu\nu q_1 q_2}(q_1-q_2)^\alpha,\\
T_6^{\mathrm{b},\mu\nu\alpha} &= \varepsilon^{\nu p q_1 q_2} q_2^\alpha q_2^\mu + \varepsilon^{\mu p q_1 q_2} q_1^\alpha q_1^\nu - \varepsilon^{\mu\nu p q_1} q_1^\alpha (q_1\cdot q_2) - \varepsilon^{\mu\nu p q_2} q_2^\alpha (q_1\cdot q_2),\\
T_7^{\mathrm{b},\mu\nu\alpha} &= -\varepsilon^{\nu p q_1 q_2} q_2^\alpha q_2^\mu + \varepsilon^{\mu p q_1 q_2} q_1^\alpha q_1^\nu - \varepsilon^{\mu\nu p q_1} q_1^\alpha (q_1\cdot q_2) + \varepsilon^{\mu\nu p q_2} q_2^\alpha (q_1\cdot q_2),\\
T_8^{\mathrm{b},\mu\nu\alpha} &= -\varepsilon^{\alpha\nu q_1 q_2} p^\mu - \varepsilon^{\alpha\mu q_1 q_2} p^\nu - \varepsilon^{\alpha\mu\nu q_2}(p\cdot q_1) - \varepsilon^{\alpha\mu\nu q_1}(p\cdot q_2),\\
T_9^{\mathrm{b},\mu\nu\alpha} &= -\varepsilon^{\alpha\nu p q_2} q_2^\mu q_1^2 + \varepsilon^{\alpha\nu p q_2} q_1^\mu (q_1\cdot q_2) + \varepsilon^{\alpha\mu p q_1} q_2^\nu (q_1\cdot q_2) - \varepsilon^{\alpha\mu p q_1} q_1^\nu q_2^2,\\
T_{10}^{\mathrm{b},\mu\nu\alpha} &= -\varepsilon^{\alpha\nu p q_2} q_2^\mu (p\cdot q_1) - \varepsilon^{\alpha\mu p q_1} q_1^\nu (p\cdot q_2) + \varepsilon^{\alpha\nu p q_2} p^\mu (q_1\cdot q_2) + \varepsilon^{\alpha\mu p q_1} p^\nu (q_1\cdot q_2),\\
T_{11}^{\mathrm{b},\mu\nu\alpha} &= \varepsilon^{\alpha\nu p q_2} q_2^\mu q_1^2 - \varepsilon^{\alpha\nu p q_2} q_1^\mu (q_1\cdot q_2) + \varepsilon^{\alpha\mu p q_1} q_2^\nu (q_1\cdot q_2) - \varepsilon^{\alpha\mu p q_1} q_1^\nu q_2^2,\\
T_{12}^{\mathrm{b},\mu\nu\alpha} &= \varepsilon^{\alpha\nu p q_2} q_2^\mu (p\cdot q_1) - \varepsilon^{\alpha\mu p q_1} q_1^\nu (p\cdot q_2) - \varepsilon^{\alpha\nu p q_2} p^\mu (q_1\cdot q_2) + \varepsilon^{\alpha\mu p q_1} p^\nu (q_1\cdot q_2),\\
T_{13}^{\mathrm{b},\mu\nu\alpha} &= \varepsilon^{\alpha p q_1 q_2} g^{\mu\nu}\big((q_1\cdot q_2) - q_2^\mu q_1^\nu\big).
\end{aligned}
\tag{3.23}
$$

Throughout this text, we will use the notation $\varepsilon^{\alpha p q_1 q_2} := \varepsilon^{\alpha\beta\gamma\delta} p_\beta (q_1)_\gamma (q_2)_\delta$ and similar. Out of these structures, $T_2^{\mathrm{b},\mu\nu\alpha}, T_4^{\mathrm{b},\mu\nu\alpha}, T_7^{\mathrm{b},\mu\nu\alpha}, T_9^{\mathrm{b},\mu\nu\alpha}$, and $T_{10}^{\mathrm{b},\mu\nu\alpha}$ are symmetric under photon crossing $(q_1,\mu) \leftrightarrow (q_2,\nu)$, and $T_1^{\mathrm{b},\mu\nu\alpha}$, $T_3^{\mathrm{b},\mu\nu\alpha}$, $T_5^{\mathrm{b},\mu\nu\alpha}$, $T_6^{\mathrm{b},\mu\nu\alpha}$, $T_8^{\mathrm{b},\mu\nu\alpha}$, $T_{11}^{\mathrm{b},\mu\nu\alpha}$, $T_{12}^{\mathrm{b},\mu\nu\alpha}$, and $T_{13}^{\mathrm{b},\mu\nu\alpha}$ are antisymmetric. The structures $T_1^{\mathrm{b},\mu\nu\alpha}, T_2^{\mathrm{b},\mu\nu\alpha}, T_3^{\mathrm{b},\mu\nu\alpha}, T_4^{\mathrm{b},\mu\nu\alpha}, T_5^{\mathrm{b},\mu\nu\alpha}$, and $T_8^{\mathrm{b},\mu\nu\alpha}$ have mass dimension 3, the others dimension 5. All corresponding scalar functions need to be of such dimension that $\mathcal{M}^{\mu\nu\alpha} = \sum_{i=1}^{13} \mathcal{F}_i^{\mathrm{b}} T_i^{\mathrm{b},\mu\nu\alpha}$ has mass dimension 1.

3.3.3 Degeneracies and Tarrach structures

It has been shown by TARRACH [226] and demonstrated, *e.g.*, in Refs. [227, 305] that it is not always possible to construct a basis of tensor structures such that the corresponding scalar functions are free of kinematic zeros and singularities. We will describe this issue and how to deal with it in the following.

Let us look at a simple example for illustration purposes: take the 2-dimensional vector space $V = \mathbb{R}^2$ over the field $\mathbb{R}$ and consider the basis $\{v_1 = (1, q_1\cdot q_2), v_2 = (-1, q_1\cdot q_2)\}$. As long as $q_1\cdot q_2 \neq 0$, we can express every vector $w \in V$ as $w = c_1 v_1 + c_2 v_2$; in particular, $w = (0,1) = (v_1+v_2)/(2q_1\cdot q_2)$, which we can also write as $2(q_1\cdot q_2)w = v_1 + v_2$. If we consider now the limit $q_1\cdot q_2 \to 0$, then $w = (0,1)$ does not have regular coefficients in this basis $\{v_1, v_2\}$ anymore, and it seems that we cannot represent w. But this is because the underlying field $\mathbb{R}$ has changed to $\mathbb{R}/(q_1\cdot q_2 \sim 0)$, where $\mathbb{R}/(q_1\cdot q_2 \sim 0)$ is the quotient set of $\mathbb{R}$ under the canonical surjection of the equivalence relation $q_1\cdot q_2 \sim 0$. Therefore, the notion of "linear independence" has changed, and we need to find another basis. If we take w as a new basis vector and drop, *e.g.*, v_2, this new basis is valid in the specific kinematic limit.

The equivalent situation is in the case of the vector space V of tensor structures with a basis $\{T_i^{\mathrm{b}}\}_{i=1}^N$ the existence of j relations

$$
\sum_{i=1}^{N} c_{ij} T_i^{\mathrm{b}} = (q_1\cdot q_2) T_{N+j}, \tag{3.24}
$$

where the coefficients c_{ij} are unique and at least one of them $\neq 0$ for a given relation j; *i.e.*, we exclude the trivial case $T_{N+j} = 0 \in V$. When looking at the basis in Eq. (3.23), one gets an idea how this happens since $q_1\cdot q_2$ occurs in some of the basis structures, but it is not easy to tell if and how exactly such relations arise for a given vector space and basis. In the limit $q_1\cdot q_2$, two problems occur: first, the basis structures T_i^{b} are not linearly independent anymore, and second, there are tensor structures T_{N+j} that cannot be represented in terms of the basis vectors. As in the simple example, the reason is that the underlying field of the vector space has changed according to $\mathbb{C} \to \mathbb{C}/(q_1\cdot q_2 \sim 0)$. In this kinematic limit, the previously constructed basis $\{T_i^{\mathrm{b}}\}_{i=1}^N$ is not a basis for the full vector space V anymore, but generates only a subspace $V' \subset V$.

In order to find the coefficients c_{ij} of the relations in Eq. (3.24) for the basis structures, one considers the following system of equations,

$$\lim_{(q_1\cdot q_2)\to 0} M^{\cancel{\text{pole}}}_{mk} M^{\text{proj}}_{kj} T^{\text{in}}_j = 0, \tag{3.25}$$

where M^{proj} denotes the matrix collecting the coefficients of the gauge projections and $M^{\cancel{\text{pole}}}$ collects the manipulations necessary to remove poles; the T^{in}_j are in this case symbolic. For $VP \to \gamma^*\gamma^*$, there are two non-trivial solutions to this system of equations, which read, translated to the basis structures,

$$\begin{aligned}
(p\cdot q_1)\big(T_9^{\text{b},\mu\nu\alpha} - T_{11}^{\text{b},\mu\nu\alpha}\big) - q_1^2\big(T_{10}^{\text{b},\mu\nu\alpha} - T_{12}^{\text{b},\mu\nu\alpha}\big) &= 2(q_1\cdot q_2)\varepsilon^{\alpha\nu pq_2}\big(q_1^\mu (p\cdot q_1) - p^\mu q_1^2\big) \\
&=: 2(q_1\cdot q_2) T_{14}^{\text{b},\mu\nu\alpha}, \\
(p\cdot q_2)\big(T_9^{\text{b},\mu\nu\alpha} + T_{11}^{\text{b},\mu\nu\alpha}\big) - q_2^2\big(T_{10}^{\text{b},\mu\nu\alpha} + T_{12}^{\text{b},\mu\nu\alpha}\big) &= 2(q_1\cdot q_2)\varepsilon^{\alpha\mu pq_1}\big(q_2^\nu (p\cdot q_2) - p^\nu q_2^2\big) \\
&=: 2(q_1\cdot q_2) T_{15}^{\text{b},\mu\nu\alpha}.
\end{aligned} \tag{3.26}$$

As nothing is special about $q_1\cdot q_2$ compared to other kinematic variables such as $p\cdot q_i$, the same situation can occur for any kinematic variable. Depending on the process, some variables might have a specific physical meaning; in our case, q_1^2 and q_2^2 are the photon virtualities and the limit $q_{1/2}^2 \to 0$ corresponds to the real-photon limit (where the axial-vector TFFs have to vanish).

The simple example we considered above suggests that we could drop two structures of the original basis and include $T_{14}^{\text{b},\mu\nu\alpha}$ and $T_{15}^{\text{b},\mu\nu\alpha}$ instead. However, this would unfortunately not solve our problem: it is clear from Eq. (3.26) that we would just shift the problem to different kinematic invariants, namely q_1^2 and q_2^2 or $p\cdot q_1$ and $p\cdot q_2$. While in some situations, singularities in other kinematic variables might not hurt anymore [305] and in other situations, additional symmetries makes it possible to absorb singularities into structures [227], we do not see such a solution in this case.

Instead, we need to extend the original basis by adding $T_{14}^{\text{b},\mu\nu\alpha}$ and $T_{15}^{\text{b},\mu\nu\alpha}$, such that we work with a generating set of 15 structures, $\{T_i^{\text{b},\mu\nu\alpha}\}_{i=1}^{15}$, which is not minimal, but generates the full vector space in any kinematic limit. This situation is similar to the one of the HLbL tensor in Ref. [227].

The extended generating set is not unique since one can always choose linear combinations of the structures. One alternative generating set is given in Sec. 3.9.3.

3.3.4 Projection of the scalar functions $\mathcal{F}_i$

Since the matrix element for $VP \to \gamma^*\gamma^*$ is written as $\mathcal{M}^{\mu\nu\alpha} = \sum_i \mathcal{F}_i T_i^{\mu\nu\alpha}$ and we have found a basis for $q_1\cdot q_2 \neq 0$ as well as an extended generating set that also works at $q_1\cdot q_2 = 0$, we now need to apply the respective mappings to the scalar functions $\mathcal{F}_i$. We can make use of the dual space framework again by noting that for a basis $\{T_i^{\text{b},\mu\nu\alpha}\}_{i=1}^{13}$, the expression

$$\varphi : V \to \mathbb{C}, \quad T_i^{\mu\nu\alpha} \mapsto \epsilon_\mu^*(q_1,\lambda_1)\epsilon_\nu^*(q_2,\lambda_2)\epsilon_\alpha(p,\lambda_V)\sum_{j=1}^{13}\mathcal{F}_j T_j^{\mu\nu\alpha}\delta_{ji} \in \mathbb{C}, \tag{3.27}$$

denotes a linear form; δ_{ji} is included explicitly to show that φ is a linear mapping as in Eq. (3.20). This linear form should be independent of the basis, or more precisely, the physical result should be independent, which is the reason for the contraction of the free LORENTZ indices. We have already explained how mappings work in the dual space; the only step that is missing here is the last one, where the linear relations obtained from the SCHOUTEN identity are used in order to reduce the set of gauge-invariant pole-free symmetrised structures to a basis (or the extended set $\{T_i^{\text{b},\mu\nu\alpha}\}_{i=1}^{15}$). This mapping is not invertible, and in contrast to the gauge projection, where it was enough to track what is mapped to 0, we now need to encode in the dual mapping how each structure is built from the basis, *i.e.*, revert what we did with the SCHOUTEN identities. We construct this dual mapping as a matrix M^{revS} and can thus obtain the scalar functions corresponding to $\{T_i^{\text{b},\mu\nu\alpha}\}$ via the concatenated dual mapping, which reads in terms of the matrices

$$\mathcal{F}_i^{\text{b}} = (M^{\text{revS}})^T_{in}\big((M^{\text{symm}})^{-1}\big)^T_{nm}\big((M^{\cancel{\text{pole}}})^{-1}\big)^T_{mk}(M^{\text{red}})^T_{kj}\mathcal{F}_j^{\text{in}}. \tag{3.28}$$

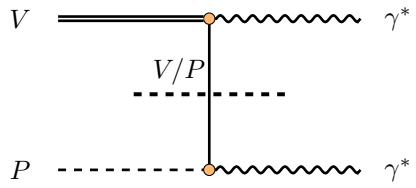

Figure 3.4: Left-hand unitarity cut for $VP \to \gamma^*\gamma^*$ with a V/P one-particle intermediate state.

3.4 Unitarity and dispersion relations for $VP \to \gamma^*\gamma^*$

Now that we know how to promote the scalar functions $\mathcal{F}_i$ in the $VP \to \gamma^*\gamma^*$ amplitude to a gauge-invariant basis or generating set, we can set up a model for them. For a complete unitary and crossing-symmetric amplitude, one needs to consider right- and left-hand cuts (RHCs and LHCs), *i.e.*, rescattering in the s-, t-, and u-channel. We consider here unitarity cuts only in the crossed channels t and u, *i.e.*, LHCs only.

3.4.1 Left-hand cuts

The lowest-lying intermediate states in the t- and u-channel are single-particle P and V states; see Fig. 3.4. These are assumed to dominate the respective amplitude. We denote the corresponding discontinuities by $\mathrm{disc}^P_{t/u}$ and $\mathrm{disc}^V_{t/u}$, with $t = (p-q_1)^2$ and $u = (p-q_2)^2$; they are given for a pseudoscalar intermediate state $P(k)$ by

$$\begin{aligned}
&\mathrm{disc}^P_t\big(-\mathrm{i}\langle\gamma^*(q_1,\lambda_1)\gamma^*(q_2,\lambda_2)|V(p,\lambda_V)P(p_P)\rangle\big)\\
&= e^2(2\pi)^4\delta^{(4)}(p+p_P-q_1-q_2)\epsilon^*_\mu(q_1,\lambda_1)\epsilon^*_\nu(q_2,\lambda_2)\epsilon_\alpha(p,\lambda_V)\,\mathrm{disc}^P_t\,\mathcal{M}^{\mu\nu\alpha}\\
&= \int \widetilde{\mathrm{d}k}\,\langle P(k)|P(-p_P)\gamma^*(q_2,\lambda_2)\rangle^*\,\langle P(k)|V(p,\lambda_V)\gamma^*(-q_1,\lambda_1)\rangle,\\
&\mathrm{disc}^P_u\big(-\mathrm{i}\langle\gamma^*(q_1,\lambda_1)\gamma^*(q_2,\lambda_2)|V(p,\lambda_V)P(p_P)\rangle\big)\\
&= e^2(2\pi)^4\delta^{(4)}(p+p_P-q_1-q_2)\epsilon^*_\mu(q_1,\lambda_1)\epsilon^*_\nu(q_2,\lambda_2)\epsilon_\alpha(p,\lambda_V)\,\mathrm{disc}^P_u\,\mathcal{M}^{\mu\nu\alpha}\\
&= \int \widetilde{\mathrm{d}k}\,\langle P(k)|P(-p_P)\gamma^*(q_1,\lambda_1)\rangle^*\,\langle P(k)|V(p,\lambda_V)\gamma^*(-q_2,\lambda_2)\rangle,
\end{aligned}\tag{3.29}$$

with $\widetilde{\mathrm{d}k} = \mathrm{d}^3k/\big((2\pi)^3 2k^0\big)$ and $\mathrm{disc}_t\, f(t;s,q_1^2,q_2^2) := f(t+\mathrm{i}\epsilon;s,q_1^2,q_2^2) - f(t-\mathrm{i}\epsilon;s,q_1^2,q_2^2)$, and similar for u. For a vector-meson intermediate state $V(k,\lambda_{\mathrm{LH}})$, the discontinuities from a t/u cut read

$$\begin{aligned}
&\mathrm{disc}^V_t\big(-\mathrm{i}\langle\gamma^*(q_1,\lambda_1)\gamma^*(q_2,\lambda_2)|V(p,\lambda_V)P(p_P)\rangle\big)\\
&= e^2(2\pi)^4\delta^{(4)}(p+p_P-q_1-q_2)\epsilon^*_\mu(q_1,\lambda_1)\epsilon^*_\nu(q_2,\lambda_2)\epsilon_\alpha(p,\lambda_V)\,\mathrm{disc}^V_t\,\mathcal{M}^{\mu\nu\alpha}\\
&= \int \widetilde{\mathrm{d}\ell}\,\langle V(k,\lambda_{\mathrm{LH}})|P(-p_P)\gamma^*(q_2,\lambda_2)\rangle^*\,\langle V(k,\lambda_{\mathrm{LH}})|V(p,\lambda_V)\gamma^*(-q_1,\lambda_1)\rangle,\\
&\mathrm{disc}^V_u\big(-\mathrm{i}\langle\gamma^*(q_1,\lambda_1)\gamma^*(q_2,\lambda_2)|V(p,\lambda_V)P(p_P)\rangle\big)\\
&= e^2(2\pi)^4\delta^{(4)}(p+p_P-q_1-q_2)\epsilon^*_\mu(q_1,\lambda_1)\epsilon^*_\nu(q_2,\lambda_2)\epsilon_\alpha(p,\lambda_V)\,\mathrm{disc}^V_u\,\mathcal{M}^{\mu\nu\alpha}\\
&= \int \widetilde{\mathrm{d}k}\,\langle V(k,\lambda_{\mathrm{LH}})|P(-p_P)\gamma^*(q_1,\lambda_1)\rangle^*\,\langle V(k,\lambda_{\mathrm{LH}})|V(p,\lambda_V)\gamma^*(-q_2,\lambda_2)\rangle.
\end{aligned}\tag{3.30}$$

As the $a_{1/2}$ meson decays primarily into $\rho\pi$, we consider $VP = \rho\pi$ in the following, and also restrict ourselves to π and ρ intermediate states for the moment. The respective amplitudes are given in terms

of the following form factors,

$$\begin{aligned}
\langle\pi^+(p_+)\pi^-(p_-)|j^\mu_{\rm em}|0\rangle &= \bar q^\mu F_\pi^V(q^2),\\
\langle\rho^+(p_+,\lambda_+)\rho^-(p_-,\lambda_-)|j^\mu_{\rm em}|0\rangle &= -\epsilon^*_\alpha(p_+,\lambda_+)\epsilon^*_\beta(p_-,\lambda_-)\times\\
&\quad\times\Big[g^{\alpha\beta}\bar q^\mu G_1(q^2)+(q^\alpha g^{\mu\beta}-q^\beta g^{\mu\alpha})G_2(q^2)-\bar q^\mu\frac{q^\alpha q^\beta}{2M_\rho^2}G_3(q^2)\Big],\\
\langle\pi^+(p_P)\rho^-(p,\lambda_V)|j^\mu_{\rm em}|0\rangle &= \epsilon_\alpha(p,\lambda_V)\varepsilon^{\mu\alpha p_P p}F_{\rho\pi}(q^2),
\end{aligned}\tag{3.31}$$

where $p_+ + p_- = q = p_P + p$ and $\bar q = p_+ - p_-$. The pion vector form factor is normalised to $F_\pi^V(0)=1$ and the normalisation of $F_{\rho\pi}$ is determined from

$$\Gamma(\rho\to\pi\gamma)=\frac{\alpha(M_\rho^2-M_\pi^2)^3}{24M_\rho^3}|F_{\rho\pi}(0)|^2,\tag{3.32}$$

where $\alpha=e^2/(4\pi)$ is the fine-structure constant. With $\Gamma_\rho = 149.1(8)\,\text{MeV}$ and $\mathcal{B}_{\rho\to\pi\gamma}=(4.5\pm0.5)\times10^{-4}$ [34], this leads to $|F_{\rho\pi}(0)|=0.73(4)\,\text{GeV}^{-1}$. From a BTT decomposition of $V_1\to V_2\gamma$ for two different vector mesons V_1 and V_2, one obtains 4 tensor structures and can introduce TFFs in analogy to the ρ form factors for later use,

$$\begin{aligned}
\langle V_1^+(p_+,\lambda_+)V_2^-(p_-,\lambda_-)|j^\mu_{\rm em}|0\rangle &= -\epsilon^*_\alpha(p_+,\lambda_+)\epsilon^*_\beta(p_-,\lambda_-)\times\\
&\quad\times\Big[g^{\alpha\beta}\big(\bar q^\mu q^2-q^\mu\Delta_{12}\big)H_1(q^2)+(q^\alpha g^{\mu\beta}-q^\beta g^{\mu\alpha})H_2(q^2)\\
&\quad-\Big(2\bar q^\mu q^\alpha q^\beta-(g^{\mu\alpha}q^\beta+g^{\mu\beta}q^\alpha)\Delta_{12}\Big)H_3(q^2)-\Big(2q^\mu q^\alpha q^\beta-(g^{\mu\alpha}q^\beta+g^{\mu\beta}q^\alpha)q^2\Big)H_4(q^2)\Big],
\end{aligned}\tag{3.33}$$

with $\Delta_{12}=M_{V_1}^2-M_{V_2}^2$. Note that there exists an additional FF H_4 for a tensor structure vanishing in the case of $V_1=V_2$. The TFF $F_{V\pi}$ for a vector meson V is defined in the same way as for the ρ. $H_{1,2,3,4}$ and $F_{V\pi}$ are assumed to be normalised and behave asymptotically similar to the respective form factors of the ρ.

With photons as external states, the pion vector form factor reads

$$\begin{aligned}
&\langle\pi^+(p_+)\pi^-(p_-)|\gamma^*(q,\lambda)\rangle\\
&=-\,\mathrm{i}e\,\epsilon_\mu(q,\lambda)\int\mathrm{d}^4x\,e^{-\mathrm{i}qx}\langle\pi^+(p_+)\pi^-(p_-)|j^\mu_{\rm em}|0\rangle=-\mathrm{i}e\,\epsilon_\mu(q,\lambda)(2\pi)^4\delta^{(4)}(p_++p_--q)\bar q^\mu F_\pi^V(q^2),
\end{aligned}\tag{3.34}$$

and the other FFs can be rewritten analogously. The vector FFs G_1, G_2, G_3 relate to the electric, magnetic, and quadrupole SACHS FFs G_C, G_M, and G_Q as [311]

$$\begin{pmatrix}G_1\\G_2\\G_3\end{pmatrix}=\begin{pmatrix}1 & 0 & -\frac{2}{3}\eta\\ 0 & 1 & 0\\ -\frac{1}{1+\eta} & \frac{1}{1+\eta} & \frac{3+2\eta}{3+3\eta}\end{pmatrix}\begin{pmatrix}G_C\\G_M\\G_Q\end{pmatrix},\tag{3.35}$$

with $\eta=-q^2/(4M_V^2)$. The normalisations of the SACHS FFs for a vector meson are, similar to the case of spin-1 gauge-bosons [312, 313], given by the charge for the electric FF, by the magnetic moment μ for the magnetic FF, and by the quadrupole moment Q for $G_Q(q^2)$,

$$eG_C(0)=e,\quad eG_M(0)=2M_V\mu,\quad eG_Q(0)=M_V^2Q.\tag{3.36}$$

With Eq. (3.35) follows

$$G_1(0)=1,\quad G_2(0)=\frac{2M_V\mu}{e},\quad G_3(0)=-1+\frac{2M_V\mu}{e}+\frac{M_V^2Q}{e}.\tag{3.37}$$

For the $W^\pm$ gauge bosons, $\mu = e/M_V$ and $Q = -e/M_V^2$ hold at tree level [313], which yields a normalisation of $G_2(0) = 2$ and $G_3(0) = 0$, where the latter relation is a fundamental result for vector mesons interacting with an electromagnetic field at tree level [314]. The high-energy behaviour can be fixed from pQCD to be $G_1(Q^2) \sim Q^{-4} \sim G_2(Q^2)$ and $G_3(Q^2) \sim Q^{-6}$ [194, 312, 315].

Inserting this into Eq. (3.29) and Eq. (3.30) yields the following expressions for the pion LHC,

$$\begin{aligned}
\operatorname{disc}_t^\pi \mathcal{M}^{\mu\nu\alpha} &= \int \widetilde{\mathrm{d}k}\,(2\pi)^4\delta^{(4)}(p-q_1-k)F_\pi^V(q_2^2)(p_\pi+k)^\nu F_{\rho\pi}(q_1^2)\varepsilon^{\mu\alpha k(-q_1)} \\
&= 2\pi\delta(t-M_\pi^2)\int\frac{\mathrm{d}^4k}{(2\pi)^4}\theta(k^0)\,(2\pi)^4\delta^{(4)}(p-q_1-k)F_\pi^V(q_2^2)(p_\pi+k)^\nu F_{\rho\pi}(q_1^2)\varepsilon^{\mu\alpha k(-q_1)} \\
&= 2\pi\delta(t-M_\pi^2)F_\pi^V(q_2^2)F_{\rho\pi}(q_1^2)(2q_1+q_2-2p)^\nu\varepsilon^{\mu\alpha q_1 p} \\
&= 2\pi\delta(t-M_\pi^2)F_\pi^V(q_2^2)F_{\rho\pi}(q_1^2)\big[2T_{26}^{\mathrm{in},\mu\nu\alpha}-2T_8^{\mathrm{in},\mu\nu\alpha}-T_{17}^{\mathrm{in},\mu\nu\alpha}\big] \\
&=: 2\pi\delta(t-M_\pi^2)\hat\rho_t^{\pi;\mu\nu\alpha}(q_1,q_2,p), \\
\operatorname{disc}_u^\pi \mathcal{M}^{\mu\nu\alpha} &= 2\pi\delta(u-M_\pi^2)F_\pi^V(q_1^2)F_{\rho\pi}(q_2^2)\big[2T_{24}^{\mathrm{in},\mu\nu\alpha}-2T_{15}^{\mathrm{in},\mu\nu\alpha}-T_6^{\mathrm{in},\mu\nu\alpha}\big] \\
&=: 2\pi\delta(u-M_\pi^2)\hat\rho_u^{\pi;\mu\nu\alpha}(q_1,q_2,p).
\end{aligned} \tag{3.38}$$

For the ρ intermediate state, we find

$$\begin{aligned}
\operatorname{disc}_t^\rho \mathcal{M}^{\mu\nu\alpha} &= \int \widetilde{\mathrm{d}k}\,(2\pi)^4\delta^{(4)}(p-q_1-k)F_{\rho\pi}(q_2^2)\varepsilon^{\nu\tau k q_2}\times \\
&\quad\times\Big[G_1(q_1^2)g_\tau^\alpha(p+k)^\mu - G_2(q_1^2)(q_1^\tau g^{\alpha\mu}-q_1^\alpha g^{\tau\mu}) - G_3(q_1^2)\frac{q_1^\tau q_1^\alpha}{2M_\rho^2}(p+k)^\mu\Big] \\
&= 2\pi\delta(t-M_\rho^2)F_{\rho\pi}(q_2^2)\Big[G_1(q_1^2)\Big(T_4^{\mathrm{in},\mu\nu\alpha}+T_6^{\mathrm{in},\mu\nu\alpha}-2T_{22}^{\mathrm{in},\mu\nu\alpha}-2T_{24}^{\mathrm{in},\mu\nu\alpha}\Big) \\
&\quad - G_2(q_1^2)\Big(T_{10}^{\mathrm{in},\mu\nu\alpha}+T_{12}^{\mathrm{in},\mu\nu\alpha}-T_{32}^{\mathrm{in},\mu\nu\alpha}\Big) - \frac{G_3(q_1^2)}{2M_\rho^2}\Big(T_{49}^{\mathrm{in},\mu\nu\alpha}-2T_{46}^{\mathrm{in},\mu\nu\alpha}\Big)\Big] \\
&=: 2\pi\delta(t-M_\rho^2)\hat\rho_t^{\rho;\mu\nu\alpha}(q_1,q_2,p), \\
\operatorname{disc}_u^\rho \mathcal{M}^{\mu\nu\alpha} &= \int \widetilde{\mathrm{d}k}\,(2\pi)^4\delta^{(4)}(p-q_2-k)F_{\rho\pi}(q_1^2)\varepsilon^{\mu\tau k q_1}\times \\
&\quad\times\Big[G_1(q_2^2)g_\tau^\alpha(p+k)^\nu - G_2(q_2^2)(q_2^\tau g^{\alpha\nu}-q_2^\alpha g^{\tau\nu}) - G_3(q_2^2)\frac{q_2^\tau q_2^\alpha}{2M_\rho^2}(p+k)^\nu\Big] \\
&= 2\pi\delta(u-M_\rho^2)F_{\rho\pi}(q_1^2)\Big[G_1(q_2^2)\Big(2T_{25}^{\mathrm{in},\mu\nu\alpha}-2T_{26}^{\mathrm{in},\mu\nu\alpha}-T_{16}^{\mathrm{in},\mu\nu\alpha}+T_{17}^{\mathrm{in},\mu\nu\alpha}\Big) \\
&\quad - G_2(q_2^2)\Big(T_{19}^{\mathrm{in},\mu\nu\alpha}-T_{20}^{\mathrm{in},\mu\nu\alpha}+T_{33}^{\mathrm{in},\mu\nu\alpha}\Big) - \frac{G_3(q_2^2)}{2M_\rho^2}\Big(2T_{57}^{\mathrm{in},\mu\nu\alpha}-T_{59}^{\mathrm{in},\mu\nu\alpha}\Big)\Big] \\
&=: 2\pi\delta(u-M_\rho^2)\hat\rho_u^{\rho;\mu\nu\alpha}(q_1,q_2,p).
\end{aligned} \tag{3.39}$$

Constructing the $\rho\pi \to \gamma^*\gamma^*$ amplitude from its imaginary part, which yields, in the case of one-particle intermediate states, just the pole residues $\hat\rho$, results in

$$\begin{aligned}
\mathcal{M}^{\mu\nu\alpha} &= \frac{1}{2\pi\mathrm{i}}\int\mathrm{d}t'\,\frac{\operatorname{disc}_t^\pi\mathcal{M}^{\mu\nu\alpha}}{t'-t} + \frac{\operatorname{disc}_t^\rho\mathcal{M}^{\mu\nu\alpha}}{t'-t} + \frac{1}{2\pi\mathrm{i}}\int\mathrm{d}u'\,\frac{\operatorname{disc}_u^\pi\mathcal{M}^{\mu\nu\alpha}}{u'-u} + \frac{\operatorname{disc}_t^\rho\mathcal{M}^{\mu\nu\alpha}}{u'-u} \\
&= \mathrm{i}\Big[\frac{\hat\rho_t^{\pi;\mu\nu\alpha}(q_1,q_2,p)}{t-M_\pi^2} + \frac{\hat\rho_t^{\rho;\mu\nu\alpha}(q_1,q_2,p)}{t-M_\rho^2} + \frac{\hat\rho_u^{\pi;\mu\nu\alpha}(q_1,q_2,p)}{u-M_\pi^2} + \frac{\hat\rho_u^{\rho;\mu\nu\alpha}(q_1,q_2,p)}{u-M_\rho^2}\Big] \\
&=: \mathrm{i}\sum_i T_i^{\mu\nu\alpha}(q_1,q_2,p)\mathcal{F}_i(s,q_1^2,q_2^2).
\end{aligned} \tag{3.40}$$

This defines the scalar functions $\mathcal{F}_i(s,q_1^2,q_2^2)$ as coefficients of the tensor structures in $\hat{\rho}_t^{\pi;\mu\nu\alpha}(q_1,q_2,p)/(t-M_\pi^2)$ and similar for $t\leftrightarrow u$ and $\pi\leftrightarrow\rho$. The scalar functions $\mathcal{F}_i$ we just constructed meet the requirements of the SCHWARZ reflection principle $f(z^*)=\big(f(z)\big)^*$. With this, Eq. (3.40) shows that $\mathcal{M}^{\mu\nu\alpha}$ cannot be a SCHWARZ function since it is defined with a relative factor of i.

3.4.2 Projected scalar functions for the LHCs

With the tensor structures projected to the basis in Eq. (3.23), we use the dual mapping described in Sec. 3.3.4 in order to obtain for the scalar functions

$$
\begin{aligned}
\mathcal{F}_1^{\mathrm{b}} =&\frac{F_{\rho\pi}(q_2^2)}{2(M_\rho^2-t)}\Big(G_1(q_1^2)-G_3(q_1^2)\Big)-\frac{F_{\rho\pi}(q_1^2)}{2(M_\rho^2-u)}\Big(G_1(q_2^2)-G_3(q_2^2)\Big),\\
\mathcal{F}_2^{\mathrm{b}} =&\frac{F_{\rho\pi}(q_2^2)}{2(M_\rho^2-t)}\Big(G_1(q_1^2)-G_3(q_1^2)\Big)+\frac{F_{\rho\pi}(q_1^2)}{2(M_\rho^2-u)}\Big(G_1(q_2^2)-G_3(q_2^2)\Big),\\
\mathcal{F}_3^{\mathrm{b}} =&-\frac{F_{\rho\pi}(q_2^2)G_2(q_1^2)}{M_\rho^2-t}+\frac{F_{\rho\pi}(q_1^2)G_2(q_2^2)}{M_\rho^2-u},\\
\mathcal{F}_4^{\mathrm{b}} =&\frac{F_{\rho\pi}(q_2^2)}{2(M_\rho^2-t)}\left(G_1(q_1^2)-G_2(q_1^2)-\frac{G_3(q_1^2)q_1^2}{4M_\rho^2}\right)+\frac{F_{\rho\pi}(q_1^2)}{2(M_\rho^2-u)}\left(G_1(q_2^2)-G_2(q_2^2)-\frac{G_3(q_2^2)q_2^2}{4M_\rho^2}\right),\\
\mathcal{F}_5^{\mathrm{b}} =&\frac{F_{\rho\pi}(q_2^2)}{2(M_\rho^2-t)}\left(G_1(q_1^2)-G_2(q_1^2)-\frac{G_3(q_1^2)q_1^2}{4M_\rho^2}\right)-\frac{F_{\rho\pi}(q_1^2)}{2(M_\rho^2-u)}\left(G_1(q_2^2)-G_2(q_2^2)-\frac{G_3(q_2^2)q_2^2}{4M_\rho^2}\right),\\
\mathcal{F}_6^{\mathrm{b}} =&\frac{F_{\rho\pi}(q_2^2)G_3(q_1^2)}{4M_\rho^2(M_\rho^2-t)}-\frac{F_{\rho\pi}(q_1^2)G_3(q_2^2)}{4M_\rho^2(M_\rho^2-u)},\\
\mathcal{F}_7^{\mathrm{b}} =&\frac{F_{\rho\pi}(q_2^2)G_3(q_1^2)}{4M_\rho^2(M_\rho^2-t)}+\frac{F_{\rho\pi}(q_1^2)G_3(q_2^2)}{4M_\rho^2(M_\rho^2-u)},\\
\mathcal{F}_8^{\mathrm{b}} =&\frac{F_{\rho\pi}(q_2^2)}{M_\rho^2-t}\Big(G_1(q_1^2)-\frac{G_2(q_1^2)}{2}-\frac{G_3(q_1^2)q_1^2}{4M_\rho^2}\Big)-\frac{F_{\rho\pi}(q_1^2)}{M_\rho^2-u}\Big(G_1(q_2^2)-\frac{G_2(q_2^2)}{2}-\frac{G_3(q_2^2)q_2^2}{4M_\rho^2}\Big),\\
\mathcal{F}_9^{\mathrm{b}} =&\frac{-1}{2q_1\cdot q_2}\left[F_{\rho\pi}(q_2^2)\left(\frac{F_\pi^V(q_1^2)}{M_\pi^2-u}+\frac{G_1(q_1^2)-\frac{G_3(q_1^2)q_1^2}{2M_\rho^2}}{M_\rho^2-t}\right)+F_{\rho\pi}(q_1^2)\left(\frac{F_\pi^V(q_2^2)}{M_\pi^2-t}+\frac{G_1(q_2^2)-\frac{G_3(q_2^2)q_2^2}{2M_\rho^2}}{M_\rho^2-u}\right)\right],\\
\mathcal{F}_{10}^{\mathrm{b}} =&\frac{1}{q_1\cdot q_2}\left[F_{\rho\pi}(q_2^2)\left(\frac{F_\pi^V(q_1^2)}{M_\pi^2-u}+\frac{G_1(q_1^2)-\frac{G_3(q_1^2)q_1^2}{2M_\rho^2}}{M_\rho^2-t}\right)\right.\\
&\left.+F_{\rho\pi}(q_1^2)\left(\frac{F_\pi^V(q_2^2)}{M_\pi^2-t}+\frac{G_1(q_2^2)-\frac{G_3(q_2^2)q_2^2}{2M_\rho^2}}{M_\rho^2-u}\right)\right]+\frac{F_{\rho\pi}(q_2^2)G_3(q_1^2)}{2M_\rho^2(M_\rho^2-t)}+\frac{F_{\rho\pi}(q_1^2)G_3(g_2^2)}{2M_\rho^2(M_\rho^2-u)},\\
\mathcal{F}_{11}^{\mathrm{b}} =&\frac{1}{2q_1\cdot q_2}\left[F_{\rho\pi}(q_2^2)\left(\frac{F_\pi^V(q_1^2)}{M_\pi^2-u}+\frac{G_1(q_1^2)-\frac{G_3(q_1^2)q_1^2}{2M_\rho^2}}{M_\rho^2-t}\right)-F_{\rho\pi}(q_1^2)\left(\frac{F_\pi^V(q_2^2)}{M_\pi^2-t}+\frac{G_1(q_2^2)-\frac{G_3(q_2^2)q_2^2}{2M_\rho^2}}{M_\rho^2-u}\right)\right],\\
\mathcal{F}_{12}^{\mathrm{b}} =&\frac{1}{q_1\cdot q_2}\left[-F_{\rho\pi}(q_2^2)\left(\frac{F_\pi^V(q_1^2)}{M_\pi^2-u}+\frac{G_1(q_1^2)-\frac{G_3(q_1^2)q_1^2}{2M_\rho^2}}{M_\rho^2-t}\right)\right.\\
&\left.+F_{\rho\pi}(q_1^2)\left(\frac{F_\pi^V(q_2^2)}{M_\pi^2-t}+\frac{G_1(q_2^2)-\frac{G_3(q_2^2)q_2^2}{2M_\rho^2}}{M_\rho^2-u}\right)\right]+\frac{F_{\rho\pi}(q_2^2)G_3(q_1^2)}{2M_\rho^2(M_\rho^2-t)}-\frac{F_{\rho\pi}(q_1^2)G_3(g_2^2)}{2M_\rho^2(M_\rho^2-u)},\\
\mathcal{F}_{13}^{\mathrm{b}} =&0.
\end{aligned}
\tag{3.41}
$$

Here, we encounter a few intricacies: $\mathcal{F}_1$ and $\mathcal{F}_2$ are initially given by a number of terms with coefficients consisting of fractions of the kinematic invariables $q_1\cdot q_2$, $p\cdot q_1$, $p\cdot q_2$, q_1^2, q_2^2, and p^2. The simple and

pole-free version given in Eq. (3.41) can be obtained by making use of *on-shell relations* for the ρ and π meson,

$$p^2 = M_\rho^2, \qquad s+t+u = M_\rho^2 + M_\pi^2 + q_1^2 + q_2^2. \tag{3.42}$$

This does not come as a surprise since the BTT procedure is supposed to construct a gauge-invariant pole-free amplitude for external, asymptotic states. Furthermore, even when using these relations, $\mathcal{F}_{9-12}$ still exhibit kinematic singularities in $q_1 \cdot q_2 = (s - q_1^2 - q_2^2)/2$ when projected to the 13 basis structures. This is due to the degeneracies in the kinematic limit $q_1 \cdot q_2 \to 0$, which we discussed in Sec. 3.3.3, and to the asymmetry of the diagram, *i.e.*, the fact that the ρ and the π meson couple to the photon in different ways.

In order to cancel those kinematic singularities, two modifications are necessary: we need to extend the basis as explained in Sec. 3.3.3 and additionally include another intermediate state in the LHC. The reason for the latter is that we can see from Eq. (3.41) that the kinematic singularities would cancel if we had

$$F_{\rho\pi}(q_1^2)\Big[F_\pi^V(q_2^2) - G_1(q_2^2) + \frac{G_3(q_2)^2 q_2^2}{2M_\rho^2}\Big] = 0 \tag{3.43}$$

and the equivalent with $(q_1 \leftrightarrow q_2)$, together with the on-shell relations in Eq. (3.42). This condition is in contradiction to the expected high-energy behaviour for the form factors involved. In order to mend this problem arising from the asymmetry of the system, we can introduce an additional effective intermediate state R in the LHC, which we think of as a heavier version of the ρ meson. We repeat the steps of expressing the discontinuities in terms of the initial tensor structures—the result of which can be found in Sec. 3.9.4—solving the dispersion integrals, and mapping the resulting scalar functions in accordance with the basis structures. This yields the following additional pieces in the projected scalar functions, where we leave out $H_3(q^2)$ and $H_4(q^2)$ as higher-order effects,

$$\begin{aligned}
\mathcal{F}_1^{\mathrm{b},R} &= \frac{F_{R\pi}(q_2^2)}{2(M_R^2-t)} H_1(q_1^2)\big[q_1^2+\Delta_{\rho R}\big] - \frac{F_{R\pi}(q_1^2)}{2(M_R^2-u)} H_1(q_2^2)\big[q_2^2+\Delta_{\rho R}\big],\\
\mathcal{F}_2^{\mathrm{b},R} &= \frac{F_{R\pi}(q_2^2)}{2(M_R^2-t)} H_1(q_1^2)\big[q_1^2+\Delta_{\rho R}\big] + \frac{F_{R\pi}(q_1^2)}{2(M_R^2-u)} H_1(q_2^2)\big[q_2^2+\Delta_{\rho R}\big],\\
\mathcal{F}_3^{\mathrm{b},R} &= -\frac{F_{R\pi}(q_2^2)H_2(q_1^2)}{M_R^2-t} + \frac{F_{R\pi}(q_1^2)H_2(q_2^2)}{M_R^2-u},\\
\mathcal{F}_4^{\mathrm{b},R} &= \frac{F_{R\pi}(q_2^2)}{2(M_R^2-t)}\Big(H_1(q_1^2)\big[q_1^2+\Delta_{\rho R}\big] - H_2(q_1^2)\Big) + \frac{F_{R\pi}(q_1^2)}{2(M_R^2-u)}\Big(H_1(q_2^2)\big[q_2^2+\Delta_{\rho R}\big] - H_2(q_2^2)\Big),\\
\mathcal{F}_5^{\mathrm{b},R} &= \frac{F_{R\pi}(q_2^2)}{2(M_R^2-t)}\Big(H_1(q_1^2)\big[q_1^2+\Delta_{\rho R}\big] - H_2(q_1^2)\Big) - \frac{F_{R\pi}(q_1^2)}{2(M_R^2-u)}\Big(H_1(q_2^2)\big[q_2^2+\Delta_{\rho R}\big] - H_2(q_2^2)\Big),\\
\mathcal{F}_6^{\mathrm{b},R} &= 0,\\
\mathcal{F}_7^{\mathrm{b},R} &= 0,\\
\mathcal{F}_8^{\mathrm{b},R} &= \frac{F_{R\pi}(q_2^2)}{M_R^2-t}\Big(H_1(q_1^2)q_1^2 - \frac{H_2(q_1^2)}{2}\Big) - \frac{F_{R\pi}(q_1^2)}{M_R^2-u}\Big(H_1(q_2^2)q_2^2 - \frac{H_2(q_2^2)}{2}\Big),\\
\mathcal{F}_9^{\mathrm{b},R} &= -\frac{F_{R\pi}(q_2^2)H_1(q_1^2)}{2(q_1\cdot q_2)(M_R-t)}\big[q_1^2+\Delta_{\rho R}\big] - \frac{F_{R\pi}(q_1^2)H_1(q_2^2)}{2(q_1\cdot q_2)(M_\rho^2-u)}\big[q_2^2+\Delta_{\rho R}\big],\\
\mathcal{F}_{10}^{\mathrm{b},R} &= \frac{F_{R\pi}(q_2^2)H_1(q_1^2)q_1^2}{(q_1\cdot q_2)(M_R-t)} + \frac{F_{R\pi}(q_1^2)H_1(q_2^2)q_2^2}{(q_1\cdot q_2)(M_\rho^2-u)},\\
\mathcal{F}_{11}^{\mathrm{b},R} &= \frac{F_{R\pi}(q_2^2)H_1(q_1^2)}{2(q_1\cdot q_2)(M_R-t)}\big[q_1^2+\Delta_{\rho R}\big] - \frac{F_{R\pi}(q_1^2)H_1(q_2^2)}{2(q_1\cdot q_2)(M_\rho^2-u)}\big[q_2^2+\Delta_{\rho R}\big],
\end{aligned}$$

$$\mathcal{F}_{12}^{\mathrm{b},R} = -\frac{F_{R\pi}(q_2^2)H_1(q_1^2)q_1^2}{(q_1\cdot q_2)(M_R-t)} + \frac{F_{R\pi}(q_1^2)H_1(q_2^2)q_2^2}{(q_1\cdot q_2)(M_\rho^2-u)},$$
$$\mathcal{F}_{13}^{\mathrm{b},R} = 0. \tag{3.44}$$

If we now impose the condition

$$F_{\rho\pi}(q_2^2)\big[G_1(q_1^2) - F_\pi^V(q_1^2)\big] + q_1^2 F_{R\pi}(q_2^2)H_1(q_1^2) = 0 \tag{3.45}$$

and its equivalent for $q_1^2 \leftrightarrow q_2^2$, setting $G_3(q_1^2)$ and $H_{3,4}(q_1^2)$ to 0, and extend our set of tensor structures from the basis $\{T_i^{\mathrm{b},\mu\nu\alpha}\}_{i=1}^{13}$ to the generating set $\{T_i^{\mathrm{b},\mu\nu\alpha}\}_{i=1}^{15}$, the kinematic singularities cancel. For this, the on-shell conditions Eq. (3.42) have to be used again.

Since the set of 15 tensor structures is not a basis, we need to ensure that no double counting occurs for the scalar functions. The tensor structures $T_i^{\mathrm{b},\mu\nu\alpha}$ and scalar functions $\mathcal{F}_i^{\mathrm{b}}$ for $i \in \{1,\dots 8,13\}$ are not affected by the TARRACH issue and are kept as $\mathcal{F}_i^{\mathrm{b}} + \mathcal{F}_i^{\mathrm{b},R}$ from Eq. (3.41) and Eq. (3.44). For $i \in \{9,10,11,12\}$ (note that $\mathcal{F}_{13}^{\mathrm{b}} + \mathcal{F}_{13}^{\mathrm{b},R}$ vanishes), we demand

$$\sum_{i=9}^{12} T_i^{\mathrm{b},\mu\nu\alpha}(\mathcal{F}_i^{\mathrm{b}} + \mathcal{F}_i^{\mathrm{b},R}) = \sum_{i=9}^{15} T_i^{\mathrm{b},\mu\nu\alpha}\mathcal{F}_i^{\mathrm{bT}}, \tag{3.46}$$

where $\mathcal{F}_i^{\mathrm{bT}}$ are the scalar functions for the generating set $\{T_i^{\mathrm{b},\mu\nu\alpha}\}_{i=1}^{15}$ related to the TARRACH problem. Starting on the left-hand side of the equation, one can reassemble the terms in the sum such that the additional summands $T_{14}^{\mathrm{b},\mu\nu\alpha}\mathcal{F}_{14}^{\mathrm{bT}} + T_{15}^{\mathrm{b},\mu\nu\alpha}\mathcal{F}_{15}^{\mathrm{bT}}$ are created, where kinematic prefactors in the tensor structures Eq. (3.26) are conveniently provided by the scalar functions. The result of this reshuffling is given by

$$\begin{aligned}
\mathcal{F}_9^{\mathrm{bT}} &= -\frac{F_{\rho\pi}(q_2^2)G_1(q_1^2)}{(M_\pi^2-u)(M_\rho^2-t)} + \frac{F_{R\pi}(q_2^2)H_1(q_1^2)}{M_\pi^2-u} - \frac{F_{\rho\pi}(q_1^2)G_1(q_2^2)}{(M_\pi^2-t)(M_\rho^2-u)} + \frac{F_{R\pi}(q_1^2)H_1(q_2^2)}{M_\pi^2-t},\\
\mathcal{F}_{10}^{\mathrm{bT}} &= \frac{2F_{\rho\pi}(q_2^2)G_1(q_1^2)}{(M_\pi^2-u)(M_\rho^2-t)} + \frac{2F_{\rho\pi}(q_1^2)G_1(q_2^2)}{(M_\pi^2-t)(M_\rho^2-u)},\\
\mathcal{F}_{11}^{\mathrm{bT}} &= \frac{F_{\rho\pi}(q_2^2)G_1(q_1^2)}{(M_\pi^2-u)(M_\rho^2-t)} - \frac{F_{R\pi}(q_2^2)H_1(q_1^2)}{M_\pi^2-u} - \frac{F_{\rho\pi}(q_1^2)G_1(q_2^2)}{(M_\pi^2-t)(M_\rho^2-u)} + \frac{F_{R\pi}(q_1^2)H_1(q_2^2)}{M_\pi^2-t},\\
\mathcal{F}_{12}^{\mathrm{bT}} &= -\frac{2F_{\rho\pi}(q_2^2)G_1(q_1^2)}{(M_\pi^2-u)(M_\rho^2-t)} + \frac{2F_{\rho\pi}(q_1^2)G_1(q_2^2)}{(M_\pi^2-t)(M_\rho^2-u)},\\
\mathcal{F}_{13}^{\mathrm{bT}} &= 0,\\
\mathcal{F}_{14}^{\mathrm{bT}} &= -2F_{R\pi}(q_2^2)H_1(q_1^2)\Big[\frac{1}{M_R^2-t} + \frac{1}{M_\pi^2-u}\Big] = -2F_{R\pi}(q_2^2)H_1(q_1^2)\frac{2(q_1\cdot q_2)-\Delta_{\rho R}}{(M_R^2-t)(M_\pi^2-u)},\\
\mathcal{F}_{15}^{\mathrm{bT}} &= -2F_{R\pi}(q_1^2)H_1(q_2^2)\Big[\frac{1}{M_R^2-u} + \frac{1}{M_\pi^2-t}\Big] = -2F_{R\pi}(q_1^2)H_1(q_2^2)\frac{2(q_1\cdot q_2)-\Delta_{\rho R}}{(M_R^2-u)(M_\pi^2-t)}.
\end{aligned} \tag{3.47}$$

Note that the pion vector form factor has vanished from these expressions due to Eq. (3.45). We collect the unaltered scalar functions $\{\mathcal{F}_i^{\mathrm{b}} + \mathcal{F}_i^{\mathrm{b},R}\}_{i=1}^{8}$ together with the modified scalar functions in Eq. (3.47) in the set $\{\mathcal{F}_i^{\mathrm{bT}}\}_{i=1}^{15}$. For the alternative generating set of tensor structures, the mapped scalar functions look different; see Sec. 3.9.3. The sums over all tensor structures and scalar functions are equivalent for both generating sets up to on-shell relations,

$$\sum_{i=1}^{15} T_i^{\mathrm{b},\mu\nu\alpha}\mathcal{F}_i^{\mathrm{bT}} \overset{\text{on-shell}}{\equiv} \sum_{i=1}^{15} T_i^{\mathrm{b2},\mu\nu\alpha}\mathcal{F}_i^{\mathrm{b2}}. \tag{3.48}$$

The condition in Eq. (3.45) is matched and the correct high-energy behaviour and normalisation ensured via a suitable choice of $H_1(q^2)$ and $F_{R\pi}(q^2)$. Assuming that $F_{R\pi}(q^2)$ has the same behaviour as $F_{\rho\pi}(q^2)$ fixes the electric FF of R to

$$H_1(q^2) = \frac{1}{q^2}\left[F_\pi^V(q^2) - G_1(q^2)\right] \tag{3.49}$$

up to normalisation, where the normalisations $F_{R\pi}(0)$ and $H_1(0)$ scale inversely to each other. In the simplest VMD model that fulfils the pQCD constraints,

$$F_\pi^V(q^2) = \frac{M_\rho^2}{M_\rho^2 - q^2}, \quad G_1(q^2) = \frac{M_\rho^2 M_{\rho'}^2}{(M_\rho^2 - q^2)(M_{\rho'}^2 - q^2)}, \quad F_{\rho\pi}(q^2) = C_{\rho\pi\gamma}\frac{M_\omega^2 M_{\omega'}^2}{(M_\omega^2 - q^2)(M_{\omega'}^2 - q^2)}, \tag{3.50}$$

this implies

$$F_{R\pi}(q_1^2)H_1(q_2^2) = -C_{\rho\pi\gamma}\frac{M_\omega^2 M_{\omega'}^2}{(M_\omega^2 - q_1^2)(M_{\omega'}^2 - q_1^2)}\frac{M_\rho^2}{(M_\rho^2 - q_2^2)(M_{\rho'}^2 - q_2^2)}. \tag{3.51}$$

Normalisation and asymptotic behaviour of $G_2(q^2)$ and by analogy of $H_2(q^2)$ suggest

$$G_2(q^2) = \frac{2M_\rho^2 M_{\rho'}^2}{(M_\rho^2 - q^2)(M_{\rho'}^2 - q^2)}, \quad H_2(q^2) = \frac{2M_\rho^2 M_{\rho'}^2}{(M_\rho^2 - q^2)(M_{\rho'}^2 - q^2)}. \tag{3.52}$$

Note that including $H_2(q^2)$ is not necessary to cancel any kinematic singularities; it is merely included for consistency reasons.

3.5 From $VP \to \gamma^*\gamma^*$ to $A/T \to \gamma^*\gamma^*$

With the $VP \to \gamma^*\gamma^*$ amplitude written in a gauge-invariant form, together with a concrete reconstruction of the scalar functions for $VP = \rho\pi$ from cuts in $\pi/\rho/R$ intermediate states in the t- and u-channel, we can now turn to our goal of describing a_1 and a_2 TFFs. The framework can potentially also be used for f_1' with $VP = K\bar{K}^*$ in the future; since we do not discuss this case here, we will now write $\rho\pi$ instead of VP. We will put most attention to the case of the a_1 meson. The a_2 can be treated in analogy, and additional details are collected in Ref. [316].

3.5.1 The couplings $a_{1/2} \to \rho\pi$

For the coupling of $a_1(p_A, \epsilon_\beta^A)$ to $\rho(p, \epsilon_\alpha^V)\pi(p_\pi)$, there are two tensor structures,

$$g^{\alpha\beta}, \quad p^\beta p_A^\alpha. \tag{3.53}$$

From the structure $\langle[V,A]P\rangle$ in terms of meson multiplet matrices, which can be found in Sec. 3.9.6, one can conclude that the two charge channels relate to each other as $a_1(\rho^+\pi^- - \rho^-\pi^+)$, which has to change sign under hermitian conjugation, such that the vertex rule should include a factor of i; this is also what one finds from RChPT [21, 317, 318]. The prefactors one finds in RChPT are not unique and can be absorbed into the coupling, such that we denote the vertex rule as

$$\mathcal{M}_{a_1\rho\pi}^{\beta\delta} = \mathrm{i}\, C_{a_1\rho\pi}\left(g^{\beta\delta}(p\cdot p_A) - p^\beta p_A^\delta\right), \qquad \mathcal{M}_{a_1\rho\pi}^{\mathrm{simp},\,\beta\delta} = \mathrm{i}\, C_{a_1\rho\pi} g^{\beta\delta}, \tag{3.54}$$

where the simplified vertex rule takes into account only the first tensor structure. It is defined here since it will be used in this work; this corresponds to an incomplete amplitude, but has advantages for the computation. Taking into account both tensor structure enforces transversality for ρ and a_1, as can be shown by contracting with the propagators in different gauges.

The coupling strength $C_{a_1\rho\pi}$ can be extracted from experimental results. Since we will restrict our calculation to the simplified vertex rule $\mathcal{M}^{\text{simp, }\beta\delta}_{a_1\rho\pi}$, the coupling constant is calculated using only this structure. Additionally, we assume that the total decay width Γ_{a_1} is saturated by the sum of the two charge-conjugated decay widths into $\rho^\pm\pi^\mp$, $\Gamma_{a_1} = \Gamma_{a_1\to\rho^+\pi^-} + \Gamma_{a_1\to\rho^-\pi^+}$. With this,

$$\begin{aligned}
\mathrm{d}\Gamma_{a_1\to\rho^+\pi^-} &= \frac{1}{32\pi^2}\overline{|\mathcal{M}^{\text{simp}}_{a_1\rho\pi}|^2}\frac{|\vec{p}|}{M_{a_1}^2}\mathrm{d}\Omega,\\
2\Gamma_{a_1\to\rho^+\pi^-} &= 2\frac{4\pi}{32\pi^2}\frac{1}{3}\left[3+\frac{\lambda_{a_1\rho\pi}}{4M_{a_1}^2M_\rho^2}\right]\frac{\sqrt{\lambda_{a_1\rho\pi}}}{2M_{a_1}^3}|C_{a_1\rho\pi}|^2 = \frac{\sqrt{\lambda_{a_1\rho\pi}}}{8\pi M_{a_1}^3}|C_{a_1\rho\pi}|^2\left[1+\frac{\lambda_{a_1\rho\pi}}{12M_{a_1}^2M_\rho^2}\right]
\end{aligned} \tag{3.55}$$

with

$$|\vec{p}| = \frac{1}{2M_{a_1}}\sqrt{\lambda(M_{a_1}^2,M_\rho^2,M_\pi^2)} =: \frac{\sqrt{\lambda_{a_1\rho\pi}}}{2M_{a_1}}, \qquad E_\rho = \frac{M_{a_1}^2+M_\rho^2-M_\pi^2}{2M_{a_1}}. \tag{3.56}$$

With $\Gamma_{a_1}^{\text{Compass}} = 380(80)\,\text{MeV}$ [319], which was obtained using a BREIT–WIGNER fit, and neglecting the second term in the bracket since it yields a correction of $\sim 4\%$, this results in

$$|C_{a_1\rho\pi}^{\text{Compass}}| = 4.4(5)\,\text{GeV}, \tag{3.57}$$

where the uncertainty estimate comes from evaluating $|C_{a_1\rho\pi}|$ for the boundary values of Γ_{a_1}. Using the complex $\mathcal{T}$-matrix pole location at $(1209 \pm 4^{+12}_{-9}) - \mathrm{i}(288^{+45}_{-10})\,\text{MeV}$ [320] and again neglecting the second term in the bracket yields

$$|C_{a_1\rho\pi}^{\text{pole}}| = 5.6^{+4}_{-2}\,\text{GeV}. \tag{3.58}$$

There are systematic sources of uncertainty here: on our side neglecting one of the tensor structures, and on the experimental side, the value obtained from a BREIT–WIGNER fit is incompatible with the one using the complex $\mathcal{T}$-matrix pole location. In order to account for this inconclusive situation, the rather conservative interval $\Gamma_{a_1} \in (250, 600)\,\text{MeV}$, which was quoted by the PDG up to 2024 [34], is taken to estimate the uncertainty, and the central value is used in this work whenever needed,

$$|C_{a_1\rho\pi}| = 4.7(1.0)\,\text{GeV}. \tag{3.59}$$

Similarly, for the decay of the tensor meson $a_2(p_T, \epsilon^T_{\beta\gamma}) \to \rho(p, \epsilon^V_\alpha)\pi(p_\pi)$, the vertex corresponds in terms of multiplet matrices to $\langle T[V,P]\rangle$ and has a factor of i for similar reasons as the a_1. Due to parity, it includes a LEVI-CIVITA tensor, which gets contracted with two independent momenta. In order to ensure transversality of the tensor and vector meson, we construct the vertex rule [283, 316, 321]

$$\mathcal{M}^{\beta\gamma\alpha}_{a_2\rho\pi} = \mathrm{i}\,C_{a_2\rho\pi}\frac{4}{M_{a_2}^2}\left[\varepsilon^{\alpha\beta pp_T}\left(p_T^\gamma(p\cdot p_T) - p^\gamma M_{a_2}^2\right) + \varepsilon^{\alpha\gamma pp_T}\left(p_T^\beta(p\cdot p_T) - p^\beta M_{a_2}^2\right)\right]. \tag{3.60}$$

In this case, it is not possible to construct a simplified vertex rule without momentum dependence due to the LEVI-CIVITA tensor. The corresponding coupling constant is extracted from the experimental decay width $\Gamma_{a_2} = 107(5)\,\text{MeV}$ and the branching ratio $\Gamma_{a_2\to 3\pi}/\Gamma_{a_2} = 70.1(2.7)\%$ [34], which does not distinguish different charge channels, such that

$$\begin{aligned}
\Gamma_{a_2\to\rho\pi} &= \frac{4\pi}{32\pi^2}\frac{1}{5}|C_{a_2\rho\pi}|^2\frac{16}{M_{a_2}^4}s^T_{\beta\gamma\beta'\gamma'}\left[\varepsilon^{\alpha\beta pp_T}\left(p_T^\gamma(p\cdot p_T) - p^\gamma M_T^2\right) + \varepsilon^{\alpha\gamma pp_T}\left(p_T^\beta(p\cdot p_T) - p^\beta M_T^2\right)\right]\\
&\quad\times\left(g_{\alpha\alpha'} - \frac{p_\alpha p_{\alpha'}}{M_\rho^2}\right)\left[\varepsilon^{\alpha'\beta' pp_T}\left(p_T^{\gamma'}(p\cdot p_T) - p^{\gamma'}M_T^2\right) + \varepsilon^{\alpha'\gamma' pp_T}\left(p_T^{\beta'}(p\cdot p_T) - p^{\beta'}M_T^2\right)\right]\\
&= \frac{\lambda_{a_2\rho\pi}^{5/2}}{20\pi M_{a_2}^5}|C_{a_2\rho\pi}|^2
\end{aligned} \tag{3.61}$$

with

$$|\vec{p}| = \frac{\sqrt{\lambda_{a_2\rho\pi}}}{2M_{a_1}}, \qquad E_\rho = \frac{M_{a_2}^2 + M_\rho^2 - M_\pi^2}{2M_{a_2}} \tag{3.62}$$

and the polarisation sum of the tensor meson [308]

$$s^T_{\beta\gamma\beta'\gamma'} := \sum_{\lambda_T} \epsilon^{\lambda_T}_{\beta\gamma}(p_T)\big(\epsilon^{\lambda_T}_{\beta'\gamma'}(p_T)\big)^* = \frac{1}{2}(s_{\beta\gamma'}s_{\beta'\gamma} + s_{\beta\beta'}s_{\gamma\gamma'}) - \frac{1}{3}s_{\beta\gamma}s_{\beta'\gamma'}. \tag{3.63}$$

With this, we find

$$|C_{a_2\rho\pi}| = 3.45(2)\,\mathrm{GeV}^{-2}. \tag{3.64}$$

3.5.2 Projection to axial-vector transition form factors

The amplitude for an axial-vector meson A coupling to two virtual photons is given by

$$\begin{aligned}
&\langle\gamma^*(q_1,\lambda_1)\gamma^*(q_2,\lambda_2)|A(p_A,\lambda_A)\rangle \\
&= -(2\pi)^4\delta^{(4)}(p_A - q_1 - q_2)e^2\epsilon^*_\mu(q_1,\lambda_1)\epsilon^*_\nu(q_2,\lambda_2)\int \mathrm{d}^4x\, e^{\mathrm{i}q_1x}\langle 0|T\{j^\mu_{\mathrm{em}}(z)j^\nu_{\mathrm{em}}(0)\}|A(p_A,\lambda_A)\rangle \\
&= \mathrm{i}(2\pi)^4\delta^{(4)}(p_A - q_1 - q_2)e^2\epsilon^*_\mu(q_1,\lambda_1)\epsilon^*_\nu(q_2,\lambda_2)\epsilon_\beta(p_A,\lambda_A)\mathcal{M}^{\mu\nu\beta}_{A\gamma^*\gamma^*}
\end{aligned} \tag{3.65}$$

and can be BTT decomposed as [308]

$$\mathcal{M}^{\mu\nu\beta}_{A\gamma^*\gamma^*} = \frac{\mathrm{i}}{M_A^2}\sum_{i=1}^{3}\tilde{T}_i^{\mu\nu\beta}F_i^A. \tag{3.66}$$

Note that, similar to the case of $\mathcal{M}^{\mu\nu\alpha}_{VP\gamma^*\gamma^*}$, the matrix element is defined with a factor of i. The tensor structures are given by

$$\begin{aligned}
\tilde{T}_1^{\mu\nu\beta}(q_1,q_2) &= \varepsilon^{\mu\nu q_1 q_2}(q_1 - q_2)^\beta, \\
\tilde{T}_2^{\mu\nu\beta}(q_1,q_2) &= \varepsilon^{\beta\nu q_1 q_2}q_1^\mu + \varepsilon^{\beta\mu\nu q_2}q_1^2, \\
\tilde{T}_3^{\mu\nu\beta}(q_1,q_2) &= \varepsilon^{\beta\mu q_1 q_2}q_2^\nu + \varepsilon^{\beta\mu\nu q_1}q_2^2.
\end{aligned} \tag{3.67}$$

Under photon crossing $\mathcal{C}_{12} : q_1 \leftrightarrow q_2, \mu \leftrightarrow \nu$, they behave as

$$\begin{aligned}
\tilde{T}_1^{\mu\nu\beta}(q_1,q_2) &\xrightarrow{\mathcal{C}_{12}} \tilde{T}_1^{\nu\mu\beta}(q_2,q_1) = -\tilde{T}_1^{\mu\nu\beta}(q_1,q_2), \\
\tilde{T}_2^{\mu\nu\beta}(q_1,q_2) &\xrightarrow{\mathcal{C}_{12}} \tilde{T}_2^{\nu\mu\beta}(q_2,q_1) = -\tilde{T}_3^{\mu\nu\beta}(q_1,q_2).
\end{aligned} \tag{3.68}$$

Thus, one can construct one symmetric and two antisymmetric structures,

$$\begin{aligned}
\tilde{T}_{a1}^{\mu\nu\beta}(q_1,q_2) &= \tilde{T}_1^{\mu\nu\beta}(q_1,q_2), \\
\tilde{T}_{a2}^{\mu\nu\beta}(q_1,q_2) &= 1/2\left[\tilde{T}_2^{\mu\nu\beta}(q_1,q_2) + \tilde{T}_3^{\mu\nu\beta}(q_1,q_2)\right], \\
\tilde{T}_s^{\mu\nu\beta}(q_1,q_2) &= 1/2\left[\tilde{T}_2^{\mu\nu\beta}(q_1,q_2) - \tilde{T}_3^{\mu\nu\beta}(q_1,q_2)\right],
\end{aligned} \tag{3.69}$$

with corresponding form factors

$$\begin{aligned}
F_{a1}^A(q_1^2,q_2^2) &= F_1^A(q_1^2,q_2^2), \\
F_{a2}^A(q_1^2,q_2^2) &= F_2^A(q_1^2,q_2^2) + F_3^A(q_1^2,q_2^2), \\
F_s^A(q_1^2,q_2^2) &= F_2^A(q_1^2,q_2^2) - F_3^A(q_1^2,q_2^2).
\end{aligned} \tag{3.70}$$

For the lowest-lying isoscalar axial-vector f_1, the respective form factors $F_i^{f_1}$ have been studied in detail and constrained with available experimental data in Refs. [144, 277]. The asymptotic behaviour in terms of the BRODSKY–LEPAGE limit [113–115] is discussed in Ref. [308]. For both virtualities vanishing, the whole amplitude has to vanish due to the LANDAU–YANG theorem. In order to still access the normalisation of these TFFs, one defines the equivalent two-photon decay width [322]

$$\tilde{\Gamma}_{A\gamma\gamma} := \lim_{q_1^2\to 0} \frac{M_A^2}{2q_1^2}\Gamma(A\to\gamma_L^*\gamma_T), \tag{3.71}$$

where the spin-averaged longitudinal-transversal (LT) width is given by [144]

$$\Gamma(A\to\gamma_L^*\gamma_T) = \frac{1}{3}\sum_{\substack{\lambda_A\in\{\pm,0\}\\ \lambda_2=\pm}} \int \mathrm{d}\Gamma^{0\lambda_2;\lambda_A}_{A\gamma^*\gamma^*}\Big|_{q_2^2=0}. \tag{3.72}$$

Since $\mathrm{d}\Gamma_{A\gamma^*\gamma^*}$ is expressed in terms of helicity amplitudes $H_{\lambda_1\lambda_2;\lambda_A}$ as [308]

$$\mathrm{d}\Gamma^{\lambda_1\lambda_2;\lambda_A}_{A\gamma^*\gamma^*} = \frac{e^4}{32\pi^2}|H_{\lambda_1\lambda_2;\lambda_A}|^2\frac{\lambda_{A12}^{1/2}}{2M_A^3}\mathrm{d}\Omega, \tag{3.73}$$

with $\lambda_{A12} := \lambda(M_A^2, q_1^2, q_2^2)$, the equivalent two-photon decay width can be expressed in terms of the normalisation of F_2^A as

$$\tilde{\Gamma}_{A\gamma\gamma} = \frac{\pi\alpha^2 M_A}{12}|F_2^A(0,0)|^2. \tag{3.74}$$

Symmetry under photon crossing shows that $|F_3^A(0,0)|^2 = |F_2^A(0,0)|^2$ and that $|F_1^A(0,0)|^2 = 0$. The axial-vector TFFs can be obtained from $\mathcal{M}^{\mu\nu\beta}_{A\gamma^*\gamma^*}\epsilon_\beta(p_A,\lambda_A)\epsilon^*_\mu(q_1,\lambda_1)\epsilon^*_\nu(q_2,\lambda_2) = \mathcal{M}_{A\gamma^*\gamma^*}$ via projection,

$$F_j^A = (-\mathrm{i}M_A^2)\mathrm{Proj}^j_{\mu\nu\beta}\mathcal{M}^{\mu\nu\beta}_{A\gamma^*\gamma^*}, \tag{3.75}$$

where the projectors are constructed taking into account not only the 3 physical tensor structures, but also a fourth one,

$$\tilde{T}_4^{\mu\nu\beta} = \varepsilon^{\mu\nu q_1 q_2}(q_1+q_2)^\beta, \tag{3.76}$$

which drops out of any physical quantity upon contraction with the axial-vector meson polarisation sum

$$\sum_{\lambda_A}\epsilon_\beta(p_A,\lambda_A)\epsilon_{\beta'}(p_A,\lambda_A)^* = -\Big(g_{\beta\beta'} - \frac{(p_A)_\beta(p_A)_{\beta'}}{M_A^2}\Big). \tag{3.77}$$

It still modifies the projectors because we do not enforce the axial-vector meson to be space-like in the $a_1\rho\pi$ vertex, but the projection to the fourth structure does not contribute to any physical quantity. The projectors are given by

$$\begin{aligned}
\mathrm{Proj}_1^{\mu\nu\beta} =& N\Big[\varepsilon^{\beta\nu q_1 q_2}q_2^\mu q_1^2 - \varepsilon^{\beta\mu q_1 q_2}q_1^\nu(q_1\cdot q_2)\Big],\\
\mathrm{Proj}_2^{\mu\nu\beta} =& N\Big[\varepsilon^{\beta\nu q_1 q_2}q_2^\mu(q_1\cdot q_2) - \varepsilon^{\beta\mu q_1 q_2}q_1^\nu q_2^2\Big],\\
\mathrm{Proj}_3^{\mu\nu\beta} =& \frac{N}{2}\Big[\varepsilon^{\beta\nu q_1 q_2}q_2^\mu q_1^2 + \varepsilon^{\beta\mu q_1 q_2}q_1^\nu q_2^2 + \varepsilon^{\mu\nu q_1 q_2}\big(q_2^\beta(q_1\cdot q_2+q_1^2) - q_1^\beta(q_1\cdot q_2+q_2^2)\big)\Big],\\
\mathrm{Proj}_4^{\mu\nu\beta} =& \frac{N}{2}\Big[-\varepsilon^{\beta\nu q_1 q_2}q_2^\mu q_1^2 + \varepsilon^{\beta\mu q_1 q_2}q_1^\nu q_2^2 + \varepsilon^{\mu\nu q_1 q_2}\big(q_2^\beta(q_1\cdot q_2-q_1^2) - q_1^\beta(q_1\cdot q_2-q_2^2)\big)\Big],
\end{aligned} \tag{3.78}$$

with

$$N = \frac{1}{2\big((q_1\cdot q_2)^2 - q_1^2 q_2^2\big)^2}. \tag{3.79}$$

For a tensor meson T, there are 5 tensor structures and transition form factors F_i^T, matching the 5 helicity amplitudes $H_{\lambda_1\lambda_2;\lambda_T}$ [308],

$$H_{+-;2+} = H_{-+;2-}, \quad H_{+0;+} = H_{-0;-}, \quad H_{0-;+} = H_{0+;-}, \quad H_{++;0} = H_{--;0}, \quad H_{00;0}. \tag{3.80}$$

The on-shell decay width $\Gamma_{T\gamma\gamma}$ depends only on the first two TFFs,

$$\Gamma_{T\gamma\gamma} = \frac{\pi\alpha^2 M_T}{5}\left(|F_1^T(0,0)|^2 + \frac{1}{24}|F_2^T(0,0)|^2\right) \tag{3.81}$$

and the projection from

$$\mathcal{M}_{T\gamma^*\gamma^*} = \sum_{i=1}^{5} \hat{T}_i^{\mu\nu\alpha\beta} \frac{1}{M_{a_2}^{n_i}} F_i^T(q_1^2, q_2^2), \qquad n_i = \begin{cases} 1, & i = 1 \\ 3, & \text{else} \end{cases}, \tag{3.82}$$

to the TFFs $F_i^T(q_1^2, q_2^2)$ can be done by constructing projectors similar to the axial-vector case [316]. Note that there is no extra factor of i in this definition.

The tensor-meson tensor structures are given by [308]

$$\begin{aligned}
\hat{T}_1^{\mu\nu\alpha\beta} &= g^{\mu\alpha}P_{21}^{\nu\beta} + g^{\nu\alpha}P_{12}^{\mu\beta} + g^{\mu\beta}P_{21}^{\nu\alpha} + g^{\nu\beta}P_{12}^{\mu\alpha} + g^{\mu\nu}\big(q_1^\alpha q_2^\beta + q_2^\alpha q_1^\beta\big) - (q_1\cdot q_2)\big(g^{\mu\alpha}g^{\nu\beta} + g^{\nu\alpha}g^{\mu\beta}\big), \\
\hat{T}_2^{\mu\nu\alpha\beta} &= \big(q_1^\alpha q_1^\beta + q_2^\alpha q_2^\beta\big)P_{12}^{\mu\nu}, \\
\hat{T}_3^{\mu\nu\alpha\beta} &= P_{11}^{\mu\alpha}P_{22}^{\nu\beta} + P_{11}^{\mu\beta}P_{22}^{\nu\alpha}, \\
\hat{T}_4^{\mu\nu\alpha\beta} &= P_{12}^{\mu\alpha}P_{22}^{\nu\beta} + P_{12}^{\mu\beta}P_{22}^{\nu\alpha}, \\
\hat{T}_5^{\mu\nu\alpha\beta} &= P_{21}^{\nu\alpha}P_{11}^{\mu\beta} + P_{21}^{\nu\beta}P_{11}^{\mu\alpha},
\end{aligned} \tag{3.83}$$

where $P_{ij}^{\mu\nu} := g^{\mu\nu}(q_i\cdot q_j) - q_j^\mu q_i^\nu$.

3.5.3 Unitarity in $a_1 \to \gamma^*\gamma^*$

We discuss now the case of the a_1. A similar calculation can be done for the a_2; we will point out where differences occur. A direct loop calculation of $a_1 \to \gamma^*\gamma^*$ would look like

$$\begin{aligned}
&\epsilon_\mu^*(q_1,\lambda_1)\epsilon_\nu^*(q_2,\lambda_2)\epsilon_\beta(p_A,\lambda_A)\,\mathcal{M}_{a_1\gamma^*\gamma^*}^{\mu\nu\beta}(s,q_1^2,q_2^2) \\
&= \epsilon_\mu^*(q_1,\lambda_1)\epsilon_\nu^*(q_2,\lambda_2)\epsilon_\beta(p_A,\lambda_A)\int\frac{\mathrm{d}^4p}{(2\pi)^4}\,\mathcal{M}_{a_1\rho\pi}^{\beta\delta}\,P_{\delta\alpha}^\rho(p)P^\pi(p-q_1-q_2)\mathcal{M}_{VP\gamma^*\gamma^*}^{\mu\nu\alpha} \\
&\overset{\text{simpl. } a_1\rho\pi}{=} \epsilon_\mu^*(q_1,\lambda_1)\epsilon_\nu^*(q_2,\lambda_2)\epsilon_\beta(p_A,\lambda_A)\,\mathrm{i}\,C_{a_1\rho\pi}\int\frac{\mathrm{d}^4p}{(2\pi)^4}P_{\beta\alpha}^\rho(p)P^\pi(p-q_1-q_2)\times \\
&\qquad\times\mathrm{i}\sum_{i=1}^{15}T_i^{\mu\nu\alpha}\mathcal{F}_i(q_1^2,q_2^2;s,t,u) \\
&=: \epsilon_\mu^*(q_1,\lambda_1)\epsilon_\nu^*(q_2,\lambda_2)\epsilon_\beta(p_A,\lambda_A)\,C_{a_1\rho\pi}\sum_{i=1}^{15}I_i^{\mu\nu\beta},
\end{aligned} \tag{3.84}$$

where $P_{\delta\alpha}^\rho(q)$ and $P^\pi(q)$ are the ρ and π meson propagators, respectively, and we inserted the simplified $a_1\rho\pi$ vertex from Eq. (3.54) and the gauge-invariant pole-free decomposition of $\mathcal{M}_{VP\gamma^*\gamma^*}^{\mu\nu\alpha}$ in the third line.

Since the constructed amplitude holds only for on-shell V and P mesons, we cannot naively use $\mathcal{M}_{\rho\pi\gamma^*\gamma^*}^{\mu\nu\alpha} = \mathrm{i}\sum_{i=1}^{15}\mathcal{F}_i^{\mathrm{bT}}T_i^{\mathrm{bT},\mu\nu\alpha}$ in a loop calculation as the real part would depend on the generating set. Therefore, we need to reconstruct the $a_1 \to \gamma^*\gamma^*$ matrix element from this on-shell amplitude using unitarity and analyticity. By virtue of the latter property, $\mathcal{M}_{a_1\gamma^*\gamma^*}$ is determined from its

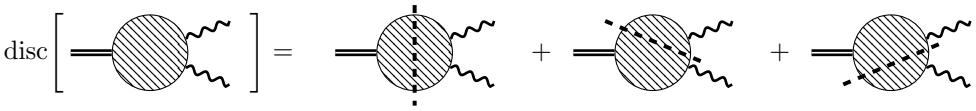

Figure 3.5: The discontinuity of a three-point function can be reconstructed from three cuts in s, q_1^2, and q_2^2.

discontinuity. CUTKOSKY'S rules [139] imply that the discontinuity of an amplitude is proportional to the sum over all possible cuts. In the case of a three-point function, one can cut in $s = (q_1 + q_2)^2$, q_1^2, and q_2^2; see Fig. 3.5. In the narrow-resonance approximation, s is not a free kinematic variable, but fixed to $M_{a_1}^2$; in this sense, we consider rather an axial-vector current here, which we later fix to be the a_1. The discontinuity in q_1^2 is given by the unitarity relation

$$\begin{aligned}&\operatorname{disc}_{q_1^2}\big(-\mathrm{i}\langle\gamma^*(q_2,\lambda_2)|\gamma^*(-q_1,\lambda_1)a_1(p_A,\lambda_A)\rangle\big) = e^2(2\pi)^4\delta^{(4)}(p_A-q_1-q_2)\operatorname{disc}_{q_1^2}\mathcal{M}_{a_1\gamma^*\gamma^*}\\ &= \sum_n \frac{1}{S_n}\int\left(\prod_{j=1}^{N_n}\widetilde{\mathrm{d}k_j}\right)\langle n|\gamma^*(q_2,\lambda_2)\rangle^*\,\langle n|\gamma^*(-q_1,\lambda_1)a_1(p_A,\lambda_A)\rangle,\end{aligned} \tag{3.85}$$

$\operatorname{disc}_{q_2^2}$ is given by the same expression with $1 \leftrightarrow 2$. Thus, knowledge about $\langle n|a_1\gamma^*\rangle$ amplitudes for suitable intermediate states $|n\rangle$ is required, which we do not have, such that we neglect $\operatorname{disc}_{q_1^2}$ and $\operatorname{disc}_{q_2^2}$ in this work. This leaves us with the discontinuity in s,

$$\begin{aligned}&\operatorname{disc}_s\big(-\mathrm{i}\langle\gamma^*(q_1,\lambda_1)\gamma^*(q_2,\lambda_2)|a_1(p_A,\lambda_A)\rangle\big) = e^2(2\pi)^4\delta^{(4)}(p_A-q_1-q_2)\operatorname{disc}_s\mathcal{M}_{a_1\gamma^*\gamma^*}\\ &= \sum_n \frac{1}{S_n}\int\left(\prod_{j=1}^{N_n}\widetilde{\mathrm{d}k_j}\right)\langle n|\gamma^*(q_1,\lambda_1)\gamma^*(q_2,\lambda_2)\rangle^*\,\langle n|a_1(p_A,\lambda_A)\rangle.\end{aligned} \tag{3.86}$$

Due to the fact that a_1 decays mainly into $\rho\pi$, considering $|n\rangle = |\rho\pi\rangle$ is assumed to capture the dominant contribution.

The subamplitude $\rho\pi \to \gamma^*\gamma^*$ emerging from this cut should be unitarised itself, which means that rescattering effects (in the s-channel) need to be taken care of. Additionally, crossing symmetry for $\rho\pi \to \gamma^*\gamma^*$ requires the inclusion of left-hand cuts arising from a unitarisation in $\rho\gamma^* \to \pi\gamma^*$, where ρ and π are the lowest-lying intermediate states. In this work, we neglect the RHCs and only take into account the LHCs, which we calculated in Sec. 3.4.1, as these are assumed to yield the dominant contribution to the $\rho\pi \to \gamma^*\gamma^*$ amplitude. Thus, we disregard parts of the $a_1\gamma^*\gamma^*$ discontinuity as well as rescattering in $\rho\pi \to \gamma^*\gamma^*$. [#7]

The dispersion relation we use for the $a_1\gamma^*\gamma^*$ amplitude reads

$$\mathcal{M}_{a_1\gamma^*\gamma^*}(s,q_1^2,q_2^2) = \frac{1}{2\pi\mathrm{i}}\int_{(M_\rho+M_\pi)^2}^{\infty}\mathrm{d}x\,\frac{\operatorname{disc}_x\mathcal{M}_{a_1\gamma^*\gamma^*}(x,q_1^2,q_2^2)}{x-s}. \tag{3.87}$$

Since we are interested in $F_i^{a_1}$, and these TFFs are SCHWARZ functions in contrast to $\mathcal{M}^{\mu\nu\beta}_{a_1\gamma^*\gamma^*}$, we continue our construction with $F_i^{a_1}(s,q_1^2,q_2^2)$, which we define to be a generalisation of the physical TFFs via $\lim_{s\to M_{a_1}^2} F_i^{a_1}(s,q_1^2,q_2^2) = F_i^{a_1}(q_1^2,q_2^2)$. With this, there is a dispersion relation in s for $F_i^{a_1}(s,q_1^2,q_2^2)$, with a $\rho\pi$ intermediate state; see Fig. 3.6. Although the $F_i^{a_1}(s,q_1^2,q_2^2)$ are SCHWARZ functions, their discontinuities in s

$$\operatorname{disc}_s F_i^{a_1}(s,q_1^2,q_2^2) = F_i^{a_1}(s+\mathrm{i}\epsilon,q_1^2+\mathrm{i}\epsilon,q_2^2+\mathrm{i}\epsilon) - F_i^{a_1}(s-\mathrm{i}\epsilon,q_1^2+\mathrm{i}\epsilon,q_2^2+\mathrm{i}\epsilon) \tag{3.88}$$

are in general not equal to their imaginary parts

$$2\mathrm{i}\,\operatorname{Im}F_i^{a_1}(s,q_1^2,q_2^2) = 2\mathrm{i}\big[F_i^{a_1}(s+\mathrm{i}\epsilon,q_1^2+\mathrm{i}\epsilon,q_2^2+\mathrm{i}\epsilon) - F_i^{a_1}(s-\mathrm{i}\epsilon,q_1^2-\mathrm{i}\epsilon,q_2^2-\mathrm{i}\epsilon)\big] \tag{3.89}$$

[#7] Additional effects in $\rho\pi \to \gamma^*\gamma^*$ such as triangle singularities are neglected, as well. These are contained in the neglected part of the $a_1\gamma^*\gamma^*$ discontinuity.

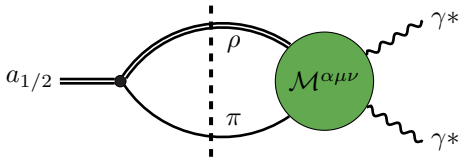

Figure 3.6: Reconstruction of the $a_{1/2}$ TFFs from the unitarity cut in s.

since $F_i^{a_1}$ can also have cuts in q_1^2 and q_2^2. These occur in the time-like region, such that we can identify $\mathrm{disc}_s\, F_i^{a_1}(s,q_1^2,q_2^2)$ with $2\mathrm{i}\,\mathrm{Im}\, F_i^{a_1}(s,q_1^2,q_2^2)$ for space-like photon virtualities. In this region, we can use the imaginary part obtained from a loop calculation as in Eq. (3.84) in order to determine the discontinuity in s.

The objects we actually calculate numerically are the integrals $\mathrm{Proj}^i_{\mu\nu\beta} I_j^{\mu\nu\beta}$, where the indeces i,j relate to the i-th TFF of a_1 and the j-th scalar function in $\mathcal{M}^{\mu\nu\alpha}_{\rho\pi\gamma^*\gamma^*}$. In terms of these objects and with $s_{\mathrm{thr}} = (M_\pi + M_\rho)^2$, we can express the TFFs for space-like virtualities as

$$\begin{aligned} F_i^{a_1}(s,q_1^2,q_2^2) &= (-\mathrm{i}M_{a_1}^2)\mathrm{Proj}^i_{\mu\nu\beta}\mathcal{M}^{\mu\nu\beta}_{A\gamma^*\gamma^*}(s,q_1^2,q_2^2) \\ &= (-\mathrm{i}M_{a_1}^2)\mathrm{Proj}^i_{\mu\nu\beta}\Big(C_{a_1\rho\pi}\sum_{j=1}^{15} I_j^{\mu\nu\beta}\Big) = (-\mathrm{i}M_{a_1}^2)C_{a_1\rho\pi}\sum_{j=1}^{15}\mathrm{Proj}^i_{\mu\nu\beta} I_j^{\mu\nu\beta} \\ &= \frac{1}{\pi}\int_{s_{\mathrm{thr}}}^{\infty}\mathrm{d}x\,\frac{(-\mathrm{i}M_{a_1}^2)C_{a_1\rho\pi}\sum_{j=1}^{15}\mathrm{Re}\left[\mathrm{Proj}^i_{\mu\nu\beta} I_j^{\mu\nu\beta}\right]}{x-s} =: \frac{1}{\pi}\int_{s_{\mathrm{thr}}}^{\infty}\mathrm{d}x\,\frac{\mathrm{Im}\, F_i^{a_1}(x,q_1^2,q_2^2)}{x-s}\,. \end{aligned} \tag{3.90}$$

For the evaluation we use the fact that this integrand decreases fast enough and formally rewrite it,

$$\begin{aligned} F_i^{a_1}(s,q_1^2,q_2^2) &= \frac{1}{\pi}\int_{s_{\mathrm{thr}}}^{\infty}\mathrm{d}x\frac{\mathrm{Im}\, F_i^{a_1}(x,q_1^2,q_2^2)}{x-s} \\ &= \frac{1}{\pi}\int_{s_{\mathrm{thr}}}^{\infty}\mathrm{d}x\frac{x\,\mathrm{Im}\, F_i^{a_1}(x,q_1^2,q_2^2)}{x(x-s)} =: \frac{1}{\pi}\int_{s_{\mathrm{thr}}}^{\infty}\mathrm{d}x\frac{E_i(x,q_1^2,q_2^2)}{x(x-s)} \\ &= \frac{1}{\pi}\int_{s_{\mathrm{thr}}}^{\infty}\mathrm{d}x\frac{E_i(x,q_1^2,q_2^2)-E_i(s,q_1^2,q_2^2)}{x(x-s)} + E_i(s,q_1^2,q_2^2)\frac{1}{\pi}\int_{s_{\mathrm{thr}}}^{\infty}\mathrm{d}x\frac{1}{x(x-s)}, \end{aligned} \tag{3.91}$$

where it is now manifest that the integral converges as long as $E_j(x,q_1^2,q_2^2)$ does not diverge in the limit $x\to\infty$.[#8] The first integral in the last line of Eq. (3.91) is evaluated numerically, whereas the second integral is analytically equal to

$$\frac{1}{s}\ln\left(\frac{s_{\mathrm{thr}}}{s_{\mathrm{thr}}-s}\right). \tag{3.92}$$

If we had not redefined the integrand according to $x\,\mathrm{Im}\, F_i^{a_1}(x,q_1^2,q_2^2) =: E_i(x,q_1^2,q_2^2)$, then the logarithm would diverge with the upper limit of the integral at ∞. One could solve this issue by introducing a subtraction, but this would require us to fix a subtraction constant, which reduces the predictive power of the model. Besides this, it is important to choose the correct branch of the logarithm, namely what is sometimes referred to as $\ln^{II}$,

$$\ln z = \ln|z| + \mathrm{i}\begin{cases}\arg z, & \arg z > 0,\\ \arg z + 2\pi, & \arg z < 0\end{cases}. \tag{3.93}$$

We are limited, however, to convergent loop integrals $I_j^{\mu\nu\beta}$, which unfortunately constrains us to the simplified version of $\mathcal{M}_{a_1\rho\pi}$ from Eq. (3.54) and to a ρ propagator that does not enforce transversality,

[#8] The trick in the last line, where $E_i(s,q_1^2,q_2^2)$ is subtracted and added in order to regularise the integrand, can already be found in [134] and [323]; it is equivalent to the Sokhotski–Plemelj formula.

$P^{\rho}_{\beta\alpha}(p) = (-\mathrm{i}g_{\beta\alpha})/(p^2 - M_\rho^2)$. This issue also prevents us from doing a similar evaluation for the a_2 due to the inevitable factor of the loop momentum p in $\mathcal{M}^{\beta\gamma\alpha}_{a_2\rho\pi}$; see Eq. (3.60). In order to overcome this problem, one needs to introduce some regularisation and renormalisation scheme, which we hope to do in the future.

3.6 Numerical evaluation

We calculate the integrals $\mathrm{Proj}^{i}_{\mu\nu\alpha} I_j^{\mu\nu\beta}$ via a PASSARINO–VELTMAN (PaVe) decomposition [324, 325], using the `Mathematica` package *FeynCalc* [220–222, 326] for the decomposition to tensor coefficients and evaluating these with the native `Fortran` library *Collier* [157–160] via an interface to `C++` [223]; we use the library *LoopTools* [155] for a cross-check. Results for these two implementations have been found to agree on three significant digits. The scalar functions are implemented as denoted in Eq. (3.47) and the text above, *i.e.*, including the TARRACH structures. The form factors $F_\pi^V, G_1, G_2, H_1, H_2$, as well as $F_{\rho\pi}$ and $F_{R\pi}$, can be varied: in the variant referred to as "full model", they are implemented as in Eq. (3.50)–Eq. (3.52), other versions are indicated.

We evaluate $E_i(s, q_1^2, q_2^2) = s\,\mathrm{Im}\,F_i^{a_1}(s, q_1^2, q_2^2)$ for a set of sampling points (s, q_1^2, q_2^2), which yields the imaginary part of the TFFs. The real part is calculated via a dispersion integral over s using two different implementations: on the one hand, *GSL* interpolation and integration methods, specifically the QAG adaptive integration algorithm with GAUSS–KRONROD rules [327], and on the other hand an adapted version of the GAUSS–LEGENDRE algorithm from the *dispersionrelations* package for `python` [328]. In practice, the upper limit of the dispersion integral is set to a high value $\Lambda = (M_\rho + M_\pi)^2 \times 10^6$, which we vary in order to ensure that the results do not depend on Λ. We evaluate the real and imaginary part of $F_i^{a_1}(s, q_1^2, q_2^2)$ at $s = M_{a_1}^2$ and space-like virtualities for $C_{a_1\rho\pi} = 4.7\,\mathrm{GeV}$. In order to account for both charge channels $\rho^+\pi^-$ and $\rho^-\pi^+$, we multiply the result by 2.

The contribution to the uncertainty that we can presently quantify comes from the coupling constant. It is indicated in some of the plots by error bands that correspond to $C_{a_1\rho\pi} \in [3.7, 5.7]$ and also taken as an error estimate of the normalisation. Both evaluation methods for the dispersive integral agree up to numerical deviations $\lesssim 10\%$, which we take as our current numerical precision. This can probably be improved in the future; at present, it is well within the $\sim 20\%$ uncertainty from $C_{a_1\rho\pi}$, where uncertainties from $C_{\rho\pi\gamma}$ and the masses are not taken into account. The presumably largest uncertainty is, however, systematic and comes from the fact that we have not yet been able to enforce transversality for the vector and axial-vector meson. At present, we cannot estimate the size of the contributions we are missing from this.

3.7 Results and discussion

Doubly-virtual TFFs depending on $(-Q_1^2, -Q_2^2) = (q_1^2, q_2^2)$ are presented as real and imaginary part in colour-coded 2d plots with logarithmic colourbars, where the region close to 0 is linear. In Fig. 3.7, $F^{a_1}_{1,2,3}$ are depicted for photon virtualities up to $2\,\mathrm{GeV}^2$, while Fig. 3.8 shows the symmetrised TFFs $F^{a_1}_{a1}$, $F^{a_1}_{s}$, and $F^{a_1}_{a2}$. For $Q_1^2 = Q_2^2$, the antisymmetric TFFs $F_1^{a_1} = F_{a1}^{a_1}$ and $F_{a2}^{a_1}$ vanish. The asymmetry in $F^{a_1}_{2,3}$ is visible, and their real parts change sign at virtualities $\sim 0.2\,\mathrm{GeV}^2$; as a consequence, $F^{a_1}_{s,a2}$ change sign at $\sim 0.2\,\mathrm{GeV}^2$ and $\sim 0.6\,\mathrm{GeV}^2$, respectively. Fig. 3.9 demonstrates the asymptotic behaviour of the symmetrised TFFs up to $50\,\mathrm{GeV}^2$.

The antisymmetric TFFs $F^{a_1}_{a1/2}$ can be divided by $(Q_1^2 - Q_2^2)$. Fig. 3.10 shows that they thus become symmetric, from which we can conclude that these TFFs can be expressed as

$$F^{a_1}_{a1/2} \sim (Q_1^2 - Q_2^2) \cdot \tilde{F}^{a_1}_{a1/2}, \tag{3.94}$$

where $\tilde{F}^{a_1}_{a1/2}$ are symmetric in the virtualities. This is similar to what was observed for the antisymmetric f_1 TFFs in Ref. [277].

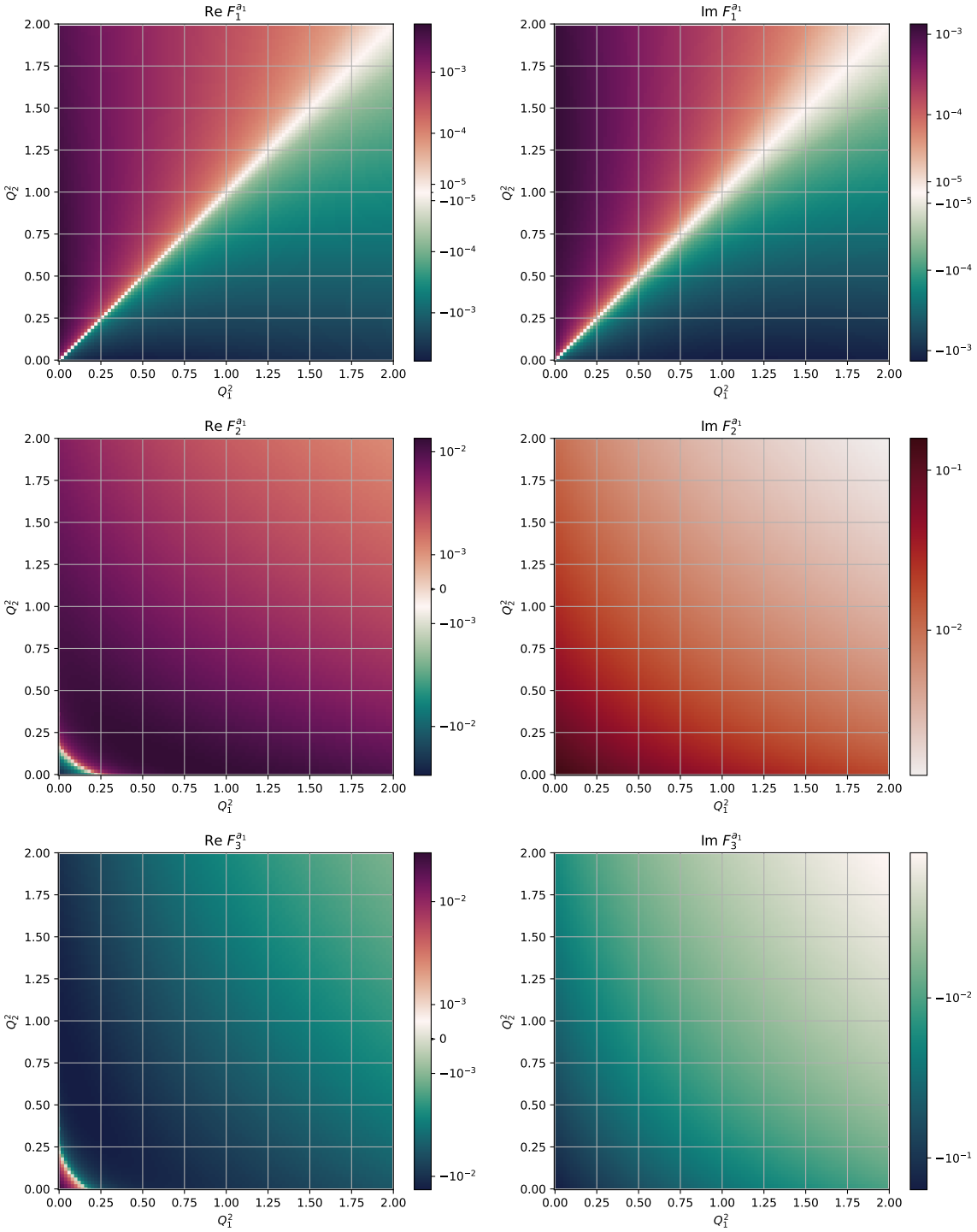

Figure 3.7: Real and imaginary parts of the a_1 TFFs, full model, for virtualities up to $2\,\mathrm{GeV}^2$.

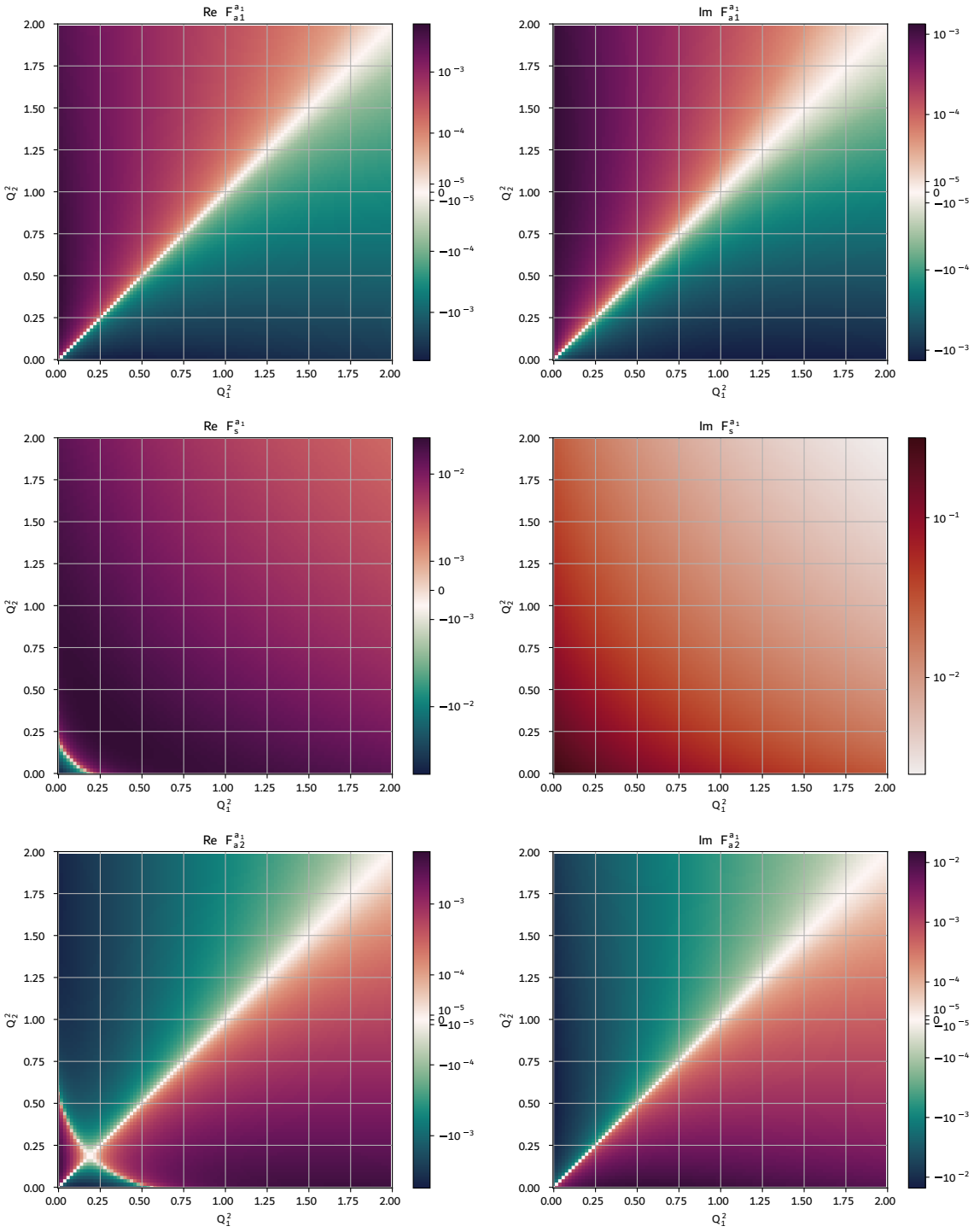

Figure 3.8: Real and imaginary parts of symmetrised a_1 TFFs, full model, for virtualities up to $2\,\mathrm{GeV}^2$.

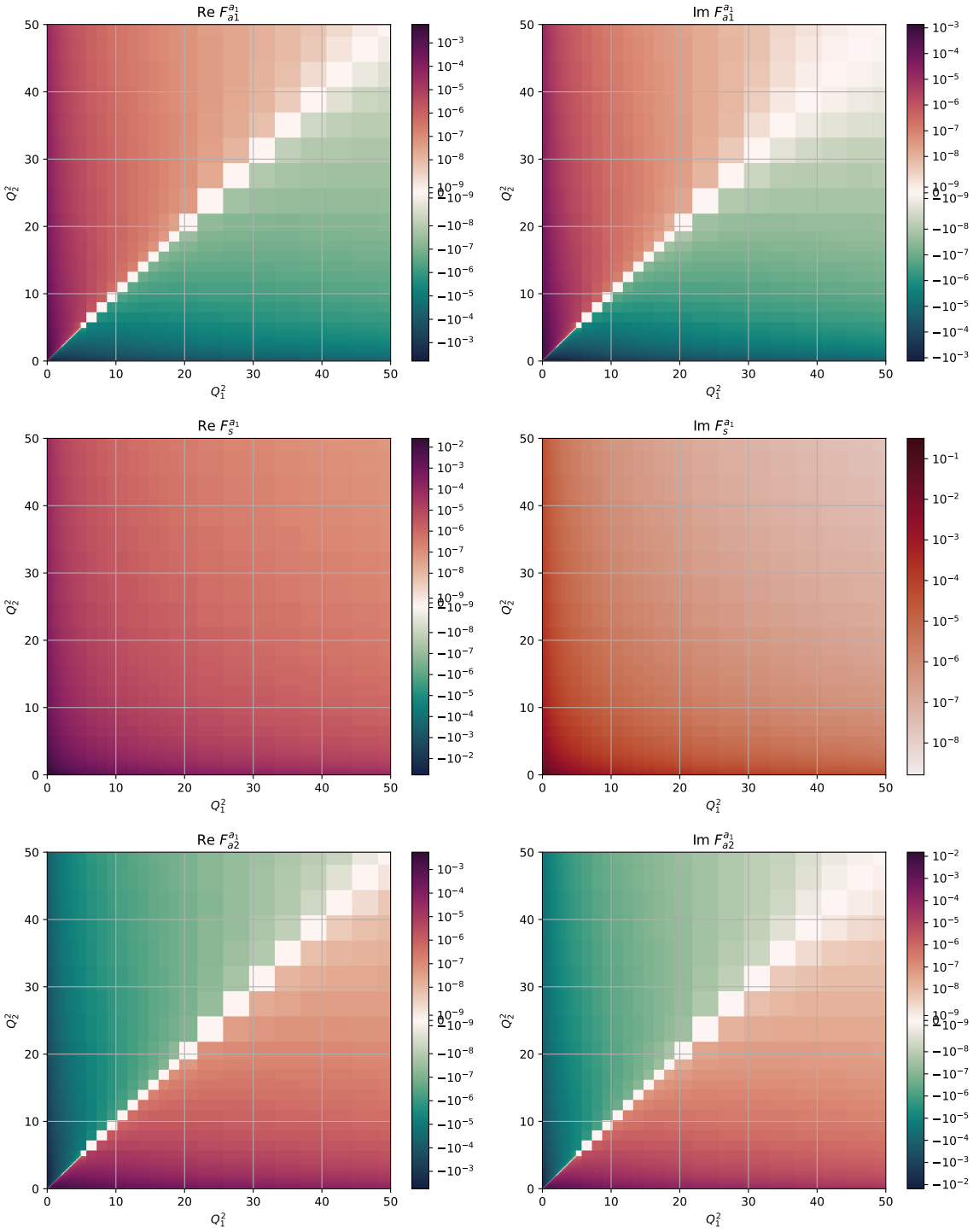

Figure 3.9: Real and imaginary parts of symmetrised a_1 TFFs, full model, for virtualities up to $50\,\mathrm{GeV}^2$. The increased pixel size at higher virtualities is due to the spacing of the sampling points.

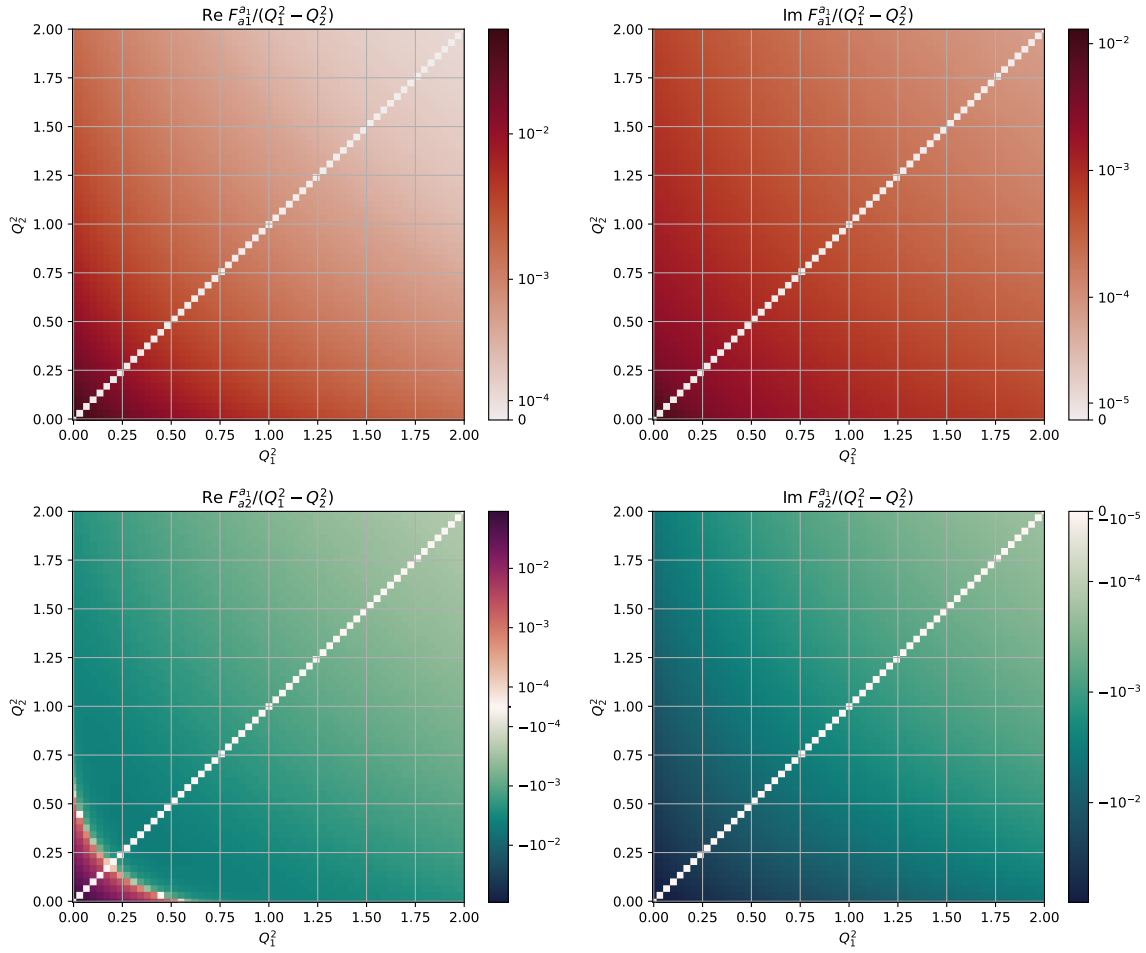

Figure 3.10: Real and imaginary part of the antisymmetric TFFs $F^{a_1}_{a1/2}/(Q_1^2 - Q_2^2)$ for virtualities below $2\,\mathrm{GeV}^2$. The white pixels on the diagonal emerge since the antisymmetric TFFs vanish there.

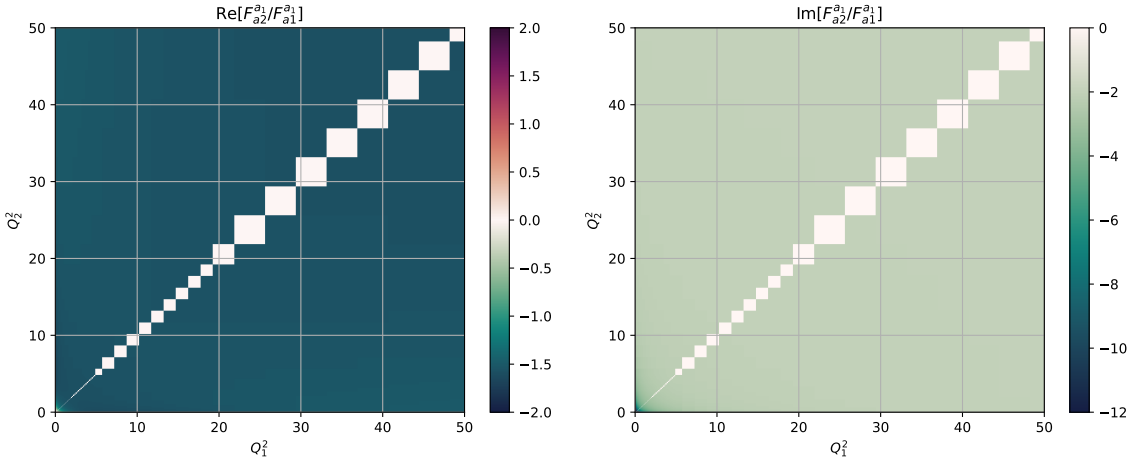

Figure 3.11: Real and imaginary part of the ratio $F^{a_1}_{a2}/F^{a_1}_{a1}$ for virtualities up to $50\,\mathrm{GeV}^2$.

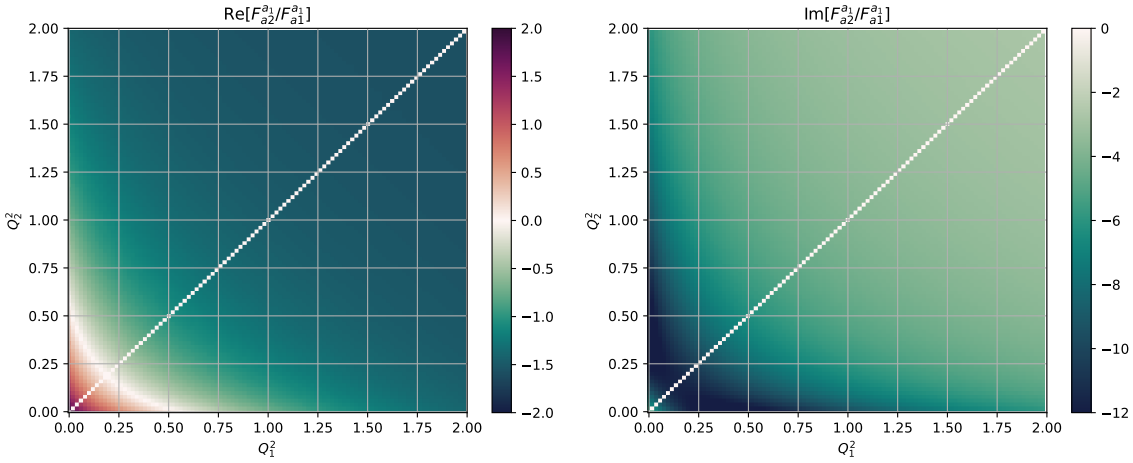

Figure 3.12: Real and imaginary part of the ratio $F^{a_1}_{a2}/F^{a_1}_{a1}$ for virtualities below $2\,\mathrm{GeV}^2$.

Moreover, we can consider the ratio $F^{a_1}_{a2}/F^{a_1}_{a1}$, see Fig. 3.11, which is asymptotically constant, whereas in the low-virtuality region, the real part exhibits a zero line and the imaginary part a minimum; see Fig. 3.12. Note that in these plots, the colourbar is linear.

For a more quantitative analysis and comparisons of different contributions, we consider two special cases of TFFs depending on one virtuality, namely the singly-virtual case ($q_1^2 = -Q^2, q_2^2 \to 0^-$) and symmetric virtualities ($q_1^2 = -Q^2, q_2^2 = -Q^2$). The limit $q_2^2 \to 0^-$ is taken in this way in order to keep virtualities space-like and implemented numerically as $q_2^2 = -5\times10^{-5}\,\mathrm{GeV}^2$. For each TFF, we present real and imaginary part for two different ranges of Q^2, at low and high virtualities, where in the latter case, the TFFs are multiplied by a suitable power of Q^2 in order to study the asymptotic behaviour. For low virtualities, error bands are shown, which represent the uncertainty from the $a_1\rho\pi$ coupling constant. Since the plots for high virtualities are merely used to empirically derive the asymptotic behaviour, no error bands are included there.

Fig. 3.13 and Fig. 3.14 demonstrate the singly-virtual behaviour of the TFFs $F^{a_1}_{1,2,3}$ and the symmetrised TFFs $F^{a_1}_{s,a1,a2}$, respectively. Here, we compare the full model variant to a simplified version

		$F_{a1}^{a_1} = F_1^{a_1}$	$F_s^{a_1}$	$F_{a2}^{a_1}$	$F_2^{a_1}$	$F_3^{a_1}$
$Q_2^2 = 0$	Re	$1/(Q_1^2\sqrt{Q_1^2})$	$1/(Q_1^2\sqrt{Q_1^2})$	$1/(Q_1^2\sqrt{Q_1^2})$	$1/(Q_1^2\sqrt{Q_1^2})$	$1/(Q_1^2\sqrt{Q_1^2})$
	Im	$1/Q_1^4$	$1/Q_1^4$	$1/Q_1^4$	$1/Q_1^4$	$1/Q_1^4$
$Q_1^2 = Q_2^2 = Q^2$	Re	–	$1/(Q^6\sqrt{Q^2})$	–	$1/(Q^6\sqrt{Q^2})$	$1/(Q^6\sqrt{Q^2})$
	Im	–	$1/Q^8$	–	$1/Q^8$	$1/Q^8$

Table 3.1: Empirically determined asymptotic behaviour of real and imaginary parts of (symmetrised) a_1 TFFs.

where $F_\pi^V = G_1 \sim 1/q^2$ and $H_1 = 0 = H_2$. In the latter variant, the electric ρ FF does not fulfil the expected asymptotic behaviour and the situation is more symmetric, such that the electric heavy-vector-meson FF H_1 is not needed for the cancellation of kinematic singularities in the scalar functions. The asymptotic behaviour of the TFFs is qualitatively the same for both versions. The effect of the implementation of the expected asymptotic behaviour in G_1 and the inclusion of $H_{1,2}$ is most notable in $F_1^{a_1}$, where the full model yields smaller results for both real and imaginary part; the latter is significantly smaller, at the maximum $\sim 50\%$, whereas the real parts are compatible within uncertainties. For $F_{2,3}^{a_1}$, the imaginary parts receive rather mild corrections well within the uncertainties, while the real parts deviate $\sim 50\%$ at the maximum. As the effects for real and imaginary parts cancel almost, this changes the normalisation of $F_{2,3}^{a_1}$ and $F_s^{a_1}$ only slightly, $\sim 4\%$, which is well within the uncertainties.

Overall, $F_1^{a_1}$ is more than one order of magnitude smaller compared to $F_{2,3}^{a_1}$. For the latter TFFs, the imaginary parts are of larger magnitude compared to the real parts, whereas the situation is reversed for $F_1^{a_1}$. With symmetric virtualities, the picture is qualitatively similar, with the exception of the asymptotic behaviour; see Fig. 3.15. The antisymmetric TFFs vanish in this case.

We can read off the normalisation of the axial-vector TFFs

$$|F_{2/3}^{a_1}(0,0)| = 0.16(4), \tag{3.95}$$

corresponding to $|F_s^{a_1}(0,0)| = 0.32(7)$, where the indicated uncertainties correspond to the uncertainty of $C_{a_1\rho\pi}$, while the systematic uncertainty in the framework cannot be quantified at present. This value can be compared to $|F_2^{a_1}(0,0)| = 0.34(6)$, estimated from U(3) symmetry, and $F_2^{a_1}(0,0) = 0.38(5)$, extracted from an analysis in the VVA framework, in Ref. [244], resulting in a relative factor of 2. The antisymmetric TFFs are normalised to 0 due to the LANDAU–YANG theorem.

Asymptotically, real and imaginary parts need to be discussed separately. From the second column in Fig. 3.13 and Fig. 3.14, a decrease $\sim 1/Q^4$ of the imaginary parts of all (symmetrised) TFFs can be concluded, whereas the real parts decrease slower, namely $\sim 1/(Q^2\sqrt{Q^2})$. The asymptotic behaviour expected from a light-cone expansion [144, 308] is $\mathcal{O}(Q^{-6})$ for $F_1^{a_1} = F_{a1}^{a_1}$, which is not fulfilled in our results, and $\mathcal{O}(Q^{-4})$ for $F_2^{a_1}$, which is fulfilled for the imaginary parts in the singly-virtual case.

For symmetric virtualities, all antisymmetric TFFs vanish identically, and accordingly, $F_2^{a_1}$ and $F_3^{a_1}$ only differ by a sign, while $F_s^{a_1}$ (not shown) is simply given by $2 \times F_2^{a_1}$; see Fig. 3.15. We observe for the TFFs with symmetric virtualities that the real parts decrease $\sim 1/(Q^6\sqrt{Q^2})$ and the imaginary parts $\sim 1/Q^8$; this is faster than expected from the light-cone expansion. We collect the asymptotic behaviour for our results in Table 3.1.

We can also compare to a version with point-like FFs as input, *i.e.*, $F_\pi^V(q^2) \equiv 1 \equiv G_1(q^2)$, $F_{\rho\pi}(q^2) \equiv C_{\rho\pi\gamma}$, $G_2(q^2) \equiv 2$, and $H_1(q^2) \equiv 0 \equiv H_2(q^2)$; see Fig. 3.16 for symmetric virtualities and Sec. 3.9.7 for the singly-virtual case. Since we keep the normalisations of the couplings, the normalisations of the TFFs are unchanged compared to the simplified model with FFs, but the asymptotic behaviour is different: imaginary and real part of the TFFs decrease $\sim 1/Q^2$ and $\sim 1/\sqrt{Q^2}$, respectively. This point-like model showcases the TFF behaviour and asymptotics resulting solely from the loop integrals, and we can see that this alone cannot accommodate the expected high-energy behaviour. The fact

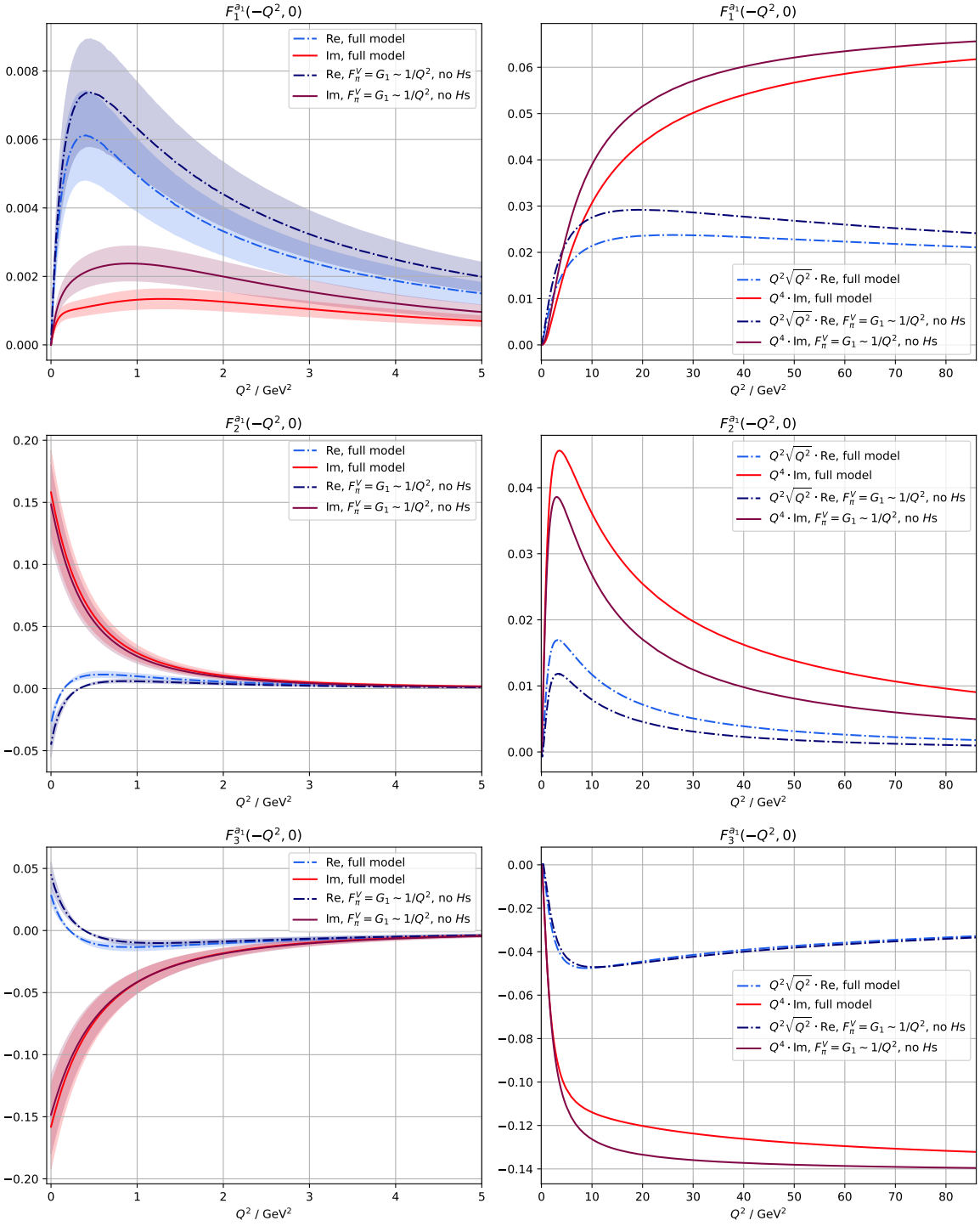

Figure 3.13: Singly-virtual a_1 TFFs: imaginary parts as solid lines, real parts as dash-dotted lines. The brighter lines correspond to the full model, whereas the darker lines show the simplified model; results shown in the second row are multiplied by factors of Q^{2n} according to Table 3.1. The error bands in the first column represent the uncertainty in the coupling constant $C_{a_1\rho\pi}$.

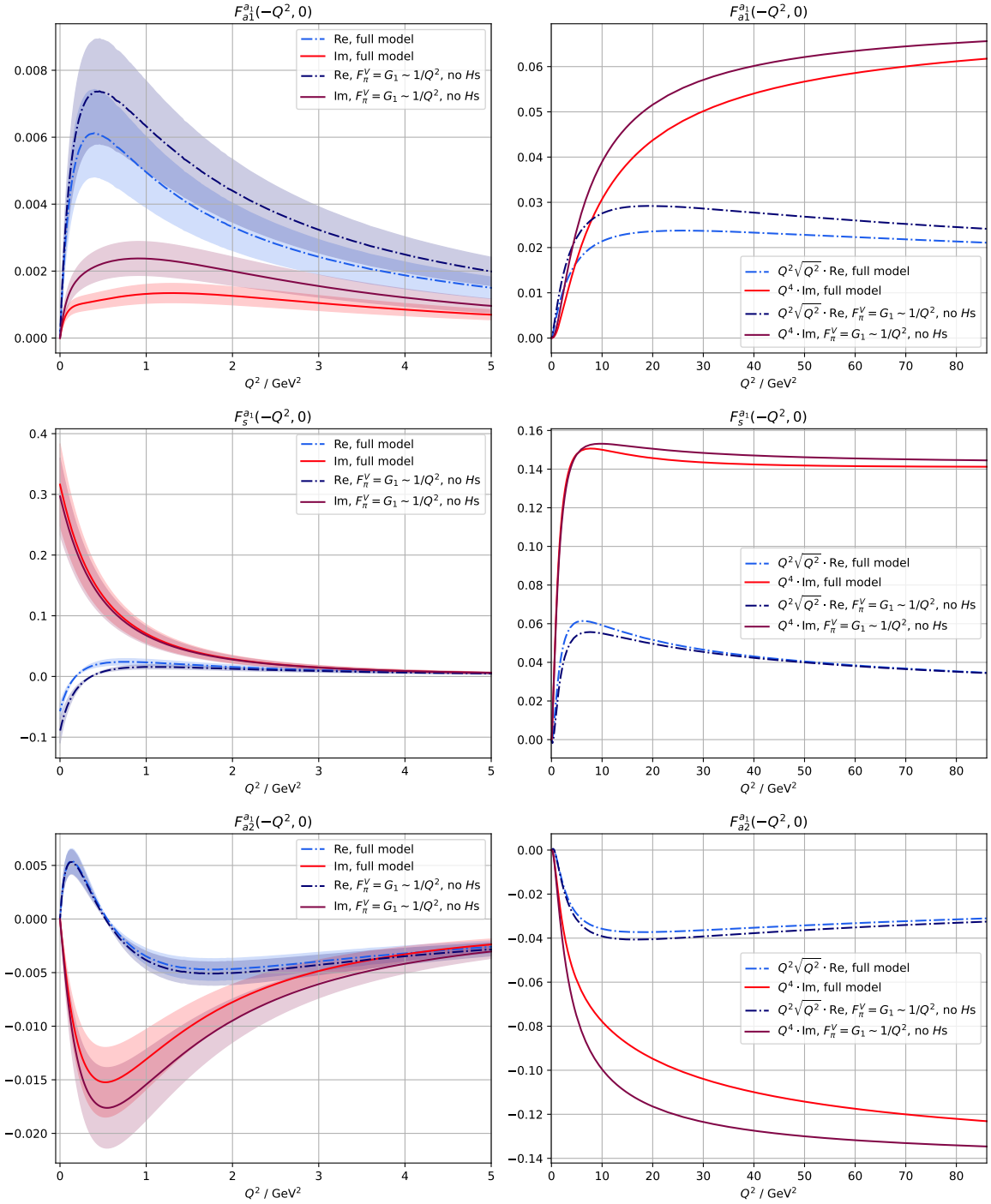

Figure 3.14: Symmetrised singly-virtual a_1 TFFs: imaginary parts as solid lines, real parts as dash-dotted lines. The brighter lines correspond to the full model, whereas the darker lines show the simplified model; results shown in the second row are multiplied by factors of Q^{2n} according to Table 3.1. The error bands in the first column represent the uncertainty in the coupling constant $C_{a_1\rho\pi}$. The diagrams in the first row of this figure are identical to the first row of Fig. 3.13 and included here in order to allow for a direct comparison to the other symmetrised TFFs.

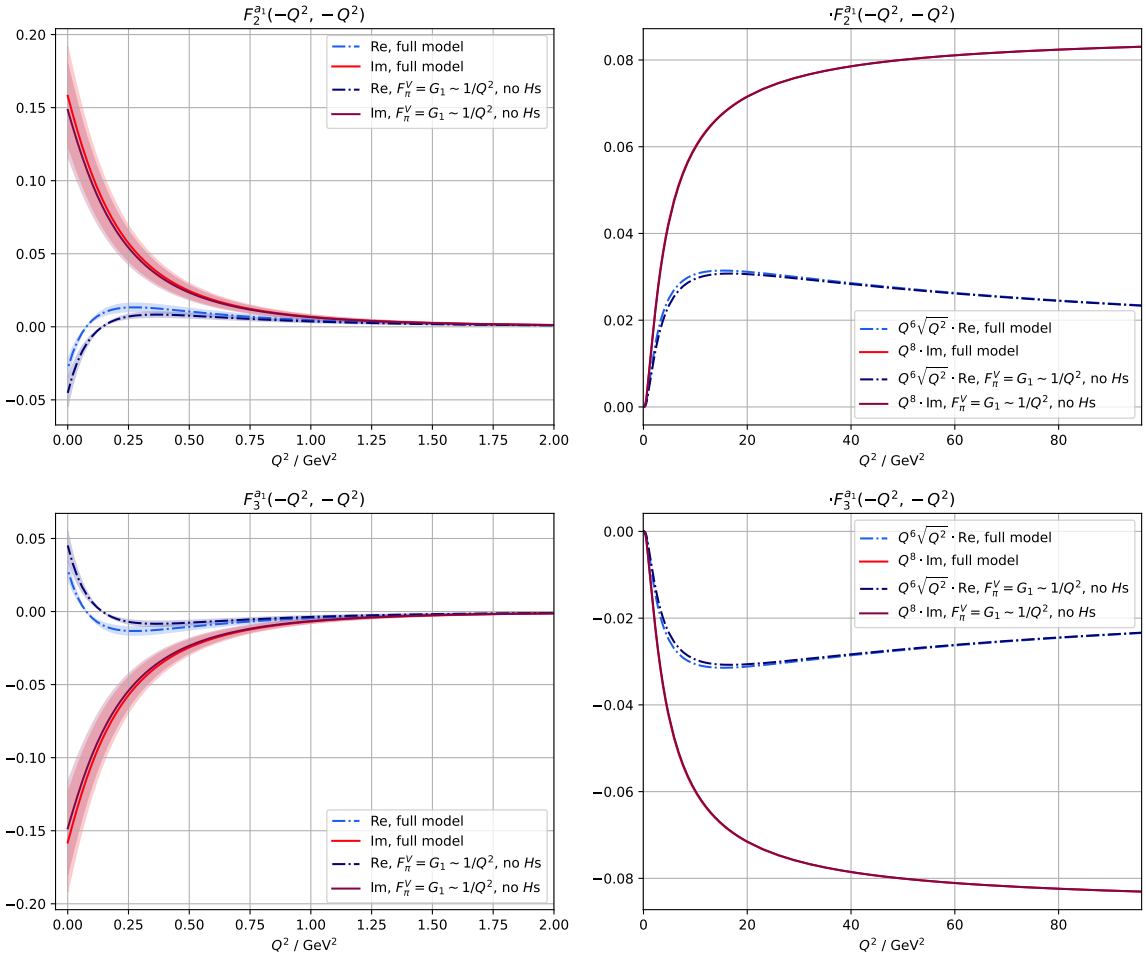

Figure 3.15: a_1 TFFs with symmetric virtualities: imaginary parts as solid lines, real parts as dash-dotted lines. The brighter lines correspond to the full model, whereas the darker lines show the simplified model; results shown in the second row are multiplied by factors of Q^{2n} according to Table 3.1. The error bands in the first column represent the uncertainty in the coupling constant $C_{a_1\rho\pi}$. $F_1^{a_1}$ vanishes identically in this case, and $F_2^{a_1}$ and $F_3^{a_1}$ are reflected versions of one another since the antisymmetric part is 0.

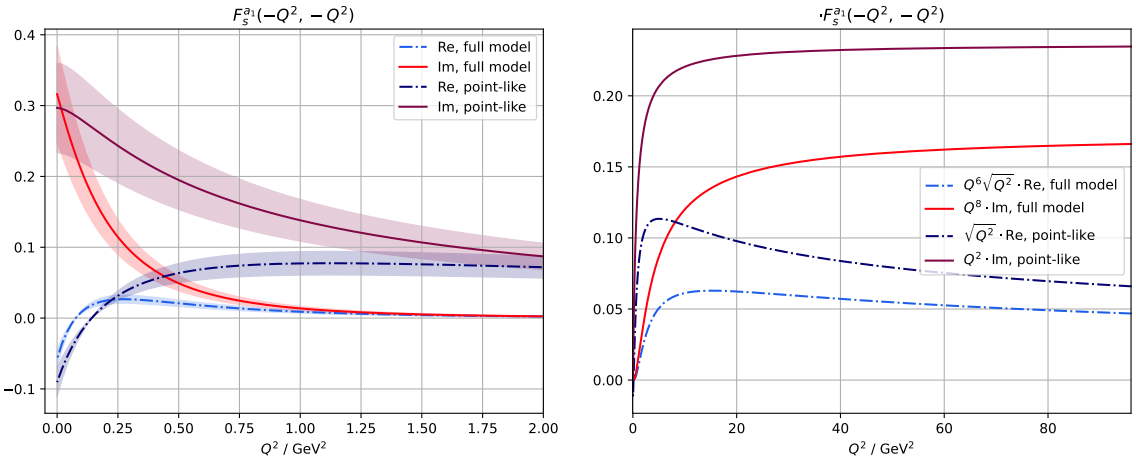

Figure 3.16: $F_s^{a_1}$ with symmetric virtualities: imaginary parts as solid lines, real parts as dash-dotted lines. The brighter lines correspond to the full model, whereas the darker lines show the model with point-like couplings; results shown in the second diagram are multiplied by factors of Q^{2n} according to Table 3.1. The error bands in the first diagram represent the uncertainty in the coupling constant $C_{a_1\rho\pi}$. $F_{a1}^{a_1}$ and $F_{a2}^{a_1}$ vanish identically in this case.

that antisymmetric TFFs vanish due to the LANDAU–YANG theorem, on the other hand, does not depend on the input form factors.

Within our framework, one can separate different contributions to the a_1 TFFs. The magnetic vector FFs G_2 for the ρ and H_2 for the heavy VM yield contributions only to $F_1^{a_1}$. While the effect of H_2 is small, $\sim 5\%$, the contribution of G_2 to the imaginary part is similar in size to the full model, but with opposite sign, and the contribution of G_2 to the real part of $F_1^{a_1}$ is $\sim 7\%$.

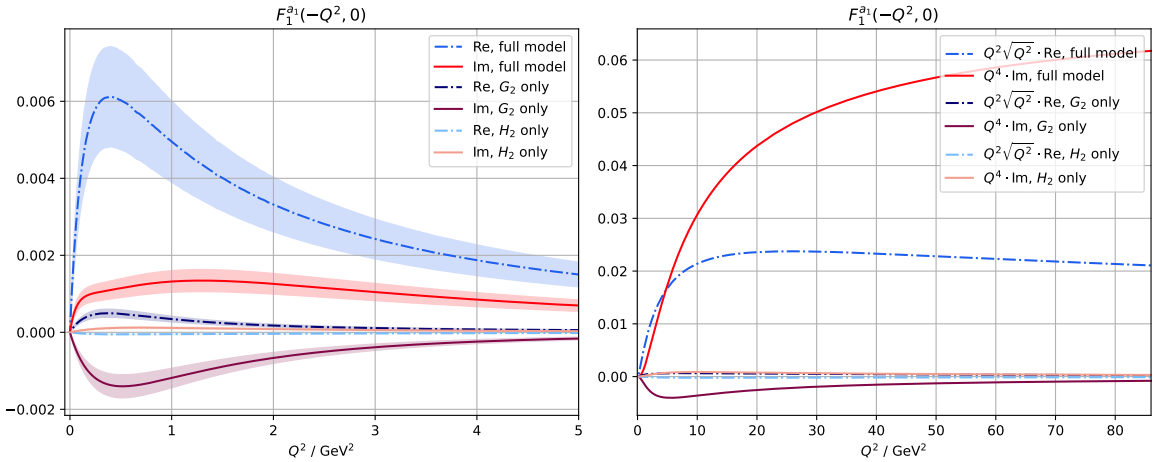

Figure 3.17: Contribution of G_2 and H_2 to singly-virtual a_1 TFFs, which vanishes for $F_{2/3}^{a_1}$; results shown in the second diagram are multiplied by factors of Q^{2n} according to Table 3.1. The full model contains both G_2 and H_2. The error bands in the first diagram represent the uncertainty in the coupling constant $C_{a_1\rho\pi}$.

3.8 Conclusion

We have constructed a framework to obtain singly- and doubly-virtual a_1 and a_2 TFFs in the space-like region from a $\rho\pi$ intermediate state and ρ, π LHCs. To this end, we have found a gauge-invariant pole-free decomposition of the $\rho\pi \to \gamma^*\gamma^*$ amplitude into tensor structures and scalar functions using the BTT procedure. In order to remove kinematic singularities in the scalar functions, we have extended the BTT basis to a generating set valid in all kinematic limits and have included an additional LHC with a heavy-vector-meson intermediate state. We calculate the imaginary parts of the $a_{1/2}$ TFFs from the loop diagram resulting from contracting the amplitude constructed in this way with an $a_{1/2} \to \rho\pi$ amplitude and reconstruct the real parts dispersively via a unitarity relation in s, which is eventually set to $M_{a_1}^2$.

Results include the normalisation and asymptotic behaviour of the a_1 TFFs, which are in the same order of magnitude, but do not agree with expectations from U(3) symmetry and results in Ref. [244] for the normalisation and partially agree with expectations from a light-cone expansion for the asymptotic behaviour. It is important to note that since we were required to use a simplified $a_1\rho\pi$ vertex, it is possible that significant contributions are missing. As our framework does not systematically enforce a NWA, imaginary parts emerge, which exceed for $F_{2/3}^{a_1}$ the real parts. $F_1^{a_1}$ has the smallest magnitude and receives the largest relative contributions from the magnetic ρ FF and the heavy-vector-meson FFs that are related to the asymmetry in the $\rho\pi$ system. A simpler model with $F_\pi^V = G_1$ describes the imaginary parts and normalisations of $F_2^{a_1}$ and $F_3^{a_1}$ similarly to the more refined model with correct asymptotic behaviour of the input FFs; the asymptotic behaviour of the TFFs is the same in both versions. Point-like couplings of π and ρ to the photons, however, result in a significantly worse asymptotic behaviour of the TFFs, demonstrating that the loop alone cannot effect the latter.

This framework is currently limited by the fact that some of the loop integrals diverge for fully transverse ρ and a_1 terms, which forces us to use a simplified version in the calculation of the a_1 TFFs, where this transversality is not given. The same difficulties also prevent the evaluation for the a_2. In order to implement full transversality and to obtain results for the a_2, we hope to extend the formalism in the future via a renormalisation procedure for the diverging loop integrals.

In this construction, we have neglected contributions required for unitarity both in the $\rho\pi \to \gamma^*\gamma^*$ and in the $a_{1/2} \to \gamma^*\gamma^*$ system. Including those would require a different approach and additional assumptions. In the context of the currently used HLbL framework, only the pole contributions for the resonances are taken into account, neglecting additional cuts, in this case 3π. A NWA for the $a_{1/2}$ TFFs, where the imaginary parts vanish, would match this approximation and might at the same time allow to construct a more unitary framework.

With these future improvements, a description of a_1, a_2, and also f_1' TFFs, which can be used as input for the HLbL contribution and for an improved understanding of these resonances in general, seems possible.

3.9 Appendix

3.9.1 Tensor structures for the $VP \to \gamma^*\gamma^*$ process and projection matrix

The initial tensor structures introduced in Sec. 3.3 are collected here, where

$$T_i^{\text{in},\mu\nu\alpha} = \epsilon_{\beta\gamma\delta\epsilon}\mathcal{M}^{\mu\nu\alpha\beta\gamma\delta\epsilon}. \tag{3.96}$$

The building blocks for $M^{\mu\nu\alpha\beta\gamma\delta\epsilon}$ are the metric tensor $g^{\mu\nu}$ and the available independent momenta $q^\mu \in \{q_1, q_2, p\}^\mu$,

$$\{K_i^{\mu\nu\alpha\beta\gamma\delta\epsilon}\}_{i=1}^{\tilde{N}} \subseteq \{gggq, ggqqq, gqqqqq, qqqqqqq\}^{\{\mu\nu\alpha\beta\gamma\delta\epsilon\}}, \tag{3.97}$$

As terms of type $qqqqqqq$ vanish upon contraction with $\epsilon_{\beta\gamma\delta\epsilon}$, there are 3 terms of type $gggq$, 30 terms of type $ggqqq$, and 27 terms of type $gqqqqq$, resulting in 60 terms in total,

$$\begin{aligned}
T_1^{\text{in},\mu\nu\alpha} &= \varepsilon^{\mu\nu\alpha q_1}\,, & T_{21}^{\text{in},\mu\nu\alpha} &= q_2^\alpha \varepsilon^{\mu\nu p q_2}\,, & T_{41}^{\text{in},\mu\nu\alpha} &= q_2^\mu q_2^\nu \varepsilon^{\alpha p q_1 q_2}\,,\\
T_2^{\text{in},\mu\nu\alpha} &= \varepsilon^{\mu\nu\alpha q_1}\,, & T_{22}^{\text{in},\mu\nu\alpha} &= p^\mu \varepsilon^{\nu\alpha q_1 q_2}\,, & T_{42}^{\text{in},\mu\nu\alpha} &= p^\mu p^\nu \varepsilon^{\alpha p q_1 q_2}\,,\\
T_3^{\text{in},\mu\nu\alpha} &= \varepsilon^{\mu\nu\alpha p}\,, & T_{23}^{\text{in},\mu\nu\alpha} &= p^\mu \varepsilon^{\nu\alpha q_1 p}\,, & T_{43}^{\text{in},\mu\nu\alpha} &= q_1^\mu q_2^\alpha \varepsilon^{\nu p q_1 q_2}\,,\\
T_4^{\text{in},\mu\nu\alpha} &= q_1^\mu\, \varepsilon^{\nu\alpha q_1 q_2}\,, & T_{24}^{\text{in},\mu\nu\alpha} &= p^\mu \varepsilon^{\nu\alpha q_2 p}\,, & T_{44}^{\text{in},\mu\nu\alpha} &= q_1^\alpha q_2^\mu \varepsilon^{\nu p q_1 q_2}\,,\\
T_5^{\text{in},\mu\nu\alpha} &= q_1^\mu \varepsilon^{\nu\alpha q_1 p}\,, & T_{25}^{\text{in},\mu\nu\alpha} &= p^\nu \varepsilon^{\mu\alpha q_1 q_2}\,, & T_{45}^{\text{in},\mu\nu\alpha} &= p^\alpha q_1^\mu \varepsilon^{\nu p q_1 q_2}\,,\\
T_6^{\text{in},\mu\nu\alpha} &= q_1^\mu \varepsilon^{\nu\alpha q_2 p}\,, & T_{26}^{\text{in},\mu\nu\alpha} &= p^\nu \varepsilon^{\mu\alpha q_1 p}\,, & T_{46}^{\text{in},\mu\nu\alpha} &= p^\mu q_1^\alpha \varepsilon^{\nu p q_1 q_2}\,,\\
T_7^{\text{in},\mu\nu\alpha} &= q_1^\nu \varepsilon^{\mu\alpha q_1 q_2}\,, & T_{27}^{\text{in},\mu\nu\alpha} &= p^\nu \varepsilon^{\mu\alpha q_2 p}\,, & T_{47}^{\text{in},\mu\nu\alpha} &= k^\alpha q_2^\mu \varepsilon^{\nu p q_1 q_2}\,,\\
T_8^{\text{in},\mu\nu\alpha} &= q_1^\nu \varepsilon^{\mu\alpha q_1 p}\,, & T_{28}^{\text{in},\mu\nu\alpha} &= -p^\alpha \varepsilon^{\mu\nu q_1 q_2}\,, & T_{48}^{\text{in},\mu\nu\alpha} &= p^\mu q_2^\alpha \varepsilon^{\nu p q_1 q_2}\,,\\
T_9^{\text{in},\mu\nu\alpha} &= q_1^\nu \varepsilon^{\mu\alpha q_2 p}\,, & T_{29}^{\text{in},\mu\nu\alpha} &= p^\alpha \varepsilon^{\mu\nu p q_1}\,, & T_{49}^{\text{in},\mu\nu\alpha} &= q_1^\alpha q_1^\mu \varepsilon^{\nu p q_1 q_2}\\
T_{10}^{\text{in},\mu\nu\alpha} &= -q_1^\alpha \varepsilon^{\mu\nu q_1 q_2}\,, & T_{30}^{\text{in},\mu\nu\alpha} &= p^\alpha \varepsilon^{\mu\nu p q_2}\,, & T_{50}^{\text{in},\mu\nu\alpha} &= q_2^\alpha q_2^\mu \varepsilon^{\nu p q_1 q_2}\,,\\
T_{11}^{\text{in},\mu\nu\alpha} &= q_1^\alpha \varepsilon^{\mu\nu p q_1}\,, & T_{31}^{\text{in},\mu\nu\alpha} &= g^{\mu\nu} \varepsilon^{\alpha p q_1 q_2}\,, & T_{51}^{\text{in},\mu\nu\alpha} &= p^\alpha p^\mu \varepsilon^{\nu p q_1 q_2}\,,\\
T_{12}^{\text{in},\mu\nu\alpha} &= q_1^\alpha \varepsilon^{\mu\nu p q_2}\,, & T_{32}^{\text{in},\mu\nu\alpha} &= g^{\mu\alpha} \varepsilon^{\nu p q_1 q_2}\,, & T_{52}^{\text{in},\mu\nu\alpha} &= q_1^\mu q_2^\alpha \varepsilon^{\mu p q_1 q_2}\,,\\
T_{13}^{\text{in},\mu\nu\alpha} &= q_2^\mu \varepsilon^{\nu\alpha q_1 q_2}\,, & T_{33}^{\text{in},\mu\nu\alpha} &= g^{\nu\alpha} \varepsilon^{\mu p q_1 q_2}\,, & T_{53}^{\text{in},\mu\nu\alpha} &= q_1^\alpha q_2^\nu \varepsilon^{\mu p q_1 q_2}\,,\\
T_{14}^{\text{in},\mu\nu\alpha} &= q_2^\mu \varepsilon^{\nu\alpha q_1 p}\,, & T_{34}^{\text{in},\mu\nu\alpha} &= q_1^\mu q_2^\nu \varepsilon^{\alpha p q_1 q_2}\,, & T_{54}^{\text{in},\mu\nu\alpha} &= k^\alpha q_1^\nu \varepsilon^{\mu p q_1 q_2}\,,\\
T_{15}^{\text{in},\mu\nu\alpha} &= q_2^\mu \varepsilon^{\nu\alpha q_2 p}\,, & T_{35}^{\text{in},\mu\nu\alpha} &= q_1^\nu q_2^\mu \varepsilon^{\alpha p q_1 q_2} & T_{55}^{\text{in},\mu\nu\alpha} &= p^\nu q_1^\alpha \varepsilon^{\mu p q_1 q_2}\,,\\
T_{16}^{\text{in},\mu\nu\alpha} &= q_2^\nu \varepsilon^{\mu\alpha q_1 q_2}\,, & T_{36}^{\text{in},\mu\nu\alpha} &= p^\nu q_1^\mu \varepsilon^{\alpha p q_1 q_2} & T_{56}^{\text{in},\mu\nu\alpha} &= p^\alpha q_2^\nu \varepsilon^{\mu p q_1 q_2}\,,\\
T_{17}^{\text{in},\mu\nu\alpha} &= q_2^\nu \varepsilon^{\mu\alpha q_1 p}\,, & T_{37}^{\text{in},\mu\nu\alpha} &= p^\mu q_1^\nu \varepsilon^{\alpha p q_1 q_2}\,, & T_{57}^{\text{in},\mu\nu\alpha} &= p^\nu q_2^\alpha \varepsilon^{\mu p q_1 q_2}\,,\\
T_{18}^{\text{in},\mu\nu\alpha} &= q_2^\nu \varepsilon^{\mu\alpha q_2 p}\,, & T_{38}^{\text{in},\mu\nu\alpha} &= p^\nu q_2^\mu \varepsilon^{\alpha p q_1 q_2}\,, & T_{58}^{\text{in},\mu\nu\alpha} &= q_1^\alpha q_1^\nu \varepsilon^{\mu p q_1 q_2}\,,\\
T_{19}^{\text{in},\mu\nu\alpha} &= -q_2^\alpha \varepsilon^{\mu\nu q_1 q_2}\,, & T_{39}^{\text{in},\mu\nu\alpha} &= p^\mu q_2^\nu \varepsilon^{\alpha p q_1 q_2}\,, & T_{59}^{\text{in},\mu\nu\alpha} &= q_2^\alpha q_2^\nu \varepsilon^{\mu p q_1 q_2}\,,\\
T_{20}^{\text{in},\mu\nu\alpha} &= q_2^\alpha \varepsilon^{\mu\nu p q_1}\,, & T_{40}^{\text{in},\mu\nu\alpha} &= q_1^\mu q_1^\nu \varepsilon^{\alpha p q_1 q_2}\,, & T_{60}^{\text{in},\mu\nu\alpha} &= p^\alpha p^\nu \varepsilon^{\mu p q_1 q_2}\,.
\end{aligned}$$

3.9.2 Schouten identities for the $VP \to \gamma^*\gamma^*$ process

The following relations arise from the Schouten identity Eq. (3.22) for the initial tensor structures $T_i^{\text{in},\mu\nu\alpha}$; only 32 of these 39 equations are independent.

$$
\begin{aligned}
-(q_1\cdot q_2)T_1^{\text{in},\mu\nu\alpha}+q_1^2T_2^{\text{in},\mu\nu\alpha}-T_4^{\text{in},\mu\nu\alpha}+T_7^{\text{in},\mu\nu\alpha}+T_{10}^{\text{in},\mu\nu\alpha}&=0\\
-q_2^2T_1^{\text{in},\mu\nu\alpha}+(q_1\cdot q_2)T_2^{\text{in},\mu\nu\alpha}-T_{13}^{\text{in},\mu\nu\alpha}+T_{16}^{\text{in},\mu\nu\alpha}+T_{19}^{\text{in},\mu\nu\alpha}&=0\\
-(p\cdot q_2)T_1^{\text{in},\mu\nu\alpha}+(p\cdot q_1)T_2^{\text{in},\mu\nu\alpha}-T_{22}^{\text{in},\mu\nu\alpha}+T_{25}^{\text{in},\mu\nu\alpha}+T_{28}^{\text{in},\mu\nu\alpha}&=0\\
(p\cdot q_1)T_1^{\text{in},\mu\nu\alpha}-q_1^2T_3^{\text{in},\mu\nu\alpha}+T_5^{\text{in},\mu\nu\alpha}-T_8^{\text{in},\mu\nu\alpha}-T_{11}^{\text{in},\mu\nu\alpha}&=0\\
(p\cdot q_1)T_2^{\text{in},\mu\nu\alpha}-(q_1\cdot q_2)T_3^{\text{in},\mu\nu\alpha}+T_6^{\text{in},\mu\nu\alpha}-T_9^{\text{in},\mu\nu\alpha}-T_{12}^{\text{in},\mu\nu\alpha}&=0\\
(p\cdot q_2)T_1^{\text{in},\mu\nu\alpha}-(q_1\cdot q_2)T_3^{\text{in},\mu\nu\alpha}+T_{14}^{\text{in},\mu\nu\alpha}-T_{17}^{\text{in},\mu\nu\alpha}-T_{20}^{\text{in},\mu\nu\alpha}&=0\\
(p\cdot q_2)T_2^{\text{in},\mu\nu\alpha}-(q_1\cdot q_2)T_3^{\text{in},\mu\nu\alpha}+T_{15}^{\text{in},\mu\nu\alpha}-T_{18}^{\text{in},\mu\nu\alpha}-T_{21}^{\text{in},\mu\nu\alpha}&=0\\
p^2T_1^{\text{in},\mu\nu\alpha}-(p\cdot q_1)T_3^{\text{in},\mu\nu\alpha}+T_{23}^{\text{in},\mu\nu\alpha}-T_{26}^{\text{in},\mu\nu\alpha}-T_{29}^{\text{in},\mu\nu\alpha}&=0\\
p^2T_2^{\text{in},\mu\nu\alpha}-(p\cdot q_2)T_3^{\text{in},\mu\nu\alpha}+T_{24}^{\text{in},\mu\nu\alpha}-T_{27}^{\text{in},\mu\nu\alpha}-T_{28}^{\text{in},\mu\nu\alpha}&=0\\
-T_6^{\text{in},\mu\nu\alpha}+T_{14}^{\text{in},\mu\nu\alpha}-T_{22}^{\text{in},\mu\nu\alpha}-T_{31}^{\text{in},\mu\nu\alpha}-T_{32}^{\text{in},\mu\nu\alpha}&=0\\
-T_9^{\text{in},\mu\nu\alpha}+T_{17}^{\text{in},\mu\nu\alpha}-T_{25}^{\text{in},\mu\nu\alpha}-T_{31}^{\text{in},\mu\nu\alpha}-T_{33}^{\text{in},\mu\nu\alpha}&=0\\
-T_{12}^{\text{in},\mu\nu\alpha}+T_{20}^{\text{in},\mu\nu\alpha}-T_{28}^{\text{in},\mu\nu\alpha}+T_{32}^{\text{in},\mu\nu\alpha}-T_{33}^{\text{in},\mu\nu\alpha}&=0\\
(p\cdot q_1)T_{16}^{\text{in},\mu\nu\alpha}-(q_1\cdot q_2)T_{17}^{\text{in},\mu\nu\alpha}+q_1^2T_{18}^{\text{in},\mu\nu\alpha}+T_{34}^{\text{in},\mu\nu\alpha}-T_{53}^{\text{in},\mu\nu\alpha}&=0\\
(p\cdot q_2)T_4^{\text{in},\mu\nu\alpha}-q_2^2T_5^{\text{in},\mu\nu\alpha}+(q_1\cdot q_2)T_6^{\text{in},\mu\nu\alpha}+T_{34}^{\text{in},\mu\nu\alpha}-T_{43}^{\text{in},\mu\nu\alpha}&=0\\
(p\cdot q_2)T_7^{\text{in},\mu\nu\alpha}-q_2^2T_8^{\text{in},\mu\nu\alpha}+(q_1\cdot q_2)T_9^{\text{in},\mu\nu\alpha}+T_{35}^{\text{in},\mu\nu\alpha}-T_{52}^{\text{in},\mu\nu\alpha}&=0\\
(p\cdot q_1)T_{13}^{\text{in},\mu\nu\alpha}-(q_1\cdot q_2)T_{14}^{\text{in},\mu\nu\alpha}+q_1^2T_{15}^{\text{in},\mu\nu\alpha}+T_{35}^{\text{in},\mu\nu\alpha}-T_{44}^{\text{in},\mu\nu\alpha}&=0\\
(p\cdot q_1)T_{25}^{\text{in},\mu\nu\alpha}-(q_1\cdot q_2)T_{26}^{\text{in},\mu\nu\alpha}+q_1^2T_{27}^{\text{in},\mu\nu\alpha}+T_{36}^{\text{in},\mu\nu\alpha}-T_{55}^{\text{in},\mu\nu\alpha}&=0\\
p^2T_4^{\text{in},\mu\nu\alpha}-(p\cdot q_2)T_5^{\text{in},\mu\nu\alpha}+(p\cdot q_1)T_6^{\text{in},\mu\nu\alpha}+T_{36}^{\text{in},\mu\nu\alpha}-T_{45}^{\text{in},\mu\nu\alpha}&=0\\
p^2T_7^{\text{in},\mu\nu\alpha}-(p\cdot q_2)T_8^{\text{in},\mu\nu\alpha}+(p\cdot q_1)T_9^{\text{in},\mu\nu\alpha}+T_{37}^{\text{in},\mu\nu\alpha}-T_{54}^{\text{in},\mu\nu\alpha}&=0\\
(p\cdot q_1)T_{22}^{\text{in},\mu\nu\alpha}-(q_1\cdot q_2)T_{23}^{\text{in},\mu\nu\alpha}+q_1^2T_{24}^{\text{in},\mu\nu\alpha}+T_{37}^{\text{in},\mu\nu\alpha}-T_{46}^{\text{in},\mu\nu\alpha}&=0\\
(p\cdot q_2)T_{25}^{\text{in},\mu\nu\alpha}-q_2^2T_{26}^{\text{in},\mu\nu\alpha}+(q_1\cdot q_2)T_{27}^{\text{in},\mu\nu\alpha}+T_{38}^{\text{in},\mu\nu\alpha}-T_{57}^{\text{in},\mu\nu\alpha}&=0\\
p^2T_{13}^{\text{in},\mu\nu\alpha}-(p\cdot q_2)T_{14}^{\text{in},\mu\nu\alpha}+(p\cdot q_1)T_{15}^{\text{in},\mu\nu\alpha}+T_{38}^{\text{in},\mu\nu\alpha}-T_{47}^{\text{in},\mu\nu\alpha}&=0\\
p^2T_{16}^{\text{in},\mu\nu\alpha}-(p\cdot q_2)T_{17}^{\text{in},\mu\nu\alpha}+(p\cdot q_1)T_{18}^{\text{in},\mu\nu\alpha}+T_{39}^{\text{in},\mu\nu\alpha}-T_{56}^{\text{in},\mu\nu\alpha}&=0\\
(p\cdot q_2)T_{22}^{\text{in},\mu\nu\alpha}-q_2^2T_{23}^{\text{in},\mu\nu\alpha}+(q_1\cdot q_2)T_{24}^{\text{in},\mu\nu\alpha}+T_{39}^{\text{in},\mu\nu\alpha}-T_{48}^{\text{in},\mu\nu\alpha}&=0\\
(p\cdot q_1)T_7^{\text{in},\mu\nu\alpha}-(q_1\cdot q_2)T_8^{\text{in},\mu\nu\alpha}+q_1^2T_9^{\text{in},\mu\nu\alpha}+T_{40}^{\text{in},\mu\nu\alpha}-T_{58}^{\text{in},\mu\nu\alpha}&=0\\
(p\cdot q_1)T_4^{\text{in},\mu\nu\alpha}-(q_1\cdot q_2)T_5^{\text{in},\mu\nu\alpha}+q_1^2T_6^{\text{in},\mu\nu\alpha}+T_{40}^{\text{in},\mu\nu\alpha}-T_{49}^{\text{in},\mu\nu\alpha}&=0\\
(p\cdot q_2)T_{16}^{\text{in},\mu\nu\alpha}-q_2^2T_{17}^{\text{in},\mu\nu\alpha}+(q_1\cdot q_2)T_{18}^{\text{in},\mu\nu\alpha}+T_{41}^{\text{in},\mu\nu\alpha}-T_{59}^{\text{in},\mu\nu\alpha}&=0\\
(p\cdot q_2)T_{13}^{\text{in},\mu\nu\alpha}-q_2^2T_{14}^{\text{in},\mu\nu\alpha}+(q_1\cdot q_2)T_{15}^{\text{in},\mu\nu\alpha}+T_{41}^{\text{in},\mu\nu\alpha}-T_{50}^{\text{in},\mu\nu\alpha}&=0\\
p^2T_{25}^{\text{in},\mu\nu\alpha}-(p\cdot q_2)T_{26}^{\text{in},\mu\nu\alpha}+(p\cdot q_1)T_{27}^{\text{in},\mu\nu\alpha}+T_{42}^{\text{in},\mu\nu\alpha}-T_{60}^{\text{in},\mu\nu\alpha}&=0\\
p^2T_{22}^{\text{in},\mu\nu\alpha}-(p\cdot q_2)T_{23}^{\text{in},\mu\nu\alpha}+(p\cdot q_1)T_{24}^{\text{in},\mu\nu\alpha}+T_{42}^{\text{in},\mu\nu\alpha}-T_{51}^{\text{in},\mu\nu\alpha}&=0\\
-(p\cdot q_1)T_{19}^{\text{in},\mu\nu\alpha}+(q_1\cdot q_2)T_{20}^{\text{in},\mu\nu\alpha}-q_1^2T_{21}^{\text{in},\mu\nu\alpha}+T_{43}^{\text{in},\mu\nu\alpha}-T_{52}^{\text{in},\mu\nu\alpha}&=0\\
-(p\cdot q_2)T_{10}^{\text{in},\mu\nu\alpha}+q_2^2T_{11}^{\text{in},\mu\nu\alpha}-(q_1\cdot q_2)T_{12}^{\text{in},\mu\nu\alpha}+T_{44}^{\text{in},\mu\nu\alpha}-T_{53}^{\text{in},\mu\nu\alpha}&=0\\
-(p\cdot q_1)T_{28}^{\text{in},\mu\nu\alpha}+(q_1\cdot q_2)T_{29}^{\text{in},\mu\nu\alpha}-q_1^2T_{30}^{\text{in},\mu\nu\alpha}+T_{45}^{\text{in},\mu\nu\alpha}-T_{54}^{\text{in},\mu\nu\alpha}&=0
\end{aligned}
$$

$$
\begin{aligned}
-p^2 T_{10}^{\text{in},\mu\nu\alpha} + (p\cdot q_2) T_{11}^{\text{in},\mu\nu\alpha} - (p\cdot q_1) T_{12}^{\text{in},\mu\nu\alpha} + T_{46}^{\text{in},\mu\nu\alpha} - T_{55}^{\text{in},\mu\nu\alpha} &= 0\\
-(p\cdot q_2) T_{28}^{\text{in},\mu\nu\alpha} + q2^2 T_{29}^{\text{in},\mu\nu\alpha} - (q_1\cdot q_2) T_{30}^{\text{in},\mu\nu\alpha} + T_{47}^{\text{in},\mu\nu\alpha} - T_{56}^{\text{in},\mu\nu\alpha} &= 0\\
-p^2 T_{19}^{\text{in},\mu\nu\alpha} + (p\cdot q_2) T_{20}^{\text{in},\mu\nu\alpha} - (p\cdot q_1) T_{21}^{\text{in},\mu\nu\alpha} + T_{48}^{\text{in},\mu\nu\alpha} - T_{57}^{\text{in},\mu\nu\alpha} &= 0\\
-(p\cdot q_1) T_{10}^{\text{in},\mu\nu\alpha} + (q_1\cdot q_2) T_{11}^{\text{in},\mu\nu\alpha} - q_1^2 T_{12}^{\text{in},\mu\nu\alpha} + T_{49}^{\text{in},\mu\nu\alpha} - T_{58}^{\text{in},\mu\nu\alpha} &= 0\\
-(p\cdot q_2) T_{19}^{\text{in},\mu\nu\alpha} + q2^2 T_{20}^{\text{in},\mu\nu\alpha} - (q_1\cdot q_2) T_{21}^{\text{in},\mu\nu\alpha} + T_{50}^{\text{in},\mu\nu\alpha} - T_{59}^{\text{in},\mu\nu\alpha} &= 0\\
-p^2 T_{28}^{\text{in},\mu\nu\alpha} + (p\cdot q_2) T_{29}^{\text{in},\mu\nu\alpha} - (p\cdot q_1) T_{30}^{\text{in},\mu\nu\alpha} + T_{51}^{\text{in},\mu\nu\alpha} - T_{60}^{\text{in},\mu\nu\alpha} &= 0
\end{aligned}
\tag{3.98}
$$

3.9.3 Alternative generating set

We can consider an alternative generating set

$$
\{T_i^{\text{b2},\mu\nu\alpha}\} := \Big\{T_1^{\text{b},\mu\nu\alpha},\dots,T_8^{\text{b},\mu\nu\alpha},\frac{1}{2}\big(T_9^{\text{b},\mu\nu\alpha}-T_{11}^{\text{b},\mu\nu\alpha}\big),T_{14}^{\text{b},\mu\nu\alpha},\frac{1}{2}\big(T_9^{\text{b},\mu\nu\alpha}+T_{11}^{\text{b},\mu\nu\alpha}\big),T_{15}^{\text{b},\mu\nu\alpha}\Big\},
\tag{3.99}
$$

with a basis

$$
\begin{aligned}
T_1^{\text{b2},\mu\nu\alpha} &= \varepsilon^{\alpha\nu q_1 q_2} q_2^\mu + \varepsilon^{\alpha\mu q_1 q_2} q_1^\nu + \big(\varepsilon^{\alpha\mu\nu q_1} + \varepsilon^{\alpha\mu\nu q_2}\big)(q_1\cdot q_2),\\
T_2^{\text{b2},\mu\nu\alpha} &= -\varepsilon^{\alpha\nu q_1 q_2} q_2^\mu + \varepsilon^{\alpha\mu q_1 q_2} q_1^\nu + \big(\varepsilon^{\alpha\mu\nu q_1} - \varepsilon^{\alpha\mu\nu q_2}\big)(q_1\cdot q_2),\\
T_3^{\text{b2},\mu\nu\alpha} &= \varepsilon^{\alpha p q_1 q_2} g^{\mu\nu} - \varepsilon^{\alpha\nu p q_1} q_2^\mu + \varepsilon^{\alpha\mu p q_2} q_1^\nu + \varepsilon^{\alpha\mu\nu p}(q_1\cdot q_2),\\
T_4^{\text{b2},\mu\nu\alpha} &= \varepsilon^{\mu\nu q_1 q_2}(q_1+q_2)^\alpha,\\
T_5^{\text{b2},\mu\nu\alpha} &= \varepsilon^{\mu\nu q_1 q_2}(q_1-q_2)^\alpha,\\
T_6^{\text{b2},\mu\nu\alpha} &= \varepsilon^{\nu p q_1 q_2} q_2^\alpha q_2^\mu + \varepsilon^{\mu p q_1 q_2} q_1^\alpha q_1^\nu - \big(\varepsilon^{\mu\nu p q_1} q_1^\alpha + \varepsilon^{\mu\nu p q_2} q_2^\alpha\big)(q_1\cdot q_2),\\
T_7^{\text{b2},\mu\nu\alpha} &= -\varepsilon^{\nu p q_1 q_2} q_2^\alpha q_2^\mu + \varepsilon^{\mu p q_1 q_2} q_1^\alpha q_1^\nu - \big(\varepsilon^{\mu\nu p q_1} q_1^\alpha - \varepsilon^{\mu\nu p q_2} q_2^\alpha\big)(q_1\cdot q_2),\\
T_8^{\text{b2},\mu\nu\alpha} &= -\varepsilon^{\alpha\nu q_1 q_2} p^\mu - \varepsilon^{\alpha\mu q_1 q_2} p^\nu - \varepsilon^{\alpha\mu\nu q_2}(p\cdot q_1) - \varepsilon^{\alpha\mu\nu q_1}(p\cdot q_2),\\
T_9^{\text{b2},\mu\nu\alpha} &= \varepsilon^{\alpha\nu p q_2}\big(q_1^\mu (q_1\cdot q_2) - q_2^\mu q_1^2\big),\\
T_{10}^{\text{b2},\mu\nu\alpha} &= \varepsilon^{\alpha\nu p q_2}\big(q_1^\mu (p\cdot q_1) - p^\mu q_1^2\big),\\
T_{11}^{\text{b2},\mu\nu\alpha} &= \varepsilon^{\alpha\mu p q_1}\big(q_2^\nu (q_1\cdot q_2) - q_1^\nu q_2^2\big),\\
T_{12}^{\text{b2},\mu\nu\alpha} &= \varepsilon^{\alpha\mu p q_1}\big(q_2^\nu (p\cdot q_2) - p^\nu q_2^2\big),\\
T_{13}^{\text{b2},\mu\nu\alpha} &= \varepsilon^{\alpha p q_1 q_2} g^{\mu\nu}\big((q_1\cdot q_2) - q_2^\mu q_1^\nu\big)
\end{aligned}
\tag{3.100}
$$

and an extension by

$$
\begin{aligned}
T_{14}^{\text{b2},\mu\nu\alpha} &= \varepsilon^{\alpha\nu p q_2}\big(p^\mu (q_1\cdot q_2) - q_2^\mu (p\cdot q_1)\big) = \frac{1}{2}\big(T_{10}^{\text{b},\mu\nu\alpha} - T_{12}^{\text{b},\mu\nu\alpha}\big),\\
T_{15}^{\text{b2},\mu\nu\alpha} &= \varepsilon^{\alpha\mu p q_1}\big(p^\nu (q_1\cdot q_2) - q_1^\nu (p\cdot q_2)\big) = \frac{1}{2}\big(T_{10}^{\text{b},\mu\nu\alpha} + T_{12}^{\text{b},\mu\nu\alpha}\big).
\end{aligned}
\tag{3.101}
$$

With this basis, the projection of the form factors $\mathcal{F}_{9,10,11,12}$ changes, such that we find (neglecting $G_{2,3}$ and $H_{2,3,4}$)

$$
\mathcal{F}_9^{\text{b2}} = \frac{2\big(2(p\cdot q_1) - q_1^2\big)}{(q_1\cdot q_2) q_1^2}\left[\frac{F_\pi^V(q_1^2) F_{\rho\pi}(q_2^2)}{M_\pi^2 - u} + \frac{G_1(q_1^2) F_{\rho\pi}(q_2^2)}{M_\rho^2 - t} + \frac{H_1(q_1^2) F_{R\pi}(q_2^2) q_1^2}{M_R^2 - t}\right] - \frac{H_1(q_1^2) F_{R\pi}(q_2^2)\Delta_{\rho R}}{(q_1\cdot q_2)(M_R^2 - t)},
$$

$$
\mathcal{F}_{10}^{\text{b2}} = -\frac{4}{q_1^2}\left[\frac{F_\pi^V(q_1^2) F_{\rho\pi}(q_2^2)}{M_\pi^2 - u} + \frac{G_1(q_1^2) F_{\rho\pi}(q_2^2)}{M_\rho^2 - t} + \frac{H_1(q_1^2) F_{R\pi}(q_2^2) q_1^2}{M_R^2 - t}\right],
$$

$$
\mathcal{F}_{11}^{\text{b2}} = \frac{2\big(2(p\cdot q_2) - q_2^2\big)}{(q_1\cdot q_2) q_2^2}\left[\frac{F_\pi^V(q_2^2) F_{\rho\pi}(q_1^2)}{M_\pi^2 - t} + \frac{G_1(q_2^2) F_{\rho\pi}(q_1^2)}{M_\rho^2 - u} + \frac{H_1(q_2^2) F_{R\pi}(q_1^2) q_2^2}{M_R^2 - u}\right] - \frac{H_1(q_2^2) F_{R\pi}(q_1^2)\Delta_{\rho R}}{(q_1\cdot q_2)(M_R^2 - u)},
$$

$$\mathcal{F}_{12}^{\mathrm{b2}} = -\frac{4}{q_1^2}\left[\frac{F_\pi^V(q_1^2)F_{\rho\pi}(q_2^2)}{M_\pi^2 - t} + \frac{G_1(q_1^2)F_{\rho\pi}(q_2^2)}{M_\rho^2 - u} + \frac{H_1(q_1^2)F_{R\pi}(q_2^2)q_1^2}{M_R^2 - u}\right]. \tag{3.102}$$

The extra factors of 2 can be determined by comparing $\sum_{i=9}^{12} T_i^{\mu\nu\alpha}\mathcal{F}_i$ for the two bases. We see that there are now poles in $(q_1 \cdot q_2)$, q_1^2, and q_2^2 in the form factors $\mathcal{F}_i^{\mathrm{b2}}$ for $i \in \{9, 10, 11, 12\}$. As with basis B_1, we extend basis B_2 as indicated and shift parts of the form factors $\mathcal{F}_{9,10,11,12}^{\mathrm{b2}}$ to $\mathcal{F}_{14,15}^{\mathrm{b2}}$, resulting in

$$\begin{aligned}
\mathcal{F}_9^{\mathrm{b2}} &= -\frac{2G_1(q_1^2)F_{\rho\pi}(q_2^2)}{(M_\rho^2 - t)(M_\pi^2 - u)} - \frac{2H_1(q_1^2)F_{R\pi}(q_2^2)(q_1^2 + \Delta_{\rho R})}{(M_R^2 - t)(M_\pi^2 - u)},\\
\mathcal{F}_{10}^{\mathrm{b2}} &= \frac{2H_1(q_1^2)F_{R\pi}(q_2^2)\Delta_{\rho R}}{(M_R^2 - t)(M_\pi^2 - u)},\\
\mathcal{F}_{11}^{\mathrm{b2}} &= -\frac{2G_1(q_2^2)F_{\rho\pi}(q_1^2)}{(M_\rho^2 - u)(M_\pi^2 - t)} - \frac{2H_1(q_2^2)F_{R\pi}(q_1^2)(q_2^2 + \Delta_{\rho R})}{(M_R^2 - u)(M_\pi^2 - t)},\\
\mathcal{F}_{12}^{\mathrm{b2}} &= \frac{2H_1(q_2^2)F_{R\pi}(q_1^2)\Delta_{\rho R}}{(M_R^2 - u)(M_\pi^2 - t)},\\
\mathcal{F}_{14}^{\mathrm{b2}} &= \frac{4G_1(q_1^2)F_{\rho\pi}(q_2^2)}{(M_\rho^2 - t)(M_\pi^2 - u)} + \frac{4H_1(q_1^2)F_{R\pi}(q_2^2)q_1^2}{(M_R^2 - t)(M_\pi^2 - u)},\\
\mathcal{F}_{15}^{\mathrm{b2}} &= \frac{4G_1(q_2^2)F_{\rho\pi}(q_1^2)}{(M_\rho^2 - u)(M_\pi^2 - t)} + \frac{4H_1(q_2^2)F_{R\pi}(q_1^2)q_2^2}{(M_R^2 - u)(M_\pi^2 - t)}.
\end{aligned} \tag{3.103}$$

3.9.4 Discontinuities for the heavier vector state R

The discontinuities in the t- and u-channel for a heavy vector meson R are expressed in terms of the set of initial tensor structures, see Sec. 3.9.1, and $\Delta_{\rho R} = M_\rho^2 - M_R^2$,

$$\begin{aligned}
&\Delta_t^R(t; s, q_1^2, q_2^2)\\
&= \epsilon_\mu(q_1, \lambda_1)\epsilon_\nu(q_2, \lambda_2)\epsilon_\alpha(p, \lambda_\rho)2\pi e^2\delta(t - M_R^2)(2\pi)^4\delta^{(4)}(p + p_\pi - q_1 - q_2)F_{R\pi}(q_2^2)\\
&\quad\Big[H_1(q_1^2)\Big((q_1^2 + \Delta_{\rho R})\big[T_4^{\mathrm{in},\mu\nu\alpha} + T_6^{\mathrm{in},\mu\nu\alpha}\big] - 2q_1^2\big[T_{22}^{\mathrm{in},\mu\nu\alpha} + T_{24}^{\mathrm{in},\mu\nu\alpha}\big]\Big) - H_2(q_1^2)\Big(T_{10}^{\mathrm{in},\mu\nu\alpha} + T_{12}^{\mathrm{in},\mu\nu\alpha} - T_{32}^{\mathrm{in},\mu\nu\alpha}\Big)\\
&\quad - H_3(q_1^2)\Big(2T_{49}^{\mathrm{in},\mu\nu\alpha} - 4T_{46}^{\mathrm{in},\mu\nu\alpha} + \Delta_{\rho R}\big[T_{10}^{\mathrm{in},\mu\nu\alpha} + T_{12}^{\mathrm{in},\mu\nu\alpha} + T_{32}^{\mathrm{in},\mu\nu\alpha}\big]\Big)\\
&\quad - H_4(q_1^2)\Big(-2T_{49}^{\mathrm{in},\mu\nu\alpha} + q_1^2\big[T_{10}^{\mathrm{in},\mu\nu\alpha} + T_{12}^{\mathrm{in},\mu\nu\alpha} + T_{32}^{\mathrm{in},\mu\nu\alpha}\big]\Big)\Big],
\end{aligned}$$

$$\begin{aligned}
&\Delta_u^R(u; s, q_1^2, q_2^2)\\
&= \epsilon_\mu(q_1, \lambda_1)\epsilon_\nu(q_2, \lambda_2)\epsilon_\alpha(p, \lambda_\rho)2\pi e^2\delta(u - M_R^2)(2\pi)^4\delta^{(4)}(p + p_\pi - q_1 - q_2)F_{R\pi}(q_1^2)\\
&\quad\Big[H_1(q_2^2)\Big((q_2^2 + \Delta_{\rho R})\big[T_{17}^{\mathrm{in},\mu\nu\alpha} - T_{16}^{\mathrm{in},\mu\nu\alpha}\big] + 2q_2^2\big[T_{25}^{\mathrm{in},\mu\nu\alpha} - T_{26}^{\mathrm{in},\mu\nu\alpha}\big]\Big) - H_2(q_2^2)\Big(T_{19}^{\mathrm{in},\mu\nu\alpha} - T_{20}^{\mathrm{in},\mu\nu\alpha} + T_{33}^{\mathrm{in},\mu\nu\alpha}\Big)\\
&\quad - H_3(q_2^2)\Big(4T_{57}^{\mathrm{in},\mu\nu\alpha} - 2T_{59}^{\mathrm{in},\mu\nu\alpha} + \Delta_{\rho R}\big[T_{19}^{\mathrm{in},\mu\nu\alpha} - T_{20}^{\mathrm{in},\mu\nu\alpha} - T_{33}^{\mathrm{in},\mu\nu\alpha}\big]\Big)\\
&\quad - H_4(q_2^2)\Big(2T_{59}^{\mathrm{in},\mu\nu\alpha} + q_2^2\big[T_{19}^{\mathrm{in},\mu\nu\alpha} - T_{20}^{\mathrm{in},\mu\nu\alpha} - T_{33}^{\mathrm{in},\mu\nu\alpha}\big]\Big)\Big].
\end{aligned} \tag{3.104}$$

3.9.5 Constants and parameters

We collect the masses and widths used throughout the calculations in Table 3.2.

	Variable	Value [34] / MeV
$\pi^{\pm}$	$M_{\pi^{\pm}}$	139.57039(17)
$K^{\pm}$	$M_{K^{\pm}}$	493.677(13)
$\rho^{\pm}(770)$	M_{ρ}	775.11(34)
	Γ_{ρ}	149.1(8)
$\omega(782)$	M_{ω}	782.66(13)
$\rho(1450)$	$M_{\rho'}$	1465(25)
$\omega(1420)$	$M_{\omega'}$	1410(60)
$a_1(1260)$	M_{a_1}	1230(40)
	Γ_{a_1}	380(80)
$a_2(1320)$	M_{a_2}	1318.2(6)
	Γ_{a_2}	107(5)

Table 3.2: Masses and widths needed for the calculations in this article, with the values taken from Ref. [34].

3.9.6 Meson multiplets

The multiplets of mesons with the same quantum numbers J^{PC} are collected in matrices,

$$
\begin{aligned}
P &= \begin{pmatrix} \frac{\pi^0}{\sqrt{2}} + \frac{\eta^8}{\sqrt{6}} + \frac{\eta^0}{\sqrt{3}} & \pi^+ & K^+ \\ \pi^- & -\frac{\pi^0}{\sqrt{2}} + \frac{\eta^8}{\sqrt{6}} + \frac{\eta^0}{\sqrt{3}} & K^0 \\ K^- & \bar{K}^0 & -\frac{2\eta^8}{\sqrt{6}} + \frac{\eta^0}{\sqrt{3}} \end{pmatrix}, \\
V_\mu &= \begin{pmatrix} \frac{\rho^0}{\sqrt{2}} + \frac{\omega^8}{\sqrt{6}} + \frac{\omega^0}{\sqrt{3}} & \rho^+ & K^{*+} \\ \rho^- & -\frac{\rho^0}{\sqrt{2}} + \frac{\omega^8}{\sqrt{6}} + \frac{\omega^0}{\sqrt{3}} & K^{*0} \\ K^{*-} & \bar{K}^{*0} & -\frac{2\omega^8}{\sqrt{6}} + \frac{\omega^0}{\sqrt{3}} \end{pmatrix}_\mu, \\
A_\mu &= \begin{pmatrix} \frac{a_1^0}{\sqrt{2}} + \frac{f_1^8}{\sqrt{6}} + \frac{f_1^0}{\sqrt{3}} & a_1^+ & K_1^+ \\ a_1^- & -\frac{a_1^0}{\sqrt{2}} + \frac{f_1^8}{\sqrt{6}} + \frac{f_1^0}{\sqrt{3}} & K_1^0 \\ K_1^- & \bar{K}_1^0 & -\frac{2f_1^8}{\sqrt{6}} + \frac{{f_1}^0}{\sqrt{3}} \end{pmatrix}_\mu, \\
T_{\mu\nu} &= \begin{pmatrix} \frac{a_2^0}{\sqrt{2}} + \frac{f_2^8}{\sqrt{6}} + \frac{f_2^0}{\sqrt{3}} & a_2^+ & K_2^{*+} \\ a_2^- & -\frac{a_2^0}{\sqrt{2}} + \frac{f_2^8}{\sqrt{6}} + \frac{f_2^0}{\sqrt{3}} & K_2^{*0} \\ K_2^{*-} & \bar{K}_2^{*0} & -\frac{2f_2^8}{\sqrt{6}} + \frac{f_2^0}{\sqrt{3}} \end{pmatrix}_{\mu\nu},
\end{aligned}
\tag{3.105}
$$

where $\eta^{8/0}$, $\omega^{8/0}$, $f_1^{8/0}$, and $f_2^{8/0}$ denote the octet and singlet state, respectively, which are mixed to form the physical states η and η', ω and ϕ, f_1 and f_1', and f_2 and f_2'.

3.9.7 Additional plots

The plots in Fig. 3.18 and Fig. 3.19 show the comparison of the full model to the point-like model, which showcases only the loop contributions and the normalisations, for (symmetrised) singly-virtual a_1 TFFs.

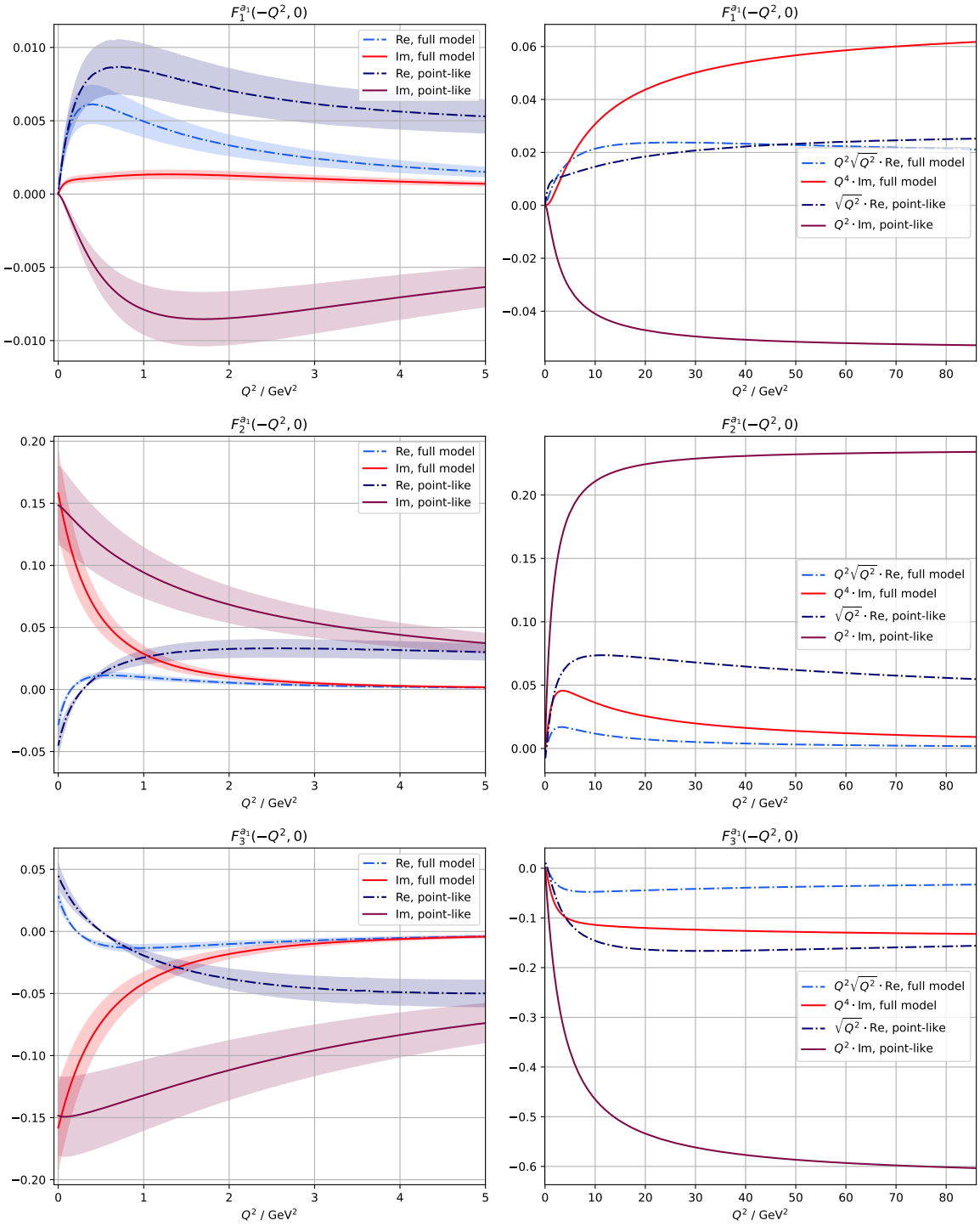

Figure 3.18: Singly-virtual a_1 TFFs: imaginary parts as solid lines, real parts as dash-dotted lines. The brighter lines correspond to the full model, whereas the darker lines show the model with point-like couplings; results shown in the second diagram are multiplied by factors of Q^{2n} according to Table 3.1. The full model contains both G_2 and H_2. The error bands in the first diagram represent the uncertainty in the coupling constant $C_{a_1\rho\pi}$.

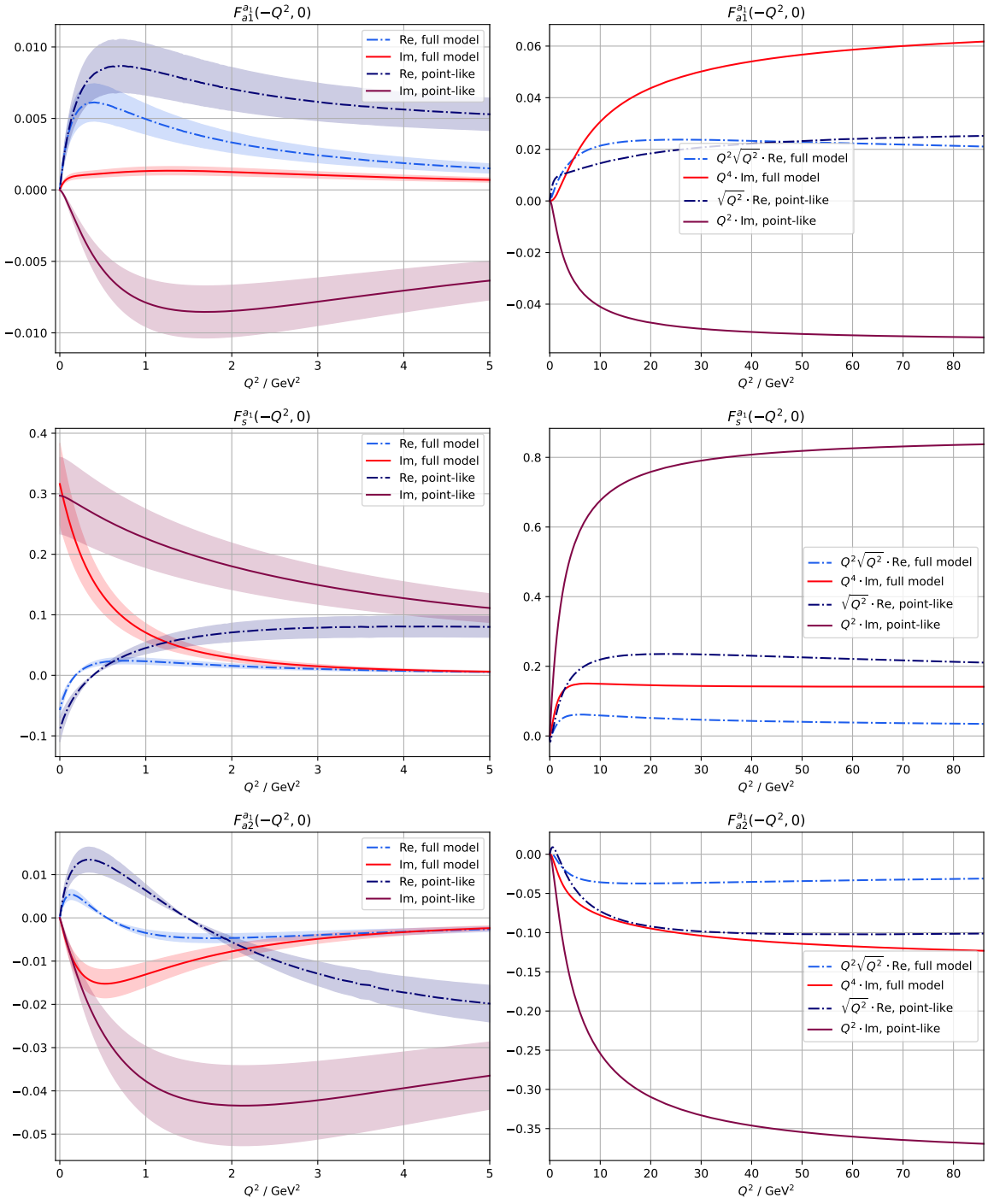

Figure 3.19: Symmetrised singly-virtual a_1 TFFs: imaginary parts as solid lines, real parts as dash-dotted lines. The brighter lines correspond to the full model, whereas the darker lines show the model with point-like couplings; results shown in the second diagram are multiplied by factors of Q^{2n} according to Table 3.1. The full model contains both G_2 and H_2. The error bands in the first diagram represent the uncertainty in the coupling constant $C_{a_1\rho\pi}$.

Chapter 4

Conclusion and outlook

Still round the corner there may wait
A new road or a secret gate
And though I oft have passed them by
A day will come at last when I
Shall take the hidden paths that run
West of the Moon, East of the Sun.

J.R.R. Tolkien, *The Return of the King* [329]

In this thesis, we have presented two projects where form factors and loop effects play a dominant role to achieve a precise prediction of hadronic processes. One concerns the decay of a pseudo-Goldstone boson to another pseudo-Goldstone boson and two leptons via a two-photon intermediate state, which is modelled via vector-meson resonances, both as intermediate states and for the form-factor description. The other project concentrates on transition form factors of resonance states, which are obtained from π and ρ intermediate states. The ρ resonance itself describes here a 2π intermediate state. Knowledge of ρ and π (transition) form factors is presumed in both projects and implemented to different orders of refinement.

The major difficulties in such endeavours lie on the one hand in the fact that loop contributions are naturally harder to calculate than tree-level effects. This required considerable numerical effort in the projects presented here and establishes a connection to the field of high-performance computing (HPC), which might become even more important in future projects in this direction. Algorithms for numerical integration in general and for the evaluation of one- or multiloop integrals in particular are already available, but need to be tested and sometimes adapted for the specific purpose, and since often several of these methods need to be combined, interference effects can occur. Ensuring numerical stability and controlling uncertainties needs to be done carefully.

On the other hand, the development of suitable frameworks can be challenging, especially since hadronic loops including resonances are in general not well-defined in the context of RChPT and dispersive methods need input, which is scarce for short-lived broader resonances. Both dispersion theory and RChPT include in principle infinite sums over intermediate states. Therefore, in any practical calculation, the truncation of these sums introduces errors, and in order to contain those, it is essential to identify and include the dominant contribution and estimate the magnitude of the error. For this, some intuition is helpful, which should be complemented with experimental observations and theoretical considerations, such as expansions in different parameters. Low-energy limits and expectations concerning the asymptotic behaviour constrain these processes at intermediate energies to some extent; matching to such constraints can help with the aforementioned goals. In some cases, one can include higher-order effects via effective terms matched to low- and high-energy limits [106, 107, 244]. We have used a similar idea when introducing an additional heavy-vector-meson intermediate

state in order to match constraints. This could be investigated more systematically by including a heavy pseudoscalar state instead.

In order to estimate systematic effects, we compared different versions of our models in both projects. In some cases, the version most convincing from a theoretical point of view yields only a minor change in the result compared to a simpler version, which implies also less numerical difficulties and more stability. This is the case for the semileptonic $\eta^{(\prime)}$ decays, where the energy-dependent dipole FFs, which fulfil all asymptotic constraints, result in almost the same numbers as the simpler monopole FFs. For these decays, the uncertainty is currently dominated by the experimental uncertainty of the coupling constants; if this changes in the future, more subtle FF effects might become relevant. For the $\eta \to \pi^0\gamma\gamma$ decay, which is less suppressed than the semileptonic process, it has already become apparent that the current models are not precise enough. The tension between the experimental results of the A2 experiment at MAMI [177] and KLOE2 [330] motivates an investigation of additional intermediate states, such as the a_2 in the s-channel [181, 331], and their interference with other intermediate states.

A somewhat similar situation can be observed for the a_1 TFFs: normalisations and asymptotic behaviour are described similarly by two versions of the model, one of them implementing the correct high-energy behaviour of the input ρ and π FFs, whereas the other one neglects the fact that ρ and π are expected to behave differently and the model should therefore be asymmetric. But the only way to find out how significant corrections are is to calculate different versions and compare them. In the TFF project, some difficulties emerged that could not be solved within this thesis, namely the renormalisation of some of the loop integrals and the inclusion into the current HLbL framework [278, 282, 301]. These tasks are left for the future, as well as an improved implementation of unitarity constraints.

With a future refinement of the HLbL framework that might take into account more intermediate states [300, 332], a good understanding of these TFFs and their subtleties becomes even more imperative than it is today. For this, it would be interesting to set up different frameworks for the TFFs: an improved version of the one presented here, where imaginary parts arise, but renormalised, and on the other hand a framework that takes into account RHCs in the $\rho\pi \to \gamma^*\gamma^*$ system, as well as a more complete description of the discontinuity in $a_{1/2} \to \gamma^*\gamma^*$, and works in the NWA. Comparing these different versions could yield insight into the effect of these different assumptions. Such a comparison could even be extended to other resonances such as the f_2.

Specifically in the case of tensor mesons, novel insights could be obtained from such frameworks. Since out of five TFFs, only F_1^T and F_2^T contribute to the on-shell decay width, the others are harder to investigate and understand. On the other hand, in holographic QCD (hQCD), only F_1^T and F_3^T contribute [284], and in the HLbL framework with four-point kinematics, more than two TFFs contributing leads to problems with spurious kinematic singularities [278]. This raises questions about the relative magnitude and asymptotic behaviour of tensor TFFs. A different point of view on these could help to figure out this situation.

On a more fundamental level, one can ask what a complete description of a resonance might even be. The difficulties to define and include resonances into models relates to this. The notion of a pole in the complex $\mathcal{T}$ matrix is probably one of the most appropriate descriptions, but it is also rather abstract. Obtaining all possible effects and interferences with other effects on an observable does not follow automatically from this definition. In this sense, investigating different frameworks for resonances that allow for an evaluation of observables can improve the understanding of the intermediate sector of strong interactions. An example for this is given in Ref. [244], where two dispersive frameworks for the VVA correlator, which imply different intermediate states, are compared.

Future experiments with improved precision require theorists to improve their understanding of higher-order effects in hadronic processes and to communicate this understanding in a suitable way, presenting results such that they can be utilised in further experimental and theoretical analyses. The semileptonic $\eta^{(\prime)}$ decays might be measured with higher event number and improved precision [152], such that a comparison with the SM result calculated in this work might yield a BSM signal. There exist multiple models for C- and CP-violating extensions of the SM. A systematic and model-independent approach to study these is given by the framework of the SM effective field theory (SMEFT), which

collects all operators at a given order of suppression by a heavy scale. The effect of such SMEFT operators on calculations in the low-energy regime can be studied, as has been done in Ref. [163]. Similarly, multiple BSM extensions could explain a potential anomalous magnetic moment of the muon. Understanding the different contributions and how they relate to and are constrained by other processes is necessary to differentiate between different BSM options. Before that, however, deviations between the SM and experiment need to be verified or falsified with high confidence.

It becomes clear in working on and presenting these projects how important it is to collaborate—between theory and experiment, between theory and HPC, between theory and lattice theory, and also within theory. Additionally, different people come with different knowledge and different ideas, and sometimes a fresh view on a project makes all the difference. Different frameworks need to be reconciled such that results can be compared or utilised for the next step, and each field requires input from outside. Some steps in this direction have been taken in this work, and more are to be taken in the future.

Bibliography

[1] Kalandra, *It gets easier*, The Line, 2020.

[2] E. Rutherford, Phil. Mag. Ser. 6 **21**, 669 (1911).

[3] W. Bothe and H. Becker, Zeitschrift für Physik **66**, 289 (1930).

[4] I. Curie and F. Joliot, CR Acad. Sci. Paris **194**, 273 (1932).

[5] J. Chadwick, Nature **129**, 312 (1932).

[6] W. Heisenberg, Z. Phys. **77**, 1 (1932).

[7] H. Yukawa, Proc. Phys. Math. Soc. Jap. **17**, 48 (1935).

[8] C. M. G. Lattes, G. P. S. Occhialini, and C. F. Powell, Nature **160**, 453 (1947).

[9] C. M. G. Lattes, G. P. S. Occhialini, and C. F. Powell, Nature **160**, 486 (1947).

[10] M. Spannowsky, *Searching for New Physics with the Large Hadron Collider*, Oct. 2025, arXiv:2510.03704 [hep-ph].

[11] A. Abada et al. (FCC), Eur. Phys. J. ST **228**, 261 (2019).

[12] G. W. Bennett et al. (Muon $g-2$), Phys. Rev. D **73**, 072003 (2006), arXiv:hep-ex/0602035.

[13] B. Abi et al. (Muon $g-2$), Phys. Rev. Lett. **126**, 141801 (2021), arXiv:2104.03281 [hep-ex].

[14] D. P. Aguillard et al. (Muon $g-2$), Phys. Rev. Lett. **131**, 161802 (2023), arXiv:2308.06230 [hep-ex].

[15] T. Aoyama et al., Phys. Rept. **887**, 1 (2020), arXiv:2006.04822 [hep-ph].

[16] R. Aliberti et al., Phys. Rept. **1143**, 1 (2025), arXiv:2505.21476 [hep-ph].

[17] L. Gan, B. Kubis, E. Passemar, and S. Tulin, Phys. Rept. **945**, 2191 (2022), arXiv:2007.00664 [hep-ph].

[18] G. Ecker, J. Gasser, A. Pich, and E. de Rafael, Nucl. Phys. B **321**, 311 (1989).

[19] G. Ecker, J. Gasser, H. Leutwyler, A. Pich, and E. de Rafael, Phys. Lett. B **223**, 425 (1989).

[20] V. Cirigliano, G. Ecker, H. Neufeld, and A. Pich, JHEP **06**, 012 (2003), arXiv:hep-ph/0305311.

[21] V. Cirigliano, G. Ecker, M. Eidemuller, R. Kaiser, A. Pich, and J. Portoles, Nucl. Phys. B **753**, 139 (2006), arXiv:hep-ph/0603205.

[22] O. Klein and Y. Nishina, Z. Phys. **52**, 853 (1929).

[23] E. Wigner, *Gruppentheorie und ihre Anwendung auf die Quantenmechanik der Atomspektren* (Fried. Vieweg und Sohn Akt.-Ges., Braunschweig, 1931), pp. 251–254.

[24] E. P. Wigner, J. Math. Phys. **1**, 409 (1960).

[25] M. D. Schwartz, *Quantum Field Theory and the Standard Model* (Cambridge University Press, 2014).

[26] E. P. Wigner, Annals Math. **40**, edited by Y. S. Kim and W. W. Zachary, 149 (1939).

[27] G. C. Wick, A. S. Wightman, and E. P. Wigner, Phys. Rev. **88**, edited by A. S. Wightman, 101 (1952).

[28] G. Luders, Kong. Dan. Vid. Sel. Mat. Fys. Med. **28N5**, 1 (1954).

[29] W. Pauli, Niels Bohr and the Development of Physics (1955).

[30] R. Jost, Helv. Phys. Acta **30**, 409 (1957).

[31] G. Luders, Annals Phys. **2**, 1 (1957).

[32] R. F. Streater and A. S. Wightman, *PCT, Spin and Statistics, and All That* (Princeton University Press, 2016).

[33] A. D. Sakharov, Pisma Zh. Eksp. Teor. Fiz. **5**, 32 (1967).

[34] S. Navas et al. (Particle Data Group), Phys. Rev. D **110**, 030001 (2024).

[35] S. L. Glashow, Nucl. Phys. **22**, 579 (1961).

[36] S. Weinberg, Phys. Rev. Lett. **19**, 1264 (1967).

[37] A. Salam, Conf. Proc. C **680519**, 367 (1968).

[38] P. W. Higgs, Phys. Lett. **12**, 132 (1964).

[39] P. W. Higgs, Phys. Rev. Lett. **13**, edited by J. C. Taylor, 508 (1964).

[40] E. Fermi, Z. Phys. **88**, 161 (1934).

[41] R. P. Feynman and M. Gell-Mann, Phys. Rev. **109**, edited by L. M. Brown, 193 (1958).

[42] E. C. G. Sudarshan and R. e. Marshak, Phys. Rev. **109**, 1860 (1958).

[43] C. S. Wu, E. Ambler, R. W. Hayward, D. D. Hoppes, and R. P. Hudson, Phys. Rev. **105**, 1413 (1957).

[44] M. Goldhaber, L. Grodzins, and A. W. Sunyar, Phys. Rev. **109**, 1015 (1958).

[45] Y. Fukuda et al. (Super-Kamiokande), Phys. Rev. Lett. **81**, 1562 (1998), arXiv:hep-ex/9807003.

[46] B. Pontecorvo, Sov. Phys. JETP **6**, 429 (1958).

[47] Z. Maki, M. Nakagawa, and S. Sakata, Prog. Theor. Phys. **28**, 870 (1962).

[48] N. Cabibbo, Phys. Rev. Lett. **10**, 531 (1963).

[49] M. Kobayashi and T. Maskawa, Prog. Theor. Phys. **49**, 652 (1973).

[50] Y. Ne'eman, Nucl. Phys. **26**, edited by R. Ruffini and Y. Verbin, 222 (1961).

[51] M. Gell-Mann, Phys. Rev. **125**, 1067 (1962).

[52] M. Gell-Mann, Phys. Lett. **8**, 214 (1964).

[53] C.-N. Yang and R. L. Mills, Phys. Rev. **96**, edited by J.-P. Hsu and D. Fine, 191 (1954).

[54] C. G. Callan Jr., R. F. Dashen, and D. J. Gross, Phys. Lett. B **63**, edited by J. C. Taylor, 334 (1976).

[55] M. A. Shifman, A. I. Vainshtein, and V. I. Zakharov, Nucl. Phys. B **166**, 493 (1980).

[56] R. J. Crewther, P. Di Vecchia, G. Veneziano, and E. Witten, Phys. Lett. B **88**, [Erratum: Phys.Lett.B 91, 487 (1980)], 123 (1979).

[57] A. Pich and E. de Rafael, Nucl. Phys. B **367**, 313 (1991).

[58] G. Barton and B. G. Smith, Nuovo Cim. **36**, 436 (1965).

[59] D. Schildknecht, Acta Phys. Polon. B **37**, edited by R. Brenner, C. P. de los Heros, and J. Rathsman, 595 (2006), arXiv:hep-ph/0511090.

[60] S. L. Adler, Phys. Rev. **137**, B1022 (1965).

[61] S. L. Adler, Phys. Rev. **139**, B1638 (1965).

[62] S. Weinberg, Phys. Rev. Lett. **18**, 507 (1967).

[63] C.-N. Yang, Phys. Rev. **77**, 242 (1950).

[64] L. D. Landau, Dokl. Akad. Nauk SSSR **60**, 207 (1948).

[65] S. R. Coleman, J. Wess, and B. Zumino, Phys. Rev. **177**, 2239 (1969).

[66] C. G. Callan Jr., S. R. Coleman, J. Wess, and B. Zumino, Phys. Rev. **177**, 2247 (1969).

[67] J. Gasser and A. Zepeda, Nucl. Phys. B **174**, 445 (1980).

[68] J. Gasser and H. Leutwyler, Phys. Rept. **87**, 77 (1982).

[69] J. Gasser and H. Leutwyler, Annals Phys. **158**, 142 (1984).

[70] J. Gasser and H. Leutwyler, Nucl. Phys. B **250**, 465 (1985).

[71] J. Gasser and H. Leutwyler, Nucl. Phys. B **250**, 517 (1985).

[72] J. Gasser and U.-G. Meißner, Nucl. Phys. B **357**, 90 (1991).

[73] H. Leutwyler, Annals Phys. **235**, 165 (1994), arXiv:hep-ph/9311274.

[74] B. Kubis, in Workshop on Physics and Astrophysics of Hadrons and Hadronic Matter Shantiniketan, India, November 6-10, 2006 (2007), arXiv:hep-ph/0703274.

[75] S. Scherer and M. R. Schindler, *A Primer for Chiral Perturbation Theory*, Vol. 830 (2012).

[76] M. Penners and H. Schäfer, *I want to break symmetry!*, Seminar at the International Conference of Physics Students, Tbilisi, 2024.

[77] E. Noether, Nachr. d. König. Gesellsch. d. Wiss. zu Göttingen **1918**, 235 (1918).

[78] J. S. Bell and R. Jackiw, Nuovo Cim. A **60**, 47 (1969).

[79] S. L. Adler, Phys. Rev. **177**, 2426 (1969).

[80] G. 't Hooft, Phys. Rev. Lett. **37**, edited by M. A. Shifman, 8 (1976).

[81] G. 't Hooft, Phys. Rev. D **14**, edited by M. A. Shifman, [Erratum: Phys.Rev.D 18, 2199 (1978)], 3432 (1976).

[82] O. Bar and U. J. Wiese, Nucl. Phys. B **609**, 225 (2001), arXiv:hep-ph/0105258.

[83] Y. Nambu, Phys. Rev. **117**, edited by J. C. Taylor, 648 (1960).

[84] Y. Nambu and G. Jona-Lasinio, Phys. Rev. **124**, edited by T. Eguchi, 246 (1961).

[85] Y. Nambu and G. Jona-Lasinio, Phys. Rev. **122**, edited by T. Eguchi, 345 (1961).

[86] C. Vafa and E. Witten, Nucl. Phys. B **234**, 173 (1984).

[87] J. Goldstone, Nuovo Cim. **19**, 154 (1961).

[88] S. Weinberg, Physica A **96**, edited by S. Deser, 327 (1979).

[89] T. D. Lee and C.-N. Yang, Nuovo Cim. **10**, edited by G. Feinberg, 749 (1956).

[90] M. Gell-Mann, R. J. Oakes, and B. Renner, Phys. Rev. **175**, 2195 (1968).

[91] J. Wess and B. Zumino, Phys. Lett. B **37**, 95 (1971).

[92] E. Witten, Nucl. Phys. B **223**, 422 (1983).

[93] A. Abbas, (2000), arXiv:hep-ph/0009242.

[94] B. Borasoy and E. Lipartia, Phys. Rev. D **71**, 014027 (2005), arXiv:hep-ph/0410141.

[95] J. Goldstone and F. Wilczek, Phys. Rev. Lett. **47**, edited by A. D. Shapere and F. Wilczek, 986 (1981).

[96] G. 't Hooft, Nucl. Phys. B **72**, edited by J. C. Taylor, 461 (1974).

[97] G. Veneziano, Nucl. Phys. B **117**, 519 (1976).

[98] E. Witten, Nucl. Phys. B **156**, 269 (1979).

[99] J. Bijnens, G. Colangelo, and G. Ecker, JHEP **02**, 020 (1999), arXiv:hep-ph/9902437.

[100] J. Bijnens and E. Pallante, Mod. Phys. Lett. A **11**, 1069 (1996), arXiv:hep-ph/9510338.

[101] L. Ametller, J. Bijnens, A. Bramon, and F. Cornet, Phys. Lett. B **276**, 185 (1992).

[102] M. Jetter, Nucl. Phys. B **459**, 283 (1996), arXiv:hep-ph/9508407.

[103] M. A. Shifman, A. I. Vainshtein, and V. I. Zakharov, Nucl. Phys. B **147**, 385 (1979).

[104] M. A. Shifman, A. I. Vainshtein, and V. I. Zakharov, Nucl. Phys. B **147**, 448 (1979).

[105] L. J. Reinders, H. Rubinstein, and S. Yazaki, Phys. Rept. **127**, 1 (1985).

[106] G. Colangelo, F. Hagelstein, M. Hoferichter, L. Laub, and P. Stoffer, Phys. Rev. D **101**, 051501 (2020), arXiv:1910.11881 [hep-ph].

[107] G. Colangelo, F. Hagelstein, M. Hoferichter, L. Laub, and P. Stoffer, JHEP **03**, 101 (2020), arXiv:1910.13432 [hep-ph].

[108] J. Bijnens, N. Hermansson-Truedsson, L. Laub, and A. Rodríguez-Sánchez, JHEP **10**, 203 (2020), arXiv:2008.13487 [hep-ph].

[109] J. Bijnens, N. Hermansson-Truedsson, L. Laub, and A. Rodríguez-Sánchez, JHEP **04**, 240 (2021), arXiv:2101.09169 [hep-ph].

[110] J. Bijnens, N. Hermansson-Truedsson, and A. Rodríguez-Sánchez, JHEP **02**, 167 (2023), arXiv:2211.17183 [hep-ph].

[111] J. Bijnens, N. Hermansson-Truedsson, and A. Rodríguez-Sánchez, JHEP **03**, 094 (2025), arXiv:2411.09578 [hep-ph].

[112] S. J. Brodsky and G. R. Farrar, Phys. Rev. D **11**, 1309 (1975).

[113] G. P. Lepage and S. J. Brodsky, Phys. Lett. B **87**, 359 (1979).

[114] G. P. Lepage and S. J. Brodsky, Phys. Rev. D **22**, 2157 (1980).

[115] S. J. Brodsky and G. P. Lepage, Phys. Rev. D **24**, 1808 (1981).

[116] H. Georgi, Phys. Lett. B **240**, 447 (1990).

[117] T.-M. Yan, H.-Y. Cheng, C.-Y. Cheung, G.-L. Lin, Y. C. Lin, and H.-L. Yu, Phys. Rev. D **46**, [Erratum: Phys.Rev.D 55, 5851 (1997)], 1148 (1992).

[118] M. B. Wise, Phys. Rev. D **45**, R2188 (1992).

[119] M. Neubert, Phys. Rept. **245**, 259 (1994), arXiv:hep-ph/9306320.

[120] E. E. Jenkins and A. V. Manohar, Phys. Lett. B **255**, 558 (1991).

[121] V. Bernard, N. Kaiser, J. Kambor, and U.-G. Meißner, Nucl. Phys. B **388**, 315 (1992).

[122] T. Regge, Nuovo Cim. **9**, 295 (1958).

[123] G. F. Chew and S. C. Frautschi, Phys. Rev. Lett. **7**, 394 (1961).

[124] R. J. Eden, P. V. Landshoff, D. I. Olive, and J. C. Polkinghorne, *The analytic S-matrix* (Cambridge Univ. Press, Cambridge, 1966).

[125] M. Froissart, Phys. Rev. **123**, 1053 (1961).

[126] H. A. Kramers, Atti Cong. Intern. Fisica (Transactions of Volta Centenary Congress) Como **2**, 545 (1927).

[127] E. Feenberg, Phys. Rev. **40**, 40 (1932).

[128] B. Kubis, *Dispersion relations: foundations*, Oct. 2025, arXiv:2510.01962 [hep-ph].

[129] H. M. Nussenzveig, *Causality and dispersion relations*, Vol. 95 (Academic Press, New York, London, 1972).

[130] J. A. Oller, *A Brief Introduction to Dispersion Relations*, SpringerBriefs in Physics (Springer, 2019).

[131] G. Colangelo, *A brief introduction to dispersive methods*, Sept. 2025, arXiv:2509.24548 [hep-ph].

[132] E. H. Wichmann and J. H. Crichton, Phys. Rev. **132**, 2788 (1963).

[133] E. Byckling and K. Kajantie, *Particle Kinematics* (University of Jyvaskyla, Jyvaskyla, Finland, 1971).

[134] J. Plemelj, Monatshefte für Mathematik und Physik **19**, 205 (1908).

[135] R. de L. Kronig, J. Opt. Soc. Am. **12**, 547 (1926).

[136] S. Weinberg, *The Quantum theory of fields. Vol. 1: Foundations* (Cambridge University Press, June 2005).

[137] G. Kallen, Helv. Phys. Acta **25**, edited by C. Jarlskog, 417 (1952).

[138] H. Lehmann, Nuovo Cim. **11**, 342 (1954).

[139] R. E. Cutkosky, J. Math. Phys. **1**, 429 (1960).

[140] D. Gomez Dumm, A. Pich, and J. Portoles, Phys. Rev. D **62**, 054014 (2000), arXiv:hep-ph/0003320.

[141] L. A. Heuser, G. Chanturia, F.-K. Guo, C. Hanhart, M. Hoferichter, and B. Kubis, Eur. Phys. J. C **84**, 599 (2024), arXiv:2403.15539 [hep-ph].

[142] G. Breit and E. Wigner, Phys. Rev. **49**, 519 (1936).

[143] I. J. R. Aitchison, Nucl. Phys. A **189**, 417 (1972).

[144] M. Zanke, M. Hoferichter, and B. Kubis, JHEP **07**, 106 (2021), arXiv:2103.09829 [hep-ph].

[145] Linkin Park, *The Catalyst*, A Thousand Suns, 2010.

[146] V. Baluni, Phys. Rev. D **19**, 2227 (1979).

[147] C. Abel et al., Phys. Rev. Lett. **124**, 081803 (2020), arXiv:2001.11966 [hep-ex].

[148] J. M. Pendlebury et al., Phys. Rev. D **92**, 092003 (2015), arXiv:1509.04411 [hep-ex].

[149] R. I. Dzhelyadin et al., Phys. Lett. B **105**, 239 (1981).

[150] R. A. Briere et al. (CLEO), Phys. Rev. Lett. **84**, 26 (2000), arXiv:hep-ex/9907046.

[151] P. Adlarson et al. (WASA-at-COSY), Phys. Lett. B **784**, 378 (2018), arXiv:1802.08642 [hep-ex].

[152] J. Elam et al. (REDTOP), Mar. 2022, arXiv:2203.07651 [hep-ex].

[153] H. Schäfer, "The Standard Model contribution to the branching ration $\eta \to \pi^0 \ell^+ \ell^-$ and similar processes", Master's thesis (Universität Bonn, Nov. 2021).

[154] R. Escribano and E. Royo, Eur. Phys. J. C **80**, [Errata: Eur. Phys. J. C **81**, 140 (2021); Eur. Phys. J. C **82**, 743 (2022)], 1190 (2020), arXiv:2007.12467 [hep-ph].

[155] T. Hahn and M. Pérez-Victoria, Comput. Phys. Commun. **118**, 153 (1999), arXiv:hep-ph/9807565.

[156] M. Zanke, "Dispersively improved vector-meson-dominance approaches to precision observables", PhD thesis (Bonn U., 2024).

[157] A. Denner and S. Dittmaier, Nucl. Phys. B **658**, 175 (2003), arXiv:hep-ph/0212259.

[158] A. Denner and S. Dittmaier, Nucl. Phys. B **734**, 62 (2006), arXiv:hep-ph/0509141.

[159] A. Denner and S. Dittmaier, Nucl. Phys. B **844**, 199 (2011), arXiv:1005.2076 [hep-ph].

[160] A. Denner, S. Dittmaier, and L. Hofer, Comput. Phys. Commun. **212**, 220 (2017), arXiv:1604.06792 [hep-ph].

[161] J. Bernstein, G. Feinberg, and T. D. Lee, Phys. Rev. **139**, edited by G. Feinberg, B1650 (1965).

[162] B. Barrett, M. Jacob, M. Nauenberg, and T. N. Truong, Phys. Rev. **141**, 1342 (1966).

[163] H. Akdag, B. Kubis, and A. Wirzba, JHEP **06**, 154 (2023), arXiv:2212.07794 [hep-ph].

[164] H. Akdag, B. Kubis, and A. Wirzba, JHEP **03**, 059 (2024), arXiv:2307.02533 [hep-ph].

[165] R. Escribano, E. Royo, and P. Sánchez-Puertas, JHEP **05**, 147 (2022), arXiv:2202.04886 [hep-ph].

[166] P. Masjuan and P. Sánchez-Puertas, JHEP **08**, 108 (2016), arXiv:1512.09292 [hep-ph].

[167] E. Weil, G. Eichmann, C. S. Fischer, and R. Williams, Phys. Rev. D **96**, 014021 (2017), arXiv:1704.06046 [hep-ph].

[168] M. Hoferichter, B.-L. Hoid, B. Kubis, and J. Lüdtke, Phys. Rev. Lett. **128**, 172004 (2022), arXiv:2105.04563 [hep-ph].

[169] C. H. Llewellyn Smith, Nuovo Cim. A **48**, [Erratum: Nuovo Cim. A **50**, 374 (1967)], 834 (1967).

[170] J. Smith, Phys. Rev. **166**, 1629 (1968).

[171] T. P. Cheng, Phys. Rev. **162**, 1734 (1967).

[172] J. N. Ng and D. J. Peters, Phys. Rev. D **46**, 5034 (1992).

[173] J. N. Ng and D. J. Peters, Phys. Rev. D **47**, 4939 (1993).

[174] R. L. Workman et al. (Particle Data Group), PTEP **2022**, 083C01 (2022).

[175] S. Prakhov et al., Phys. Rev. C **72**, 025201 (2005).

[176] S. Prakhov et al., Phys. Rev. C **78**, 015206 (2008).

[177] B. M. K. Nefkens et al. (A2 at MAMI), Phys. Rev. C **90**, 025206 (2014), arXiv:1405.4904 [hep-ex].

[178] I. Danilkin, O. Deineka, and M. Vanderhaeghen, Phys. Rev. D **96**, 114018 (2017), arXiv:1709.08595 [hep-ph].

[179] E. Oset, J. R. Peláez, and L. Roca, Phys. Rev. D **67**, 073013 (2003), arXiv:hep-ph/0210282.

[180] E. Oset, J. R. Peláez, and L. Roca, Phys. Rev. D **77**, 073001 (2008), arXiv:0801.2633 [hep-ph].

[181] J. Lu and B. Moussallam, Eur. Phys. J. C **80**, 436 (2020), arXiv:2002.04441 [hep-ph].

[182] R. Escribano, S. Gonzàlez-Solís, R. Jora, and E. Royo, Phys. Rev. D **102**, 034026 (2020), arXiv:1812.08454 [hep-ph].

[183] L. G. Landsberg, Phys. Rept. **128**, 301 (1985).

[184] S.-s. Fang, B. Kubis, and A. Kupść, Prog. Part. Nucl. Phys. **120**, 103884 (2021), arXiv:2102.05922 [hep-ph].

[185] C. Terschlüsen and S. Leupold, Phys. Lett. B **691**, 191 (2010), arXiv:1003.1030 [hep-ph].

[186] C. Terschlüsen, S. Leupold, and M. F. M. Lutz, Eur. Phys. J. A **48**, 190 (2012), arXiv:1204.4125 [hep-ph].

[187] S. P. Schneider, B. Kubis, and F. Niecknig, Phys. Rev. D **86**, 054013 (2012), arXiv:1206.3098 [hep-ph].

[188] I. V. Danilkin, C. Fernández-Ramírez, P. Guo, V. Mathieu, D. Schott, M. Shi, and A. P. Szczepaniak, Phys. Rev. D **91**, 094029 (2015), arXiv:1409.7708 [hep-ph].

[189] R. A. Briceño, J. J. Dudek, R. G. Edwards, C. J. Shultz, C. E. Thomas, and D. J. Wilson, Phys. Rev. Lett. **115**, 242001 (2015), arXiv:1507.06622 [hep-ph].

[190] R. A. Briceño, J. J. Dudek, R. G. Edwards, C. J. Shultz, C. E. Thomas, and D. J. Wilson, Phys. Rev. D **93**, [Erratum: Phys. Rev. D **105**, 079902 (2022)], 114508 (2016), arXiv:1604.03530 [hep-ph].

[191] C. Alexandrou et al., Phys. Rev. D **98**, [Erratum: Phys. Rev. D **105**, 019902 (2022)], 074502 (2018), arXiv:1807.08357 [hep-lat].

[192] M. Niehus, M. Hoferichter, and B. Kubis, JHEP **12**, 038 (2021), arXiv:2110.11372 [hep-ph].

[193] G. R. Farrar and D. R. Jackson, Phys. Rev. Lett. **35**, 1416 (1975).

[194] A. I. Vainshtein and V. I. Zakharov, Phys. Lett. B **72**, 368 (1978).

[195] V. L. Chernyak and A. R. Zhitnitsky, Phys. Rept. **112**, 173 (1984).

[196] A. Rittenberg and G. R. Kalbfleisch, Phys. Rev. Lett. **15**, 556 (1965).

[197] M. J. Bazin, A. T. Goshaw, A. R. Zacher, and C. R. Sun, Phys. Rev. Lett. **20**, 895 (1968).

[198] M. R. Jane et al., Phys. Lett. B **59**, 99 (1975).

[199] C. Gatto (REDTOP), Oct. 2019, arXiv:1910.08505 [physics.ins-det].

[200] S. Okubo, Phys. Lett. **5**, 165 (1963).

[201] G. Zweig, "An SU(3) model for strong interaction symmetry and its breaking. Version 2", in *Developments in the Quark Theory of Hadrons. Vol. 1. 1964 - 1978*, edited by D. B. Lichtenberg and S. P. Rosen (Feb. 1964), pp. 22–101.

[202] J. Iizuka, Prog. Theor. Phys. Suppl. **37**, 21 (1966).

[203] M. Hoferichter, B. Kubis, S. Leupold, F. Niecknig, and S. P. Schneider, Eur. Phys. J. C **74**, 3180 (2014), arXiv:1410.4691 [hep-ph].

[204] M. Hoferichter, B.-L. Hoid, and B. Kubis, JHEP **08**, 137 (2019), arXiv:1907.01556 [hep-ph].

[205] B.-L. Hoid, M. Hoferichter, and B. Kubis, Eur. Phys. J. C **80**, 988 (2020), arXiv:2007.12696 [hep-ph].

[206] M. N. Achasov et al., Phys. Rev. D **94**, 112001 (2016), arXiv:1610.00235 [hep-ex].

[207] B. Aubert et al. (BaBar), Phys. Rev. D **76**, [Erratum: Phys. Rev. D **77**, 119902 (2008)], 092005 (2007), arXiv:0708.2461 [hep-ex].

[208] J. P. Lees et al. (BaBar), Phys. Rev. D **97**, 052007 (2018), arXiv:1801.02960 [hep-ex].

[209] S. Holz, J. Plenter, C.-W. Xiao, T. Dato, C. Hanhart, B. Kubis, U.-G. Meißner, and A. Wirzba, Eur. Phys. J. C **81**, 1002 (2021), arXiv:1509.02194 [hep-ph].

[210] M. Hoferichter, B. Kubis, and D. Sakkas, Phys. Rev. D **86**, 116009 (2012), arXiv:1210.6793 [hep-ph].

[211] M. Hoferichter, B. Kubis, and M. Zanke, Phys. Rev. D **96**, 114016 (2017), arXiv:1710.00824 [hep-ph].

[212] F. Stollenwerk, C. Hanhart, A. Kupść, U.-G. Meißner, and A. Wirzba, Phys. Lett. B **707**, 184 (2012), arXiv:1108.2419 [nucl-th].

[213] B. Kubis and J. Plenter, Eur. Phys. J. C **75**, 283 (2015), arXiv:1504.02588 [hep-ph].

[214] S. Holz, C. Hanhart, M. Hoferichter, and B. Kubis, Eur. Phys. J. C **82**, [Addendum: Eur. Phys. J. C **82**, 1159 (2022)], 434 (2022), arXiv:2202.05846 [hep-ph].

[215] G. Colangelo, M. Hoferichter, B. Kubis, M. Procura, and P. Stoffer, Phys. Lett. B **738**, 6 (2014), arXiv:1408.2517 [hep-ph].

[216] M. Hoferichter and P. Stoffer, JHEP **07**, 073 (2019), arXiv:1905.13198 [hep-ph].

[217] A. Crivellin and M. Hoferichter, Phys. Rev. D **108**, 013005 (2023), arXiv:2211.12516 [hep-ph].

[218] C. Adolph et al. (COMPASS), Phys. Rev. D **95**, 032004 (2017), arXiv:1509.00992 [hep-ex].

[219] F. von Hippel and C. Quigg, Phys. Rev. D **5**, 624 (1972).

[220] V. Shtabovenko, R. Mertig, and F. Orellana, Comput. Phys. Commun. **207**, 432 (2016), arXiv:1601.01167 [hep-ph].

[221] V. Shtabovenko, R. Mertig, and F. Orellana, Comput. Phys. Commun. **256**, 107478 (2020), arXiv:2001.04407 [hep-ph].

[222] R. Mertig, M. Bohm, and A. Denner, Comput. Phys. Commun. **64**, 345 (1991).

[223] H. Schäfer, M. Zanke, Y. Korte, and B. Kubis, Phys. Rev. D **108**, 074025 (2023), arXiv:2307.10357 [hep-ph].

[224] T. Hahn, Comput. Phys. Commun. **168**, 78 (2005), arXiv:hep-ph/0404043.

[225] W. A. Bardeen and W. K. Tung, Phys. Rev. **173**, [Erratum: Phys. Rev. D **4**, 3229 (1971)], 1423 (1968).

[226] R. Tarrach, Nuovo Cim. A **28**, 409 (1975).

[227] G. Colangelo, M. Hoferichter, M. Procura, and P. Stoffer, JHEP **09**, 074 (2015), arXiv:1506.01386 [hep-ph].

[228] B. Moussallam, Eur. Phys. J. C **73**, 2539 (2013), arXiv:1305.3143 [hep-ph].

[229] B. Moussallam, Eur. Phys. J. C **81**, 993 (2021), arXiv:2107.14147 [hep-ph].

[230] S. Giovannella (KLOE-2), *Light meson decays at KLOE/KLOE-2*, Talk at the *ECT** workshop, Trento, 2023.

[231] M. Ablikim et al. (BESIII), Phys. Rev. D **96**, 012005 (2017), arXiv:1612.05721 [hep-ex].

[232] M. Ablikim et al. (BESIII), Phys. Rev. D **100**, 052015 (2019), arXiv:1906.10346 [hep-ex].

[233] B. Di Micco et al. (KLOE), Acta Phys. Slov. **56**, 403 (2006).

[234] D. Kehr, *Licht*, Wo soll ich suchen, 2013.

[235] T. Aoyama, M. Hayakawa, T. Kinoshita, and M. Nio, Phys. Rev. Lett. **109**, 111808 (2012), arXiv:1205.5370 [hep-ph].

[236] S. Volkov, Phys. Rev. D **100**, 096004 (2019), arXiv:1909.08015 [hep-ph].

[237] S. Volkov, Phys. Rev. D **110**, 036001 (2024), arXiv:2404.00649 [hep-ph].

[238] T. Aoyama, M. Hayakawa, A. Hirayama, and M. Nio, Phys. Rev. D **111**, L031902 (2025), arXiv:2412.06473 [hep-ph].

[239] R. H. Parker, C. Yu, W. Zhong, B. Estey, and H. Müller, Science **360**, 191 (2018), arXiv:1812.04130 [physics.atom-ph].

[240] L. Morel, Z. Yao, P. Cladé, and S. Guellati-Khélifa, Nature **588**, 61 (2020).

[241] X. Fan, T. G. Myers, B. A. D. Sukra, and G. Gabrielse, Phys. Rev. Lett. **130**, 071801 (2023), arXiv:2209.13084 [physics.atom-ph].

[242] A. Czarnecki, W. J. Marciano, and A. Vainshtein, Phys. Rev. D **67**, [Erratum: Phys.Rev.D 73, 119901 (2006)], 073006 (2003), arXiv:hep-ph/0212229.

[243] C. Gnendiger, D. Stöckinger, and H. Stöckinger-Kim, Phys. Rev. D **88**, 053005 (2013), arXiv:1306.5546 [hep-ph].

[244] J. Lüdtke, M. Procura, and P. Stoffer, JHEP **04**, 130 (2025), arXiv:2410.11946 [hep-ph].

[245] M. Hoferichter, J. Lüdtke, L. Naterop, M. Procura, and P. Stoffer, (2025), arXiv:2503.04883 [hep-ph].

[246] T. Blum, P. A. Boyle, V. Gülpers, T. Izubuchi, L. Jin, C. Jung, A. Jüttner, C. Lehner, A. Portelli, and J. T. Tsang (RBC, UKQCD), Phys. Rev. Lett. **121**, 022003 (2018), arXiv:1801.07224 [hep-lat].

[247] D. Giusti, V. Lubicz, G. Martinelli, F. Sanfilippo, and S. Simula (ETM), Phys. Rev. D **99**, 114502 (2019), arXiv:1901.10462 [hep-lat].

[248] S. Borsányi et al., Nature **593**, 51 (2021), arXiv:2002.12347 [hep-lat].

[249] C. Lehner and A. S. Meyer, Phys. Rev. D **101**, 074515 (2020), arXiv:2003.04177 [hep-lat].

[250] G. Wang, T. Draper, K.-F. Liu, and Y.-B. Yang (χQCD), Phys. Rev. D **107**, 034513 (2023), arXiv:2204.01280 [hep-lat].

[251] C. Aubin, T. Blum, M. Golterman, and S. Peris, Phys. Rev. D **106**, 054503 (2022), arXiv:2204.12256 [hep-lat].

[252] M. Cè et al., Phys. Rev. D **106**, 114502 (2022), arXiv:2206.06582 [hep-lat].

[253] C. Alexandrou et al. (ETM), Phys. Rev. D **107**, 074506 (2023), arXiv:2206.15084 [hep-lat].

[254] T. Blum et al. (RBC, UKQCD), Phys. Rev. D **108**, 054507 (2023), arXiv:2301.08696 [hep-lat].

[255] S. Kuberski, M. Cè, G. von Hippel, H. B. Meyer, K. Ottnad, A. Risch, and H. Wittig, JHEP **03**, 172 (2024), arXiv:2401.11895 [hep-lat].

[256] A. Boccaletti et al., (2024), arXiv:2407.10913 [hep-lat].

[257] S. Spiegel and C. Lehner, Phys. Rev. D **111**, 114517 (2025), arXiv:2410.17053 [hep-lat].

[258] T. Blum et al. (RBC, UKQCD), Phys. Rev. Lett. **134**, 201901 (2025), arXiv:2410.20590 [hep-lat].

[259] D. Djukanovic, G. von Hippel, S. Kuberski, H. B. Meyer, N. Miller, K. Ottnad, J. Parrino, A. Risch, and H. Wittig, JHEP **04**, 098 (2025), arXiv:2411.07969 [hep-lat].

[260] C. Alexandrou et al. (ETM), Phys. Rev. D **111**, 054502 (2025), arXiv:2411.08852 [hep-lat].

[261] A. Bazavov et al. (Fermilab Lattice, HPQCD, MILC), Phys. Rev. D **111**, 094508 (2025), arXiv:2411.09656 [hep-lat].

[262] A. Bazavov et al. (Fermilab Lattice, HPQCD,, MILC), Phys. Rev. Lett. **135**, 011901 (2025), arXiv:2412.18491 [hep-lat].

[263] A. Keshavarzi, D. Nomura, and T. Teubner, Phys. Rev. D **101**, 014029 (2020), arXiv:1911.00367 [hep-ph].

[264] L. Di Luzio, A. Keshavarzi, A. Masiero, and P. Paradisi, Phys. Rev. Lett. **134**, 011902 (2025), arXiv:2408.01123 [hep-ph].

[265] A. Kurz, T. Liu, P. Marquard, and M. Steinhauser, Phys. Lett. B **734**, 144 (2014), arXiv:1403.6400 [hep-ph].

[266] P. Masjuan and P. Sanchez-Puertas, Phys. Rev. D **95**, 054026 (2017), arXiv:1701.05829 [hep-ph].

[267] G. Colangelo, M. Hoferichter, M. Procura, and P. Stoffer, JHEP **04**, 161 (2017), arXiv:1702.07347 [hep-ph].

[268] M. Hoferichter, B.-L. Hoid, B. Kubis, S. Leupold, and S. P. Schneider, JHEP **10**, 141 (2018), arXiv:1808.04823 [hep-ph].

[269] G. Eichmann, C. S. Fischer, E. Weil, and R. Williams, Phys. Lett. B **797**, [Erratum: Phys. Lett. B **799**, 135029 (2019)], 134855 (2019), arXiv:1903.10844 [hep-ph].

[270] J. Bijnens, N. Hermansson-Truedsson, and A. Rodríguez-Sánchez, Phys. Lett. B **798**, 134994 (2019), arXiv:1908.03331 [hep-ph].

[271] J. Leutgeb and A. Rebhan, Phys. Rev. D **101**, 114015 (2020), arXiv:1912.01596 [hep-ph].

[272] L. Cappiello, O. Catà, G. D'Ambrosio, D. Greynat, and A. Iyer, Phys. Rev. D **102**, 016009 (2020), arXiv:1912.02779 [hep-ph].

[273] P. Masjuan, P. Roig, and P. Sánchez-Puertas, J. Phys. G **49**, 015002 (2022), arXiv:2005.11761 [hep-ph].

[274] I. Danilkin, M. Hoferichter, and P. Stoffer, Phys. Lett. B **820**, 136502 (2021), arXiv:2105.01666 [hep-ph].

[275] D. Stamen, D. Hariharan, M. Hoferichter, B. Kubis, and P. Stoffer, Eur. Phys. J. C **82**, 432 (2022), arXiv:2202.11106 [hep-ph].

[276] J. Leutgeb, J. Mager, and A. Rebhan, Phys. Rev. D **107**, 054021 (2023), arXiv:2211.16562 [hep-ph].

[277] M. Hoferichter, B. Kubis, and M. Zanke, JHEP **08**, 209 (2023), arXiv:2307.14413 [hep-ph].

[278] M. Hoferichter, P. Stoffer, and M. Zillinger, JHEP **04**, 092 (2024), arXiv:2402.14060 [hep-ph].

[279] E. J. Estrada, S. Gonzàlez-Solís, A. Guevara, and P. Roig, JHEP **12**, 203 (2024), arXiv:2409.10503 [hep-ph].

[280] O. Deineka, I. Danilkin, and M. Vanderhaeghen, Phys. Rev. D **111**, 034009 (2025), arXiv:2410.12894 [hep-ph].

[281] G. Eichmann, C. S. Fischer, T. Haeuser, and O. Regenfelder, Eur. Phys. J. C **85**, 445 (2025), arXiv:2411.05652 [hep-ph].

[282] M. Hoferichter, P. Stoffer, and M. Zillinger, JHEP **02**, 121 (2025), arXiv:2412.00178 [hep-ph].

[283] S. Holz, M. Hoferichter, B.-L. Hoid, and B. Kubis, JHEP **04**, 147 (2025), arXiv:2412.16281 [hep-ph].

[284] L. Cappiello, J. Leutgeb, J. Mager, and A. Rebhan, JHEP **07**, 033 (2025), arXiv:2501.09699 [hep-ph].

[285] G. Colangelo, M. Hoferichter, A. Nyffeler, M. Passera, and P. Stoffer, Phys. Lett. B **735**, 90 (2014), arXiv:1403.7512 [hep-ph].

[286] T. Blum, N. Christ, M. Hayakawa, T. Izubuchi, L. Jin, C. Jung, and C. Lehner, Phys. Rev. Lett. **124**, 132002 (2020), arXiv:1911.08123 [hep-lat].

[287] E.-H. Chao, R. J. Hudspith, A. Gérardin, J. R. Green, H. B. Meyer, and K. Ottnad, Eur. Phys. J. C **81**, 651 (2021), arXiv:2104.02632 [hep-lat].

[288] E.-H. Chao, R. J. Hudspith, A. Gérardin, J. R. Green, and H. B. Meyer, Eur. Phys. J. C **82**, 664 (2022), arXiv:2204.08844 [hep-lat].

[289] T. Blum, N. Christ, M. Hayakawa, T. Izubuchi, L. Jin, C. Jung, C. Lehner, and C. Tu (RBC, UKQCD), Phys. Rev. D **111**, 014501 (2025), arXiv:2304.04423 [hep-lat].

[290] Z. Fodor, A. Gérardin, L. Lellouch, K. K. Szabó, B. C. Toth, and C. Zimmermann, Phys. Rev. D **111**, 114509 (2025), arXiv:2411.11719 [hep-lat].

[291] T. Aoyama, T. Kinoshita, and M. Nio, Atoms **7**, 28 (2019).

[292] M. Davier, A. Hoecker, B. Malaescu, and Z. Zhang, Eur. Phys. J. C **77**, 827 (2017), arXiv:1706.09436 [hep-ph].

[293] A. Keshavarzi, D. Nomura, and T. Teubner, Phys. Rev. D **97**, 114025 (2018), arXiv:1802.02995 [hep-ph].

[294] G. Colangelo, M. Hoferichter, and P. Stoffer, JHEP **02**, 006 (2019), arXiv:1810.00007 [hep-ph].

[295] M. Davier, A. Hoecker, B. Malaescu, and Z. Zhang, Eur. Phys. J. C **80**, [Erratum: Eur.Phys.J.C 80, 410 (2020)], 241 (2020), arXiv:1908.00921 [hep-ph].

[296] K. Melnikov and A. Vainshtein, Phys. Rev. D **70**, 113006 (2004), arXiv:hep-ph/0312226.

[297] A. Gérardin, H. B. Meyer, and A. Nyffeler, Phys. Rev. D **100**, 034520 (2019), arXiv:1903.09471 [hep-lat].

[298] J. Aldins, T. Kinoshita, S. J. Brodsky, and A. J. Dufner, Phys. Rev. D **1**, 2378 (1970).

[299] J. Lüdtke, M. Procura, and P. Stoffer, JHEP **04**, 125 (2023), arXiv:2302.12264 [hep-ph].

[300] E. Kaziukėnas, M. Procura, and P. Stoffer, *Dispersive Approach to Hadronic Light-by-Light in Triangle Kinematics*, Talk at the 8th Plenary Workshop of the Muon $g-2$ Theory Initiative, Orsay, 2025.

[301] M. Hoferichter, P. Stoffer, and M. Zillinger, Phys. Rev. Lett. **134**, 061902 (2025), arXiv:2412.00190 [hep-ph].

[302] G. A. Schuler, F. A. Berends, and R. van Gulik, Nucl. Phys. B **523**, 423 (1998), arXiv:hep-ph/9710462.

[303] H. Lehmann, K. Symanzik, and W. Zimmermann, Nuovo Cim. **1**, 205 (1955).

[304] P. Stoffer, "Dispersive Treatments of $K_{\ell 4}$ Decays and Hadronic Light-by-Light Scattering", PhD thesis (University of Bern, Dec. 2014), arXiv:1412.5171 [hep-ph].

[305] D. Drechsel, G. Knöchlein, A. Y. Korchin, A. Metz, and S. Scherer, Phys. Rev. C **57**, 941 (1998), arXiv:nucl-th/9704064.

[306] G. Eichmann, C. S. Fischer, and W. Heupel, Phys. Rev. D **92**, 056006 (2015), arXiv:1505.06336 [hep-ph].

[307] G. Fischer, *Lineare Algebra, Eine Einführung für Studienanfänger*, 11., aktualisierte Aufl. 1997 (Vieweg, Braunschweig/Wiesbaden, 1997).

[308] M. Hoferichter and P. Stoffer, JHEP **05**, 159 (2020), arXiv:2004.06127 [hep-ph].

[309] M. Jacob and G. C. Wick, Annals Phys. **7**, 404 (1959).

[310] X.-L. Ren, I. Danilkin, and M. Vanderhaeghen, Phys. Rev. D **107**, 054037 (2023), arXiv:2212.03086 [hep-ph].

[311] H. Haberzettl, Phys. Rev. D **100**, 036008 (2019), arXiv:1905.06299 [nucl-th].

[312] S. J. Brodsky and J. R. Hiller, Phys. Rev. D **46**, 2141 (1992).

[313] K. J. Kim and Y.-S. Tsai, Phys. Rev. D **7**, 3710 (1973).

[314] T. D. Lee and C.-N. Yang, Phys. Rev. **128**, 885 (1962).

[315] B. L. Ioffe and A. V. Smilga, Nucl. Phys. B **216**, 373 (1983).

[316] E. Lymperiadou, "A model for light tensor meson transition form factors", Master's thesis (Universität Bonn, 2025).

[317] D. Gomez Dumm, A. Pich, and J. Portoles, Phys. Rev. D **69**, 073002 (2004), arXiv:hep-ph/0312183.

[318] D. G. Dumm, P. Roig, A. Pich, and J. Portoles, Phys. Lett. B **685**, 158 (2010), arXiv:0911.4436 [hep-ph].

[319] M. Aghasyan et al. (COMPASS), Phys. Rev. D **98**, 092003 (2018), arXiv:1802.05913 [hep-ex].

[320] M. Mikhasenko, A. Pilloni, M. Albaladejo, C. Fernández-Ramírez, A. Jackura, V. Mathieu, J. Nys, A. Rodas, B. Ketzer, and A. P. Szczepaniak (JPAC), Phys. Rev. D **98**, 096021 (2018), arXiv:1810.00016 [hep-ph].

[321] F. Giacosa, T. Gutsche, V. E. Lyubovitskij, and A. Faessler, Phys. Rev. D **72**, 114021 (2005), arXiv:hep-ph/0511171.

[322] H. Aihara et al. (TPC/Two Gamma), Phys. Rev. D **38**, 1 (1988).

[323] N. Muskhelishvili, *Singular Integral Equations*, 2nd ed. (P. Noordhoff N.V., 1953).

[324] G. Passarino and M. J. G. Veltman, Nucl. Phys. B **160**, 151 (1979).

[325] G. 't Hooft and M. J. G. Veltman, Nucl. Phys. B **153**, 365 (1979).

[326] V. Shtabovenko, R. Mertig, and F. Orellana, Comput. Phys. Commun. **306**, 109357 (2025), arXiv:2312.14089 [hep-ph].

[327] M. Galassi et al., *GNU Scientific Library Reference Manual (3rd Ed.)* 2024.

[328] G. Chanturia, L. A. Heuser, and M. Penners, *Dispersion Relations*, 2025.

[329] J. Tolkien, *The Return of the King* (George Allen and Unwin, 1955).

[330] D. Babusci et al. (KLOE-2), (2025), arXiv:2505.09285 [hep-ex].

[331] R. Escribano, S. Gonzàlez-Solís, and E. Royo, (2025), arXiv:2510.00787 [hep-ph].

[332] J.-N. Toelstede, E. Kaziukėnas, M. Procura, and P. Stoffer, *Update on HLbL in soft kinematics*, Talk at the 8th Plenary Workshop of the Muon $g-2$ Theory Initiative, Orsay, 2025.

[333] J. Tolkien, *The Fellowship of the Ring* (George Allen and Unwin, 1954).

Acknowledgements

> I don't know half of you half as well as I should like; and I like less than half of you half as well as you deserve.
>
> J.R.R. Tolkien, *The Fellowship of the Ring* [333]

Really daring to put myself into this work would not have been possible without the people close to me. First of all, I want to thank my supervisor Bastian Kubis for giving me the chance to become a theoretical physicist, not only during this PhD, but since the first lectures by him and Christoph Hanhart I had the chance to attend, and specifically for the opportunity to write a Bachelor's and a Master's thesis in his group. His amazing teaching and supervision qualities and constant effort to be kind to people and make the difference that we all would like to see inspired and formed me, both in physics and beyond. His enormous knowledge in many aspects of life as well as the fruits of his work, the group in Bonn, continue to impress me. I am grateful to Christoph Hanhart for being my second supervisor and someone I could always approach with a question, as well as for his comments and questions on my project that led to further clarifications. I want to express my gratitude to Pablo Sánchez-Puertas for joining the endeavour of the TFF project and enduring all my questions there, for many helpful discussions and constant encouragement.

The awesome group in Bonn has a big share in this work: Marvin Zanke, Yannis Korte, and Eirini Lymperiadou, with whom I have directly worked on these projects. Thanks for many discussions, I am glad that we could figure things out together.

I am glad that I had the honour to be a part of AG Kubis. These projects would not have come to the same success without countless questions I was asked and I could ask, and discussions resulting from those. Thanks that we could share sorrows and joy, both physics and non-physics related, for the collaboration in teaching, for many shared lunch and coffee breaks, and for many board-game nights, excursions, and visits in museums and concerts: Melisa Akdag, Nienke Balz, Gio Chanturia, Leon Heuser, Simon Holz, Yaxuan 'Coco' Huang, Simon Mutke, Elena Nitsche, Miriam Penners, Dominic Schuh, Dominik Stamen, and Marcel Welter, as well as others who where there during my Bachelor's and Master's thesis, and Bachelor's and Master's students who enriched the group by joining for their time. My gratitude encompasses also the other members of the HISKP theory department and the Diversity in Physics group in Bonn, who all do not only work on exciting physics, but also foster a friendly and welcoming environment for this work.

A significant motivation for the second project in this thesis came from the $g-2$ Theory Initiative, the workshops of which in Bern, Tsukuba, and Orsay I had the chance to partake in. Discussion there and at the workshop on Precision tests of fundamental physics with light mesons in Trento, as well as at the Workshop on Chiral Dynamics in Bochum provided valuable input and motivation for both projects.

I have to thank my track&field group in Bonn for helping me keep my sanity via sport, as well as many friends outside of physics. Finally, I want to thank my family, my partner's family, and my partner Ole Pinner for their unwavering support and encouragement.

Financial support by the DFG through the funds provided to the Sino–German Collaborative Research Center TRR110 “Symmetries and the Emergence of Structure in QCD” (DFG Project-ID 196253076 – TRR 110) and the Ministerium für Kultur und Wissenschaft des Landes Nordrhein-Westfalen through the funds provided to NRW fair is gratefully acknowledged.